UNIVERSITY OF NOTTINGHAM

DEPARTMENT OF CIVIL ENGINEERING

CYCLIC SIMPLE SHEAR TESTING OF GRANULAR MATERIAL

by

Peter Ansell

March 1977

UNIVERSITY OF NOTTINGHAM

DEPARTMENT OF CIVIL ENGINEERING

CYCLIC SIMPLE SHEAR TESTING OF GRANULAR MATERIAL

by

Peter Ansell, B.Sc.

Thesis submitted to the University of Nottingham
for the degree of Doctor of Philosophy

March 1977

To my parents

CONTENTS

ACKNOWLEDGEMENTS

The author would like to thank all those who have given help and advice during this research project. In particular:

Professor R.C. Coates, B.Sc.(Eng.), Ph.D., C.Eng., F.I.C.E., F.I.Struct.E., for providing the facilities of the Department of Civil Engineering,

Dr. S.F. Brown, B.Sc., Ph.D., C.Eng., M.I.C.E. and Dr. R.W. Sparrow, B.A., B.A.I., Ph.D., C.Eng., M.I.C.E. for their careful supervision,

The Science Research Council for providing a Research Studentship,

British Rail and the Transport and Road Research Laboratory for financing the experimental work,

Mr. R.F. Steel and his staff in the Faculty of Applied Science Workshop,

Mr. J.G. Redfern, B.A. and his staff in the Department of Civil Engineering Laboratories,

Mr. D. Syson and his staff in the Faculty of Applied Science Electronics Workshop,

Miss S.A. Bowering for preparing the photographs in this thesis,

Miss J.L. Clerbaut for typing this thesis with her usual neatness and efficiency.

ABSTRACT

A simple shear apparatus with the facility to provide cyclic shear stress reversals on samples of dry granular material has been developed for investigating the effect of this stress regime on materials which are used in road pavements and rail track permanent way. Cyclic shear stresses are a feature of the stress conditions which occur in these situations. The development of the apparatus is described in some detail including the design of contact stress transducers to measure the boundary stresses. Difficulties were encountered with the Mk1 version due to the effects of non-uniform dilation. A larger, Mk2 apparatus was designed to incorporate a split top platen so as to obviate these problems. A single size limestone material was used throughout to model a railway ballast. Several series of repeated constant load simple shear tests on samples 210 mm x 140 mm x 30 mm deep consisting of nominally 3 mm size particles were carried out in the Mk2 apparatus. The test programme included unidirectional and bidirectional repeated loading and certain features of the programme were quite novel. Block load tests were also carried out to investigate the response to a variety of loads. The permanent shear strain behaviour under unidirectional repeated load was characterised by a relatively large initial strain followed by a linear accumulation of shear strain with respect to the logarithm of the number of load cycles. The recoverable strain behaviour under repeated loading was characterised by a settling down period of several thousand load cycles to reach an equilibrium value which was dependent on the applied load. Initial dilation was found to be a factor which considerably influenced the subsequent permanent volumetric strain behaviour, particularly under unidirectional loading. Models of some aspects of the material's response to cyclic loading are presented in both graphical and mathematical form.

LIST OF FIGURES

LIST OF PLATES

NOTATION

φ	angle of shearing resistance
σ	normal stress
τ_m	mean shear stress
τ_r	repeated (peak to peak) shear stress
τ_c	cyclic (single amplitude) shear stress
R_m	mean shear stress ratio = τ_m/σ
R_c	cyclic shear stress ratio = τ_c/σ
γ_p	permanent shear strain
γ_r	recoverable shear strain
γ_c	cyclic (single amplitude) shear strain
v_p	permanent volumetric strain
v_r	recoverable volumetric strain
G	shear modulus = τ_r/γ_r
N	number of cycles
K_o	coefficient of earth pressure at rest

Note: The 1972 edition of PD 5686, "The Use of SI Units" (13) indicates that the term "pascal", symbol Pa, has been accepted by the Conférence Générale des Poids et Mesures as the official term for a newton per square metre and this has been adopted herein. Throughout the text, strains are evaluated as per cent and compressive volumetric strains are regarded as positive. Symbols other than those listed above are defined and used for restricted applications as the need arises.

A conversion table is given on the following page since the literature includes SI, MKS, CGS and Imperial units. The units quoted in the text are those used by the particular author; this avoids the use of suspiciously precise numbers in the text. Also, where Imperial unit equipment has been used in the laboratory, these units are quoted.

UNITS	in	lbf	lbf/in^2	mm	kgf	kgf/cm^2	$tonne/m^2$	N	N/mm^2	kPa
1 in	1			25.4						
1 lbf		1			0.45359237			4.44822		
1 lbf/in^2			1			0.070307	0.70307		0.00689476	6.89476
1 mm	0.0393701			1						
1 kgf		2.20462			1			9.80665		
1 kgf/cm^2			14.2233			1	10		0.0980665	98.0665
1 $tonne/m^2$			1.42233			0.1	1		0.00980665	9.80665
1 N		0.224809			0.101972			1		
1 N/mm^2			145.038			10.1972	101.972		1	1000
1 kPa			0.145038			0.0101972	0.101972		0.001	1

Conversion Table - Imperial/Metric

"It's only the shear that's simple"

CHAPTER ONE

INTRODUCTION

1.1 Background

Pavement design in Great Britain is currently based on previous experience and empirical results from full-scale testing. The materials involved in road construction are manufactured and placed according to Department of the Environment publications such as the Specification for Road and Bridge Works (21) and Road Note 29 (22). However, this method cannot cope with changes in environmental conditions, construction materials or innovative construction techniques because the performance of a particular pavement cannot be directly extrapolated with confidence beyond the conditions under which it has served.

One of the guiding themes of pavement materials research has been the development of a "structural" design method for flexible pavements. This involves the evaluation of a pavement in terms of load carrying parameters in a manner similar to that used for the relatively rational methods of design in structural concrete and steelwork. Such a design method would be able to cater for new conditions and materials. A similar technique would also be applicable to the evaluation of rail track permanent way. However, very little new permanent way is being laid at the present time and so improved design methods are not currently so important in the case of railways. Nevertheless, materials research is relevant to the railway situation for investigating the factors influencing track bed deterioration which occurs mainly as permanent deformation in the granular ballast.

There are considerable differences between the philosophies

associated with the evaluation of road pavements and permanent way. In the case of a flexible road pavement, the design is carried out partly with the intention of limiting the permanent deformations to reasonable levels and partly to prevent premature cracking of the bituminous bound layers. The aim of this approach is to render structural maintenance of the pavement a comparatively rare event. With conventional rail track, using individual sleepers supported by a granular ballast, much higher levels of permanent deformation are acceptable but information is required on its likely rate of accumulation so that track maintenance programmes can be formulated. Track maintenance, in the form of cleaning and recompaction of the ballast to restore the line and level of the track, has been an accepted feature of conventional systems. However, present maintenance techniques are not very effective and, with escalating labour costs, this maintenance has become increasingly expensive; British Rail are currently allocating the order of £75 million annually to this aspect of track rehabilitation. The possibility of using alternative, mechanised methods of track maintenance is currently an important part of the track bed research programme. The philosophy associated with the continuous concrete slab track bed currently being developed by British Rail is somewhat different. In service, the slab cracks and becomes "flexible"; so the approach is closer to that of a flexible road pavement where permanent deformations are limited in the design process. With this type of track bed, maintenance costs should be lower.

The successful implementation of a more rational, structural design approach depends on information being available from three main areas. Firstly, information regarding the likely traffic

loading spectrum to which the pavement will be subjected must be available. Secondly, a method of analysis is needed to evaluate the stresses induced in the pavement under traffic. At present, there are essentially two approaches to this problem using either layered system theory (84) or finite element techniques (24). The simplest analyses use linear elastic theory to predict the induced stresses and strains. Dehlen and Monismith (20) have shown this to be satisfactory where the main structural layer of the pavement is of bituminous bound material supported by a stiff cohesive subgrade, provided that high ambient temperatures are not involved in which case the viscous properties of the bitumen become more significant. However, in the case of unbound granular materials contributing a major proportion of the strength of the pavement, the non-linear elastic properties of these materials have to be taken into account. This non-linearity means that parameters, such as elastic modulus, which define the behaviour of the material are not constants but depend on the stress level to which the material is being subjected. This stress dependency can be accommodated in the analysis by the use of iterative techniques. The third aspect of the requirements of a structural design approach is an experimental knowledge of these elastic properties so that appropriate values can be used in the analysis. It is important that the test conditions used to investigate these properties simulate the in situ stress conditions as closely as possible. This characterisation of material properties under realistic stress conditions is an essential part of the structural design approach. It also contributes to the longer term objective of developing models for materials which can predict their in situ performance from the results of a series of relatively straightforward standard tests in which the stress conditions

do not necessarily bear any relation to the in situ conditions.

With the rapidly increasing cost of the bituminous materials used in flexible road pavements, it would seem expedient to utilise as much as possible of the available strength of unbound granular materials. In the railway situation, a major part of the track bed deterioration is associated with permanent deformation in the granular ballast and considerable savings would seem possible if a more effective track maintenance procedure could be developed. With the foregoing in mind, this project has been concerned with investigating the behaviour of granular material under appropriate laboratory test conditions and the choice of test method is discussed in the following section.

1.2 Laboratory Simulation of the In Situ Stress Regime

Fig. 1 shows the stresses induced on an element in a road pavement when a static wheel load is placed sequentially in three different positions relative to the particular element being considered. If the wheel load were to roll at a steady speed between the two extreme positions, the stresses would vary with time as shown in Fig. 2. The vertical and radial stress pulses are of a similar shape with the radial stresses being smaller and the pulse time longer. The variation of the shear stresses with time is completely different in character; involving a shear stress reversal as the wheel passes over the element concerned. This, therefore, is the stress regime which must be reproduced as closely as possible in the laboratory tests if the results are to be used with confidence in a pavement design procedure.

The stress regime in the rail track bed situation is similar where continuous rail support is provided by a concrete slab track bed.

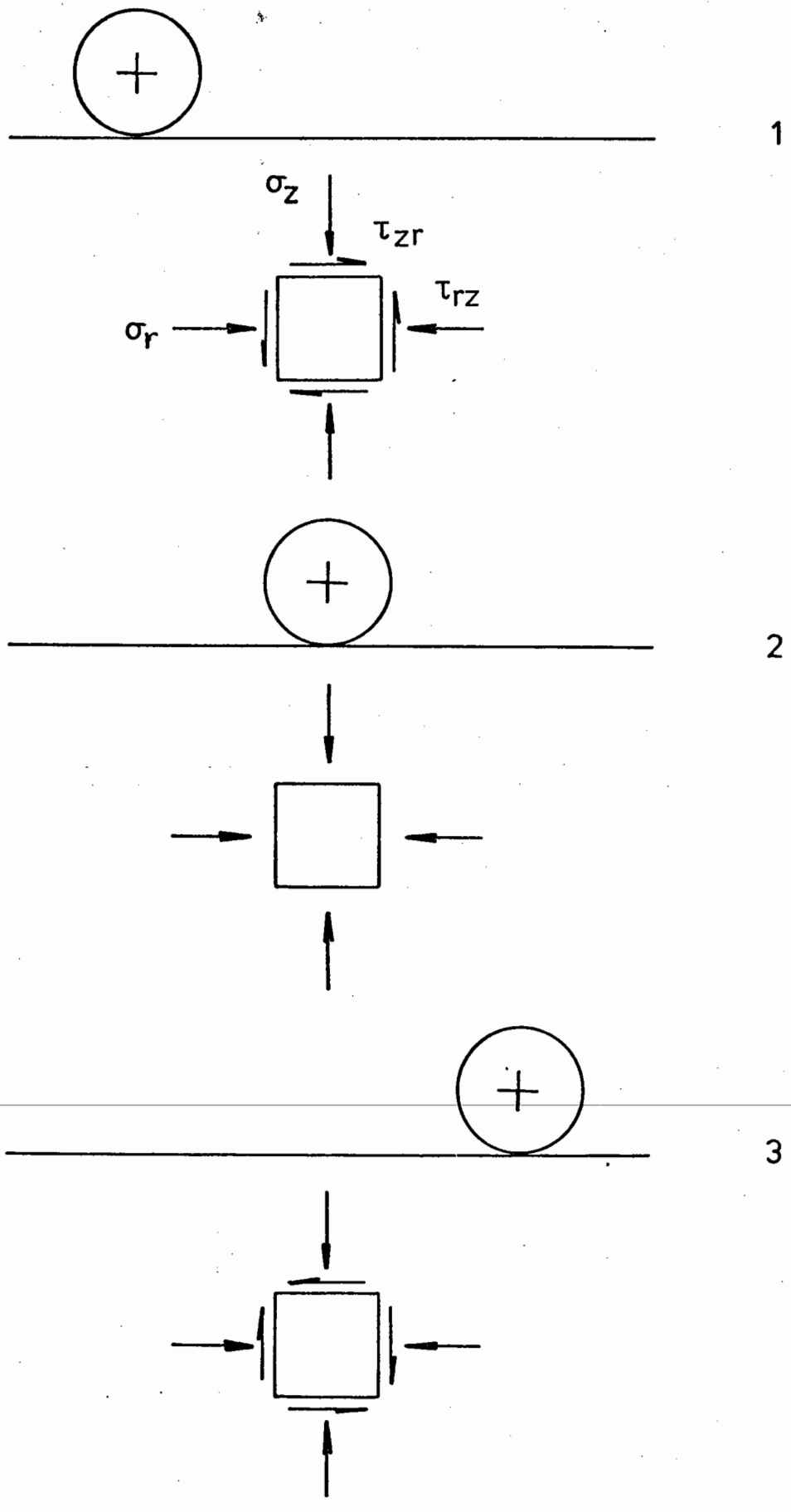

Fig. 1 Pavement stresses developed under static wheel loads

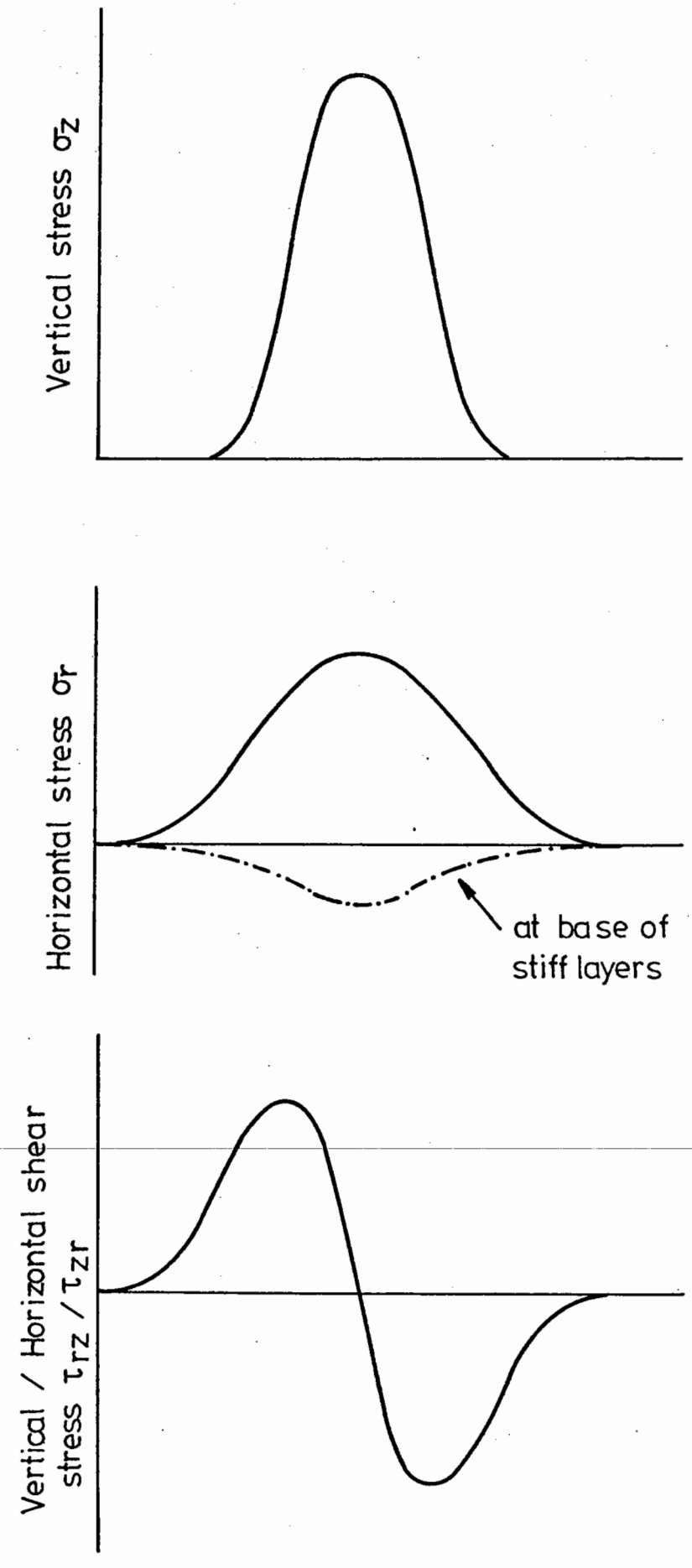

Fig. 2 Variation of pavement stresses under rolling wheel loads

However, in the case of conventional rail track with individual sleepers, the stress regime is somewhat different though shear stress reversal still occurs at points located between sleepers.

At the present time, there is no single piece of laboratory equipment capable of simultaneously applying the stress patterns shown in Fig. 2 to a test specimen. The repeated load triaxial test can pulse both of the normal stresses, σ_z and σ_r but cannot reproduce the required shear stress reversal because the triaxial test involves the application of normal stresses to a sample; shear stresses cannot be applied directly. Thus, the in situ element which corresponds to the stress conditions in the repeated load triaxial test must only be subject to principal stresses and, as shown in Fig. 3, this element rotates as the wheel load moves past. Consequently, the permanent deformations of the sample, measured in the directions of the applied stresses, will be somewhat greater than the required deformations in the actual pavement. This is because the principal stresses acting on the in situ element when the wheel load is not directly over it are generally less than those acting when the load is directly over the element. It can be seen, therefore, that the repeated load triaxial test only correctly simulates the in situ stress conditions at the central position when no shear stresses are developed on the vertical element. Peacock and Seed (57, 71) have considered the differences between field conditions and those developed in the repeated load triaxial test in some detail. In particular, they have pointed out that, in a triaxial test, the major principal stress can only act in either a vertical or a horizontal direction. Reorientation of the principal axes, other than through the full right angle, is impossible.

The standard direct shear box, which Casagrande developed (26)

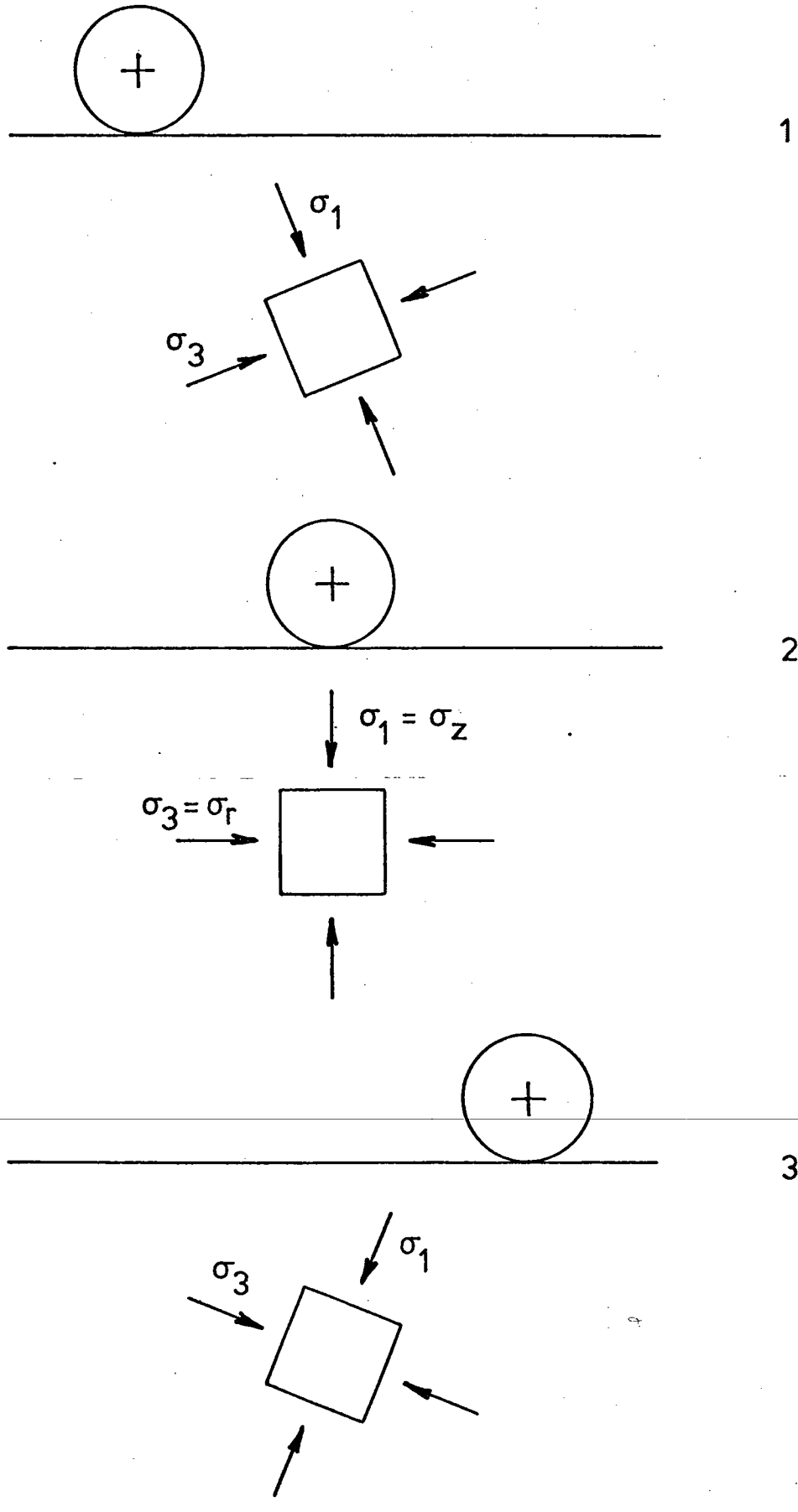

Fig. 3 Rotation of the principal stress element

at the Massachusetts Institute of Technology during the period 1930-32, applies shear forces directly to the faces of the sample and the test procedure is much simpler than that for the triaxial test. However, the stress conditions in the box are far from uniform and often indeterminate. Also, progressive failure is induced on a pre-selected plane which is unlikely to be representative. At the ends of the box the shear strains are concentrated at the shear plane and are a maximum. In the centre they are more uniformly distributed through the thickness and are a minimum (64, 77). Other failings of the direct shear test include the tendency for the box to tilt at light loads and the possibility of tension zones developing in parts of the sample under light normal loads. In view of these drawbacks, the direct shear test is not really suitable for research work where detailed stress-strain information is required. However, with its relative simplicity, the direct shear test does have a place in engineering practice, for example as a comparative strength test or for the analysis of shear in backfill behind retaining walls (16, 31).

In addition to road pavement and permanent way design, there are other instances where the shear stress reversal referred to above is of importance and where the shortcomings of the direct shear test are equally relevant. Firstly, earthquakes can be considered (47) to be represented by a series of horizontal cyclic shear stresses propagating upwards through the soil strata and a considerable portion of the literature, particularly that published in the United States, has been devoted to this aspect of cyclic shear stress reversal. Secondly, a much more recent application is the cyclic shear stress reversal, due to wave action, which occurs beneath the foundations of the gravity type of oil production platforms currently being used in the North

Sea (7). This application has dominated the recent European literature on cyclic shear stress reversal.

Recognition of the serious shortcomings of the direct shear test for research purposes led to the development of the "simple shear apparatus", of which essentially two versions have emerged. The apparatus developed in Sweden (38) and Norway (8) is relatively straightforward whereas that produced at the University of Cambridge (6, 64, 65, 80) is relatively complex. Both versions overcome the major drawbacks associated with the direct shear box and repeated load versions have been developed (27, 28, 57, 75, 82).

The research work described in what follows has been concerned with the development of a piece of equipment which incorporates the important features of other simple shear devicess and is able to apply cyclic shear stress reversal to a granular material while still remaining relatively uncomplicated in its design. Following a study of the relevant literature, which is summarised in Chapter Two, a Mk1 apparatus was developed and this is described in Chapter Three. The results obtained from this apparatus were found to be unsatisfactory due to non-uniform dilation of the sample. A larger Mk2 apparatus, incorporating a split top platen, was developed to overcome this problem and this is described in Chapter Four. The results of a programme of repeated load simple shear tests on crushed limestone samples consisting of nominally 3 mm size particles are presented in Chapters Five, Six and Seven. The material chosen for the tests was essentially a model material for railway ballast. Certain aspects of the test programme, such as the unidirectional repeated load simple shear tests, are quite novel; no similar tests appear to have been reported elsewhere in the literature. Various empirical models for the

response of the material to repeated loading in simple shear are developed and the conclusions and recommendations for further work are presented in Chapters Eight and Nine respectively.

CHAPTER TWO

A REVIEW OF THE LITERATURE

2.1 Introduction

In order to recognise some of the problems involved in the design and development of a simple shear apparatus, a fairly extensive search of the literature was made. A considerable proportion of the literature is concerned with the investigation of various stress-strain characteristics of cohesive materials. Indeed, most of the pioneer work on the simple shear apparatus seems to have been directed at cohesive material. This work was studied, even though this project was primarily concerned with granular material, because it was felt that some of the mechanical problems associated with the simple shear apparatus would be relevant to the mode of testing and not simply to the material under test.

The previous chapter has set out some of the main criticisms of the standard direct shear test and, over the last century or so, various researchers have attempted to devise other methods for the shear testing of soils. The development of these methods is presented in what follows though the descriptions are not necessarily in chronological order; the order of presentation has generally been governed by the particular type of apparatus and mode of test concerned. Several writers have reported research work aimed at identifying and investigating the important parameters affecting the inter-particle friction characteristics of granular material and this is also summarised in the review.

2.2 Novel Shear Tests

Several novel approaches to devising an alternative shear test

for soils have been reported in the literature and various novel methods of using existing pieces of equipment have also been described. Housel (33) used a double direct shear apparatus to test cohesive soil. This method, which Sowers (77) attributes to Collin in 1846, involved the transverse loading of a sample contained in a tube made up of three cylinders, Fig. 4. The outer pair were clamped and the central cylinder loaded. Sowers points out that the stress and strain conditions in this apparatus are unlikely to be any better than those in the direct shear box. Sowers also mentions a shear box, developed by Peltier in the Central Laboratory of Bridges and Roads of France, which had movable sides enabling the intermediate principal stress to be controlled. However, the stress distribution would probably have been non-uniform.

In 1963, Poellot and Yoshimi (60) reported a novel type of test whereby an unconfined rectangular sample of cohesive material, 10 in. x 4 in. x 1 in. deep was subjected to shear loading as shown in Fig. 5. The sample was sandwiched between two steel plates supported on steel rollers so as to maintain a constant volume. Weights were placed on the upper plate to prevent overturning. Since the complementary shear stresses on the ends of the sample are obviously absent, normal stresses must be induced on the upper and lower faces to maintain static equilibrium and so pure shear conditions, Section 2.3, cannot apply. However, it was assumed that, for a long shallow specimen, the effects of the normal stresses would be confined to the ends of the specimen and could be neglected. The tests were long term and so the exposed faces of the sample were smeared with grease to control the moisture content during a test. Determination of the strain distribution was carried out photographically; an ink grid being transferred onto the sides of the sample before the grease was applied.

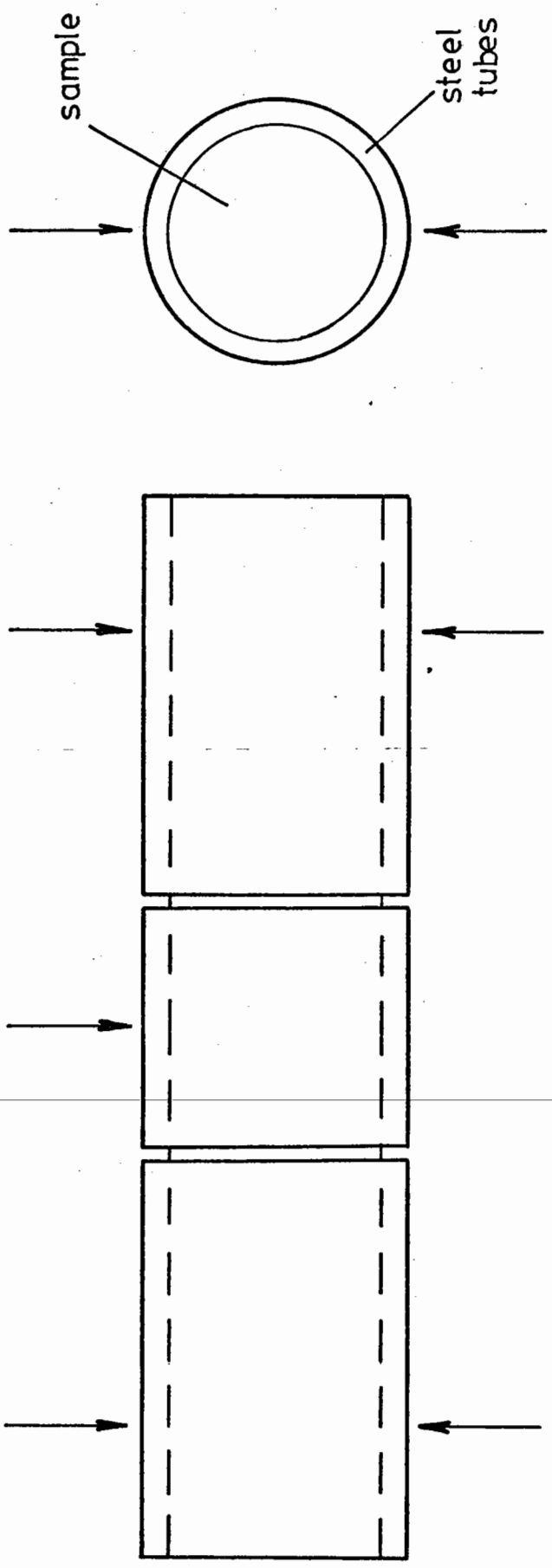

Fig. 4 Double direct shear test

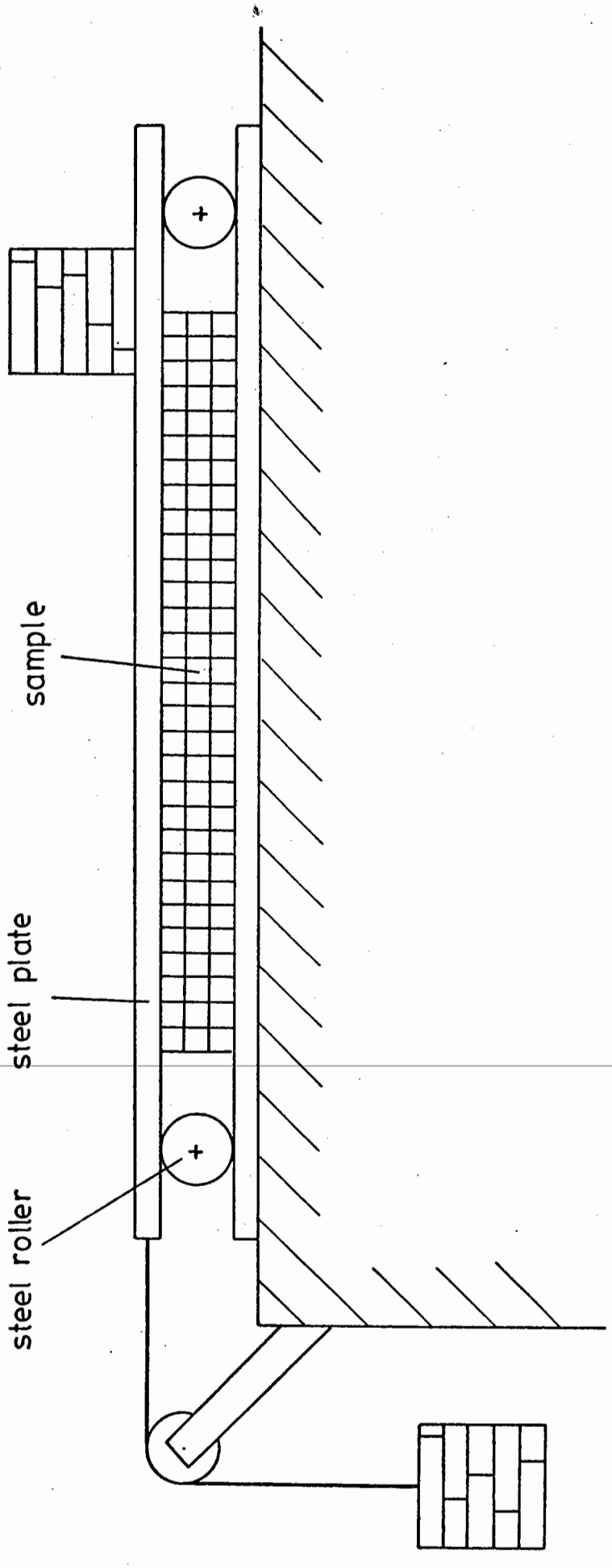

Fig.5 Simple shear apparatus (After Poellot and Yoshimi (60))

Another drawback of the standard direct shear test is the limited shear strains which can be accommodated by the apparatus. This is of particular importance when residual values for the shear strength of a material are required. Marsh (53) has described tests on clay samples to determine the residual shear strength using a modified standard direct shear box method involving repeated reversal of the direction of travel of the shear box. An alternative approach has been described by Hvorslev (34) who developed a continuous direct shear apparatus consisting of an annular shear box which permitted unlimited displacements. The shear force was applied to the sample as a torque; the upper half of the box moving relative to the fixed lower half. However, the stresses in this arrangement are still undefined and the strains non-uniform; varying with the distance from the centre of rotation. This apparatus has mainly been utilised for research concerned with large strain effects (77).

Ishibashi and Sherif have recently, 1974, described (36) a Torsional Simple Shear Device which overcomes the strain non-uniformity problem associated with Hvorslev's apparatus. Their apparatus used a 4 in. outside diameter annular specimen enclosed in a triaxial type cell and the sample had a varying depth as shown in Fig. 6. When a torque is applied to the specimen, the tangential deformation is given by $r\theta$ giving a shear strain equal to $r\theta/h$. If now the ratios r_1/r_2 and h_1/h_2 are made equal, the shear strains throughout the sample will be uniform.

2.3 Simple Shear Stress Conditions

The easiest stress conditions to analyse in terms of shear strength are those of pure shear, shown in Fig. 7(a). However,

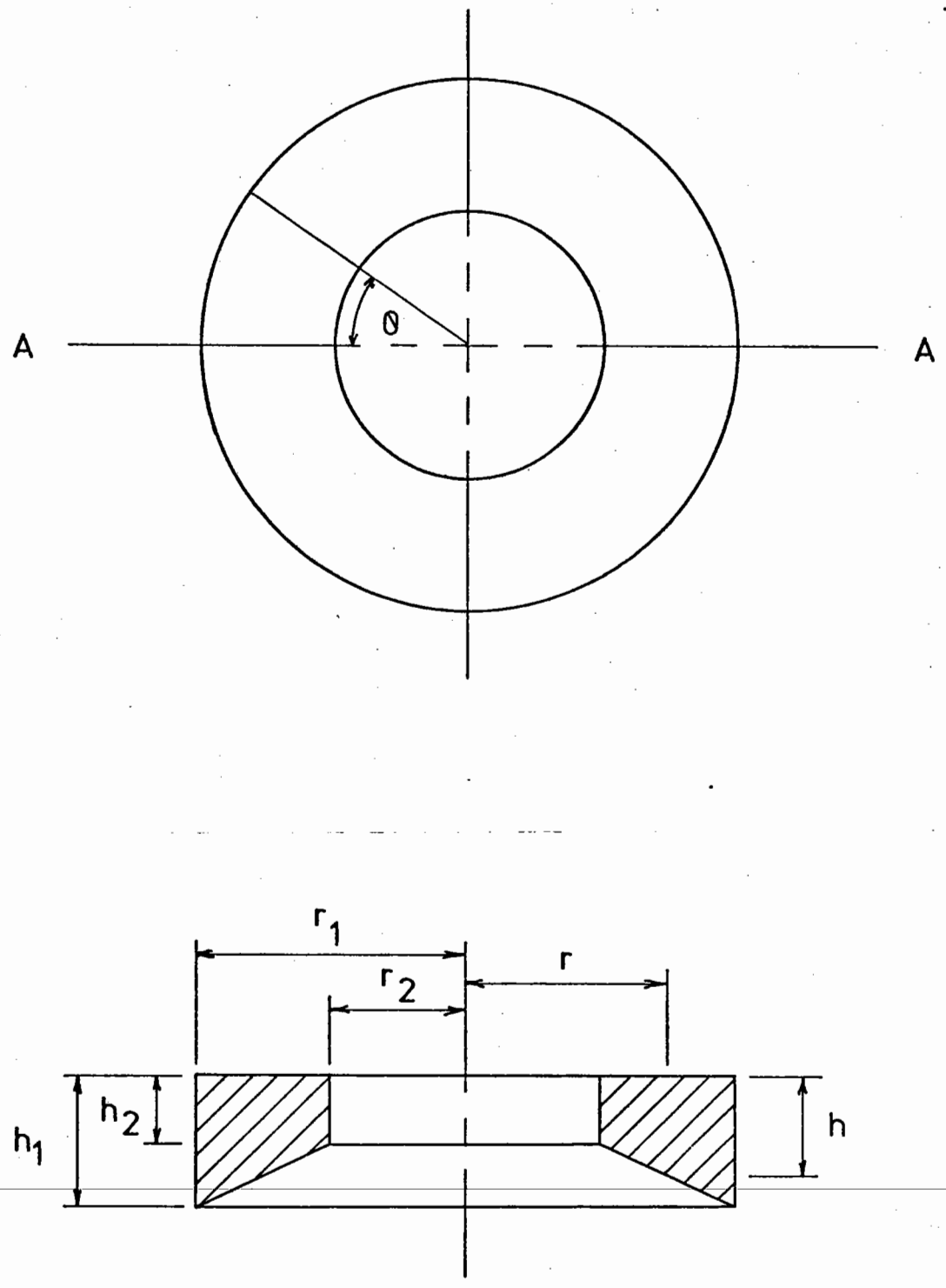

Section A-A

Fig. 6 Torsional Simple Shear Device (after Ishibashi and Sherif (36))

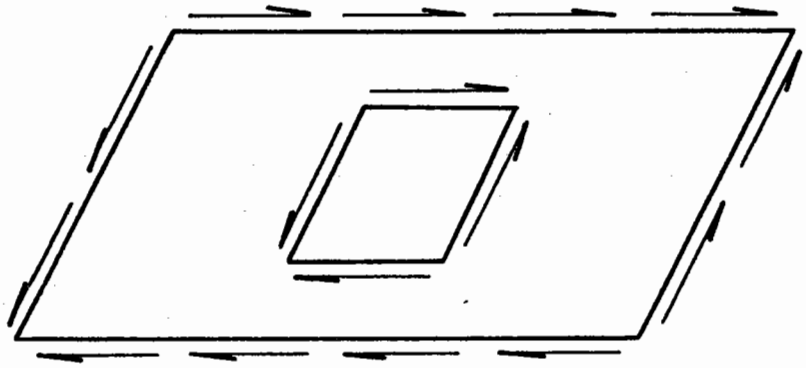

(a) Pure shear

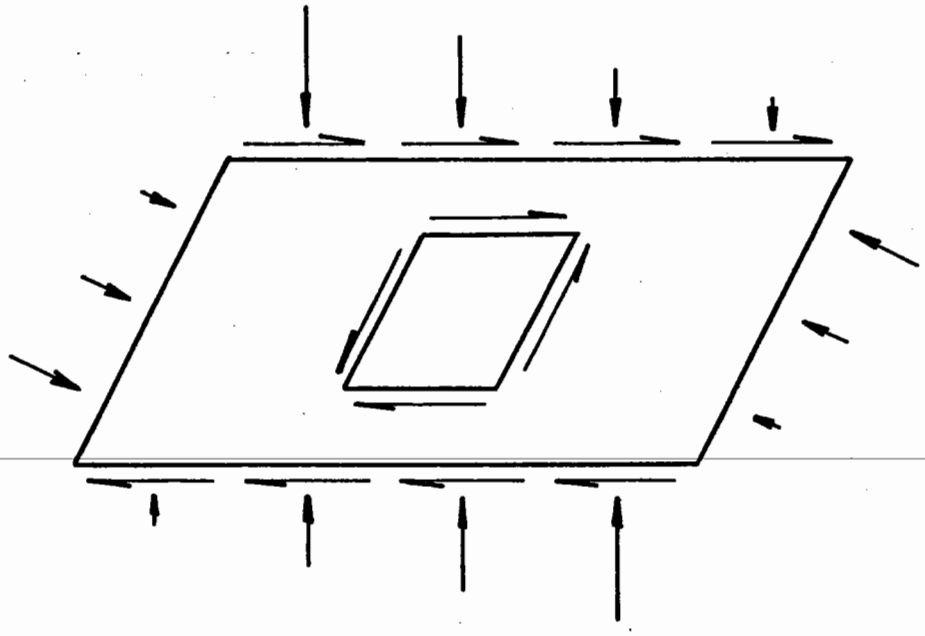

(b) Simple shear

Fig. 7 Shear stress conditions

Roscoe (64) has expressed doubts as to whether any piece of apparatus can impose uniform shear stress on the surfaces of a sample along with the required complementary shear stresses. Under conditions of simple shear, as shown in Fig. 7(b), a non-uniform normal stress distribution must be developed on the faces of the sample in order to maintain static equilibrium. Thus, the stress conditions developed under conditions of simple shear will be quite complex. However, it should be noted that the stress distribution shown in Fig. 7(b) is not intended to be representative of the actual distribution developed under these conditions.

In spite of this complexity, theoretical stress analyses by several authors have shown that the non-uniformities associated with simple shear are quite localised at the ends of the specimen; stress conditions in the central zone are reasonably uniform. The shear stresses on planes parallel to the ends of the sample increase towards the centre and the stress conditions at the centre of the sample correspond closely to those of pure shear, Fig. 7(b). The results of a linear elastic analysis by Roscoe (64) and a discrete particle computer solution by Round (66) are compared in Fig. 8. Strictly speaking, Roscoe's solution is only applicable to elastic materials but it should be reasonably accurate for soils in the initial stages of deformation and give some guidance on the likely stress distribution at larger deformations (64). The application of Round's computer program, developed at the University of Nottingham, to the behaviour of particulate materials in the simple shear apparatus is further discussed in Chapter Four. The non-linear finite element analyses described by Duncan and Dunlop (23) have also indicated that the stress non--uniformities in simple shear are confined to the ends of the sample.

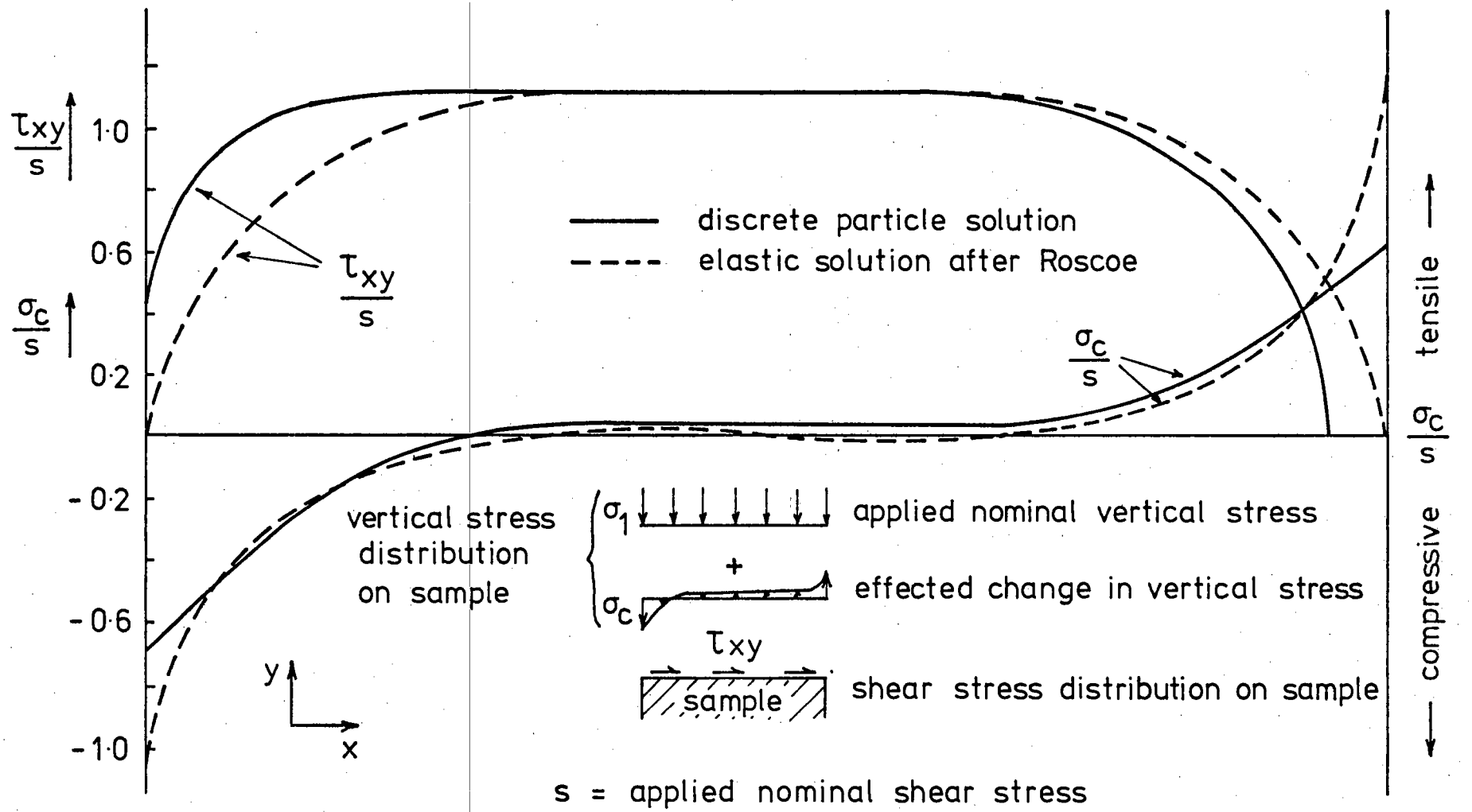

Fig. 8 Predicted stress distribution on the top sample face in the simple shear box (after Round (66))

The development of failure zones in a soft clay sample subjected to increasing strain in simple shear was monitored and the results, Fig. 9, showed that failure was progressive from the ends towards the centre of the sample. The authors did not consider that this effect would be very significant unless the soil had a marked shear resistance reduction after the peak strength had been mobilised. A recent paper by Prevost and Hoeg (61) has extended the existing analyses of simple shear (23, 51, 64) by considering the effects of partial differential slippage at the interfaces between the sample and the apparatus. Such slipping was found to have a very disruptive effect on the shear and normal stress distributions; inducing severe non-uniformities. Their analysis also showed that the lateral stresses on a sample subjected to conditions of simple shear strain were likely to change during the course of the straining. Measurements of lateral stress changes in simple shear tests on sands have confirmed the analytical pattern of behaviour (61, 89).

2.4 Simple Shear Tests

Work at the Swedish Geotechnical Institute (S.G.I.), reported by Kjellman (38) in 1951, appears to be the earliest attempt to produce a piece of apparatus providing improved stress and strain conditions. A cylindrical sample 60 mm in diameter and 20 mm high was confined by a rubber membrane reinforced on the outside by aluminium rings which prevent lateral strain, Fig. 10. However, there will almost certainly be some lateral deformation between these rings and so the lateral stresses will be even more indeterminate than in the standard direct shear box (77). The shear stresses will also be non-uniform since they must be tangential to the circular boundary unless the sides

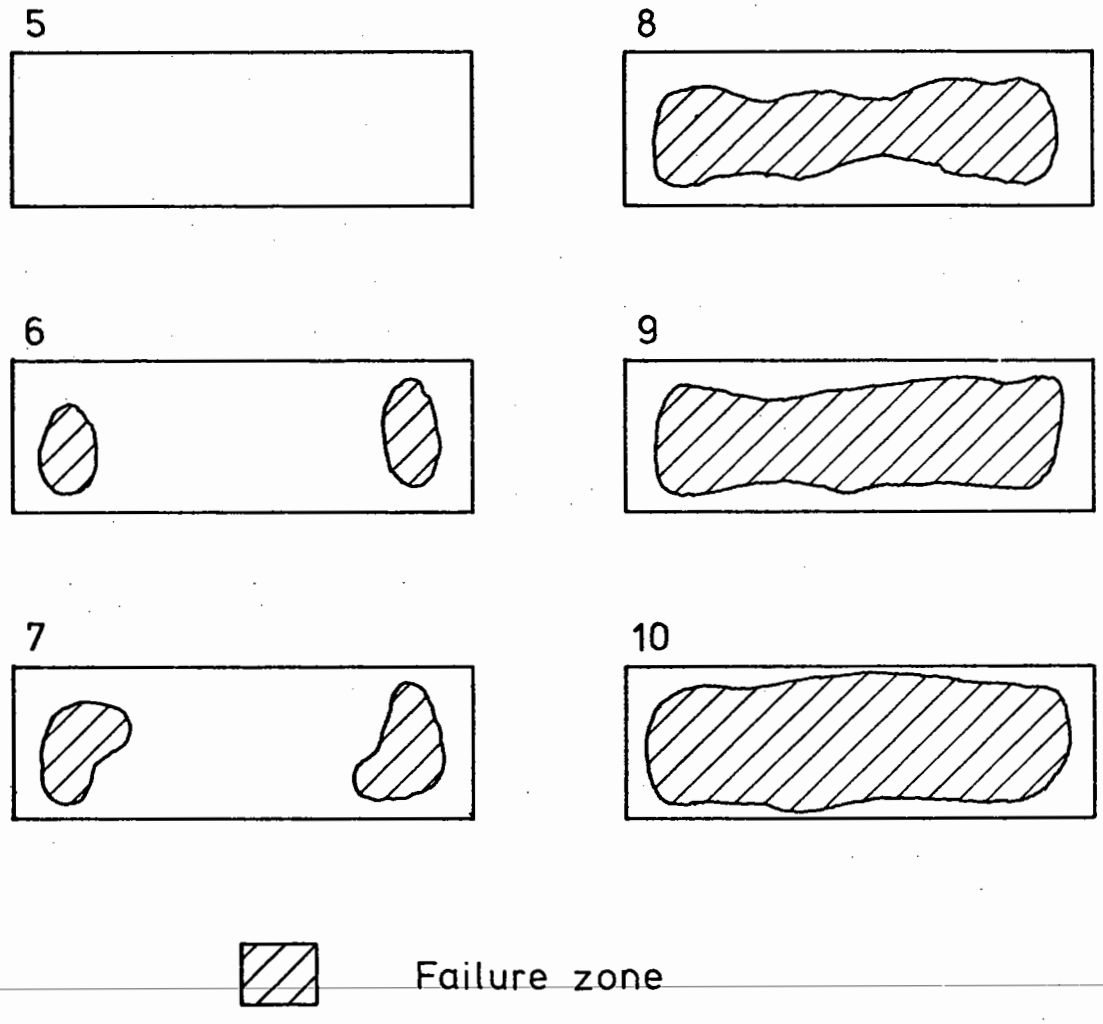

Fig. 9 Progressive failure for a soft clay in simple shear (after Duncan and Dunlop (23))

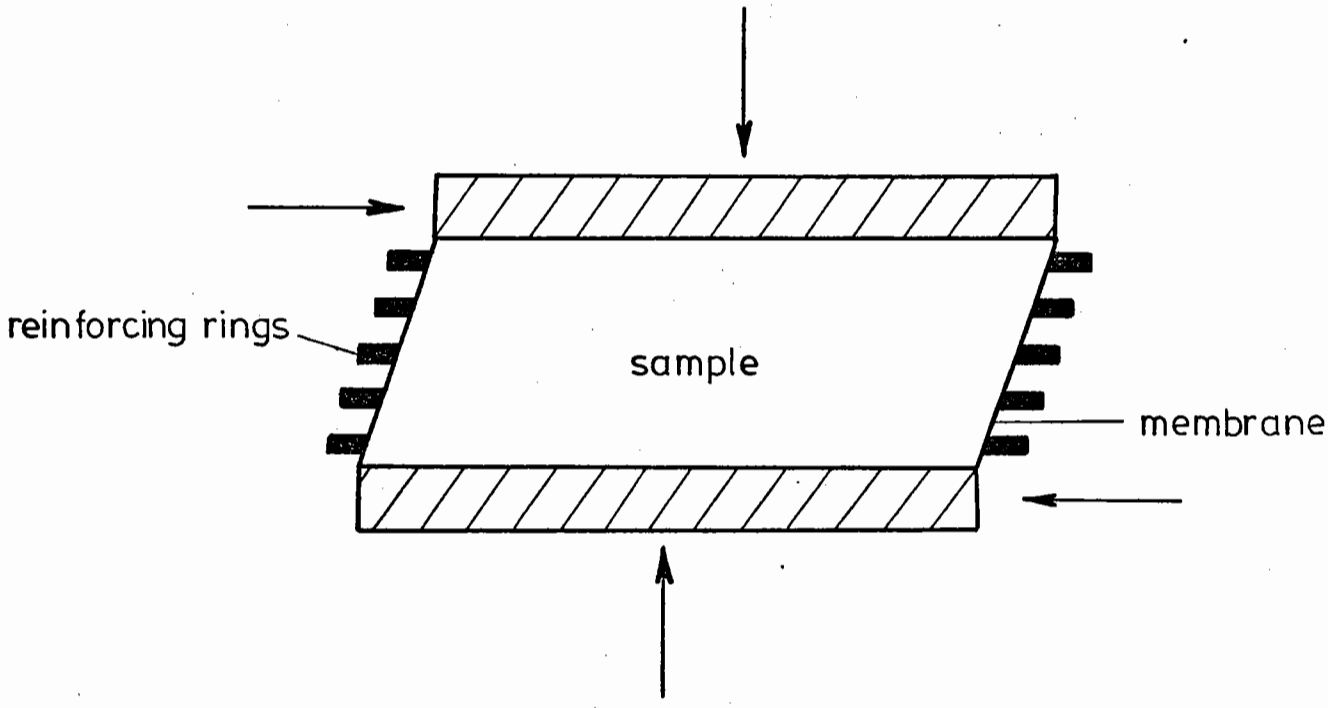

Fig.10 S.G.I Simple Shear Apparatus for routine tests

impose complementary vertical shear stresses on the sample and Roscoe (64) considers this unlikely. The shear deformation, consisting of an angular distortion, is approximately equal at all points and can be considered reasonably uniform over the height of the sample. Also, the area of the failure surface remains fairly constant during the test in contrast to the reduction of this area during the standard direct shear test. The Swedish Geotechnical Institute describe this device as a "routine test" apparatus. A mechanically intricate "research" apparatus was also built (38) and this attempted to apply pure shear directly to a square sample. However, the deformations which the apparatus could accommodate were very limited and little work with it seems to have been reported.

An apparatus similar to that developed by the Swedish Geotechnical Institute has been described by Bjerrum and Landva (8). This was developed at the Norwegian Geotechnical Institute (N.G.I.) and employs a sample 80 mm in diameter and 10 mm high. The confining rubber membrane was reinforced by a spiral binding of wire. The stress conditions induced on the sample by this apparatus were investigated by Lucks et al (51) using a finite element technique. They concluded that the stress concentrations were quite local at the edges of the sample and about 70% of the sample was subject to reasonably uniform stress conditions.

In 1953, Roscoe (64) described the (MkI) Cambridge Simple Shear Apparatus which could apply simple shear strain to a sample 60 mm square in plan and approximately 22 mm high. End and edge effects were reduced by lining the sides of the split box with rubber membranes lubricated with silicone grease. There was, however, a "dead zone", approximately 2 mm deep adjacent to the loading piston at the top of

the sample which was not subjected to shear strain. A series of tests using striped plasticene samples were carried out in both the standard direct shear box and the simple shear apparatus. Some typical results are shown in Fig. 11 and these illustrate the very severe strain non-uniformities produced in the former apparatus and the comparatively very uniform strains produced by the latter apparatus. The linear elastic analysis of simple shear by Roscoe (64), previously referred to in Section 2.3, showed the bulk of the sample to be in pure shear and tensile zones in the upper leading and lower trailing edges of the sample to be almost eliminated provided the average normal stress was approximately equal to the average shear stress. This prototype (MkI) apparatus was suitable only for rapid undrained tests and Roscoe reported (64) that tests had only been carried out using relatively firm cohesive or dry cohesionless samples.

In a later (MkVI) version of the simple shear apparatus, contact stress transducers were used (65) to measure the induced boundary stresses and the results suggested that the stress conditions over the central third of the sample were, in fact, more uniform than those on the outer thirds. At this stage of development, the apparatus was no longer of the "split box" type but had solid walls and the dead zone had been eliminated in the MkV version. Subsequent developments of the Cambridge Simple Shear Apparatus have been described by Bassett (6). In some versions, the strain distribution in the sample was examined by the development of X- and γ-ray techniques using lead shot reference targets embedded in the sample. The sides of the apparatus were made of plate glass so as to be transparent to these electro-megnetic waves. The results showed conditions in the central third to be reliable and representative of the average conditions applied to the whole sample.

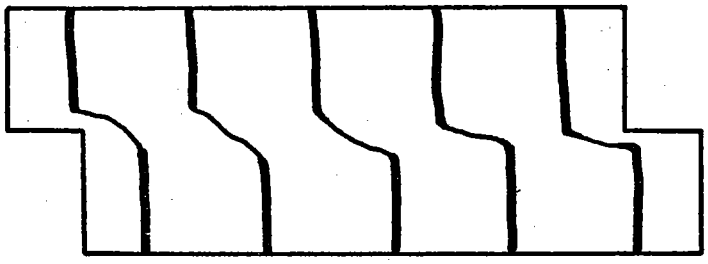

Direct shear

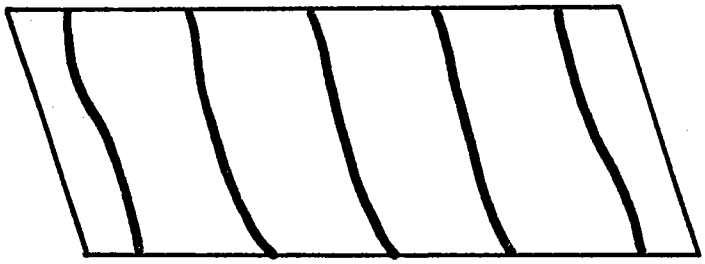

Simple shear
(Dead zone removed)

Fig.11 Shear strain distribution in direct and simple shear tests (After Roscoe (64))

2.5 Repeated Load Simple Shear Tests

Improved versions of the Roscoe type simple shear apparatus (64), modified for repeated loading, have been used by Peacock and Seed (57) and Finn, Bransby and Pickering (27, 28) in their studies of the liquefaction of saturated undrained sands due to the cyclic shear stress reversals which occur during earthquakes. The process of liquefaction is not directly relevant to this work but it so dominates the American literature on the subject of cyclic shear stress reversal that some explanation of it must be made. If a saturated sand is subjected to ground vibrations, it tends to compact and thus decrease in volume. If drainage is unable to occur, then the tendency to decrease in volume will result in an increase in the pore water pressure until it builds up to the point where it is equal to the overburden pressure. The effective stress thus tends to zero and the sand liquefies, losing its strength completely. A detailed review of the various liquefaction studies has been presented by Martin, Finn and Seed (54).

Silver and Seed (75, 76) used a modified N.G.I. Simple Shear Apparatus for a series of repeated constant strain tests on a dry, uniform angular quartz sand of 1 mm maximum particle size. The apparatus could produce controlled strain amplitudes in the range 0.01 to 0.5% on a sample 20 mm high and 80 mm in diameter. The tests were carried out at a frequency of 1 Hz. The results (75) showed that, with decreasing vertical stress and increasing shear strain, there was a marked decrease in the shear modulus, G, as defined in Fig. 12. A slight increase in shear modulus with increasing number of load cycles was observed and a decrease in shear modulus with decreasing relative density was also noted. The relationship between the shear modulus and

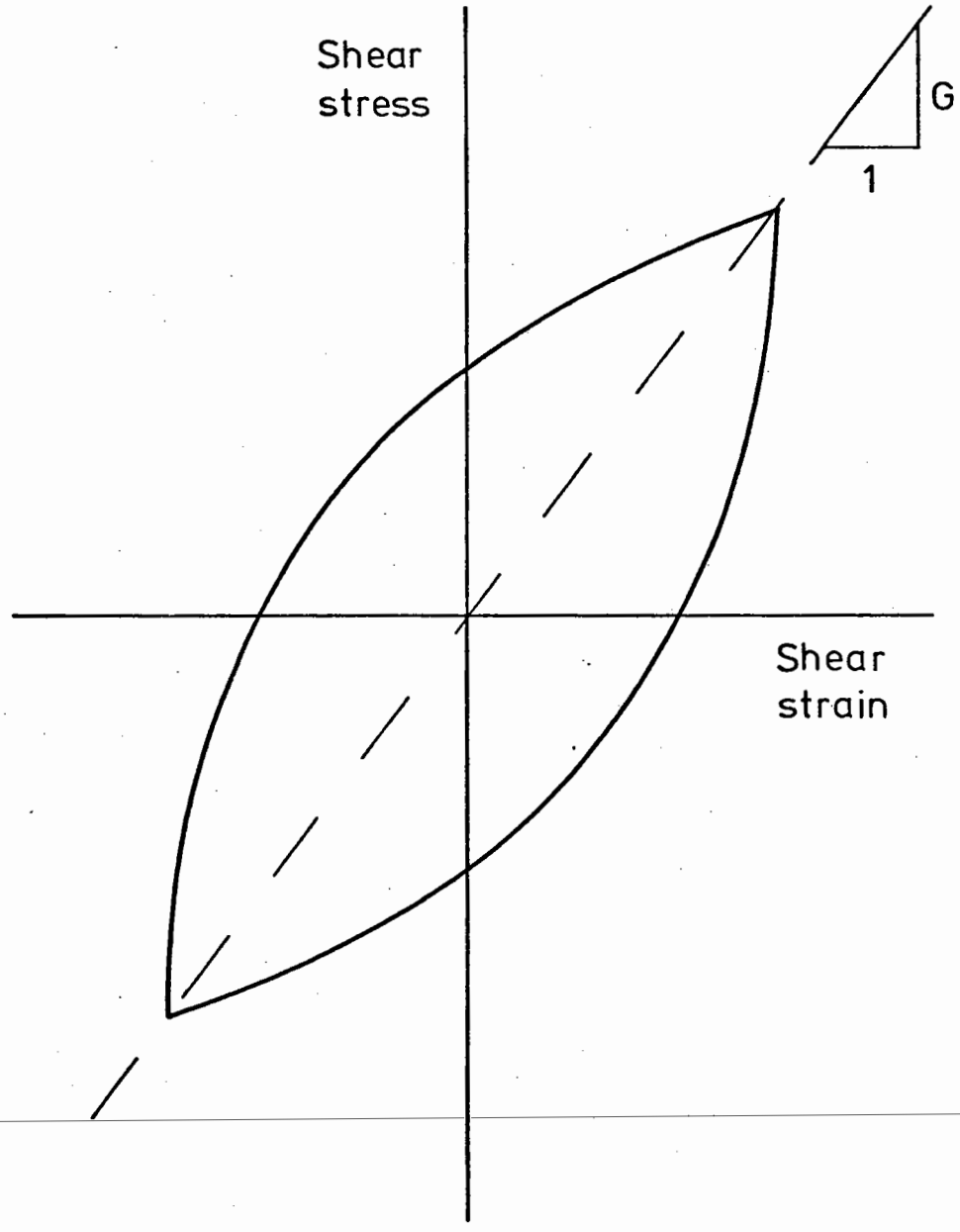

Fig.12 Definition of shear modulus (after Silver and Seed (75))

vertical stress for a given shear strain amplitude and relative density gave a straight line plot on a log-log basis as shown in Fig. 13. This relationship can be represented by the equation:

$$G = K_m \sigma_v^m$$

where G = shear modulus

K_m = value of G when $\sigma_v = 1$

σ_v = vertical stress

m = slope of the line on the log-log plot

It was found that the values of the exponent, m, varied between 0.5 and 0.7 depending on the shear strain amplitude. Further details of this relationship were given in a subsequent paper by Park and Silver (56), Fig. 66.

From their measurements of the volume change behaviour of sands under repeated constant shear strain conditions, Silver and Seed (76) suggested that the vertical strain due to compaction depended only on the shear strain amplitude where this exceeded 0.05%. The applied vertical stress did not significantly affect the volume change behaviour at the higher strain amplitudes in the range studied. It was also found that there was significantly more volume change at relative densities below 60%. The first few loading cycles were found to be important when considering the behaviour of the sand; in the range considered, as much vertical compaction occurred in the first 10 cycles as in the next 40. In a subsequent paper, Seed and Silver (72) used these results in developing a method of analysis for estimating the settlement of dry sands during earthquakes. Reasonably good agreement with laboratory scale tests was obtained.

Youd (86, 87, 88) has also reported an investigation of the

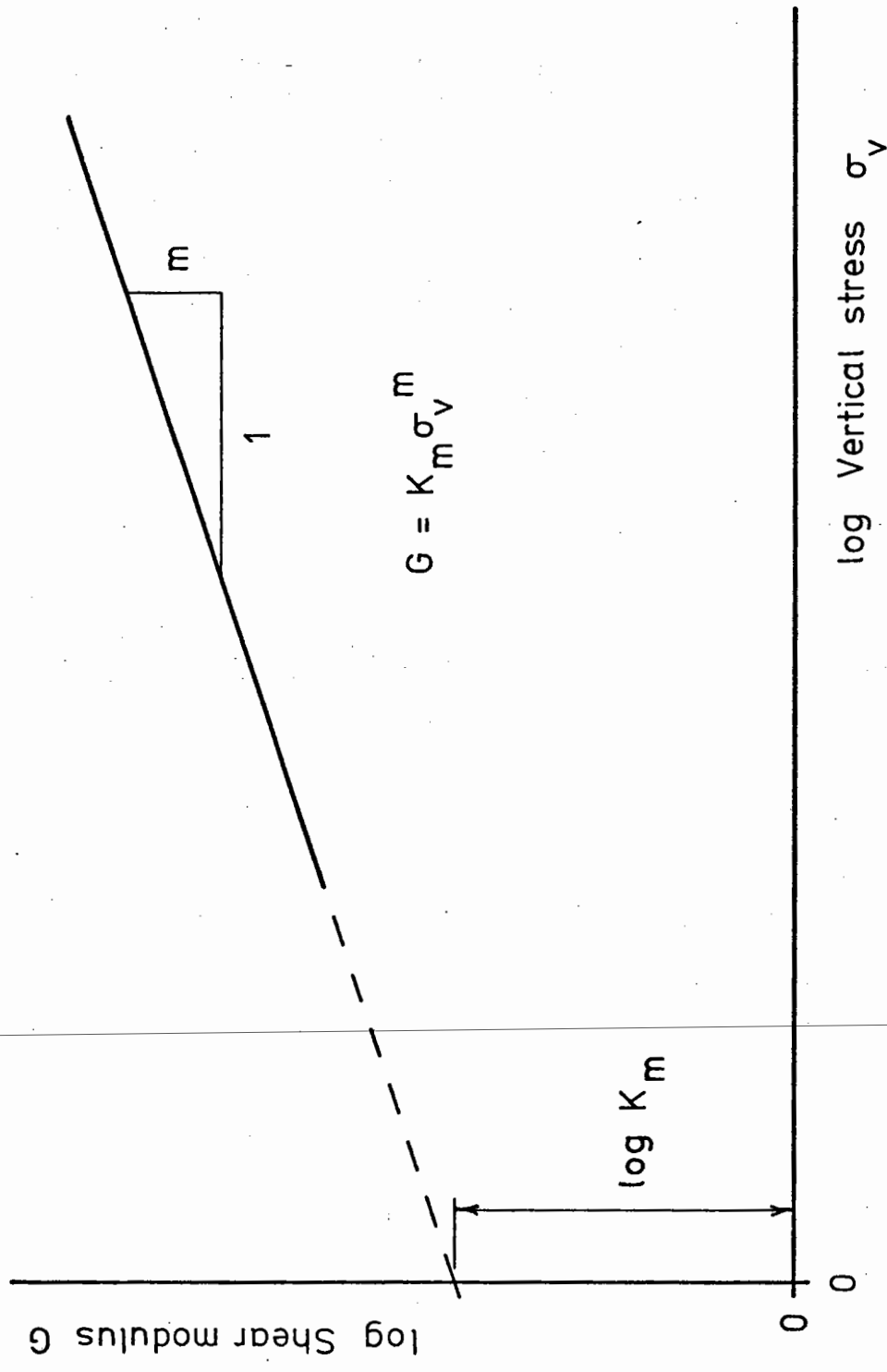

Fig.13 Shear modulus - vertical stress relationship (after Silver and Seed (75))

volume change characteristics during vibration and repeated simple shear straining using a modified N.G.I. Simple Shear Apparatus. He concluded that shear strain was the primary factor governing the compaction of granular materials. He also found that the maximum densities obtained by repeated simple shear straining exceeded those obtained by standard compaction techniques.

2.6 Other Repeated Load Tests

The work at the University of Nottingham reported by Sparrow (78) in 1965 appears to have been the first attempt to subject soil samples to repeated direct shear loading. The apparatus was devised with the intention of investigating the effect of repeated shear stress reversals occurring in the foundations of permanent way. The sample, 2 in. square in plan and approximately $\frac{1}{8}$ in. deep, was confined between two ribbed loading platens by a rubber membrane. In comparison with the samples used by other researchers, this specimen was very thin. The intention was to provide a short drainage path suitable for repeated loading tests on remoulded cohesive soils in which excess pore pressures could dissipate; allowing effective stresses to be evaluated. The repeated shear loads were applied by pneumatic rams operated by compressed air.

A repeated load Biaxial Shear Box has been designed at the British Railways Technical Centre, Derby (79) and work using this apparatus at the University of Nottingham has been reported by Phillips (58). The apparatus was developed in connection with the track bed research programme being undertaken at Derby. It applied repeated loads to a 10 cm cube of model ballast material in order to simulate in situ track loading. Six rams operated by compressed air provided the dynamic loads; one pair of rams acting in opposition along each of the

Cartesian axes. The apparatus, as described by Phillips, used air logic circuits to control the repeated loading. The four rams in the horizontal plane each carried a vertical platen which was interleaved along its vertical edges with the two adjacent platens. These four platens could, therefore, move independently of each other to allow the plan dimensions of the sample to vary continuously through the infinite number of rectangles between the limiting squares 5 cm x 5 cm and 15 cm x 15 cm. The two platens attached to the vertical rams covered the horizontal edges of the other four interleaved platens. These two rigid platens, being 20 cm square, were large enough to cover these edges even when the plan size of the sample was at its maximum of 15 cm x 15 cm. They were slightly separated from the other four platens by the sample itself during the setting up procedure. The sample consisted of dry, crushed Ballidon limestone with a grading from $\frac{1}{2}$ in. down to $\frac{1}{4}$ in. and it was separated from the loading platens by rubber membranes. The vertical rams were defined to represent the in situ horizontal direction parallel to the sleepers and the other two pairs of rams represented the vertical direction and the horizontal direction parallel to the rails.

The aim of the work using this apparatus was to firstly monitor the permanent deformation of the sample due to repeated loading in the in situ vertical direction and then to investigate the subsequent behaviour after the material had been tamped by temporarily changing the direction of the principal stresses. Various degrees and methods of tamping were used and several interesting points regarding the effectiveness of tamping emerged. This work also confirmed the strain relationship, presented by Shenton (73), which was obtained from the results of a repeated load triaxial test programme on a rail

track ballast material. The relationship, which governs the permanent strain, ε_N, after any number of load cycles, N, and the permanent strain produced by the first load cycle ε_1, is given by:

$$\varepsilon_N = \varepsilon_1(1 + 0.2 \log N)$$

This means that the whole of the subsequent permanent deformation of the ballast can be predicted from information obtained from the first load cycle. Shenton further reported that this equation was independent of stress, porosity and type of ballast material within the limits of test programme.

Repeated load triaxial tests on granular materials at constant confining stresses have also been reported by Morgan (55) and Barksdale (5). Morgan investigated the effect of confining pressure, deviator stress and degree of saturation on the permanent and recoverable strain behaviour of two sands. He found that, up to $2x10^6$ load cycles, permanent axial strain continued to accumulate but that after $2x10^5$ load cycles the rate of increase was very small. In addition, he found that the resilient modulus depended mainly on the confining pressure and that it increased with increasing confining pressure. There was a slight decrease in modulus with increasing deviator stress and it generally reached a constant value after 10^4 load cycles. Barksdale (5) reported repeated load triaxial tests on samples of a wide variety of unstabilised roadbase materials. His tests consisted of up to 10^5 deviator stress pulses at a constant confining pressure. The plastic strain developed after 10^5 load cycles was a non-linear function of the deviator stress. For small values of deviator stress, at a given confining pressure, the plastic strain was almost proportional to the deviator stress. With increasing deviator

stress, the development of plastic strain increased at an increasing rate until the plastic strains became very large as the apparent yield stress of the material was reached. The plastic strain was also very strongly dependent on the confining pressure; decreasing with increasing confining pressure. Soaking and reduced density of the material produced increased plastic strains. The results also indicated that only sufficient fines should be used in a crushed stone base to permit proper compaction so as to minimise the amount of rutting in the base. Although there was a considerable degree of scatter in the results, Barksdale developed a hyperbolic plastic stress-strain law for the plastic strain behaviour and used this in proposing a method for predicting pavement rut depths.

Variable confining pressure repeated load triaxial tests seem to have only recently been given detailed consideration in the literature (1, 2, 15). This is probably due to the more complicated experimental techniques required for this type of test. Timmerman and Wu (85) have reported tests of this type on a dry sand. The repeated loads were produced by modulating applied static pressures with cyclic deviator and confining pressures. They found that the overall dynamic strains increased with the number of load cycles but at a rapidly decreasing rate. It is interesting to note that apparently no distinction was made between permanent and recoverable strains in the presentation of their results. Within the range studied, the soil deformation consisted primarily of shear deformation; the contribution of volumetric deformation remained small and this effect has also been noted by Youd (88). Timmerman and Wu also found that, if the principal stress ratio under repeated loading was kept below a certain threshold level, the final shear strain developed was only slightly greater than that obtained in

a static test. Various threshold phenomena for many types of soil have been widely reported in the literature, e.g. (14, 30, 45, 55). Jumps in the overall dynamic axial strain versus load cycles curve were also observed by Timmerman and Wu between cycles 10 and 2000 and these seemed to be unpredictable. For all specimens, the strain did not increase significantly after 2000 cycles and the strain after 10,000 cycles was taken to be the final strain. The frequency of the cyclic loading, in the range 2.5 Hz to 25 Hz, was found to affect the rate of strain but not the final strain. They attributed the difference in the strain increment per cycle to the longer pulse durations at the lower frequencies. Similar lack of frequency effects on the final strains for sands have been reported elsewhere in the literature. Boyce found that frequency, in the range 0.1 to 20 Hz, had little effect on the recoverable strain behaviour in his repeated load triaxial tests with variable confining pressure (9). The purpose of the tests was to measure the strains which occurred when samples of a dry, well graded limestone of 38 mm maximum particle size, were subjected to a wide range of stress conditions. He found that the principal factors affecting the recoverable strains were the mean normal stress and the ratio between the deviator stress and the normal stress. Permanent strain was primarily dependent on the applied stress ratio.

In general, the literature would seem to indicate that, in the case of uniform granular materials such as railway ballast, permanent deformation continues to accumulate under repeated loading (62, 73). In the case of graded materials, the permanent deformation eventually settles down to an approximately steady value (9, 14, 55) unless the applied loads are sufficient to cause a "runaway" condition. However, this should only be regarded as a broad generalisation since exceptions,

such as Barksdale's results (5), do appear in the literature.

2.7 Comparisons of Simple Shear with Triaxial Tests

Despite the comments made in Chapter One regarding the limitations of the repeated load triaxial test, a considerable portion of the literature, e.g. (25, 28, 48, 57, 70) has been devoted to attempts to simulate the repeated shear stress reversal, such as that which occurs during earthquakes, using this type of test. This work was concerned with the liquefaction resistance of saturated undrained sands and a great deal of attention has been paid to correlating the liquefaction resistances obtained in the repeated load triaxial test with those obtained in the cyclic simple shear test. It is interesting to note the different methods used by the various authors who have attempted this correlation. The main difficulty was in defining a suitable index for the confining conditions in the simple shear test to allow comparison with triaxial tests where the confining conditions are indicated by the effective confining stress, σ_c'. Peacock and Seed (57) used the effective vertical stress, σ_v', as the equivalent index of confinement in the simple shear test. Using this index, they concluded that liquefaction resistances obtained from repeated load simple shear tests would be 50 to 55% of those obtained from triaxial tests. However, some of this discrepancy would seem to be attributable to the particular experimental techniques used by them.

Finn, Pickering and Bransby (28) suggested that the effective vertical stress, σ_v', was not a good index of the confinement of the sample for comparison with the effective confining stress, σ_c', in the triaxial test. The confining conditions in the simple shear test involve σ_v' vertically and $K_o\sigma_v'$ horizontally. The effective mean

normal stress was therefore defined as $\frac{1}{2}(\sigma_v' + K_o\sigma_v')$ and, using this index of confinement, the results obtained from the two types of test corresponded exactly. However, it should also be noted that Finn et al (28) used experimental techniques which were an improvement on those used by Peacock and Seed (57) for their simple shear tests. The degree of correlation achieved by Finn et al (28) provided improved confidence that both tests measured a physical property of the soil and not some phenomenon peculiarly related to the interaction of the sample and the apparatus. Subsequently, Park and Silver (56) went a stage further in defining the index of confinement in the simple shear tests as $\frac{1}{3}(\sigma_v' + 2K_o\sigma_v')$. This index is a mean of the normal stresses in three directions and good agreement between the two types of test was obtained using this method.

Seed and Peacock (71) have examined, in considerable detail, the merits and limitations of simple shear and triaxial tests conducted under cyclic loading conditions. As regards the simple shear test, they pointed out that the applied shear stress, τ, is not the maximum shear stress in the sample. It can be seen from Fig. 14 that the maximum shear stress, τ_{max}, is given by:

$$\tau_{max}^2 = \tau^2 + \left[\frac{\sigma_o'(1 - K_o)}{2}\right]^2$$

However, it can be shown, Appendix A, that the effect of this is unlikely to be very great, certainly in the case of single load tests. Seed and Peacock also noted problems of ensuring uniformity of strains throughout the sample and difficulties encountered in providing a uniform shear stress. The importance of an efficient boundary stress transfer mechanism was recognised and data presented to demonstrate this point. Difficulties associated with preparing test specimens in a uniform

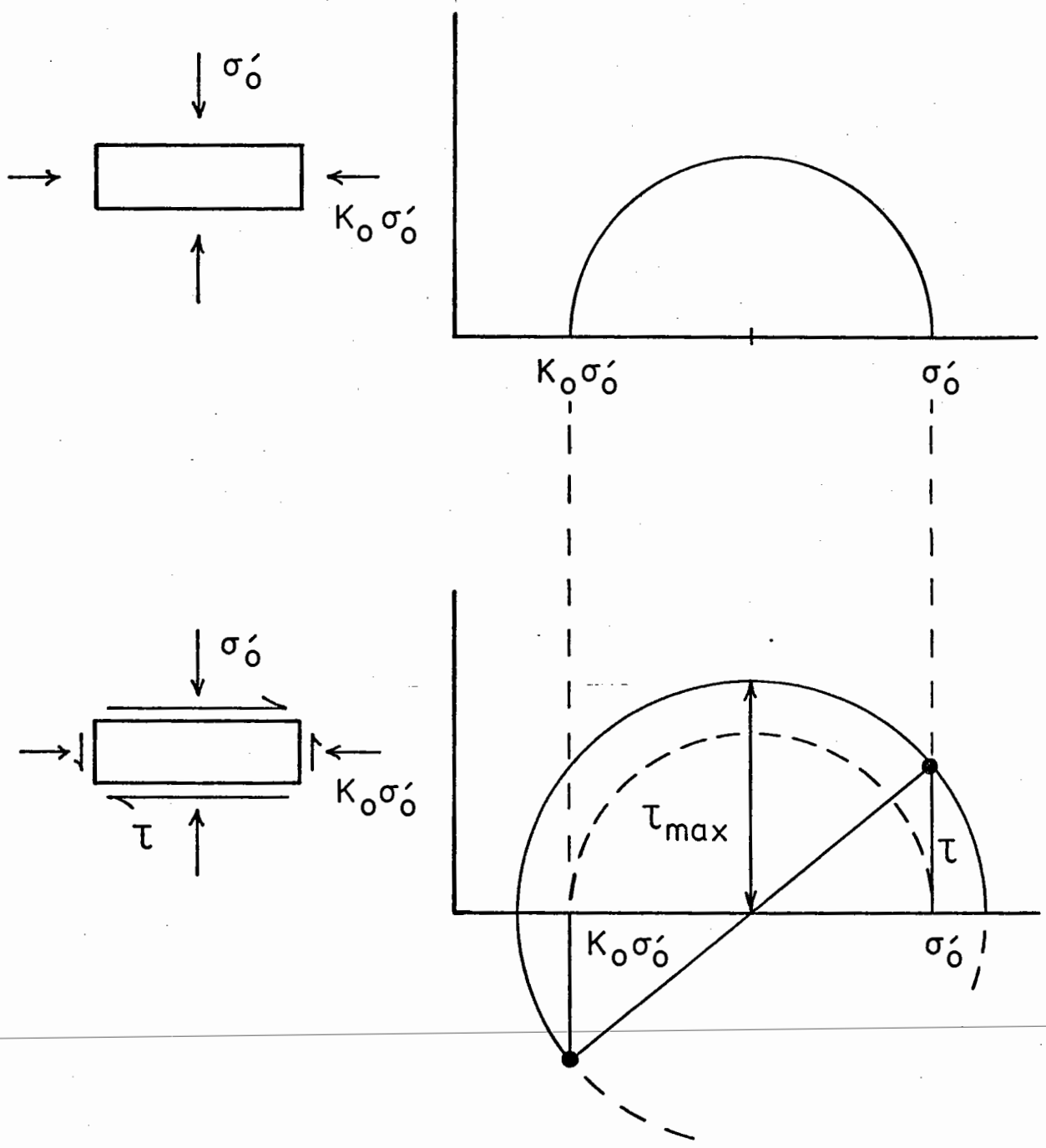

Fig. 14 Simple shear stress conditions
(after Seed and Peacock (71))

condition representative of field conditions were also noted. Seed and Peacock concluded that the net effect of the limitations of the test procedures involved in the simple shear test, along with the non--uniformities in the stress conditions, was for samples to fail under lower applied stresses than would be required in the field. This discrepancy could well be substantial, depending on the actual equipment and test procedures used. Ladd (43) has presented triaxial test data which indicate that the behaviour of saturated undrained reconstituted sand samples may be significantly affected by the method of sample preparation.

2.8 Shearing Resistance of Particulate Materials

In connection with the influence of various material parameters on the behaviour of particulate materials, Koerner (39) used the angle of shearing resistance, with the dilation component removed, as a measure of soil strength. He found that the soil strength increased with increasing angularity and decreasing sphericity of the particles. At a given relative density, the effect of grading on the soil strength was slight and with decreasing effective size, d_{10}, there was an increase in strength, particularly with particles less than 0.06 mm in diameter. In dealing with the components of the drained angle of shearing resistance, φ_d, Koerner used the equation:

$$\tau = \sigma \tan(\varphi_f + \varphi_\delta)$$

where τ = shear strength

σ = normal stress on the shear plane

φ_f = frictional component of φ_d

φ_δ = dilational (volume change) component of φ_d

Koerner indicated that particle shape affected the value of φ_f and not φ_δ. Also, as shearing progressed the value of φ_d tended towards a lower limiting value corresponding to φ_f, indicating that the dilation component of φ_d cannot be relied upon as a contributor to the soil strength over the entire failure path. For this reason, emphasis was placed on investigating the factors influencing the value of the frictional component of φ_d.

Further work by Koerner (40) on the behaviour of single mineral soils indicated that flaky mineral particles may have a tremendous effect on the overall behaviour of a soil even when they are in a minority. The behaviour of soils consisting solely of flaky particles showed a characteristically large volume decrease and terminal orientation of the particles was also noticeable. Koerner (40) also questioned the application of the angle of friction, φ_μ, to soil particles where this is obtained from direct shear type experiments on minerals in their bulk form. Tests of this type have been described by Rowe (68) and also by Horn and Deere (32). Koerner's doubts were based on a very poor correlation between experimental data and various theories relating this angle of friction to the angle of shearing resistance and he suggested (39) that φ_μ, rather than being a mineralogical constant, increased with decreasing particle size.

Lee and Seed (49) have also examined the shear strength of sand in considerable detail, again using components of the angle of shearing resistance. They concluded that the drained shearing resistance of sand was governed by three components and thus the shear strength could be expressed as:

Measured shear strength = strength due to sliding friction
± dilatancy effects
+ crushing and rearranging effects

It will be noted that the dilatancy contribution can be positive or negative depending on whether the volume increases or decreases during shear. This concept was illustrated by Lee and Seed in the form of an idealised Mohr diagram shown in Fig. 15. The influence of particle crushing only becomes significant at high confining pressures. Youd (86) employed a slightly different approach to these components of shearing resistance in defining various "energy barriers" which have to be overcome for a sand to shear and hence change its density.

Kirkpatrick (37) studied the influence of grain size and grading on the shearing behaviour of granular materials in standard triaxial tests. He concluded that the frictional component, φ_f, of the soil strength was independent of the particle size and grading. The observed influence of particle shape was very slight. However, φ_f was dependent on the surface roughness and mineralogy of the particles. As regards the overall shear strength, represented by φ' in Kirpatrick's work, this decreased with increasing particle size in the range studied; 0.3 mm to 2 mm. No clear conclusions could be drawn for the effect of grading on φ'. Kirpatrick also considered that variations in φ' were caused, in part, by the varying contribution provided by dilatancy. Various methods of calculating the contribution of dilation to the shearing resistance of granular materials have been presented in the literature. The pioneer work in this respect seems to be that of Taylor (81) who used an energy method to evaluate the effect of dilation. In their study of rockfill materials, Marachi, Chan and Seed (52) found that particle shape had a much greater effect on the

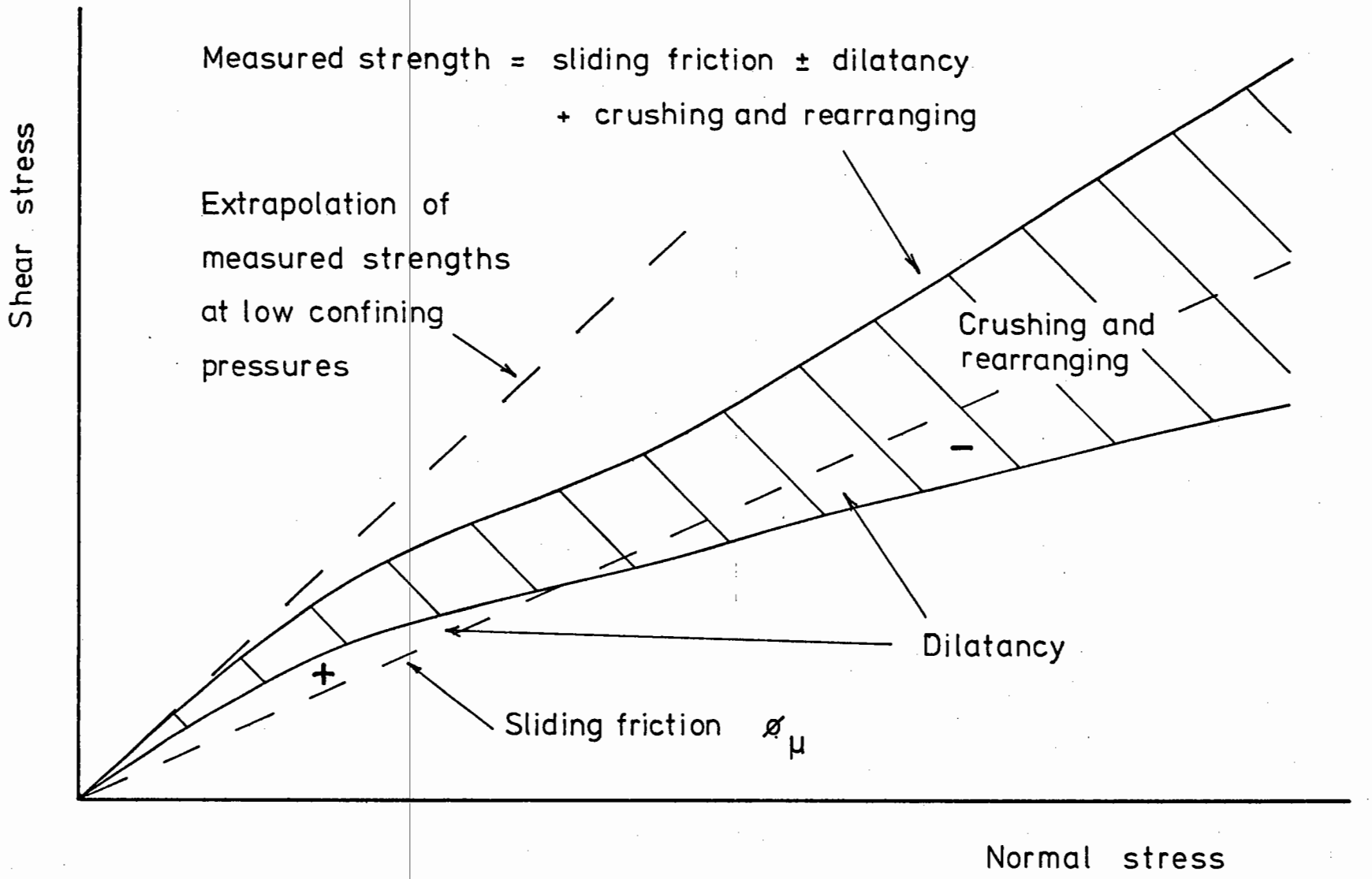

Fig.15 Idealised Mohr diagram (after Lee and Seed (49))

strength characteristics than did mineralogy. They were concerned with the possibility of modelling field rockfill gradings by producing grain size distribution curves parallel to the actual curve and then testing this grading in triaxial compression as representative of the field material. This technique seemed to provide a useful method for predicting the strength and deformation characteristics of field rockfill materials from the results of laboratory tests.

Leps (50) has reported tests on actual field rockfill materials using large triaxial machines to investigate the effect of confining pressure on the angle of shearing resistance. He also considered the influence of relative density, grading and particle shape with similar general conclusions to those of other authors.

Pike (59) has reported some large direct shear box tests to investigate the effect of material properties on the behaviour of road-base aggregates. He found that improving the compaction or using a better grading affected the strength of the material only inasmuch as it modified the dry density achieved by the compaction procedure. A similar effect was noted for the influence of moisture content on the direct shear strength. However, in the case of increasing particle angularity or surface roughness, which caused a decrease in the dry density, Pike observed an increased shear strength. It would appear that the change in the interlocking strength of the material was more significant than the effect on dry density in this case. Pike also noted a non-linear relationship between peak shear stress and normal stress over an extended range of normal stresses.

CHAPTER THREE

THE Mk1 SIMPLE SHEAR APPARATUS

3.1 Description of the Apparatus

Plate I shows a general view of the Mk1 Simple Shear Apparatus and Fig. 16 shows a diagrammatic section through the actual shear box. Plate II shows the upper and lower platens removed from the apparatus. The main frame, which carried two pairs of single-acting air rams mounted in opposition, was adopted from Sparrow's original apparatus (78) which was developed in the University. The "shear cell" arrangement in that apparatus was replaced by a shear box capable of imposing simple shear strain on a sample, Fig. 17.

The apparatus, mounted on an electric vibrating table for sample preparation purposes, confined a rectangular sample 87 mm x 51 mm x 10 mm deep between rigid boundaries. It was felt that a relatively shallow sample would localise end effects away from the central third where Roscoe's (64) linear elastic analysis indicated that stress conditions were reasonably uniform. To eliminate difficulties with sealing arrangements, the apparatus was designed for use with any granular materials. Thus, effective stresses could be evaluated without any need for pore pressure measurement which can be a source of considerable experimental difficulty in repeated load tests. Boundary contact stress transducers (load cells) were developed as part of this project in order to monitor the applied stresses on the central third of the sample. The successful use of contact stress transducers in the Cambridge Simple Shear Apparatus has been reported by Bransby (10). The load cells developed for use in the apparatus described herein were somewhat simpler than those used at Cambridge. Separate cells were used to measure the applied normal and shear stresses.

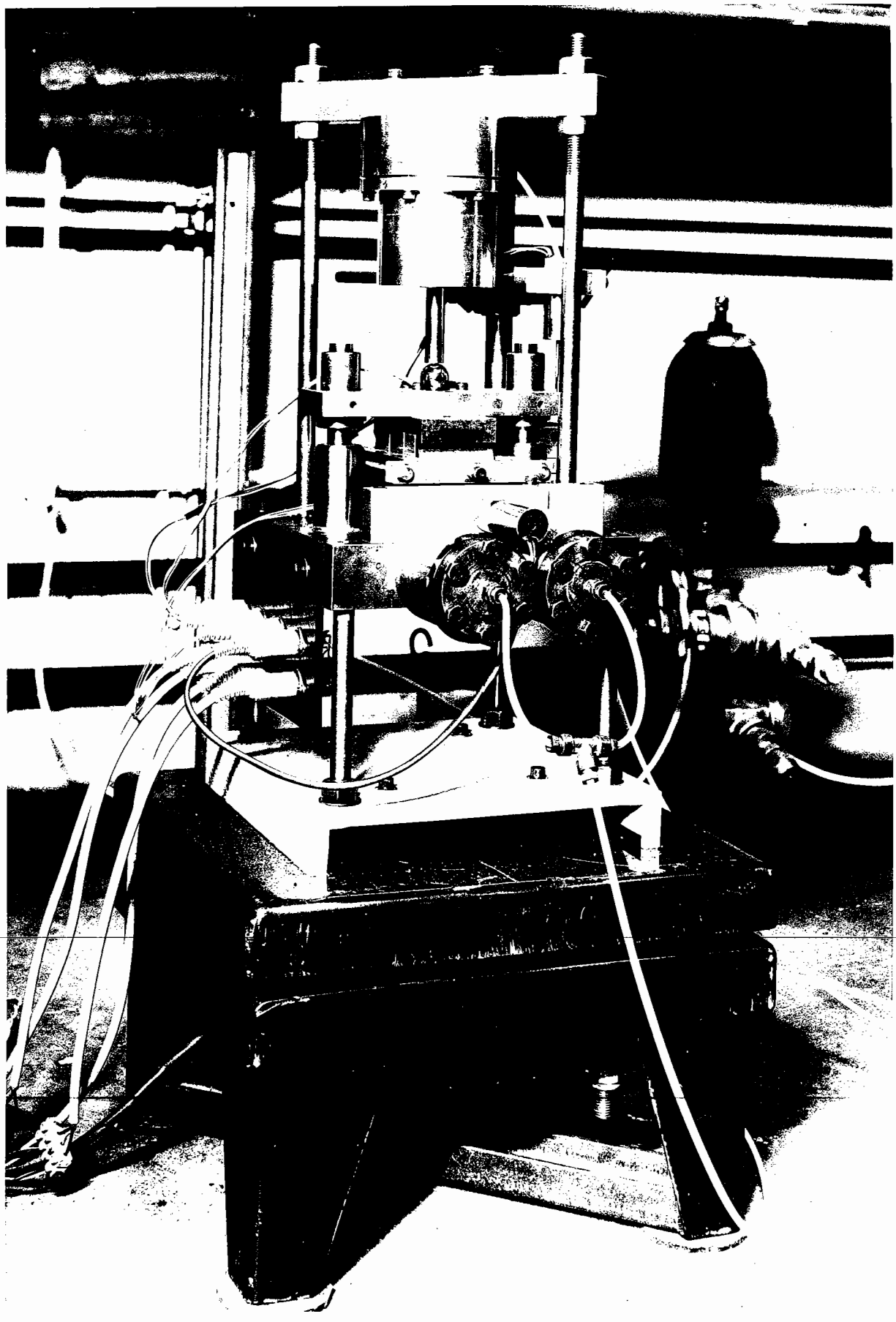

Plate I The Mkl Simple Shear Apparatus

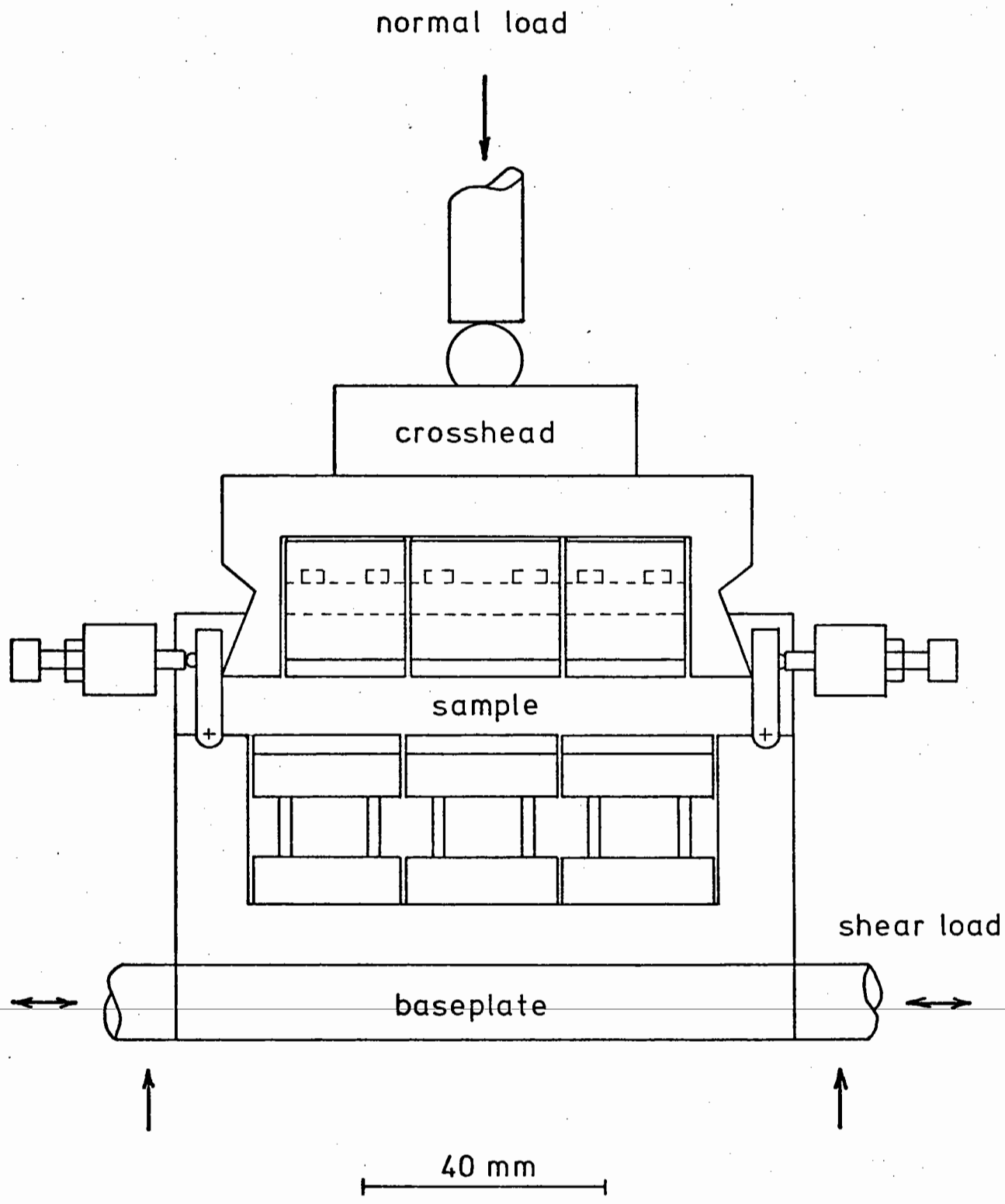

Fig.16 Schematic longitudinal section of the Mk1 Simple Shear Apparatus

Plate II The Mk1 Loading Platens

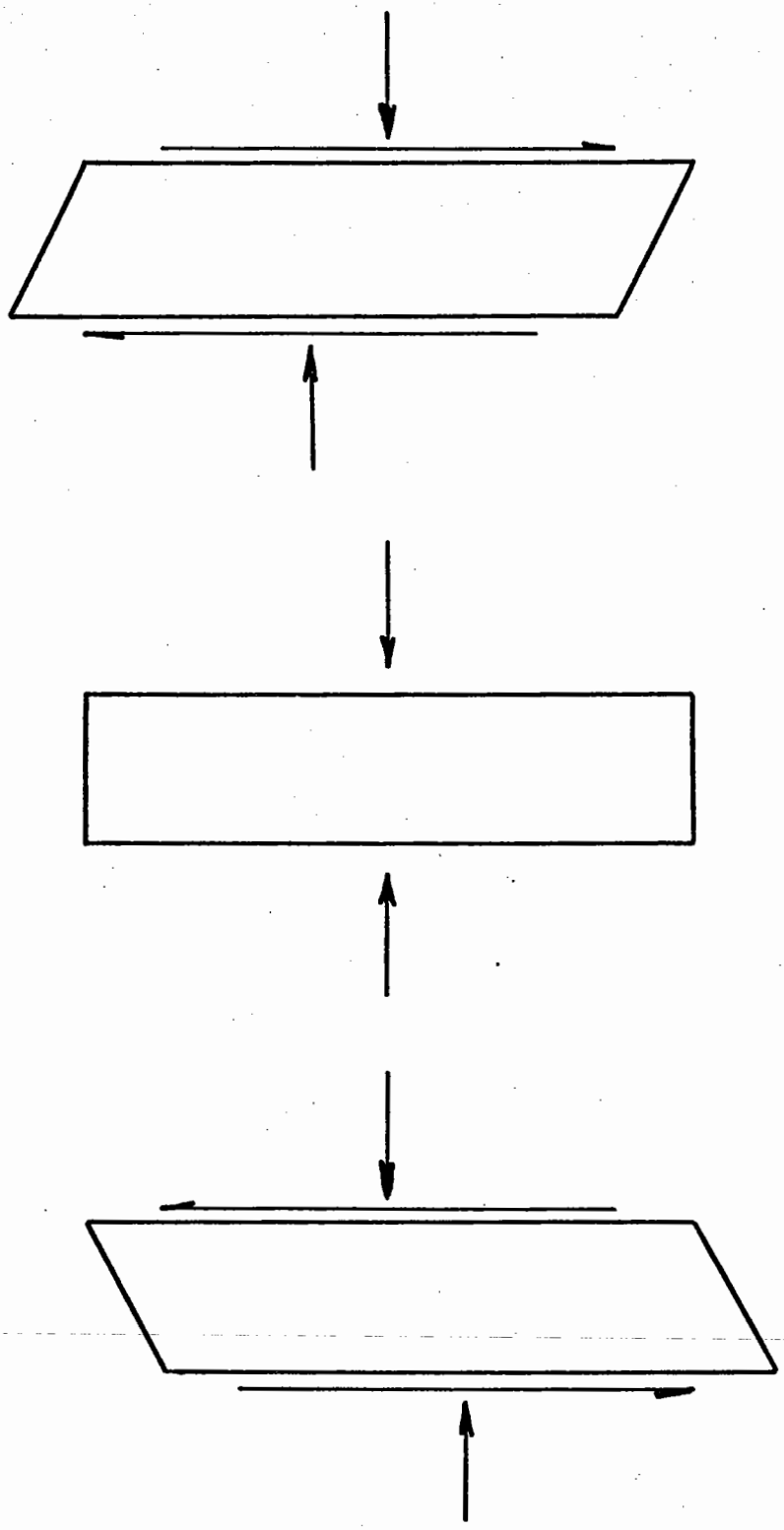

Fig.17 Sample deformation mode in the simple shear apparatus

The lower platen of the shear box, which contained the shear load cells, consisted of a steel channel machined from solid and steel side plates were screwed onto this. The side plates extended 20 mm above the base of the sample place, Plate II. The lower platen was screwed to a steel plate supported in the main frame by the four air rams running in linear bearings. This steel plate also carried adjustable limit stops to control the maximum possible shear deformations. The top platen, which contained the normal load cells, was also a channel section machined from solid steel and it fitted between the side plates. Vee-slots were cut in the outer end faces of the top platen to accommodate the hinged end plates during deformation. The top platen was supported by a crosshead carrying two linear bearings which engaged with hardened steel guide pins mounted on the main frame. The platen was thus free to move in the vertical direction while being almost rigidly restrained in the horizontal plane.

The end plates were designed so as to allow a shear distortion angle of 20°, corresponding to 36% shear strain, on either side of the central position and they were pivoted about their rounded lower edges in semi-cylindrical slots. The end plates were formed by cutting a notch into one long edge of a steel plate and soldering a length of silver steel rod into this, Fig. 18. Locating cones were machined into each end of the rod and these engaged with spring loaded stub axles mounted in the side plates so as to position the rounded edge of the end plate in the semi-cylindrical slot cut in the end of the channel forming the lower platen. The clearance between these concentric semi-cylinders was such as to allow the end plates to pivot about their lower edges while maintaining a close fit at the corner of the sample. This method of mounting the end plates was much simpler than that

the stiffer zones caused by the ends of the channel which housed the normal load cells in the Mk1 apparatus. The vee-slots which accommodate the end plates as the sample deforms have been machined directly into the side of each of the outer normal load cells, Fig. 24 and Plate VI. This arrangement allows the top platen to have a uniform stiffness over its whole length. Further details of the development and calibration of the Mk2 load cells are given in Appendix B. In the lower platen, the stiffer zones between the end plates and the shear load cells in the Mk1 apparatus have been removed by mounting the end plates immediately adjacent to the load cells. The end plates are pivoted in the same way as for the Mk1 apparatus and were again designed to accommodate a shear distortion angle of 20^{o}, corresponding to 36% shear strain, on either side of the central position.

The base of the shear box consisted of a channel machined from solid mild steel with raised side plates, extending 65 mm above the base of the sample space, screwed to it. The normal load cells fitted between the side plates as in the Mk1 apparatus. A working clearance of 0.1 mm was allowed between adjacent parts of the apparatus though this was subsequently increased slightly where necessary. The three normal load cells were each carried by a separate crosshead though provision was made for the crossheads to be locked together during sample preparation. Each crosshead carried two linear bearings which engaged with hardened steel pins mounted in the sides of the main frame, Fig. 25, which consisted of another steel channel on the base of which the lower half of the shear box travelled. The two line bearings which accommodated the travel of the shear box were similar in concept to those used in commercially available direct shear boxes. The lower half of each bearing consisted of two hardened steel rods mounted side

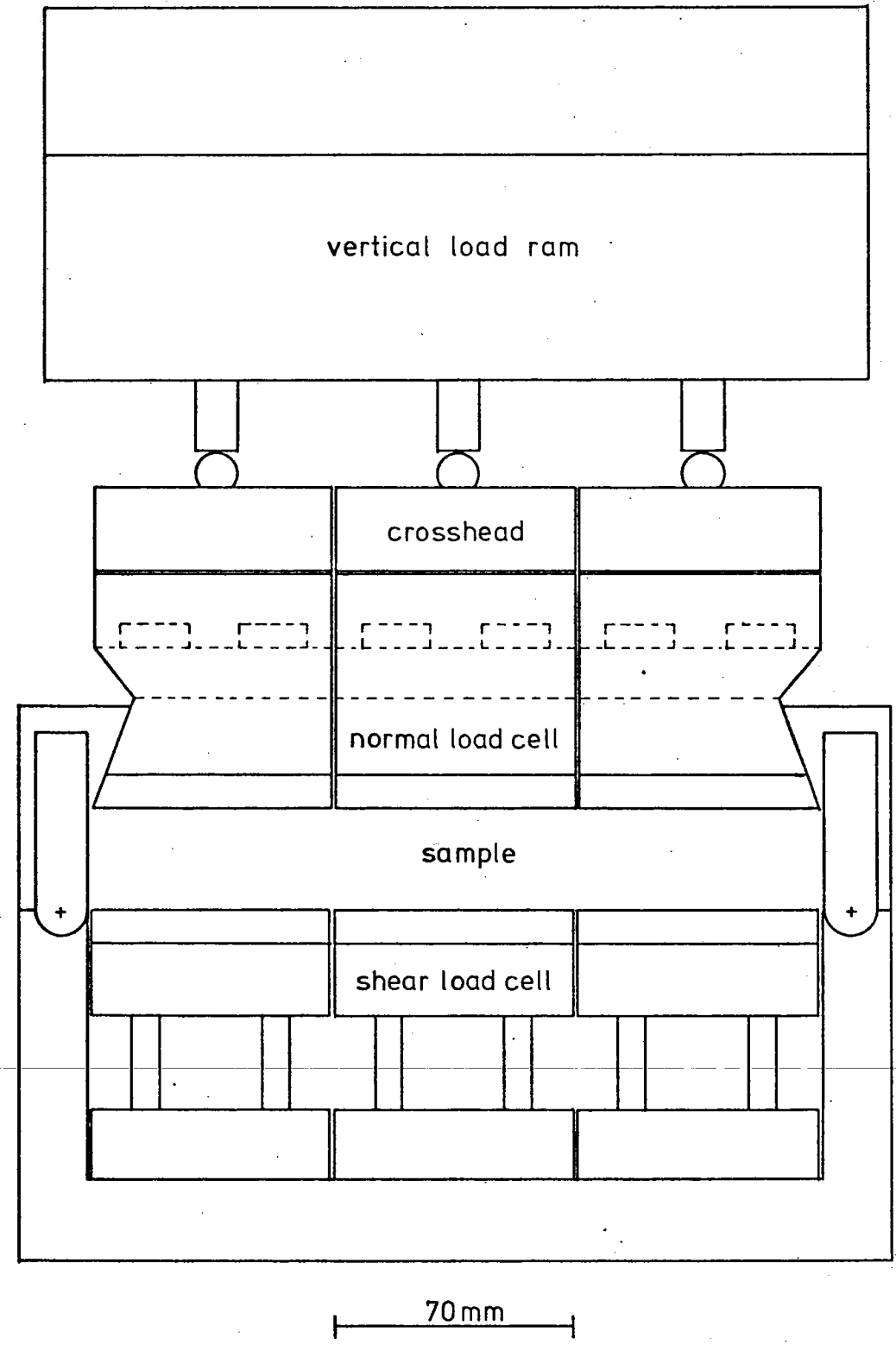

Fig. 24 Schematic longitudinal section of the Mk2 Simple Shear Apparatus

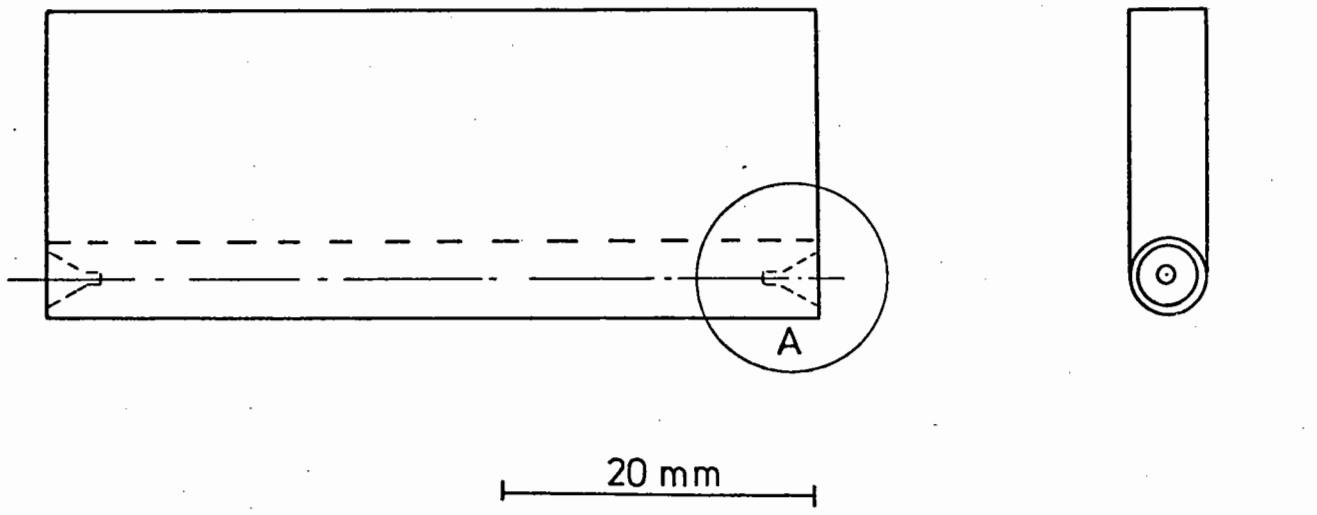

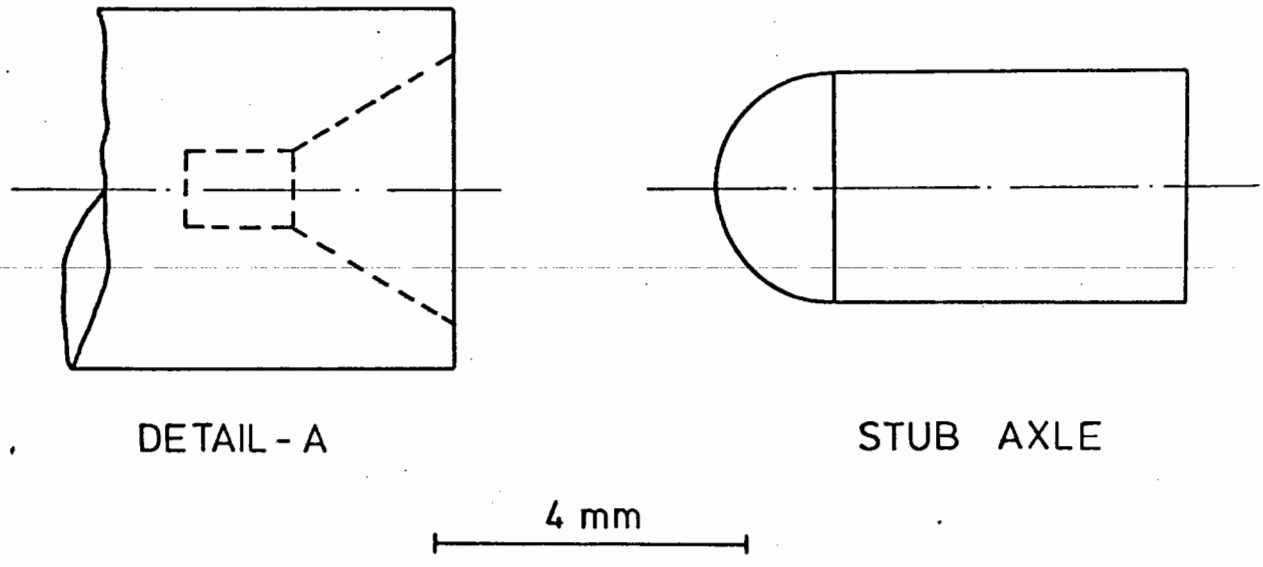

Fig.18 Detail of end flap and stub axle for simple shear box

devised by Roscoe (64) for the Cambridge Simple Shear Apparatus. His method involved external hinges to bring the effective axis of rotation of the end plates into exact coincidence with the corner of the sample. With the system adopted here, this coincidence was not exact. However, since end effects were likely to be quite localised and the applied stresses were being measured over the central third, it was felt that this lack of coincidence was unlikely to be very important. The inner faces of the end plates were held in close proximity to the edges of the top platen by a clamping frame which can be seen in Plate I. The frame consisted of two lengths of aluminium square section bar connected by a pair of brass rods. A setscrew and locknut were fitted at the midpoint of each bar and a cone was machined into the inner end of the setscrew so as to locate on a steel ball recessed into the outer face of the end plate. This frame constrained the end plates to move in conjunction with each other without the need to force them against the edges of the top platen. A working clearance of 0.5 mm was allowed between adjacent parts of the apparatus where necessary. These clearance gaps would have been filled with silicone rubber if particle trapping had become a serious problem.

The vertical load on the sample was provided by an air ram acting through a steel ball onto the crosshead, Plate I, and it was supported by a portal mounted on the main frame. The ram was designed to incorporate a linear bearing and a Bellofram rolling diaphragm so as to minimise frictional resistance to the piston.

The average shear strain in the sample was monitored by a linear variable differential transformer (LVDT) having a linear range of $\pm$0.500 in. and it was supported by a clamp mounted on the main frame, Plate I. The core of the LVDT was lightly spring loaded against the

end of the lower platen. The vertical movement of the top platen was monitored by a ±0.200 in. linear range LVDT supported by a magnetic base attached to the main frame, Plate IV. The LVDT's were both DC in, DC out and operated on a 24.0 V supply.

3.2 Boundary Conditions

Loading plates were attached to the active faces of the load cells in the platens and these formed the interface between the platens and the sample. The preparation of the faces of these loading plates has been the subject of some attention in the literature and various mechanisms to transfer the shear loads from the loading platens to the sample have been reported. The effect of using loading plate surfaces which are insufficiently rough to transmit the shear faces to the sample effectively has been demonstrated by Finn, Pickering and Bransby (28) using striped plasticene samples. The results showed that for samples where no relative motion occurred between the loading plates and the sample there was a comparatively uniform deformation. If relative motion did occur, then only the central region was resisting the shear load and parts of the sample near the surfaces were undeformed. The apparent strength of a soil tested in this way would be substantially less than its real strength. A theoretical investigation of this slippage problem by Prevost and Hoeg (61) was referred to in Chapter Two and their results showed quite dramatic changes in the stress distribution when differential slip occurred.

Investigating the relative performance of three types of loading plates, Finn et al (28) found that plain sand-blasted hardened steel plates gave lower liquefaction resistances than either plates with grains of sand glued to them or ribbed hardened steel plates. These

latter two types gave similar resistances. Finn et al have also shown that it is not sufficient for the top and bottom loading platens simply to have appropriate roughness characteristics; the platens must be properly seated on the sample to ensure that the surface roughness can be mobilised effectively. In their tests, this effective contact was achieved by applying an extra seating load after consolidation to the desired effective stress level. The seating load was removed prior to testing. The sample preparation technique employed at Cambridge (80) obviated any need for a seating load. It was found that pouring the sand onto the sand coated lower platen formed a suitable interface. The upper interface was formed afresh for each test by lowering the Araldite coated top platen onto the sample and then allowing the resin to cure before testing.

Since vibratory compaction, with the top platen in place, was to be used for the work reported herein, it was felt that a reasonable interface would be produced by the sample preparation procedure. A ribbed plate design was initially adopted for the loading platens. Square section ribs were machined onto the faces of the loading plates. The ribs were 1 mm square in cross section and spaced at 3 mm centres leaving a slot 2 mm wide between each pair of ribs. The nominally 1 mm size particles, which were to be used in the Mk1 apparatus, could therefore be accommodated in the slots and provide an effective interface between the loading platen and the sample. However, during the early development of the apparatus, these loading plates were replaced by a design similar to that used at Cambridge with the MkVII Simple Shear Apparatus (80) which it was felt would provide an even better interface. The new loading plates were rectangular and the same size as the ribbed plates. The outer surface was machined into the form

of a shallow tray with a lip 0.75 mm deep and 0.75 mm wide all round the edge. These plates were screwed to the load cells and then the trays were cleaned with Inhibisol to remove any grease. A mould release agent, Araldite QZ 19, was then painted on the face of the loading plate and allowed to dry. The release agent formed a thin film over the base of the tray. A small quantity of Araldite was then prepared; 1 part by weight of AY 105 mixed with 1 part by weight of HY 953F. A layer of Araldite was then spread as evenly as possible over the base of each of the trays. The mixture was quite viscous at room temperature and so it was rather difficult to obtain an even layer. This was overcome to a large extent by placing the platens in an oven at a temperature of approximately 70^{o}C for about 10 minutes. The Araldite then flowed under gravity to form a more even layer. Following this, an excess of the granular material was poured over the prepared faces of the platens. The material not adhering to the loading plates was then tipped off and the platens replaced in the oven to cure the adhesive. The completed loading plates are shown in Plate II. It was quite simple to remove the hardened material by prising it up from the edge when the loading plate had to be removed or the interface replaced.

3.3 Contact Stress Transducers (Load Cells)

Only the general considerations regarding the design of the load cells are given in this section; more detailed considerations are presented in Appendix B along with details of the calibration techniques used.

For an instrument to measure a physical quantity accurately, it is vital that it should be designed so as to affect the measured quantity as little as possible though it is obviously impossible to

reduce this effect to zero. Here, this requirement demands that the deflections of the active faces of the contact stress transducers should not be so large as to significantly affect the stress distribution on the sample. To help with this, three load cells were placed in line on the loading platens, Fig. 16, so that each platen had a uniform stiffness over most of its length. Only the central transducers were strain gauged, however; the outer transducers were dummies machined from the same material to a similar design. In connection with this uniformity of loading platen stiffness, it has been noted (11) that solid dummy load cells were incorporated into the platen arrangement used for the MkVII Cambridge Simple Shear Apparatus. The dummy cells at the corners of the loading platens were solid blocks of aluminium so the ratio of the vertical stiffness of the dummy cells to that of the active cell was about 100:1. Apparently, the effect of this non--uniformity has not been investigated. The load cells were machined from solid aluminium and Plate III shows the two active cells. The active faces of these cells were 50 mm x 20 mm and the loading plates were screwed to these faces. The dummy shear load cells were identical to the active cell. However, to accommodate the dummy normal load cells in the top platen, it was necessary to make these slightly narrower than the active cell. The design of these cells was adjusted accordingly so as to maintain a uniform platen stiffness in the vertical direction.

3.4 Data Monitoring Equipment

The electrical connections to the load cells and the LVDT's were made via a patchboard attached to the side of the main frame, Plate I. A 4.0 V DC input for the strain gauge Wheatstone Bridge circuits in the

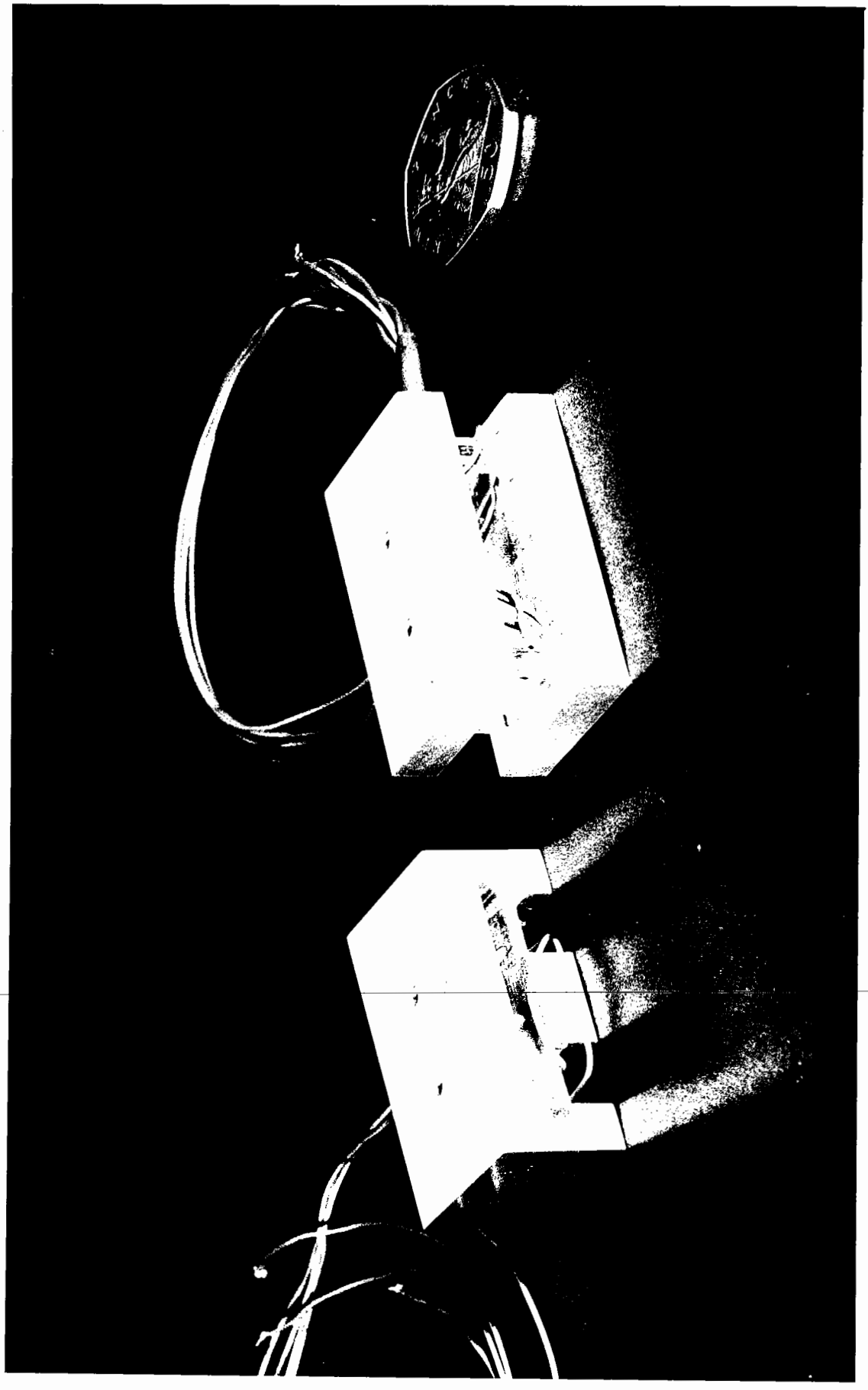

Plate III The Mkl Load Cells

load cells was provided by a Farnell Type L30 stabilised voltage supply unit. This unit had a lower noise level on the output voltage than any other units which were readily available. Such noise can cause problems with data recording equipment if it becomes excessive. Inspection of the noise level on these particular Farnell units using a sensitive cathode ray oscilloscope indicated a 50 Hz noise waveform having a double amplitude of 0.4 mV. This represents only 0.01% of the 4.0 V output voltage. The 24.0 V DC supply for the LVDT's was provided by a similar unit.

The four basic outputs from the apparatus were: shear load, horizontal deformation, normal load and vertical deflection. These were recorded using two Bryans Southern, Series 28000, two-pen flatbed chart recorders. The out of balance bridge voltages corresponding to shear and normal load were also displayed on two Solartron A220 digital voltmeters. A Philips PM2421 digital multimeter was used to monitor the vertical LVDT output during sample preparation and the bridge input voltage during a test.

3.5 The Material

3.5.1 Choice of material

The material chosen for use in the Mk1 Simple Shear Apparatus was a crushed limestone of nominally 1 mm particle size. It consisted, in fact, of particles passing BS Sieve No. 14 and retained on BS Sieve No. 25. This gave a metric size range of 1.2 mm down to 0.6 mm respectively. A nominally single size material was chosen to model a railway ballast. The limestone was obtained from the Amalgamated Roadstone Corporation at Chipping Sodbury and a well graded material from this limestone has been used for repeated load triaxial testing at the University of

Nottingham (9). A similar size fraction of a crushed granite was compared with the limestone under a low power microscope. The limestone, being much less flaky, was chosen as being more appropriate for the simulation of a railway ballast.

3.5.2 Compaction trials

Various tests were carried out to establish the compaction characteristics of the limestone. In order to evaluate parameters such as void ratio and porosity from the density values obtained in these compaction trials it was necessary to know the specific gravity of the material. This was determined according to BS 1377:1967 (12) as 2.72.

A preliminary investigation of the vibration compaction characteristics of the material was carried out using a shallow steel box clamped to the vibrating table. A similar vibrating table to that used for this project has been described by Boyce (9) as being capable of producing accelerations of up to 4 g at 50 Hz on loads up to 30 kg. Research by Kolbuszewski and Alyanak (42) has shown that granular materials tend towards their maximum density at accelerations of about 2 g. From the results obtained using the noaminally 1 mm single size particles it appeared that the compacted density of the material was constant within the range of accelerations produced by the vibrating table. This is not too surprising considering the fairly uniform nature of the material. A brief investigation also indicated that the compacted density was not significantly affected by small surcharge weights. The value obtained for the compacted density was 1.56 Mg/m^3 which corresponds to a void ratio of 0.74 or a porosity of 0.43.

To determine a minimum density for the material, tests similar in principle to those described by Kolbuszewski (41) were carried out.

One test involved slowly pouring the material into the box used for the vibration compaction tests from "zero height" and then carefully scraping the surface level with the top edge of the box using a straight edge. The other test involved placing a known weight of the material into a 500 ml measuring cylinder and then filling the cylinder with water and putting a stopper in the end. The cylinder was inverted several times and then set upright on the bench and the volume of the material noted. These tests were repeated several times to obtain an average value. The results from the two types of test were, in fact, the same; giving a minimum density of 1.27 Mg/m^3 corresponding to a void ratio of 1.14 or a porosity of 0.53.

An attempt was made to determine a maximum density using a California Bearing Ratio mould and an electric vibrating hammer. However, difficulty was experienced in satisfactorily compacting the top layer of the sample and some degradation of the material occurred. The results obtained indicated a maximum density of 1.66 Mg/m^3 and a void ratio of 0.64 or a porosity of 0.39. Using this somewhat suspect value for the minimum void ratio, a relative density of 0.78 is obtained for the material as compacted on the vibrating table. However, it would seem probable that the correct value for the relative density is somewhat higher.

On the subject of vibrating compaction, Green and Reades (29) have reported that, for dense and medium dense conditions, more uniform samples were produced by tamping than by vibration techniques. However, Kolbuszewski and Alyanak (42), D'Appolonia (19) and Boyce (9) have confirmed the effectiveness of vibratory compaction techniques and the method was certainly suited to this project. It would also appear to be inherently more repeatable than tamping techniques.

3.5.3 Standard strength tests on the material

Standard direct shear and triaxial compression tests were carried out on the material to determine a value for the angle of shearing resistance using each of these methods. A φ value of 55° was obtained from the standard direct shear test and a value of 52° from the triaxial compression test. Details of the experimental techniques used and the results obtained are presented in Appendix C.

3.6 Sample Preparation

From the experience gained during the compaction trials, the following sample preparation technique was devised. Firstly, the shear box was set in the central position using the top platen and the end plates, clamped in the vertical position, as guides. The end plate clamping screws can be seen in the side of the shear box in Plate II. Using the value for compacted density previously obtained, sufficient material was weighed out to produce a sample 10 mm deep. The top platen was removed and the material spread evenly over the lower platen using a spatula ensuring that it filled the corners of the box. The clamping frame was then placed over the box, the top platen replaced and the frame fitted to the end plates. The clamping screws were then released and the magnetic base carrying the vertical LVDT was positioned on the main frame. To compact the sample, the amplitude (and thus the acceleration) of the vibration was successively increased and decreased using the vibrating table control box. After about four cycles of this process, it was found that the vertical LVDT output was constant at the end of each cycle when the vibration was reduced to zero. Checks carried out using this method indicated that a compacted density of about 1.50 Mg/m^3 was obtained quite consistently. Following

compaction, the vertical loading ram was fitted and the sample was then ready for testing.

3.7 Preliminary Tests

The preliminary tests using the Mk1 Simple Shear Apparatus were in the form of stress controlled single load tests; the intention being to obtain an angle of shearing resistance for the material to compare with those obtained from the strain controlled direct shear and triaxial tests. The single load tests in the simple shear apparatus were performed by incrementally increasing the applied shear load until failure, in the form of very large shear deformations, occurred. It will be seen, in what follows, that considerable difficulties were encountered with these tests and, even though an explanation for these difficulties was obtained, it was necessary to design a Mk2 apparatus to incorporate the modifications considered necessary to overcome the problems.

The first tests were conducted before the simple shear apparatus and the associated sample preparation techniques had been finalised in the form already described. However, these tests did provide an insight into the modifications necessary. The results of these single load tests are shown in Fig. 19 where it should be noted that only two different normal loads were used yet a wide spread of normal stresses was indicated by the normal stress transducer. This wide variation for nominally identical tests suggested that the sample densities were inconsistent and probably non-uniform and hence that the sample preparation procedure was unsatisfactory. The results displayed a rather inconsistent scatter well below the failure lines defined by the standard tests which are also shown for comparison in Fig. 19. For these load controlled simple shear tests, failure was defined as the point where large

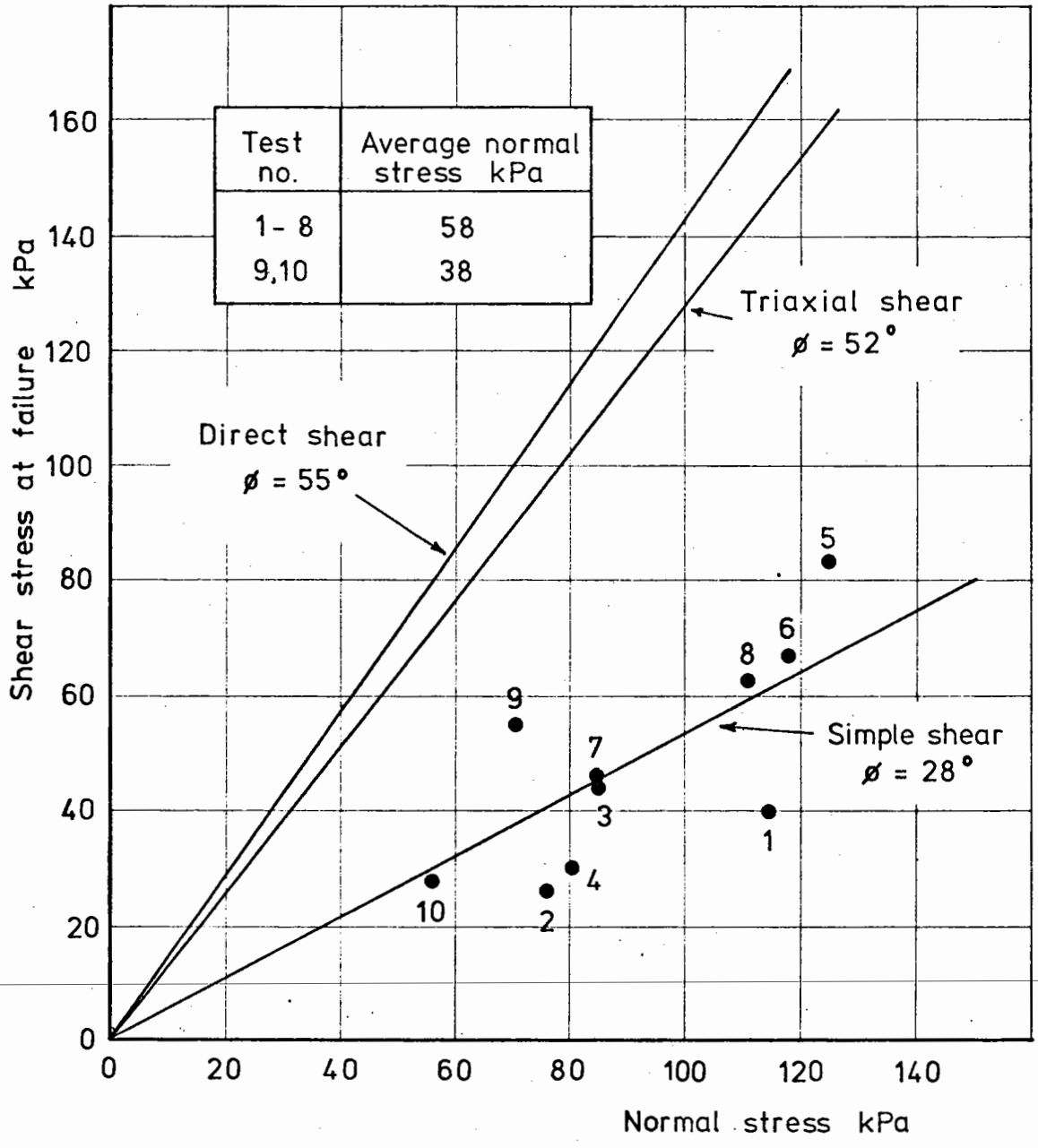

Fig. 19 Results from single load shear tests

deformations occured for a small increase in shear load. However, some difficulty was experienced in identifying this point and this will be discussed later. Another feature of these tests was that the normal stress, as recorded by the load cell, increased as the test proceeded. This seemed to indicate that dilation of the sample was being impeded by friction in the mechanics of the apparatus.

Much tighter control of the compaction procedure and some mechanical modifications brought the apparatus to the stage described earlier. The results obtained from single load tests using this apparatus are shown in Fig. 20 where points are plotted corresponding to average failure stresses on a total force/loaded area basis in addition to those corresponding to the transducer outputs from the central third of the sample. Evidence of the improvement in the consistency of the compaction procedure was provided by the points corresponding to tests at equal vertical loads being much closer together than before. It can also be seen that, on an average stress basis, the failure line for the material was similar to those defined by the standard tests. However, the failure line defined by the transducer outputs was still well below these lines. Some over-registration by the normal stress transducer and a large under-registration by the shear stress transducer was present. The indicated shear stress was, in fact, only about 50% of the calculated average value. Checks on the calibrations of the transducers showed the original calibrations to be satisfactory. Quite reasonable lines were defined by the experimental data and it was considered that this indicated the apparatus to be having a real, consistent effect on the material. The problem was one of interpretation of the data.

Up to this point, no account had been taken of any possible

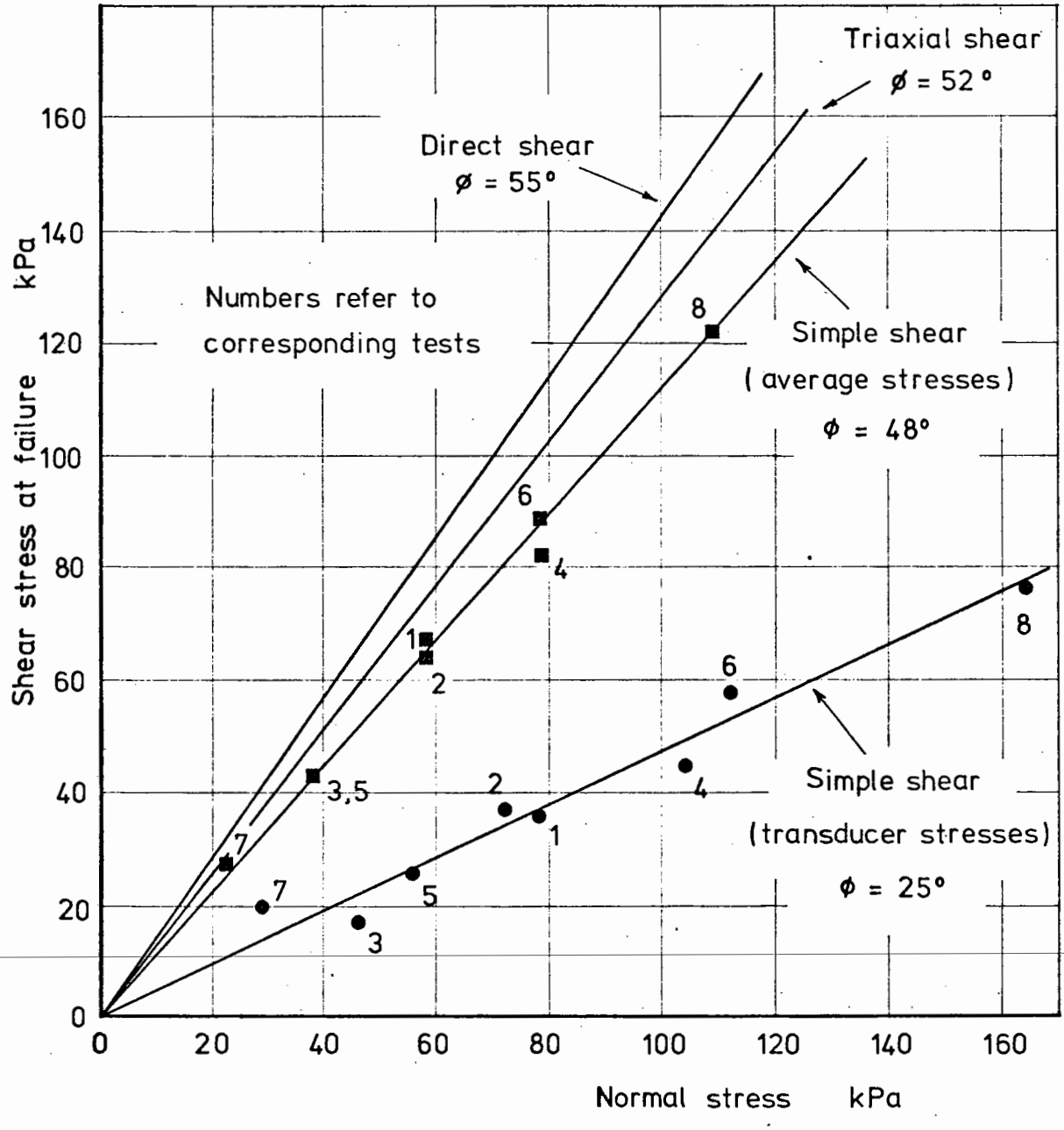

Fig. 20 Results from single load shear tests

frictional losses in the horizontal linear bearings carrying the shear rams; the use of contact stress transducers within the shear box itself made this unnecessary. Several checks were carried out to investigate any effect which might have been present. These showed that the frictional losses involved were quite small but there was a tendency for a stick-slip effect to develop at high normal loads. This might have been due to grit in the bearings themselves or possibly due to wear; this part of the system had been used previously in Sparrow's apparatus (78). To overcome this problem of reacting the normal load against the linear bearings, the vertical loading frame was modified so as to simply squeeze the top and bottom platens together; reacting the vertical loading ram directly against the base of the shear box. The modified loading frame can be seen in Plate IV. It was suspended by a steel wire using a counterweight arrangement and located on the top platen by a steel ball which engaged with a cone in a steel sleeve fitted over the ends of the loading rod. Another steel ball was positioned at the midpoint of the lower crossmember of the frame and this engaged with a cone in the base of a roller plate shown in Plate V. When in position, the steel rollers acted on the underside of the steel plate carried by the shear rams. This arrangement provided a reaction for the vertical loading ram which could also accommodate the lateral movement of the lower platen during a test.

3.8 Behaviour of the Modified Apparatus

Several tests were carried out with the apparatus in this modified form and the observed behaviour was quite consistent. Three test results are shown in Figs 21, 22 and 23 where the outputs from each of the four transducers during a test are plotted against the average shear

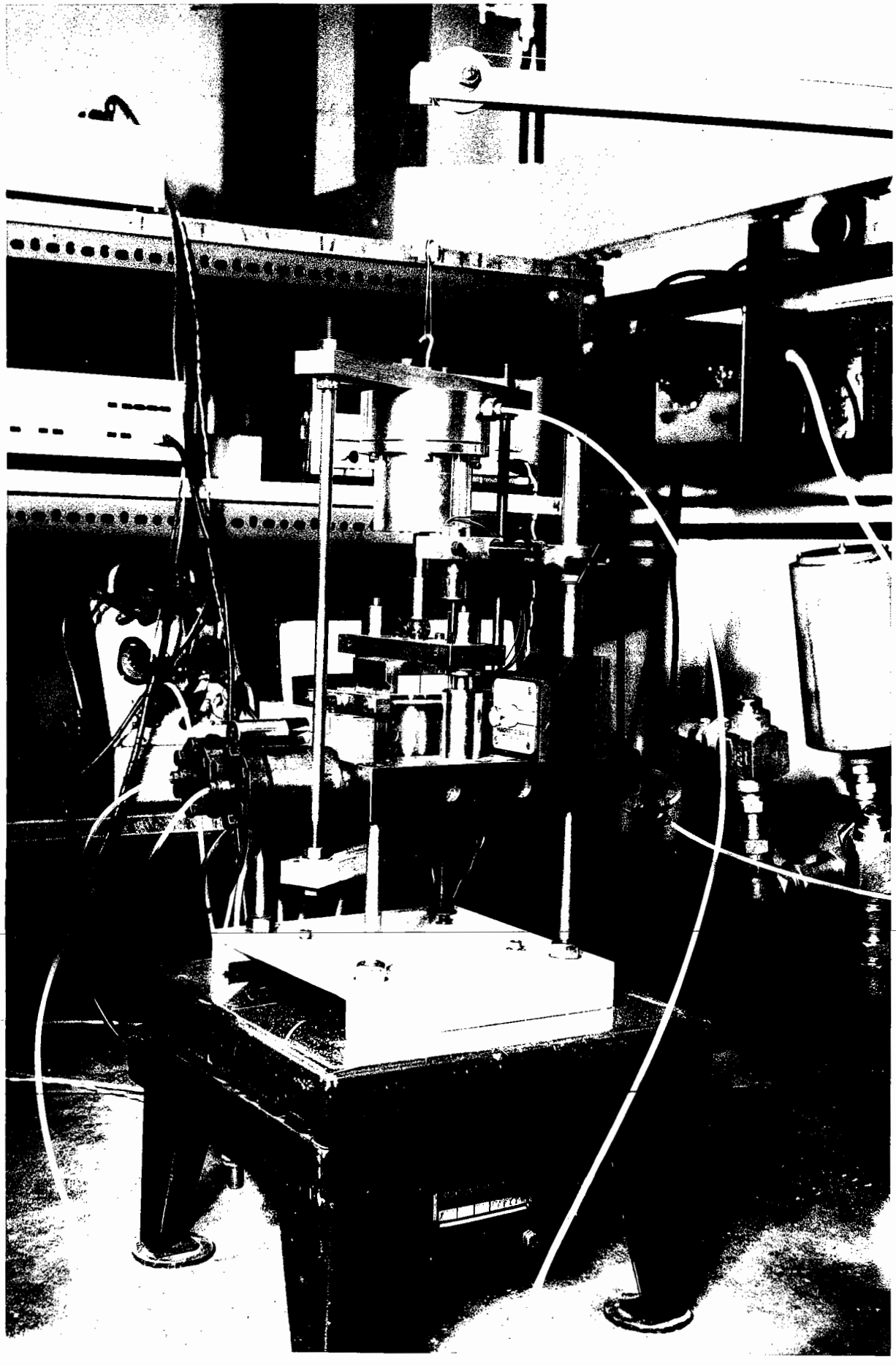

Plate IV Modified Vertical Loading Frame

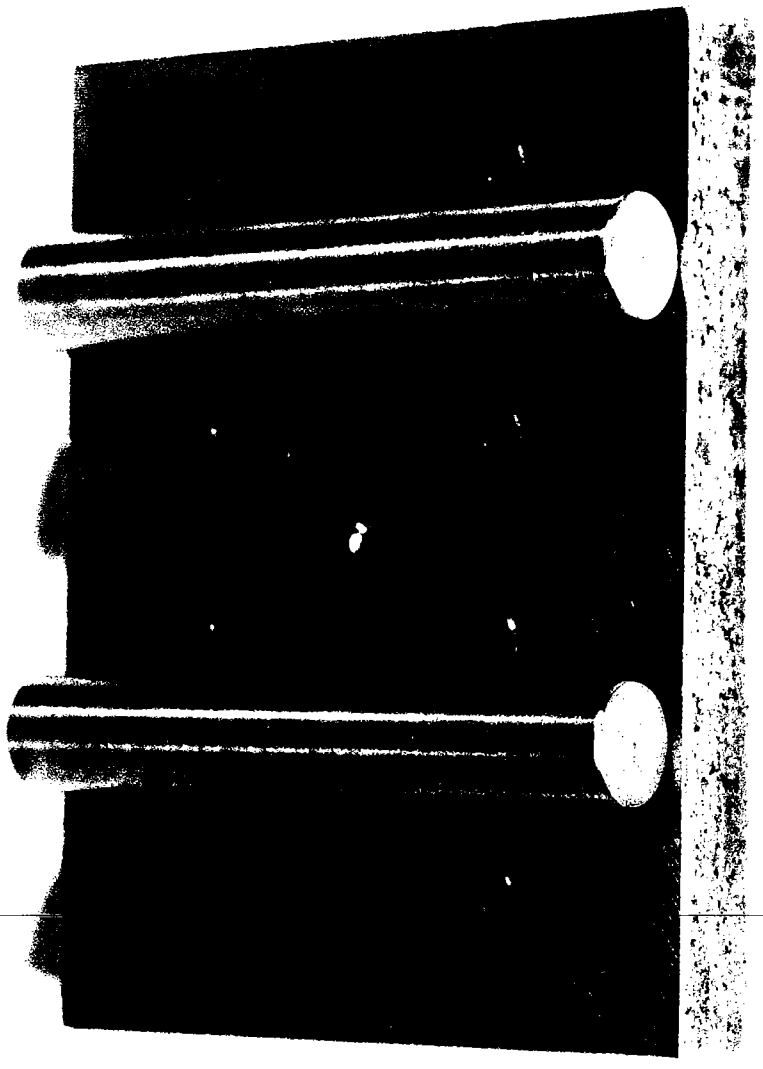

Plate V Roller Plate

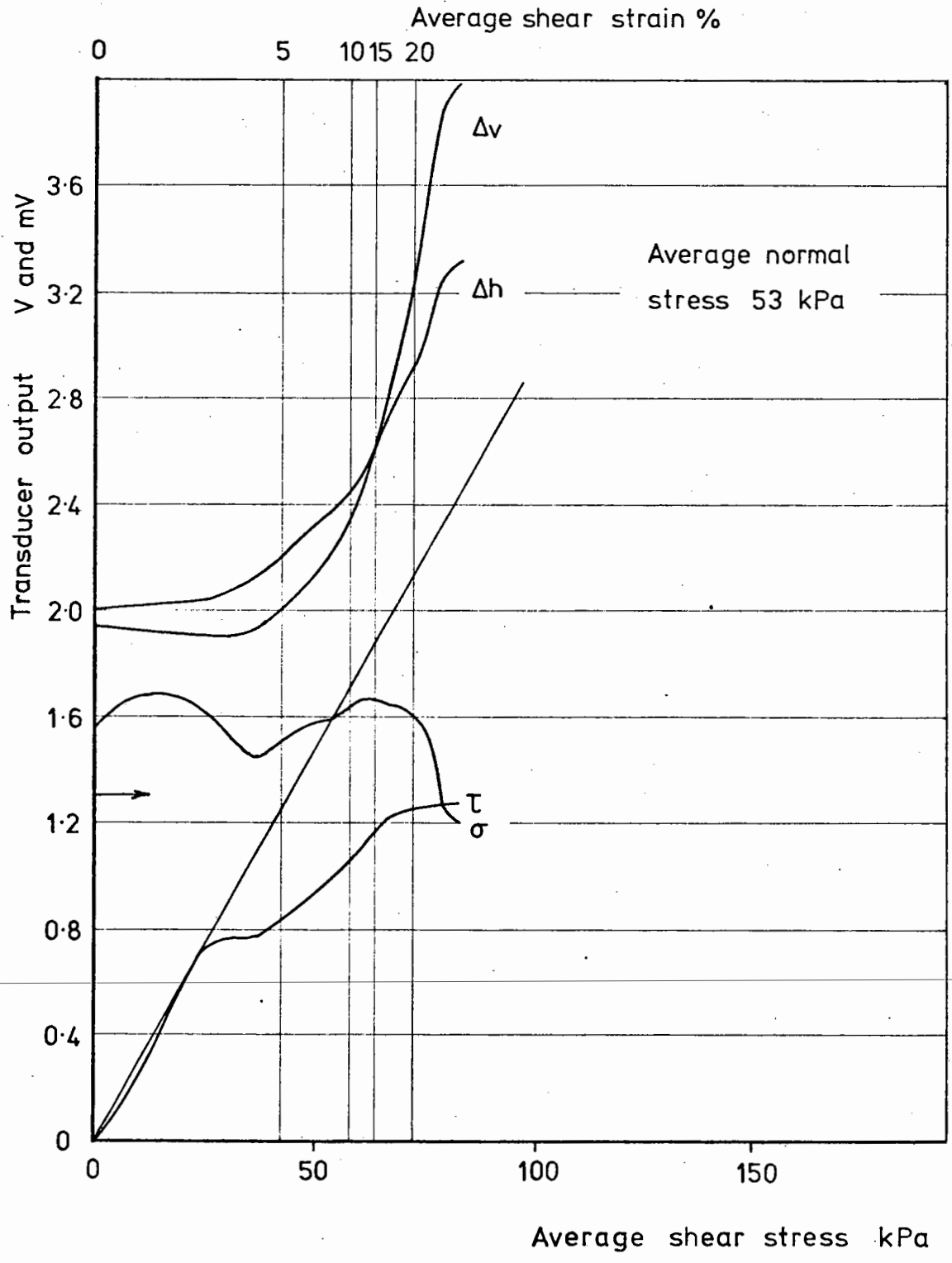

Fig. 21 Single load shear test - output data

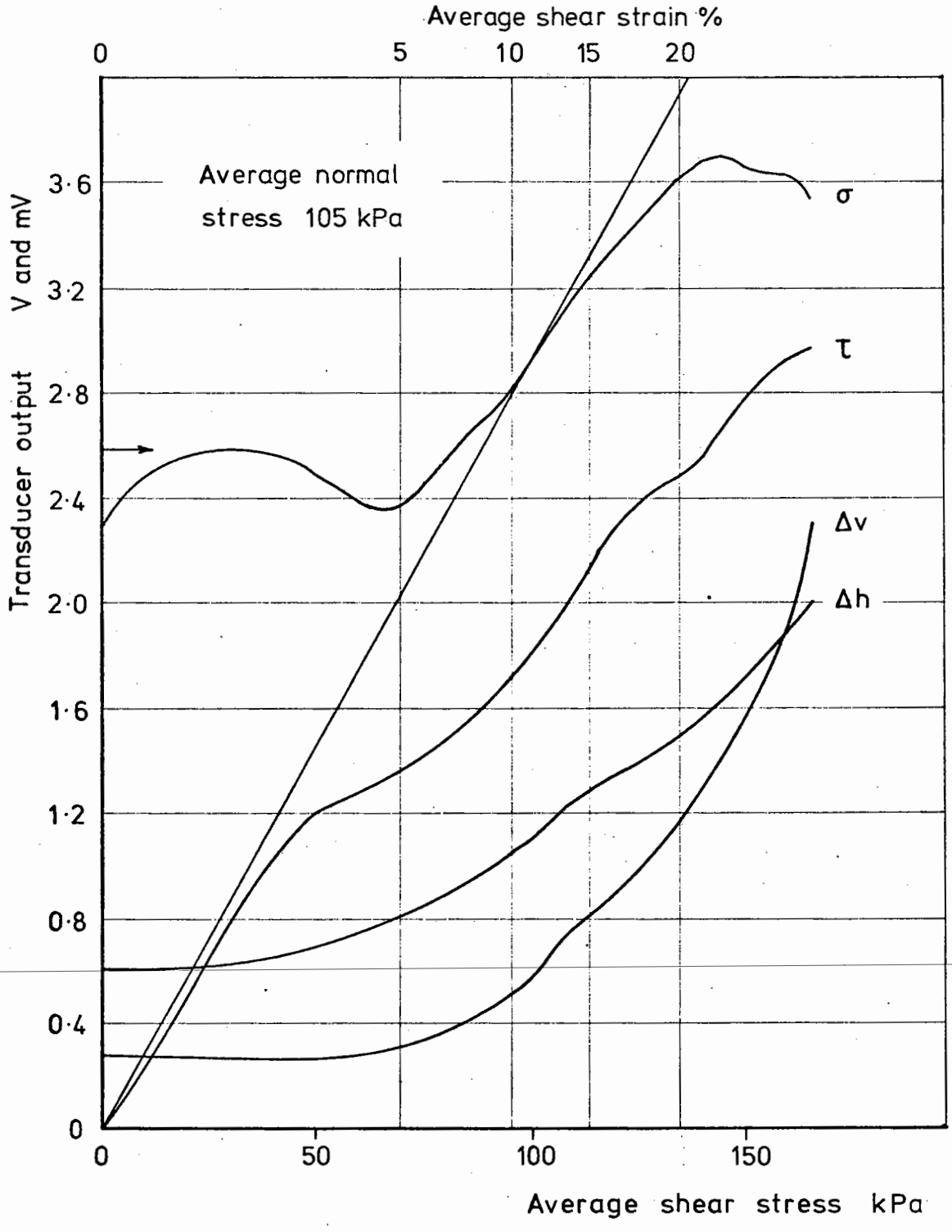

Fig. 22 Single load shear test - output data

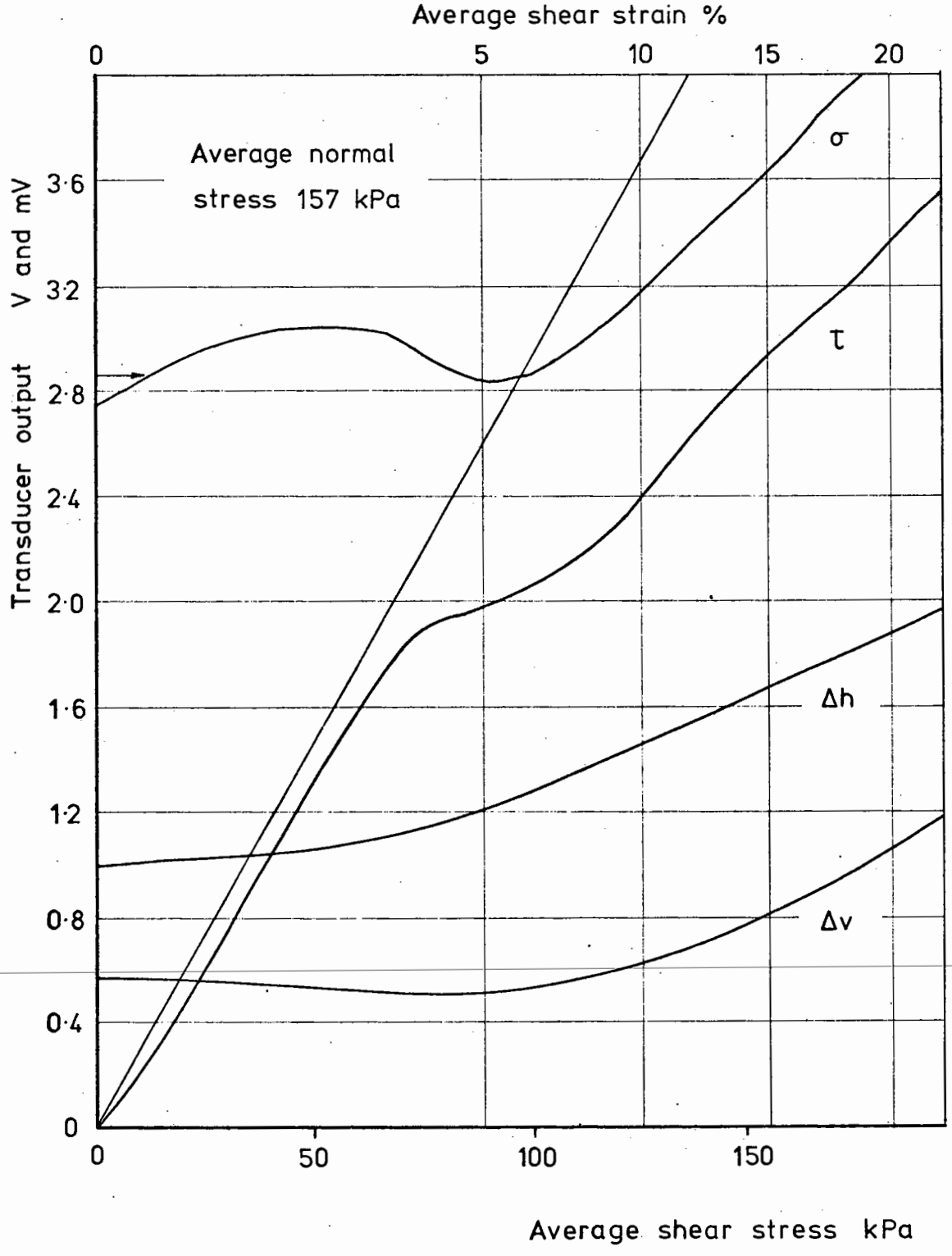

Fig.23 Single load shear test - output data

stress which is representative of the total shear load applied to the apparatus. To avoid excessive overlapping, the origin for each line is purely arbitrary. Calibration lines for the two contact stress transducers are indicated by the solid straight line for the shear stress, τ, and by the arrow for the normal stress, σ. Corresponding deformations are indicated by the LVDT outputs, Δh and Δv respectively. The output from the shear stress transducer followed the calibration line initially and then broke away quite sharply before turning again to follow a line almost parallel to the calibration line. The breakaway appeared to come immediately after the initial peaking of the normal stress and the upturn came just as the normal stress reached the low point of the trough. This trough also coincided with the onset of vertical dilation as indicated by the vertical deformation, Δv.

An explanation for this behaviour can be found by reference to Fig. 9 which shows the progressive failure of a soft clay in simple shear after Duncan and Dunlop (23) who used a finite element analysis to produce the results shown. The extent of the failure zones in Fig. 9 is governed by the undrained shear strength of the clay but the underlying stress distribution must be a general one. For a granular material, therefore, dilation would start at the ends of the sample before it started in the central zone. This being so, there would be a tendency for these outer areas to lift the rigid top platen and thus reduce the normal stress recorded by the central transducer, as indicated by the trough. Under a reduced normal stress, the shear stress carried by the central zone would also be reduced as indicated by the initial breakaway from the calibration line. This coupling of the normal and shear stresses has also been noted by Prevost and Hoeg (61). As the shear strain increased further, the central zone would

begin to dilate and so the boundary stresses in this zone would increase as indicated by the graphs.

The basic problem appeared to be one of the rigid top platen being lifted by the early dilation occurring in the outer zones of the sample. This would presumably have upset the boundary stress distribution but since only the central load cells were strain gauged, it was not possible to monitor the stresses acting on the outer zones of the sample. To remove the effect of the dilation of the outer zones on the central zone, it was necessary to split the top platen into three sections, each with its own load cell, moving independently of each other. This involved the three normal load cells having individual crossheads and loading rams. This arrangement did not prevent progressive failure from occurring because a simple shear strain condition was still being applied to the sample. However, the dilation which accompanied the early failure at the ends of the sample could not directly affect the central zone. The Mk1 apparatus was not large enough to accommodate the mechanics of three independently mounted crossheads and so a larger Mk2 Simple Shear Apparatus was designed and this is described in the following chapter.

3.9 Concluding Remarks

On arriving at the above explanation of the observed behaviour, it might have been possible to test the hypothesis by using a less strongly dilatant material such as a clay. This possibility was rejected for several reasons:

(a) the hypothesis appeared to be a likely explanation of the observed behaviour,

(b) the apparatus had been designed for use with dry granular material,

(c) it had been originally intended to replace the Mk1 apparatus with a larger version at some stage and this was required to accommodate the design modifications considered necessary,

(d) the opportunity could be taken to modify the loading arrangements with particular regard to minimising frictional losses,

(e) the likely time required to design and commission a new apparatus made further delay undesirable.

CHAPTER FOUR

THE Mk2 SIMPLE SHEAR APPARATUS

4.1 Introduction

Having decided to design a larger apparatus, it was necessary to determine the practicable size in terms of applied loads and the required stress levels. The governing criteria were the size and maximum recommended working pressure for the large, Class 4 Bellofram rolling diaphragms which were to be used to load the sample. These factors constrained the Mk2 apparatus to being not more than three times larger than the Mk1 apparatus. Even so, the weight of the new version necessitated the installation of an overhead crane travelling on a rolled steel joist to handle the apparatus. A larger, more powerful vibrating table was also required for sample preparation and a Worthington-Simpson Type MTT8 two stage air compressor was installed to provide pressures up to 350 lbf/in^2.

4.2 Details of the Apparatus

The shear box in the Mk2 apparatus, Plate VI, was, in essence, a scaled up version of that in the Mk1 apparatus. The size of the sample space has been increased to 210 mm x 140 mm x 30 mm deep. The Mk2 load cells were basically the same as those used in the Mk1 apparatus except for their size. All six load cells were strain gauged so that some indication of the stress distribution in the new apparatus could be obtained. The active face of each load cell was 140 mm x 70 mm and the loading plates were of the tray type, as described in Section 3.2. The three shear load cells were identical. However, in the case of the outer normal load cells, a modification was made to remove

Note: Scale in inches

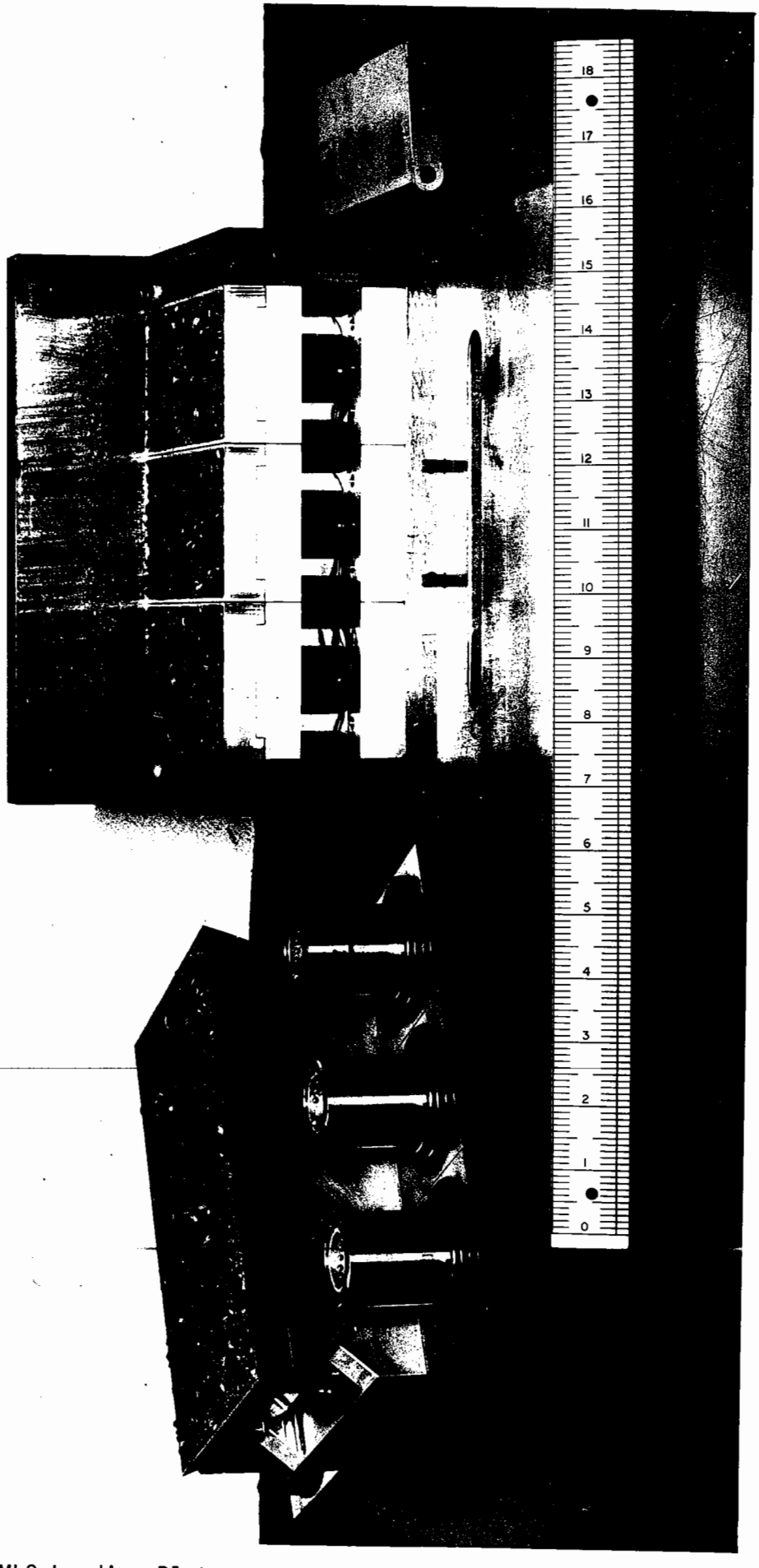

Plate VI The Mk2 Loading Platens

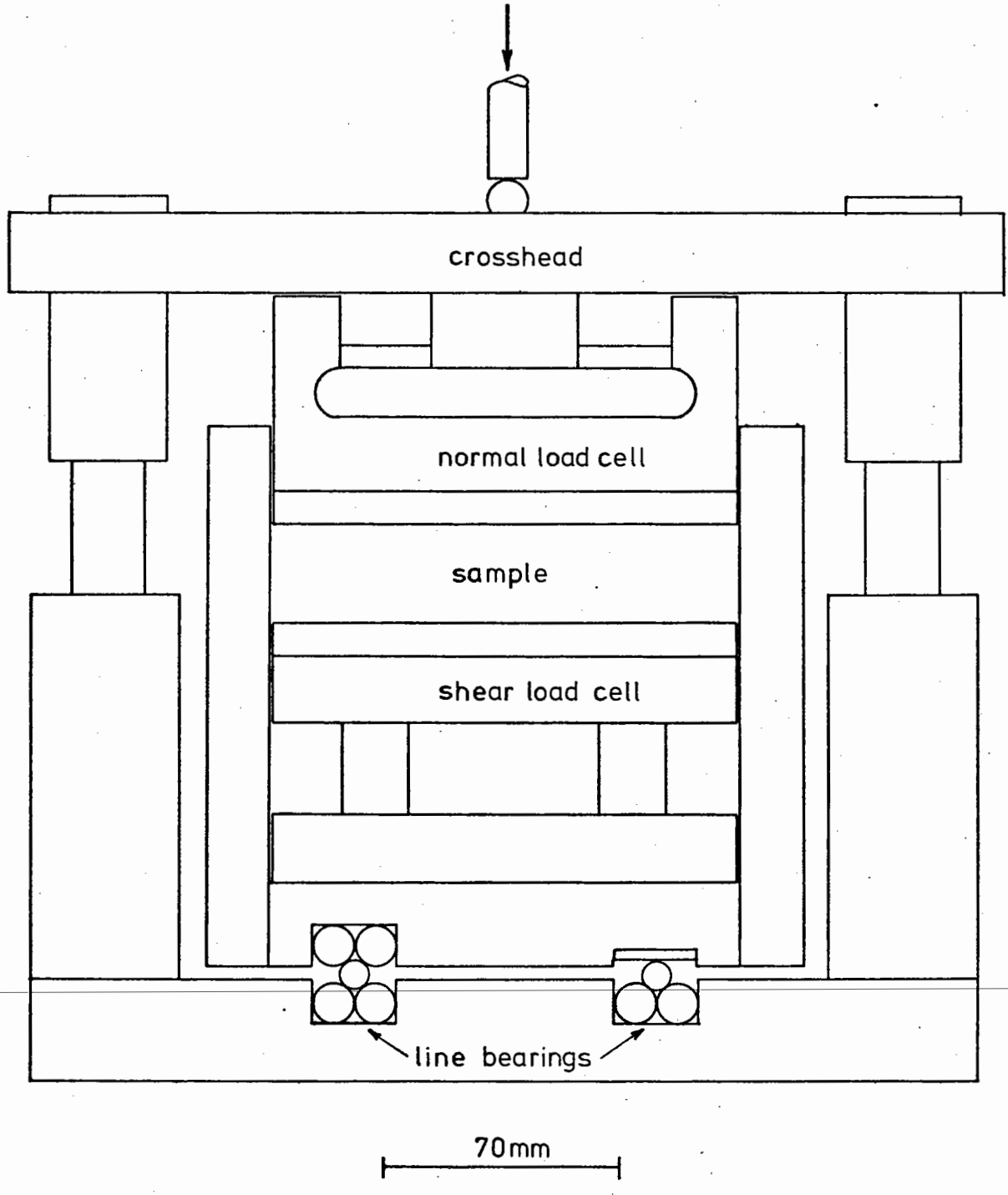

Fig. 25 Schematic transverse section of the Mk2 Simple Shear Apparatus

by side in a slot cut into the base of the main frame, Fig. 25. Steel balls, retained in a brass strip, ran in the groove formed between each pair of rods. The upper half of one bearing was a similar pair of rods mounted in the base of the shear box. The groove formed between these rods restrained the box in the transverse direction. The upper half of the other bearing consisted of a hardened steel strip set into the base of the box. In this way, the vertical load was reacted directly against the base of the shear box in a simpler manner than that adopted for the Mk1 apparatus. A clamping frame was again used to control the motion of the hinged end plates.

The shear loads were provided by a single-acting air ram at each of the apparatus. Each ram was capable of providing a thrust of about 18 kN which would produce an average shear stress of about 600 kPa on the sample. These rams were supplied by the British Railways Technical Centre at Derby. They were originally used for the Biaxial Shear Box apparatus described in Section 2.6. It was intended that each of these rams would act through a load cell fixed to the end of the shear box so that the total applied shear load could be monitored accurately. However, some difficulty was experienced in developing a satisfactory total shear load cell and the results obtained from the cells used were regarded as being only approximate. A separate loading ram was required for each section of the top platen and so three air cylinders were combined to form a single unit made from aluminium, Fig. 24. This was necessary so as to allow the vertical axes of the loading rams to be placed sufficiently close together. The rams were operated from a common regulated air pressure line and they were capable of producing a combined thrust of over 13 kN, producing an average normal stress of 450 kPa on the sample. All of the rams incorporated Bellofram rolling

diaphragms and the loading rods were carried by linear bearings to reduce frictional resistance. With the arrangements described above, all the loads were applied by the flat ends of loading rods acting on steel balls and so no transverse loads could be transferred to the rods themselves.

The loading frame for the Mk2 apparatus was made up of rolled steel channel sections. The apparatus itself was mounted on one crossmember and the vertical loading rams were carried by another, removable, cross-member. The shear load rams were supported by steel plates bolted to the vertical members at each end of the frame, Plate VII. Due to the large size and weight of the Mk2 apparatus, it was impracticable to mount it on a vibrating table as was done with the Mk1 version. An overhead travelling crane was used to transfer the apparatus between the loading frame and the vibrating table.

Sample deformations were monitored in a manner similar to that described in Section 3.1 for the Mk1 apparatus. Horizontal movement of the lower half of the shear box was measured using a $\pm$0.500 in. linear range LVDT with the core extension lightly spring loaded against the shear box. The LVDT was supported by a clamp fixed to the main frame. The vertical movement of the crossheads was measured using three $\pm$0.200 in. linear range LVDT's mounted in a clamp supported by pillars fitted to the side of the main frame, Plate VIII. Again, the LVDT's were all of the DC in, DC out type and operated on a 24.0 V supply.

4.3 Data Monitoring Equipment

There were 12 output signals from the assembled apparatus: 3 from the normal load cells, 3 from the shear load cells, 2 from the total

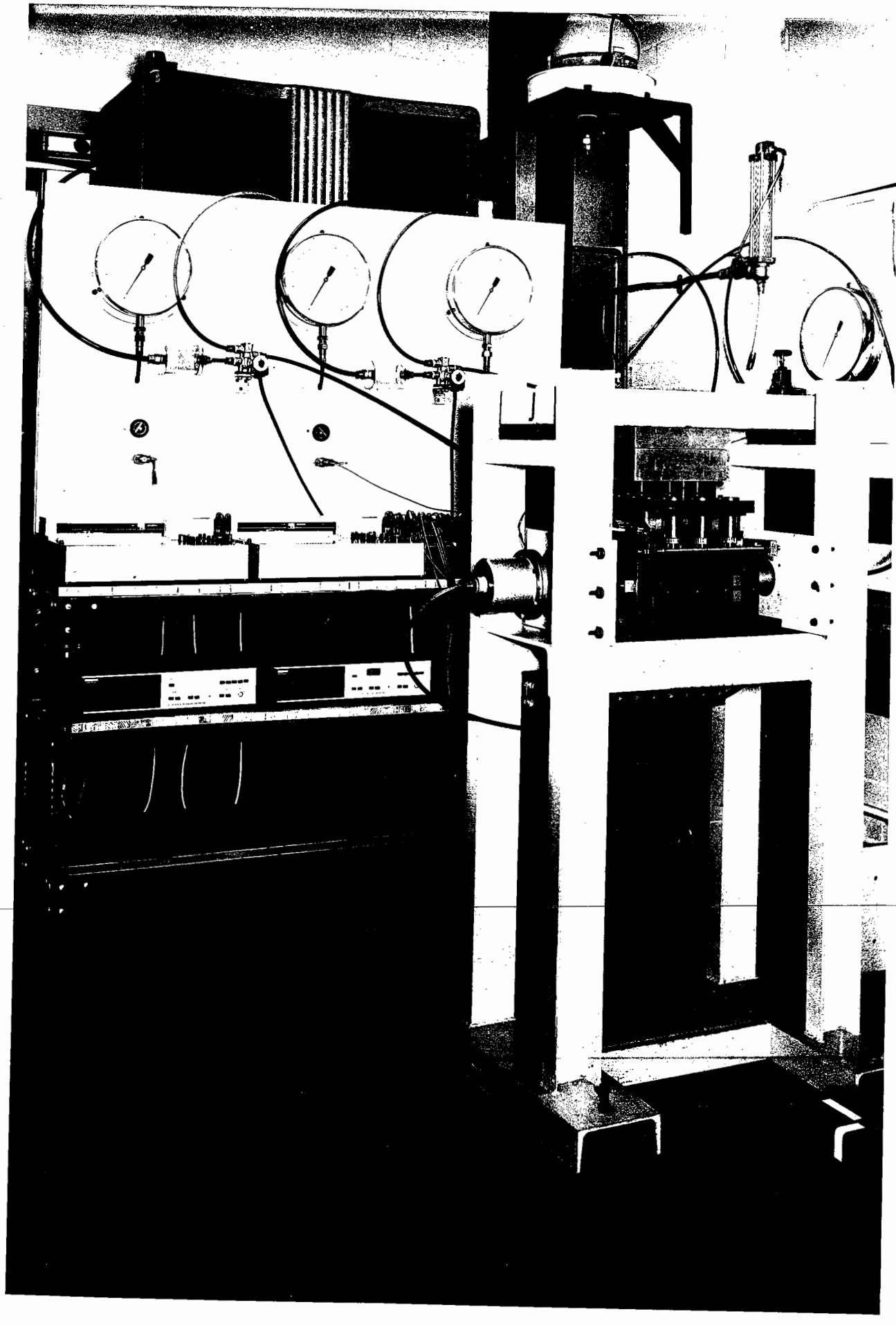

Plate VII General View of Mk2 Testing Equipment

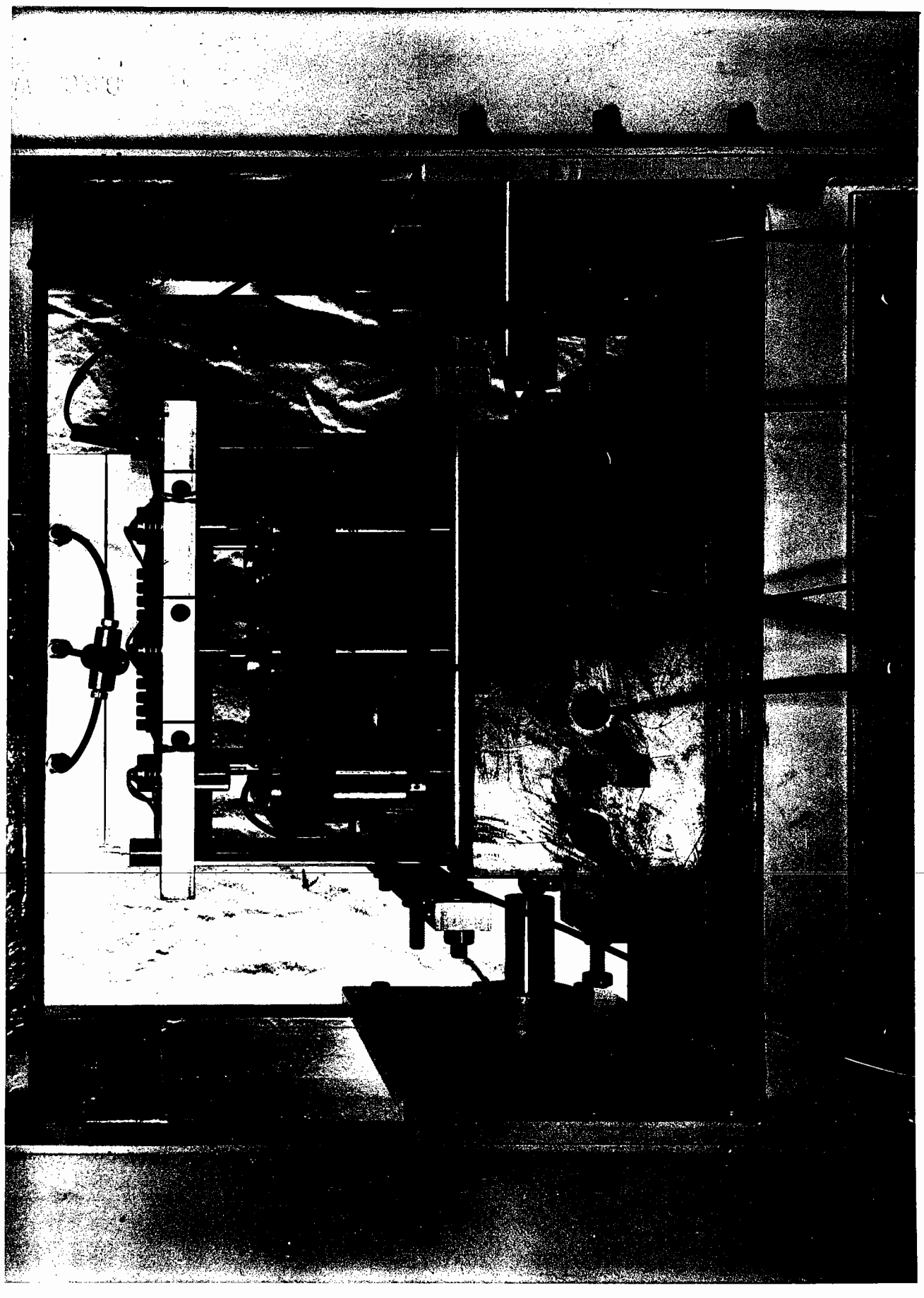

Plate VIII The Mk2 Simple Shear Apparatus

shear load cells, 3 from the vertical LVDT's and 1 from the horizontal LVDT. The outputs from the 8 load cells were taken via a patchboard on the side of the loading frame to a multi-channel balancing box and then to a two-gang, multi-channel selector switch. A Solartron A220 digital voltmeter (DVM) was connected to each gang of the switch. The outputs from the LVDT's were connected directly to the selector switch as were the input voltages for the Wheatstone Bridge circuits and the LVDT's. This arrangement allowed any required voltage to be monitored by simply selecting the relevant channel on the switch and the appropriate range on the DVM; no reconnecting of components was necessary.

The possibility of logging the 12 data channels on paper or magnetic tape was examined briefly. It appeared that relatively low scanning speeds precluded the former method. Hyde (35) has described the use of a 14 channel FM tape recorder for data logging in analogue form. A high speed analogue to digital converter linked to a digital computer was then used to process the data. While this method appeared very suitable, in that it overcame the problem of scanning speed, difficulties could have arisen with matching of the transducers to the amplifiers in the tape recorder and so the technique was not pursued further.

Permanent records of any four outputs could be obtained using two Bryans Southern, Series 28000, two-pen flatbed chart recorders. Generally, these were used to monitor the outputs from the central normal and shear load cells, the central vertical LVDT and the horizontal LVDT. A Bryans Southern, Series 29000 XY Recorder was used to produce hysteresis loops during the course of the repeated load tests by plotting the output from the central shear load cell against that from the horizontal LVDT. In the case of single load tests to failure, this

same arrangement automatically produced the stress-strain curve for the test. In addition, for the single load tests, where scanning speed was not an important factor, it was possible to record all 12 output channels on paper tape using a Solartron data logging system. The punched tape was interpreted using a computer teletype and the data processed manually.

4.4 Control Equipment

The general arrangement of the compressed air control equipment is shown in Fig. 26. A supply pressure of up to 350 lbf/in^2 was available. This supply was filtered and regulated before passing to the main control equipment. Fairchild Kendall Model 10 precision regulators, capable of handling pressures in the range 5-400 lbf/in^2, were used throughout the control equipment. Gas cylinders were used in the pressure lines as reservoirs. For the shear load rams it was necessary to have quite large reservoirs in the line so as to allow a reasonable frequency for the repeated loading. The bore of the connecting pipes was another limiting factor in this respect; $\frac{3}{8}$ in. outside diameter Enots nylon tubing was used for most of the pipework.

Solenoid valves were installed to control the flow of air to the shear rams. Initially, these were Danfoss Type EVP 302 NC but preliminary tests indicated that the 2 mm exhaust orifice and the $\frac{1}{8}$ in. BSP connections severely restricted the air flow from the rams during unloading and hence limited the loading frequency which could be achieved. With these valves, the cycle time was limited to a minimum of about 4 seconds (0.25 Hz). This proved unacceptably slow and so larger valves were installed. The Asco Type 8321 NC was an internal pilot operated solenoid valve having a $^9/_{32}$ in. exhaust orifice and

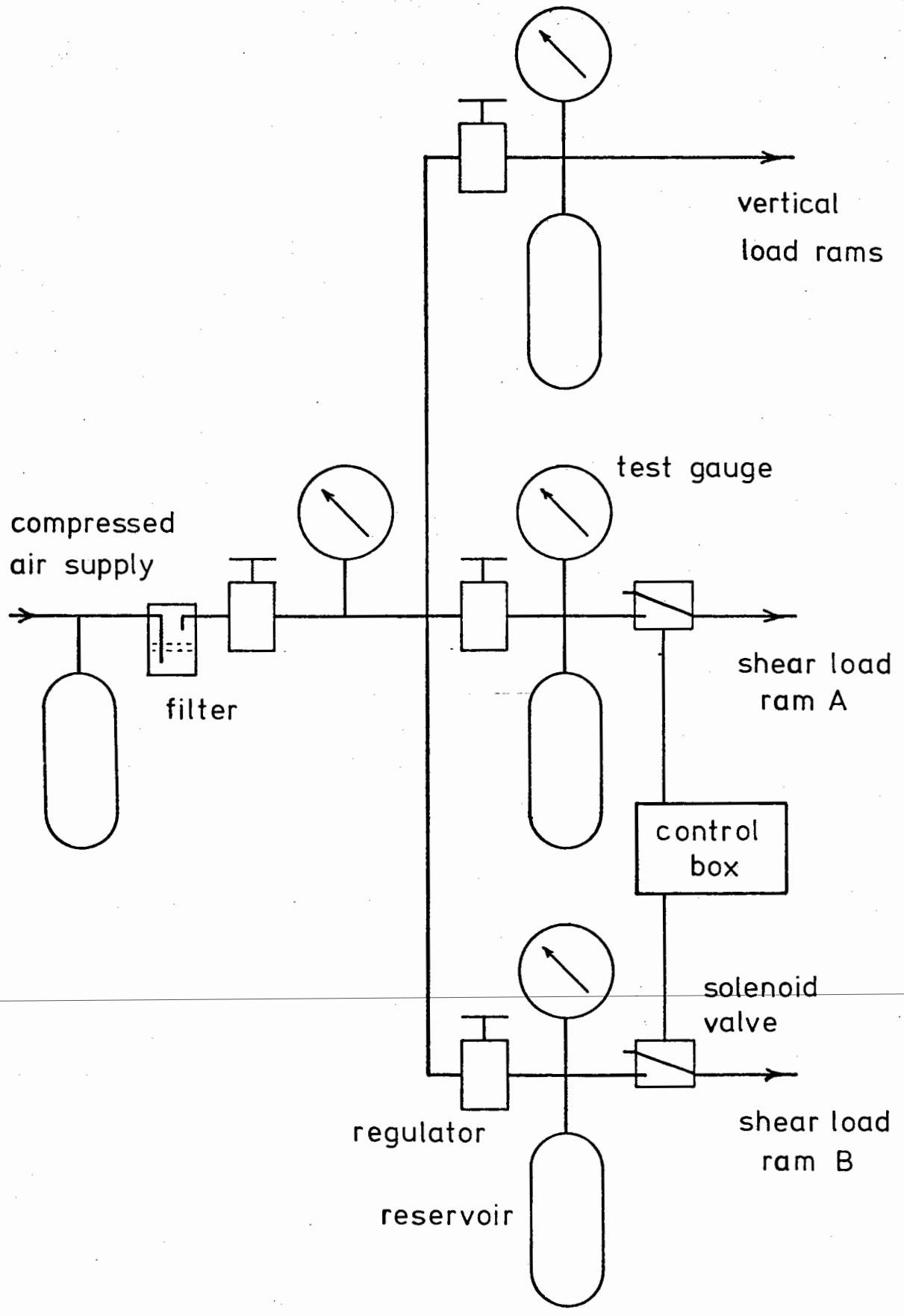

Fig. 26 Pneumatic control arrangements

$\frac{3}{8}$ in. NPTF connections. These valves enabled the cycle time to be reduced to about 2.8 seconds (0.36 Hz) and this was used for all the repeated load tests. Although quite small, this reduction in the cycle time was significant when carrying out tests of about 10^4 cycles duration.

The solenoid valves were actuated by an electronic timing switch which had the facility to independently vary the ON time of the valves and the OFF time between switching one valve out and the other in. This provided the possibility of varying the load pulse time and also having a variable rest period between load pulses. However, this latter facility was not utilised for the work described herein; the OFF control was set at zero for the entire test programme. No provision for cycling the vertical load was developed during the course of this project and some difficulties with the phasing of the two stress pulses are foreseen if the cycle time is to remain less than about 5 seconds.

The loading waveforms produced by the control equipment are shown in Fig. 27. These waveforms are outputs from the central shear load cell in each case. Waveform (a) corresponds to the unidirectional repeated load tests and waveform (b) to the bidirectional repeated load tests. The rounding of the corners of the square waveform was due to the falling pressure gradient at the end of an inlet or exhaust operation. Attempts to produce a waveform closer to the sine waveforms shown in Fig. 2 using throttle valves proved unsuccessful due to repeatability problems. The effect of the throttle valve was very severe; producing a very rapid transition from a square wave to a peaked, almost triangular, waveform. Similar difficulties have been reported by Morgan (55). Chan and Mulilis (17) have recently described

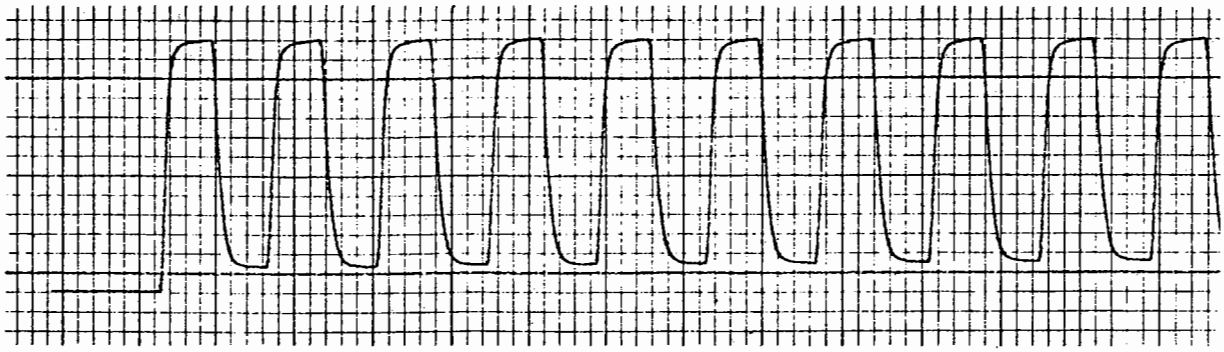

(a) Waveform for unidirectional load

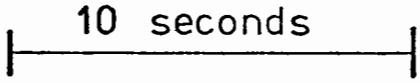

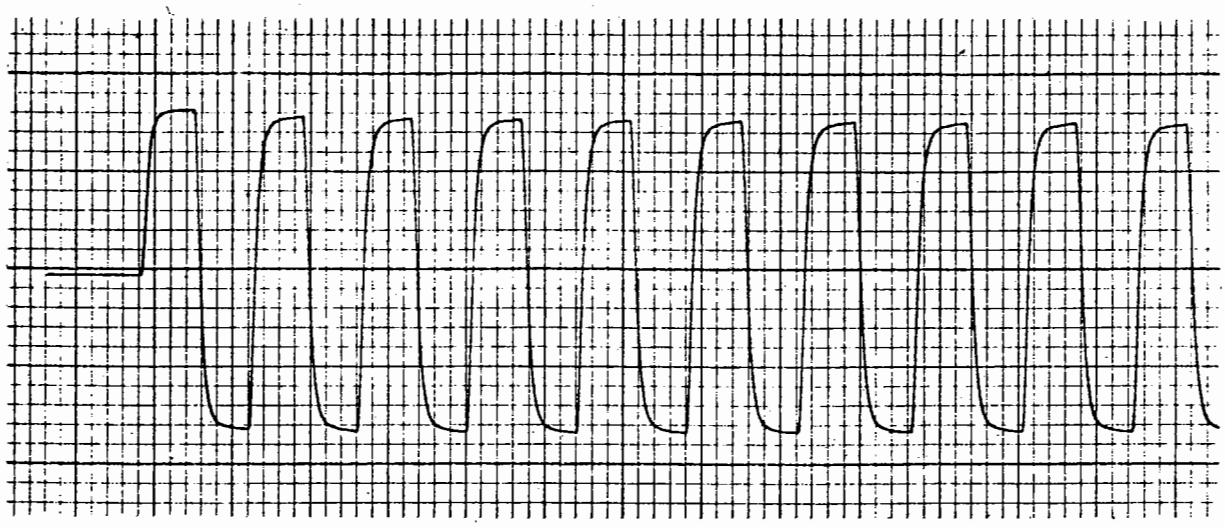

(b) Waveform for bidirectional load

Fig. 27 Waveforms for repeated load tests

a pneumatic sinusoidal loading system using commercially available components and the waveform produced by the system would seem to be quite acceptable. Studies by Lee (46), Lee and Fitton (47) and Thiers and Seed (83) have indicated that the type of waveform used can have some effect on the results obtained from repeated load tests, particularly in the case of clays. The square waveform has been found to be a rather more severe loading condition than a peaked, triangular waveform. The use of a square waveform in this work was, therefore, conservative and on the safe side.

An electrical limit switch was used as a fail-safe device to curtail the command signals to the solenoid valves if a very large shear deformation occurred during the repeated load tests. The limit switch, which can be seen in Plate VIII below the horizontal LVDT, consisted of a spring-tipped screwed brass rod mounted in a perspex bush to isolate it electrically from the shear box. If a very large shear deformation did occur, then a low voltage electrical circuit was completed by the shear box touching the spring and this tripped a relay in the control box.

4.5 The Material

4.5.1 Choice of material

The same crushed limestone material as had been used in the Mk1 apparatus was chosen for use in the Mk2 apparatus. The size fraction obtained for the larger apparatus was that passing a $\frac{3}{16}$ in. BS Sieve and retained on BS Sieve No. 7. This defined a metric size range of 4.8 mm down to 2.4 mm and this material is referred to as nominally 3 mm particle size. The specific gravity of this size fraction was determined, according to BS 1377:1967 (12) as 2.69 in comparison with

the value of 2.72 reported in Section 3.5.2 for the nominally 1 mm size particles of this material. Boyce (9) has reported a value of 2.71 for all the size fractions of this limestone which was also used for his work. These values are fairly typical of limestones in general.

4.5.2 Compaction trials

Tests similar to those described in Section 3.5.2 were carried out for the nominally 3 mm particles to establish the compaction characteristics of the larger material. Deposition through water gave an average minimum density of 1.20 Mg/m^3 corresponding to a porosity of 0.55. Slow pouring in air gave a somewhat higher density of 1.34 Mg/m^3 corresponding to a porosity of 0.50. This higher value was probably due to difficulties experienced in pouring the material from "zero height". The value of 1.20 Mg/m^3 was taken as the minimum density.

In view of the difficulties encountered in obtaining a value for the maximum density of the smaller material, no attempt was made to repeat the test for the larger material. To obtain a value for the compacted density for use in preliminary calculations, a box of the material was compacted on the vibrating table with zero surcharge. This gave a density of 1.58 Mg/m^3 which corresponds to a porosity of 0.41. A series of compaction trials was carried out in the Mk2 apparatus to establish a suitable sample preparation technique and also to determine a value for the compacted density of the samples produced. In the Mk1 apparatus, the samples were compacted by cycling the amplitude of the vibration from zero to a maximum and back to zero until no increase in compaction was indicated by the LVDT used to monitor the movement of the top platen, Section 3.6. With the Mk2 apparatus, this technique was not quite so effective since full

compaction was not achieved after just a few cycles of the vibration amplitude. However, the increase in compaction produced by each cycle did become quite small after about three cycles and so a method involving four cycles of the vibration amplitude was adopted and further details of this are given in Section 4.6. The central vertical LVDT output was simply used as a check on the compaction procedure. A similar check on the repeatability of the procedure was made by measuring the height of the top of the crossheads above a reference point on the main frame. This measurement was used to plot Fig. 28 which shows the compacted (reference) height versus the sample weight. The graph indicates a value of 76.4 mm as the datum from which the actual sample height could be calculated and the slope of the line indicates a compacted density of 1.62 Mg/m^3 corresponding to a porosity of 0.40. The slightly higher compacted density was probably due to the surcharge weight of the top platen. The compaction procedure adopted was found to be quite satisfactory and, over the whole test programme, the range of porosities of the samples produced was less than 0.02.

Table 1 contains all the results obtained from the various compaction trials using both size fractions of the material. Reference should be made to the appropriate sections of the text for details of the procedures used.

4.5.3 Triaxial compression tests on the material

An angle of shearing resistance of 50° was obtained from a series of triaxial compression tests carried out on the nominally 3 mm material. Details of the experimental procedure are given in Appendix C. A large, standard direct shear box was not available so a φ value could not be obtained using this method.

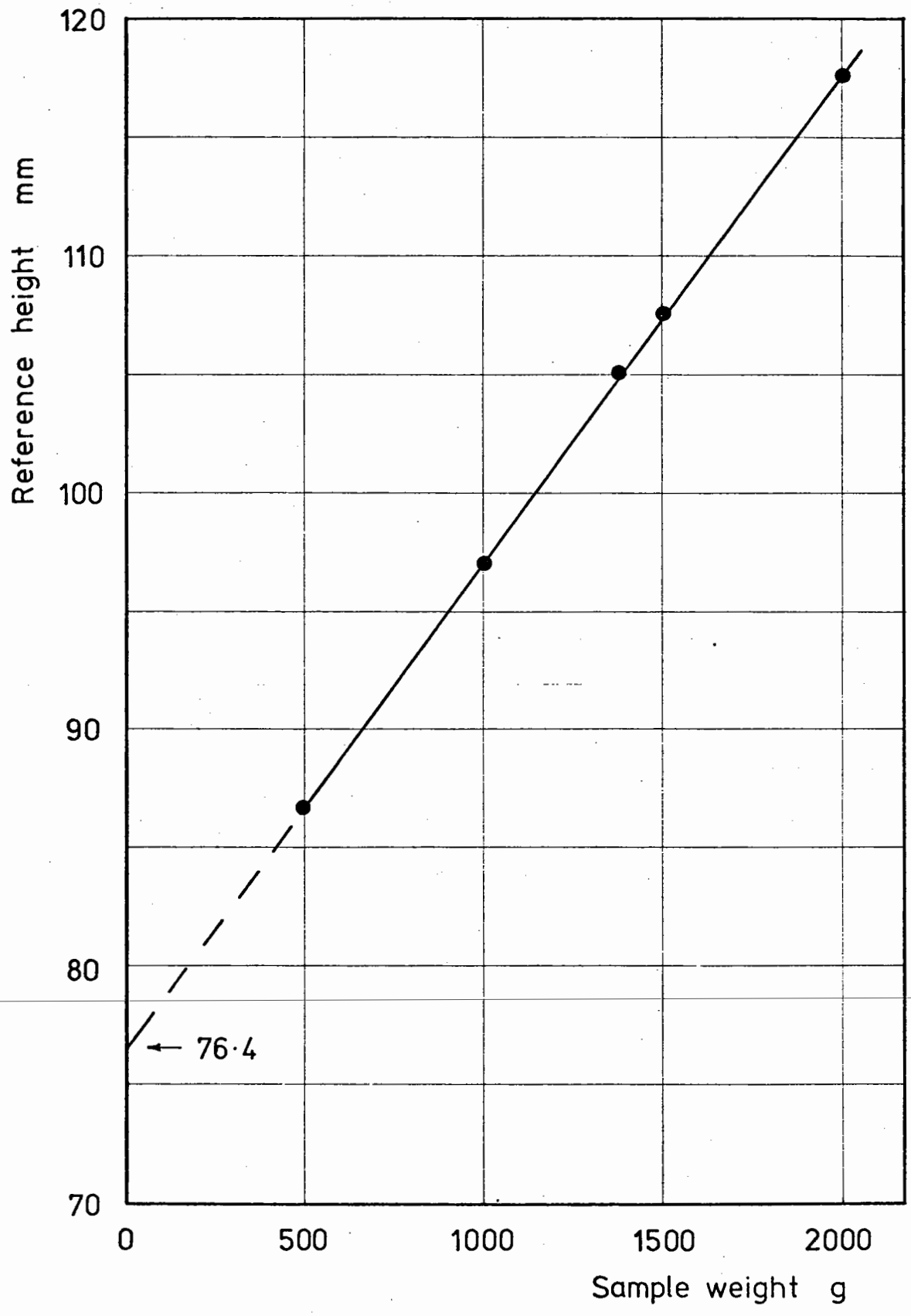

Fig. 28 Compaction trial results

Material: Passing B.S. Sieve No. 14 retained BS Sieve No. 25

Specific Gravity: 2.72

	Compaction Method						
	Water Deposition	Air Pouring	Vibration	CBR Mould	Triaxial Test	Direct Shear	Simple Shear
Density Mg/m^3	1.27	1.27	1.56	(1.66)	1.54	1.48	1.50
Void Ratio	1.14	1.14	0.74	(0.64)	0.77	0.84	0.81
Porosity	0.53	0.53	0.43	(0.39)	0.44	0.46	0.45

Material: Passing $\frac{3}{16}$ in. BS Sieve retained BS Sieve No. 7

Specific Gravity: 2.69

	Compaction Method						
	Water Deposition	Air Pouring	Vibration	CBR Mould	Triaxial Test	Direct Shear	Simple Shear
Density Mg/m^3	1.20	1.34	1.58	-	1.49	-	1.62
Void Ratio	1.24	1.01	0.70	-	0.81	-	0.66
Porosity	0.55	0.50	0.41	-	0.45	-	0.40

Note: Refer to text for explanation of compaction methods.

( ) indicates doubtful values.

Table 1 Results of Compaction Trials

4.6 Sample Preparation

Plate IX shows the starting point for sample preparation with the main frame clamped to the vibrating table. The base of the shear box was held in the central position by adjusting the limit stops which can be seen in Plate IX at the lower centre of the main frame. When in contact with the shear box, the limit stops engaged with a recess in each end of the box so that they also provided vertical restraint. During a test, the stops were used to prevent damage to the apparatus by excessive movement of the base of the shear box.

The complete top platen was fitted over the six guide pins and supported by a spacer so that the edges of the outer normal load cells were just below the top of the end plates. The end plates were then locked in position, using clamping screws mounted in the sides of the box, allowing a small clearance between the edge of the load cell and the end plate so that the top platen could easily be removed.

Having removed the top platen, a length of soft 3 mm diameter PVC sleeving was inserted along the lower edge of each end plate. This prevented particles from being trapped by the movement of the end plates. A known, fixed amount of material was scooped into the shear box and the surface of the sample was levelled using the scoop. The clamping frame was then put over the main frame before the top platen was replaced on the clamping frame fitted to the end plates.

The carrier for the vertical LVDT's was then fitted to the pillars mounted on the side of the main frame. Only the central LVDT was used for compaction checking purposes since the three crossheads were locked together at this stage, Plate X. The sample was compacted using four cycles of the vibration amplitude. Each cycle lasted about 5 seconds. The procedure adopted was to steadily increase the control

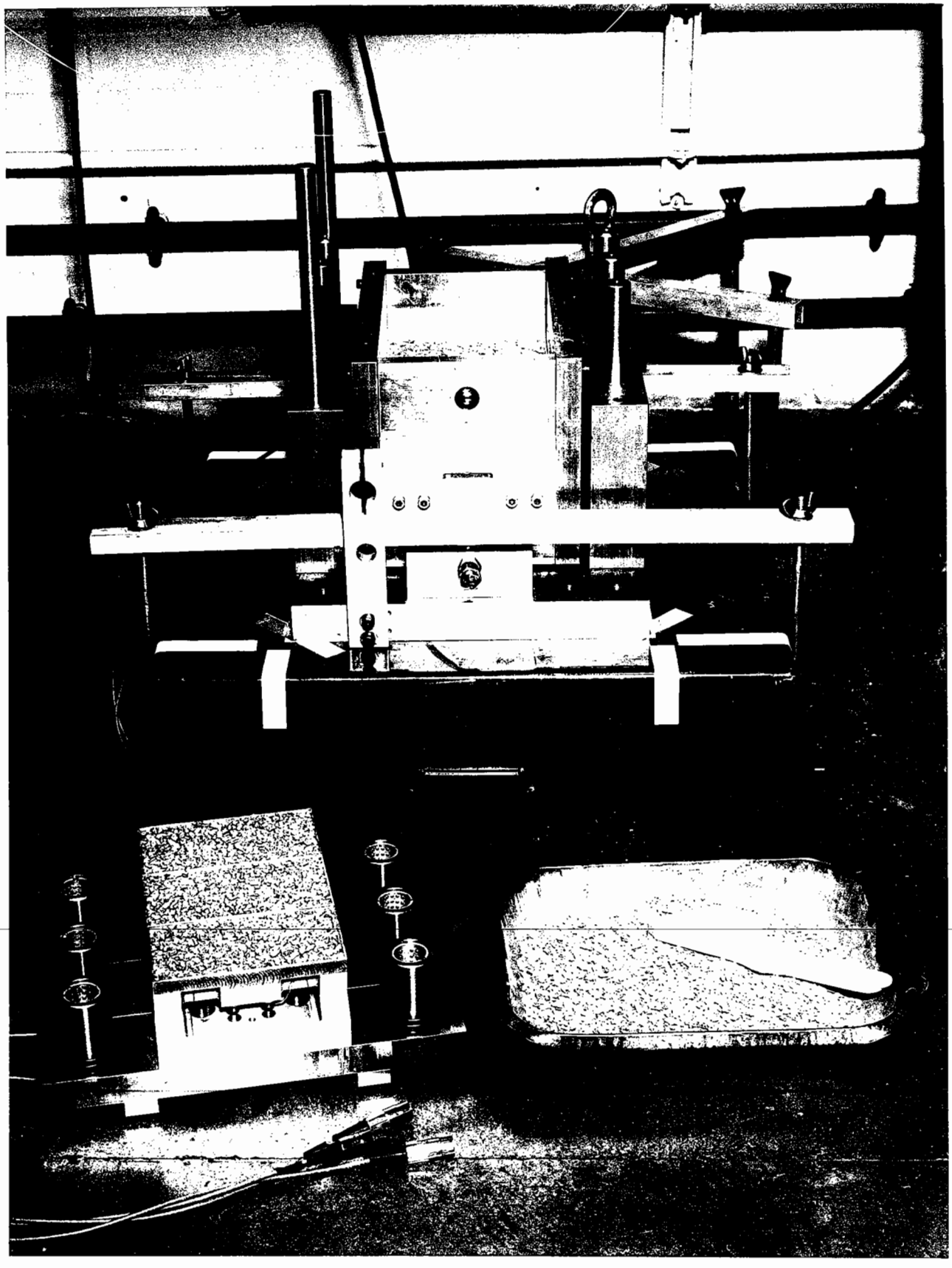

Plate IX Start of Sample Preparation

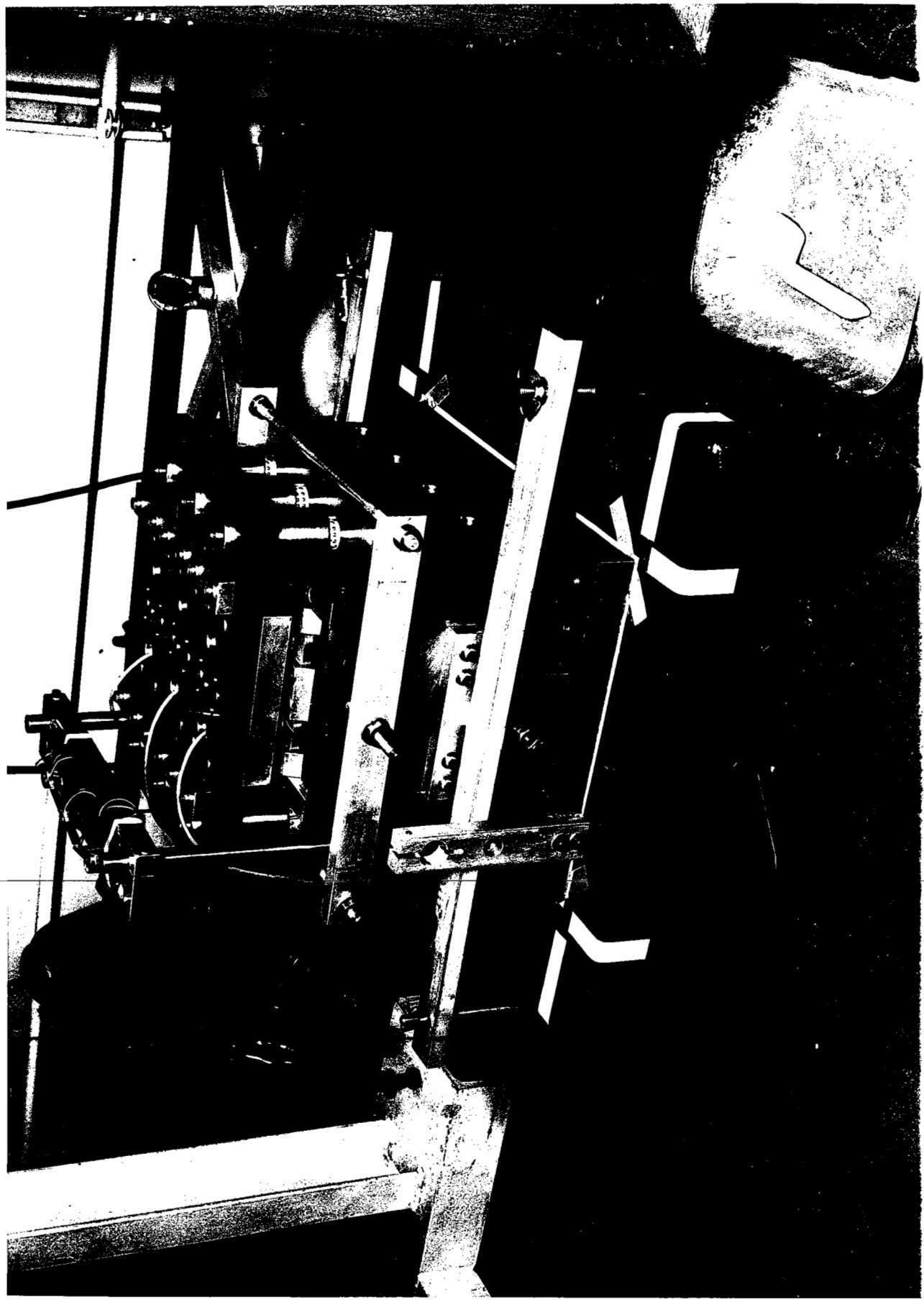

Plate X End of Sample Preparation

box setting to level 4 and back to zero for the first two cycles, level 5 for the third cycle and level 4 again for the last cycle. This method produced samples of a consistent density as indicated by measurements of the reference height mentioned in Section 4.5.2.

The clamps holding the main frame to the vibrating table were then released and the apparatus transferred to the loading frame using the overhead crane and a 4-legged spider frame screwed to the base plate of the main frame. The spider frame can be seen behind the vibrating table in Plate X. The apparatus was bolted to the loading frame and the various transducers were fitted and connected up. The crossmember carrying the vertical loading rams was bolted onto the loading frame and the clamps locking the sections of the top platen together were removed. The shear load rams were then brought into contact with the steel balls on the total shear load cells. Finally, the limit stops were backed off and the end plate locking screws were released ready for the test to begin. The assembled apparatus is shown in Plates VII and VIII.

The above procedure was reversed to remove a sample after a test. When the apparatus had been transferred back to the vibrating table and the top platen removed, the shear box was lifted from the main frame using the overhead crane and a smaller spider frame which located onto the side plates of the box. The sample was then tipped out and any remaining particles were either brushed away or blown out using an air line. A piece of steel shim was used to check that the clearance gaps around the load cells were free from trapped particles.

4.7 Single Load Tests

4.7.1 Test details

A short series of single load tests, Series S, was carried out to

compare the behaviour of the Mk2 apparatus with that of the Mk1 version. Apart from size, the only major mechanical difference between the two versions was the independent mounting of each of the normal load cells in the Mk2 apparatus to form a split top platen.

The basic format of these tests was similar to that described for the single load tests in the Mk1 apparatus, Section 3.7. The samples were incrementally loaded to failure in simple shear to obtain an angle of shearing resistance for comparison with the value of 50° obtained from the triaxial tests, Appendix C. The control equipment for the single load simple shear tests was somewhat simpler than that described in Section 4.4. The solenoid valves were bypassed so that the load applied by the shear ram was controlled directly by a precision air regulator.

The sample was set up as described in Section 4.6 and all the Wheatstone Bridge load cell circuits were balanced to give zero initial output. Appropriate senstivities and zero positions were selected for the chart recorders and the initial readings for all the transducers were then scanned by the data logger referred to in Section 4.3. These outputs were similarly recorded after the vertical load had been applied and again after each increment of shear load. The outputs from the central shear and normal load cells were monitored continuously on the chart recorders during these single load tests as were the horizontal and central vertical LVDT's. The stress-strain curve for the test was produced automatically using the xy recorder as described in Section 4.3 and this was of some assistance in estimating the failure load. Defining the failure point for a test was a considerable problem, as it had been with the Mk1 apparatus.

4.7.2 Test results

The stress-strain curve for one of the single load tests is shown in Fig. 29. However, this is not entirely typical in that it shows some tendency to reach a peak shear stress. Some of the stress-strain curves showed a tendency for the shear stress to increase slightly at each increment of shear load even when large deformations were occurring. This situation made precise analysis of the results rather difficult although Fig. 30, which is of the same type as Figs 21, 22 and 23, shows that the apparatus was behaving much better than the Mk1 version. In particular, the output, σ, from the normal stress transducer was much closer to its expected value throughout the test and the shear stress transducer output, τ, also remained much closer to its calibration line up to the point where failure was imminent as indicated by the lines for the horizontal, Δh, and vertical, Δv, deformations becoming very steep.

Fig. 31 shows the variation of the three shear load cell outputs with increasing shear ram force. The total of the three outputs is also shown and this indicates some deficit when compared with the equivalence line. This deficit was probably taken up on the sides and ends of the shear box. This explanation is substantiated to a large extent by the theoretical analysis of simple shear conditions by Prevost and Hoeg (61) which was referred to previously. There could also have been some mechanical friction losses but these ought to have been small. The distribution of the shear load over the length of the sample indicated in Fig. 31 shows that higher shear stresses were induced adjacent to the corners of the box which were opening out. The shear stress over the central zone was initially higher than the outer zone stresses but the distribution changed during the test to bring the central zone shear stress between the other two values.

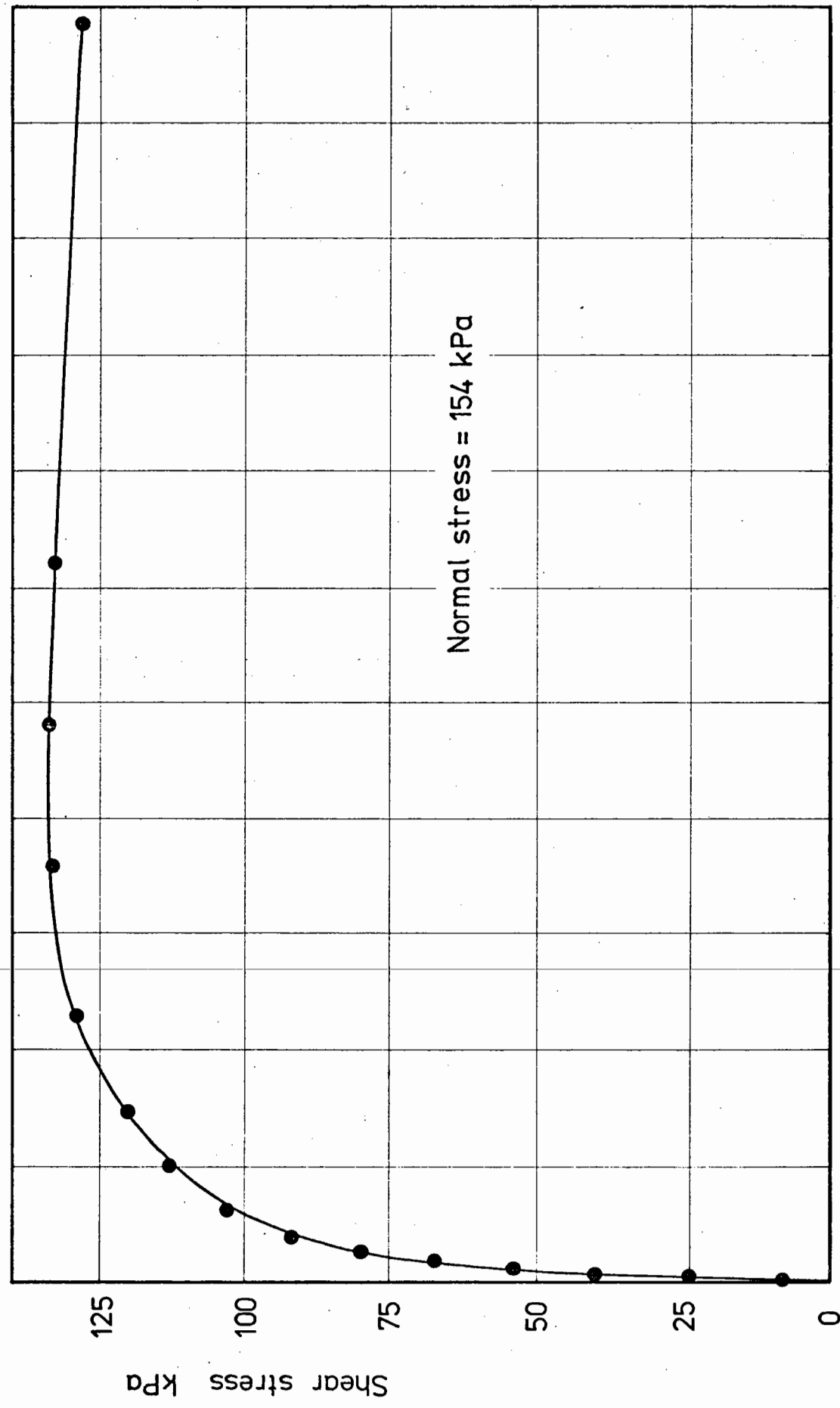

Fig.29 Stress-strain curve for single load test

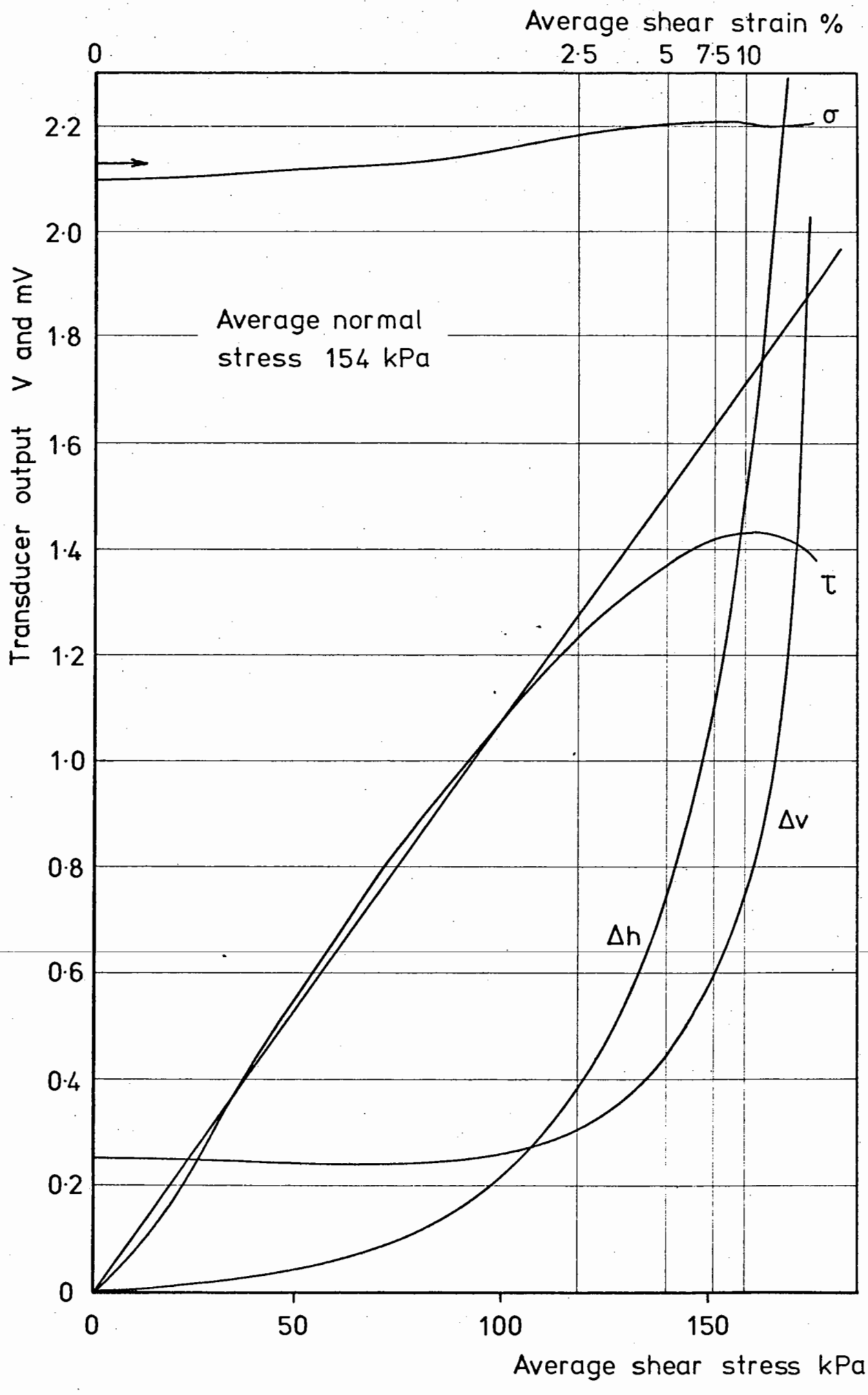

Fig. 30 Single load test - output data

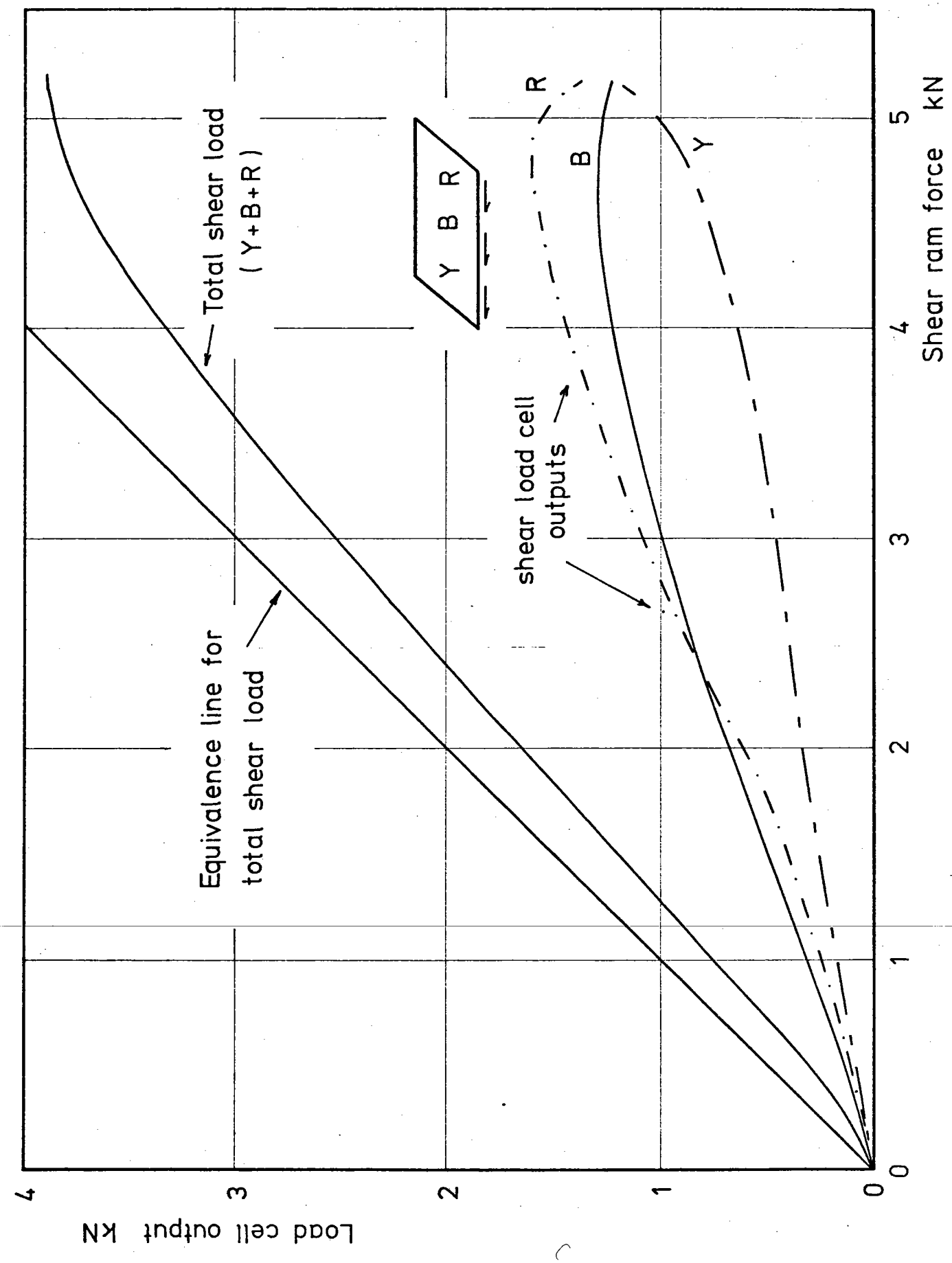

Fig. 31 Single load test - shear load data

The discrete particle computer solution of the stress conditions immediately prior to failure in a simple shear apparatus with rigid boundaries by Round (66) was referred to in Chapter Two. His analysis also indicated the shear stresses adjacent to the opening corners to be the higher. However, this analysis also indicated that the central zone shear stress should be higher than the outer zone stresses just prior to failure. This difference between the experimental results and the analysis was probably due to the independently mounted normal load cells in the Mk2 apparatus since in a test conducted with the normal load cells locked together, the central zone shear stress at failure was the highest. In contrast to Round's results, the elastic analysis of simple shear by Roscoe (64) indicated a symmetrical shear stress distribution with the highest value in the centre, Fig. 8. However, as was pointed out in Chapter Two, Roscoe's analysis is only valid for elastic materials though the results should be applicable to soils in the first stages of deformation and provide a guide to the behaviour for large deformations (64).

From the results of his analysis, Round has recently suggested (67) the possibility of using unequal vertical loads on the three zones of the sample to compensate for the non-uniform normal stress distribution produced under simple shear conditions and thus improve the uniformity of the stress conditions in the central zone. Ideally, it would be necessary to have independent control over the normal stresses on the upper and lower faces of each zone and to vary them during a test in order to achieve ideal stress conditions on the central zone. Static equilibrium would be preserved by complementary shear stresses induced on the ends of the sample. However, this theoretical arrangement would be totally impracticable.

It is interesting to note that the overall behaviour of the Mk2 apparatus in the test with the normal load cells locked together to form a rigid top platen was much better than that observed in the Mk1 apparatus. This could be due partly to the improved mechanical design of the Mk2 apparatus and partly to the fact that the range of particle sizes was somewhat greater for the larger material which might have reduced its potential for dilation. However, Fig. 30 indicates that this material does behave in a strongly dilatant manner at failure.

Fig. 32 shows the results of the single load, Series S tests evaluated on the same basis as for the Mk1 single load test results shown in Fig. 20. The triaxial test result is also included for comparison. It can be seen that there was again some discrepancy between the results obtained from the different test methods and analytical techniques. However, these results were a considerable improvement on those obtained with the Mk1 apparatus and Fig. 30 shows that the apparatus was behaving in the desired manner, certainly up to the point where failure was imminent. A fuller understanding of the behaviour of the apparatus could probably have been obtained using a strain controlled test procedure. However, this was not possible.

The results of the single load, Series S tests described in this section allowed attention to be directed towards implementing a repeated load test programme with some confidence.

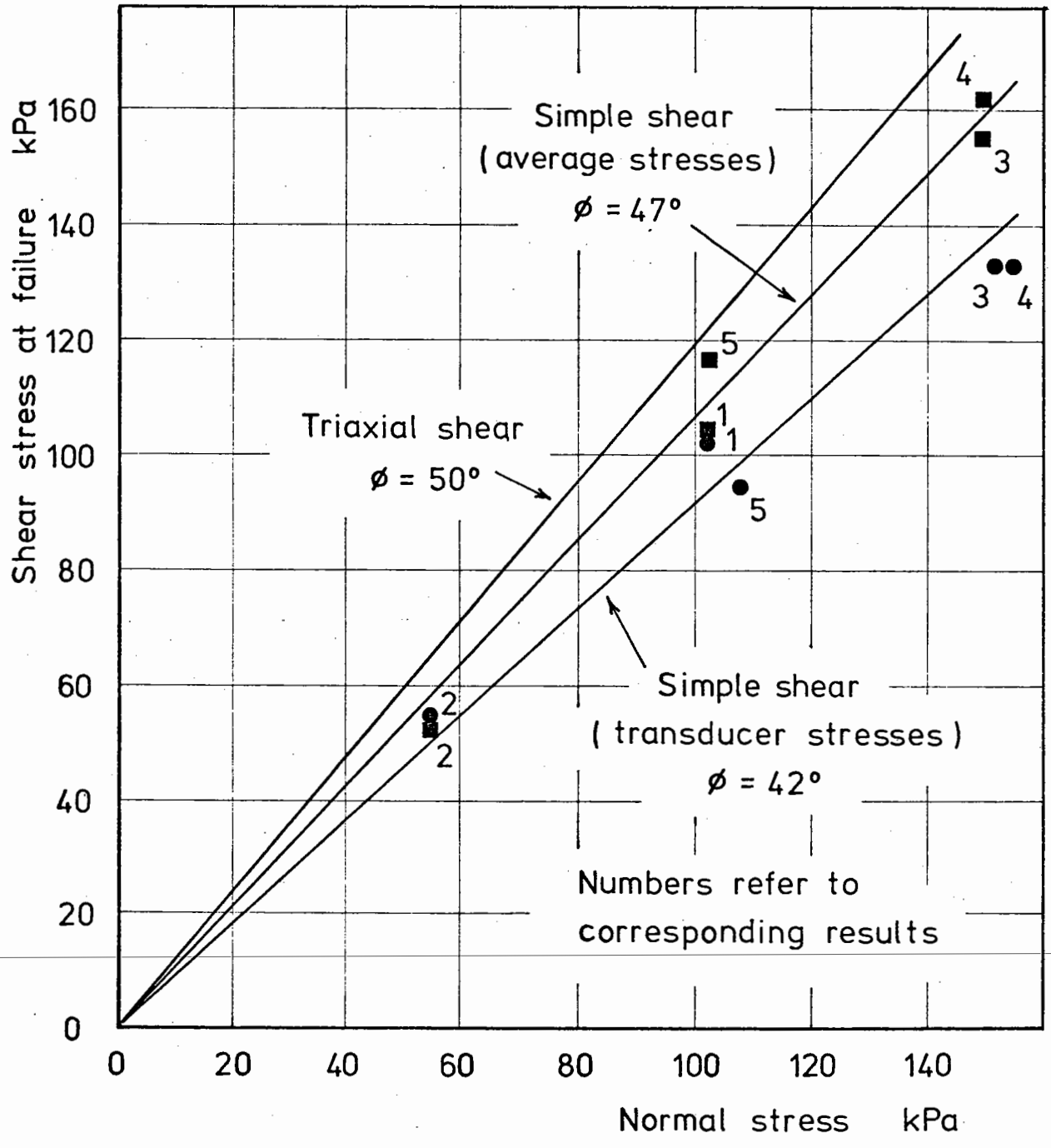

Fig. 32 Results from single load tests

CHAPTER FIVE

UNIDIRECTIONAL REPEATED LOAD TESTS (SERIES A)

5.1 Introduction

The first series of repeated load tests, Series A, involved monitoring the response of the material when subjected to unidirectional shear stress pulses which were a known fraction of the static failure strength. This type of loading corresponds to the lateral load pulse developed beneath a railway sleeper by the out of balance centripetal force when a train negotiates a curve at a speed different from the design speed which determines the superelevation of the track.

This chapter gives brief details of the test procedure and data logging techniques followed by the test results and the presentation of various models to predict certain aspects of the material's response to unidirectional repeated load. The idealised test programme devised for Series A is shown in Fig. 33. The stress paths were constrained to be vertical lines because no facility for cycling the normal stress had been developed. A value of 45° was taken for the angle of shearing resistance of the material. This value lies between the two results obtained from the single load tests described in Chapter Four and it is also a convenient value in that the tangent is unity.

5.2 Test Details

Sixteen Series A tests were carried out and, as shown in Fig. 33, three normal stresses were used: 95, 190 and 285 kPa nominal. Five tests were at the lowest stress level and four at the highest. The remaining seven tests at the intermediate stress level also included one or two tests for repeatability. However, a duplicate test, in

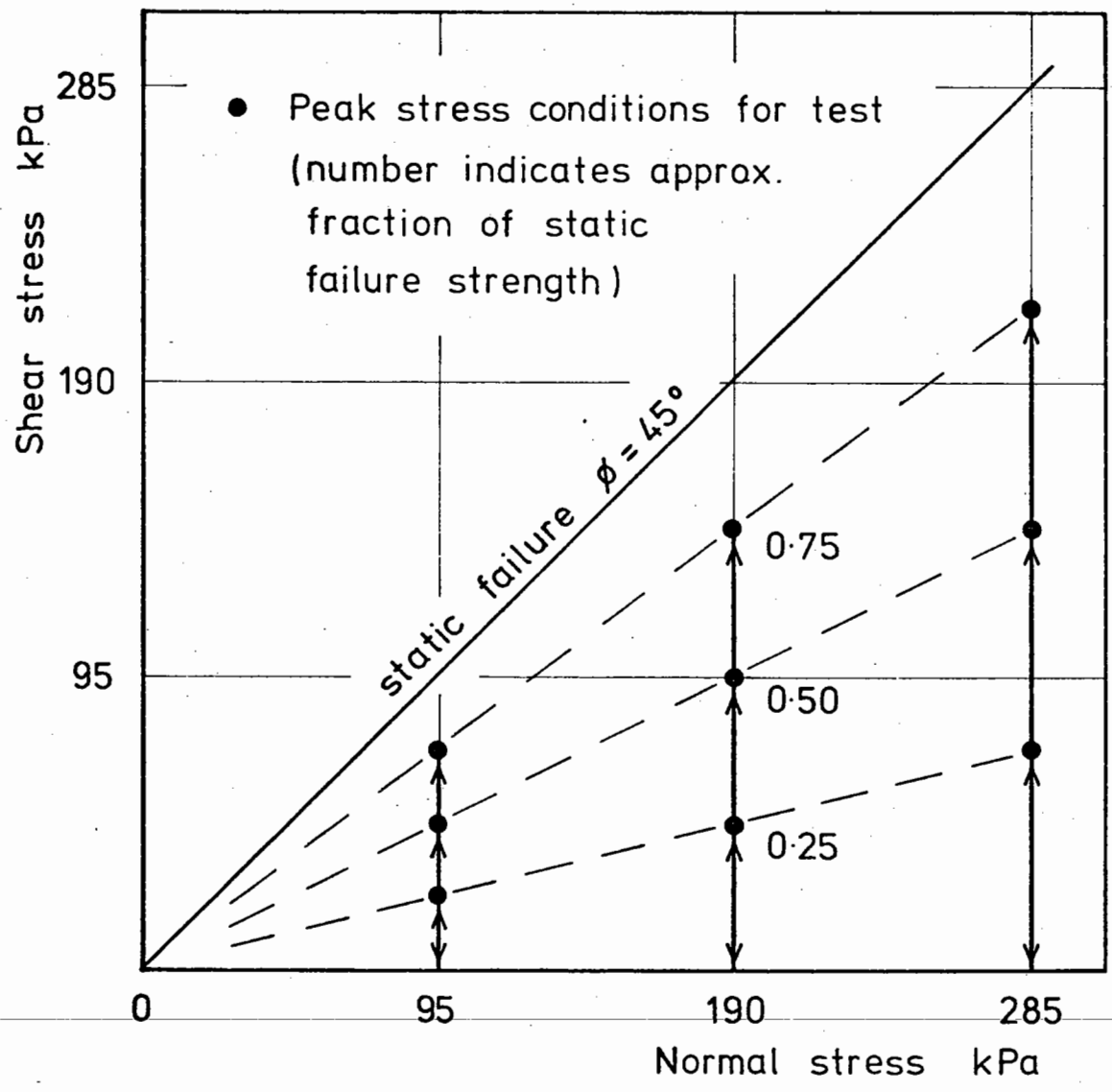

Fig. 33 Stress paths for unidirectional repeated load tests

terms of the cyclic shear stress level measured over the central zone, was difficult to arrange exactly and so the degree of correlation of the test results was also used as an indication of repeatability.

For the Series A tests, the sample was set up as described in Section 4.6 and the Wheatstone Bridge load cell circuits were balanced to give zero initial output. Suitable sensitivities and zero positions were then chosen for the chart recorders. The initial readings for all the transducers were recorded manually. These readings were repeated after the vertical load had been applied and again at the end of the test. These results were used as a check on the deformations indicated by the chart recorders. The recorders were used to monitor the same outputs as for the Series S tests described in Chapter Four. The stress-strain curve on the xy recorder became a hysteresis loop for the repeated load tests. In certain tests, it was impossible to produce a reasonably large loop because of the limiting sensitivity of the xy recorder and so no attempt has been made to analyse the loops on a quantitative basis.

The electronic control box was set so as to actuate only one of the solenoid valves for these tests. The pressure of the air admitted to the shear ram was preset using the precision regulator. With this arrangement, control of the first load cycle was just as good as in the subsequent cycles and this was thought to be useful considering the apparent importance of the first few load cycles as was mentioned in the literature review. Problems with control during the first load cycle have been encountered by various researchers in the Department when using a servo-controlled technique which was developed at Nottingham (18) for repeated load triaxial tests.

The shear stress and shear deformation traces for the first few

load cycles of Test A02 are shown in Fig. 34. A continuous record was taken for the first 20 cycles. Subsequently, several cycles were recorded at suitable intervals on a logarithmic basis. The majority of the Series A tests were of between 10^4 and $3x10^4$ cycles duration, the latter figure representing an overnight test. Several tests were taken to 10^5 cycles to investigate the possibility of a dramatic change in behaviour though none was found. Tests to 10^5 cycles took just over 3 days. A test to 10^6 cycles would have taken over a month and so no tests were taken beyond about 10^5 cycles. Drained repeated load triaxial testing of a Coteau Dolomite ballast material reported by Raymond (62) has also shown no dramatic change in behaviour up to 10^5 cycles. However, similar tests on a sand have shown (63) a sudden increase in the rate of accumulation of permanent axial strain at about 10^4 cycles, particularly at stress levels where the cyclic deviator stress was a large proportion of the deviator stress at failure in a standard triaxial test at the same confining pressure. There was no evidence of this latter type of behaviour in any of the tests reported herein. The behaviour displayed by the sand was presumably caused by the different shape characteristics of the particles.

5.3 Definition of Parameters

In order to be able to analyse and compare the results of the whole repeated load test programme on a common basis, it was necessary to define various parameters to describe the test conditions and the associated response of the material. Fig. 35 shows some of the parameters used for this purpose and reference should also be made to Fig. 34 to see how these parameters can be applied to the actual wave-forms. Fig. 35(a) shows a generalised shear stress pulse in an

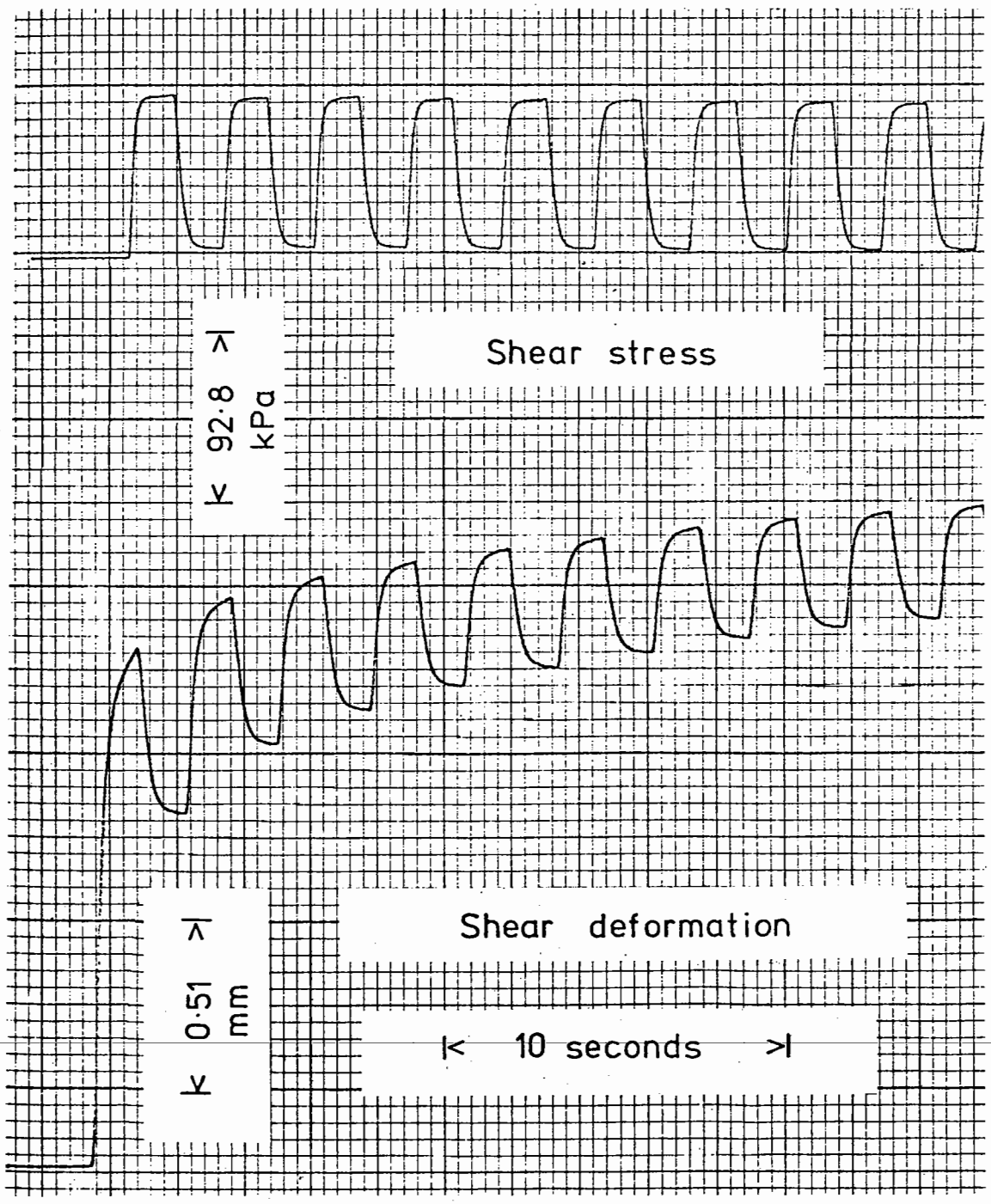

Fig.34 Example of chart recorder trace

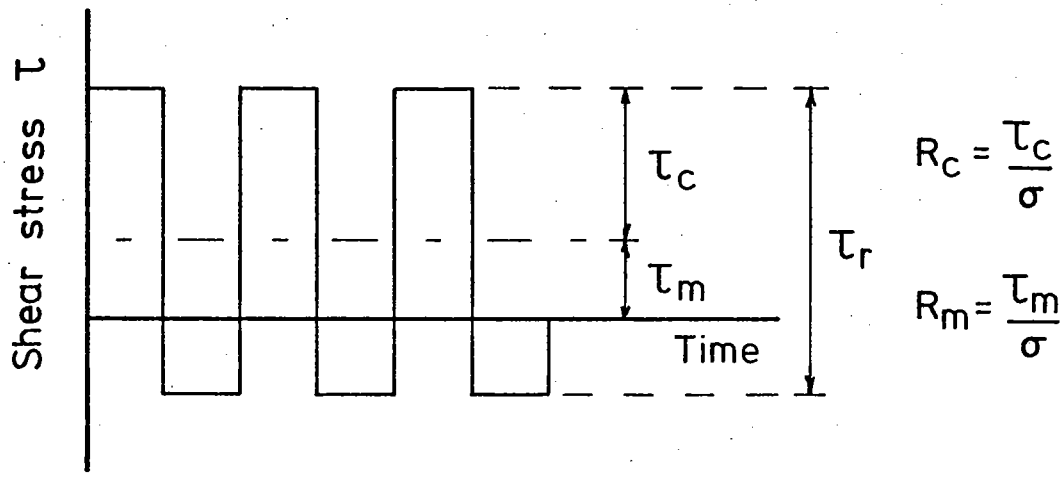

(a) Idealised repeated load waveform

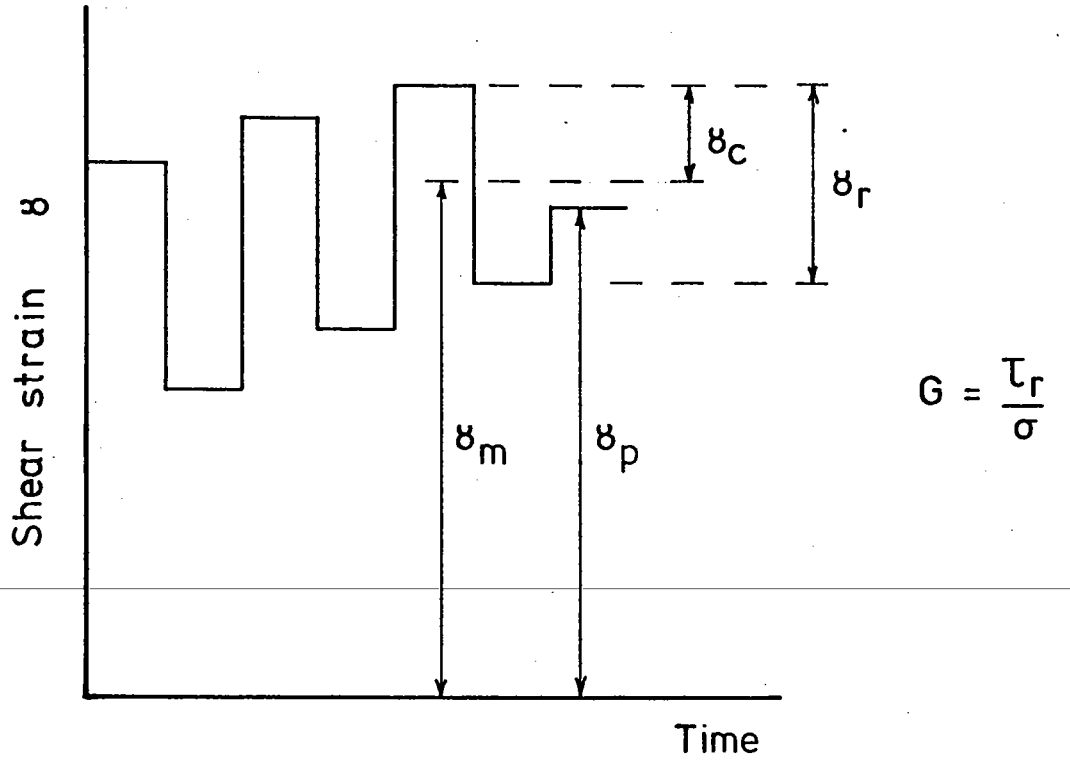

(b) Idealised response to (a)

Fig. 35 Idealised waveforms

idealised form and Fig. 35(b) shows an idealised shear deformation response to this loading.

The shear stress pulse is defined by its mean level, τ_m, and its amplitude which is the cyclic shear stress, τ_c. The double amplitude is referred to as the repeated shear stress, τ_r. This leads to the definition of the mean shear stress ratio, R_m, as τ_m/σ and the cyclic shear stress ratio, R_c as τ_c/σ, where σ is the applied normal stress. The response of the material is divided into two parts: permanent strain and recoverable strain. In the case of shear strain, these components are defined in Fig. 35(b) as γ_p and γ_r respectively. The single amplitude strain, γ_c, is less convenient to use because the mean level, γ_m, is continuously changing. Also, γ_p and γ_r represent the actual physical parameters which could be measured in situ for comparison with the laboratory results. The shear modulus, G, for the material is defined as τ_r/γ_r. Volumetric strains, v_p and v_r, are defined in a manner similar to that used above for the shear strain parameters. Since the plan area of the sample remains constant, the deformation indicated by the vertical LVDT is proportional to the volumetric strain. Compressive volumetric strains are defined as positive. Where it becomes necessary to refer to one of these parameters at a particular stage in a test, the cycle number, N, is placed in parentheses after the parameter, e.g. $R_c(10)$ represents the cyclic shear stress ratio at cycle 10.

With reference to Figs 27(a), 34 and 35, it can be seen that the applied shear load waveform does not correspond to ideal unidirectional loading in which $\tau_c/\tau_m = 1$ since the central shear stress transducer output does not return to zero at the end of each stress pulse. However, the average value of the ratio τ_c/τ_m at cycle 10 for the

Series A tests was 0.77 from which it can be shown that the average residual shear stress at the end of cycle 10 was only 13% of the peak value.

In calculating the strains, the initial sample height has been used to calculate permanent strains and the instantaneous height used for the recoverable strains. This conforms with the method which would have to be used to reduce field data for comparison purposes since the depth of the material would only be monitored at intervals. Theoretically, an integral technique should be used to evaluate permanent strain on a cycle by cycle basis. An approximation to this could be obtained by using an average value for the sample height over a convenient number of cycles, say a decade. However, preliminary calculations showed that this approximation was not worthwhile since the difference between using the approximation and using the initial height was negligible. Consequently, the permanent strains which are reported differ only slightly from the actual strains. In general, the permanent volumetric strains were compressive and so the quoted permanent shear strains are fractionally smaller than the true values.

5.4 Permanent Shear Strain

The general behaviour observed in the Series A tests was for a considerable permanent shear deformation to occur in the first load cycle as was seen in Fig. 34. This was followed by a steadily increasing permanent shear strain which was linear with respect to the logarithm of the number of load cycles as can be seen in Fig. 36, which shows the permanent shear strain data for the Series A tests at each of the three levels of normal stress. Only the decade and final points are plotted though about 30 readings were taken during each test.

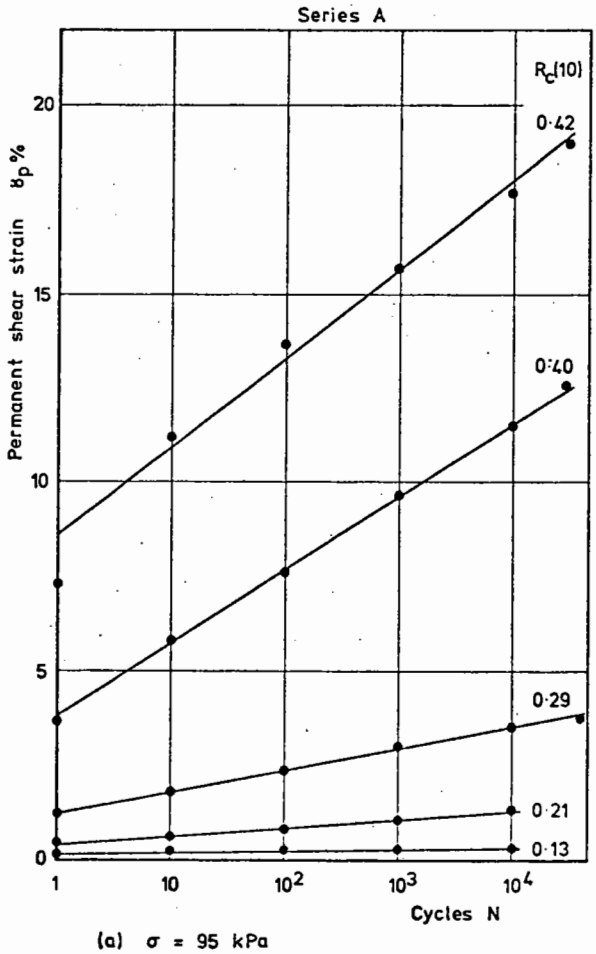

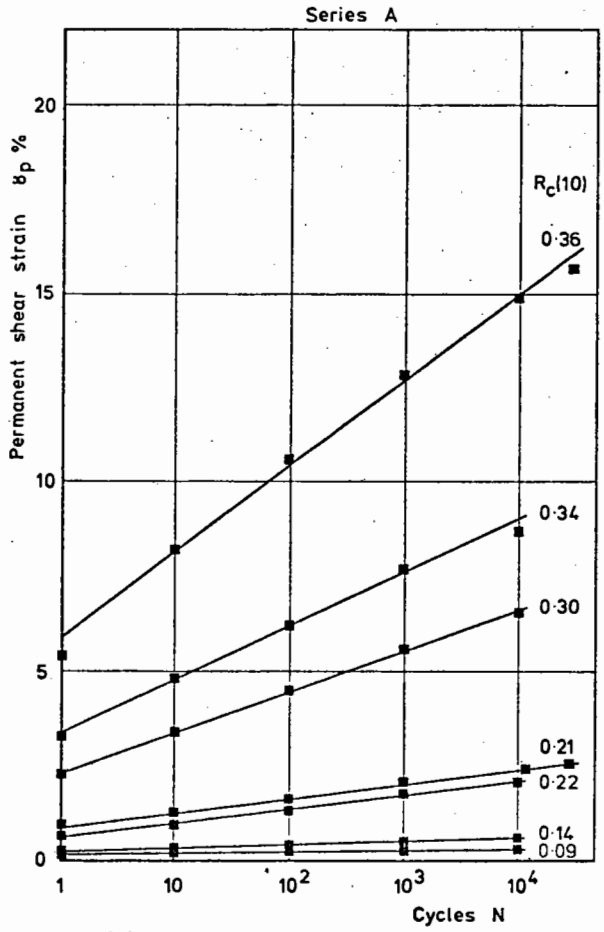

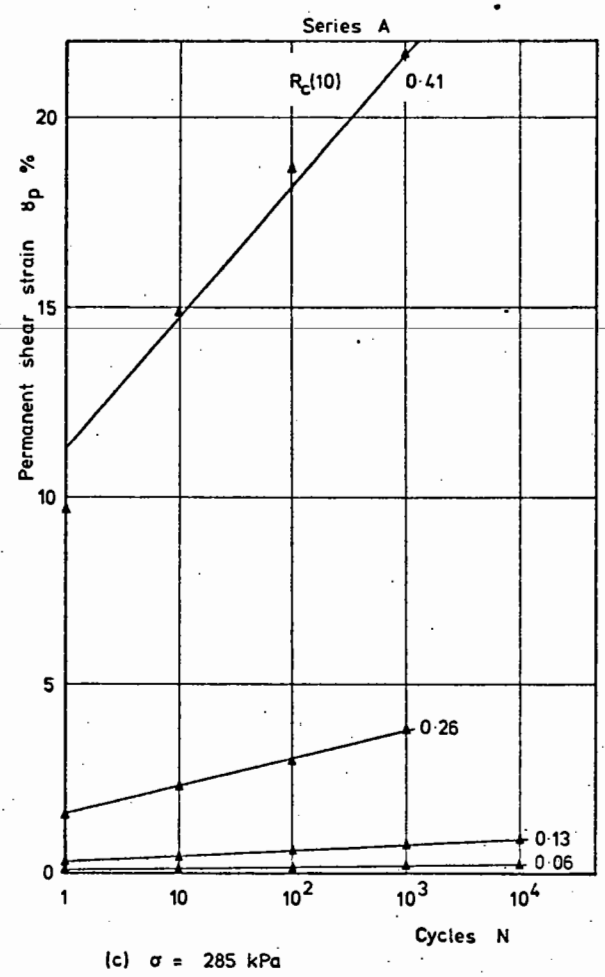

Fig.36 Permanent shear strain results - Series A

The plotted values are also tabulated in Appendix D.

The regression lines shown were fitted to all the readings using a least squares computer program developed for this purpose. The data points were generally a very good fit to the lines; the average coefficient of correlation being 0.9955. As the value of the cyclic shear stress ratio approached 0.5, which represents the static failure strength of the material for unidirectional loading, the relationships tended to depart slightly from linearity. This effect at cyclic stress ratios which are high in relation to the static failure strength, has also been noted by Raymond (62) in triaxial repeated load tests on Coteau Dolomite ballast material.

In Section 4.7.2, it was noted that the sum of the loads indicated by the three shear load cells was less than that applied by the shear ram and a similar situation was observed in the repeated load tests. For the Series A tests, the sum of the shear load cell readings was, on average, 72% of the shear ram load and this was distributed between the three load cells in the ratio 0.38:0.37:0.25 with the highest and lowest values being adjacent to the corners of the shear box which were opening and closing respectively. These figures correspond to the situation at about cycle 1000; they were not constant over the whole test. Hence, during a test the stress ratios R_m and R_c were not constant. In fact, they decreased slightly as the test proceeded, particularly at cyclic shear stress ratios in excess of about 0.4. This partly explains the slight non-linearity of the data points in tests at high cyclic shear stress ratios. The reduction in cyclic shear stress ratio, measured over the central zone, as the test proceeded was probably due partly to a stress redistribution over the length of the sample and partly to an increase in the proportion of the

shear load taken up on the sides and ends of the shear box as the sample compacted (61, 89), thus effectively increasing the value of the K_o coefficient. In view of this, it was necessary to select values for the stress ratios which could be considered as representative of the test conditions. A preliminary evaluation of the correlation between the permanent shear strain and the cyclic shear stress ratio at several points during the Series A tests indicated that the cyclic shear stress ratio at cycle 10, $R_c(10)$, could be used as a representative value and this was adopted for all the repeated load tests.

The regression lines shown in Fig. 36 for the permanent shear strain results can be defined in terms of an intercept, I, with the cycle 1 ordinate and a slope, $\Delta\gamma_p$/decade. A model for the permanent shear strain behaviour has been developed by correlating these parameters with the cyclic shear stress ratio, $R_c(10)$, and details of this are given in Appendix E. The slight effect of the applied normal stress on the permanent shear strain behaviour has been ignored in the development of the model and this is explained in the appendix. The model is of the form:

$$\gamma_p(N) = I + \Delta\gamma_p/\text{decade} \ (\log N)$$

where $$I = 0.05117 \ (204644)^{R_c(10)}$$

and $$\Delta\gamma_p/\text{decade} = 0.03006 \ (67608)^{R_c(10)}$$

The model is only applicable in the range $0.13 < R_c(10) < 0.42$ for reasons which are also given in the appendix. The calculated value of γ_p% should be corrected to 2 significant figures. A graphical representation of the model is given in Fig. 37 and this enables the permanent shear strain after any number of cycles, up to 10^4, to be

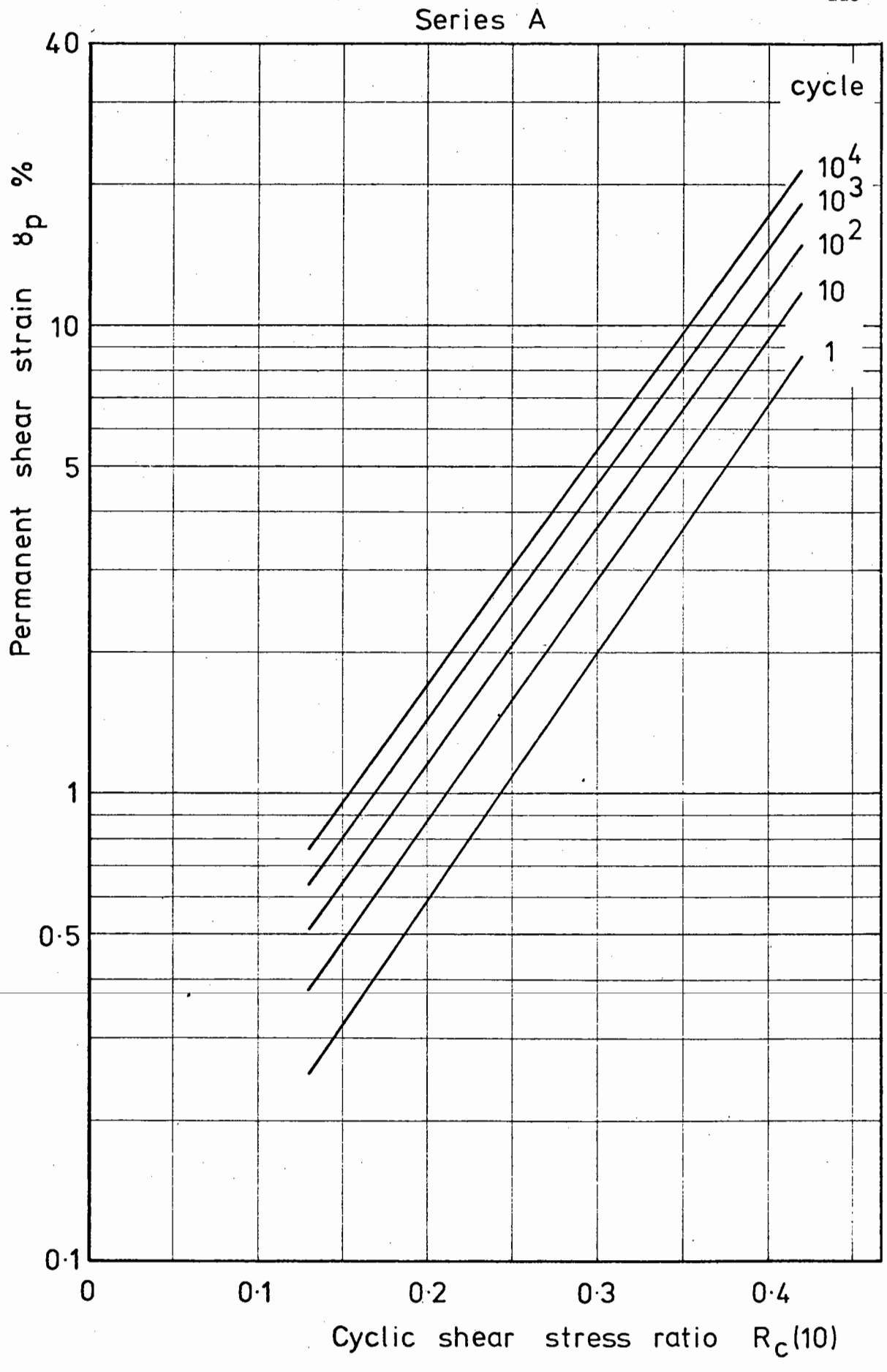

Fig. 37 Model for permanent shear strain based on $R_c(10)$

obtained from the appropriate cyclic shear stress ratio.

The model is of a similar form to that developed by Shenton (73) for permanent axial strain in repeated load triaxial tests and this was described in Section 2.6. A directly analogous model would be of the form:

$$\gamma_p(N) = \gamma_p(1)(1 + C\log N)$$

where C is a constant. However, although the model described above can be expressed in this form, the value of C is not constant. It can be seen that the reciprocal of the coefficient C is equal in magnitude to the intercept of the permanent shear strain line with the abscissa and is thus quite sensitive to small variations in the experimental results.

A comparison of the permanent shear strain model with some of the test data is shown in Fig. 38. In general, the model is more accurate for the intermediate level of normal stress at low to medium cyclic shear stress ratios; $0.13 < R_c(10) < 0.32$. This is due partly to the slight effect of normal stress on the permanent shear strain behaviour referred to earlier and partly to the sensitivity of the logarithmic scales used to develop the model. Fig. 39 is a development of Fig. 37 and is an alternative method of presentation for repeated load test results in the form of a strain contour chart. Further reference to this type of chart is made in Chapter Seven where the block load test results are considered. A more comprehensive model for the permanent shear strain behaviour is described following the presentation of the recoverable shear strain results.

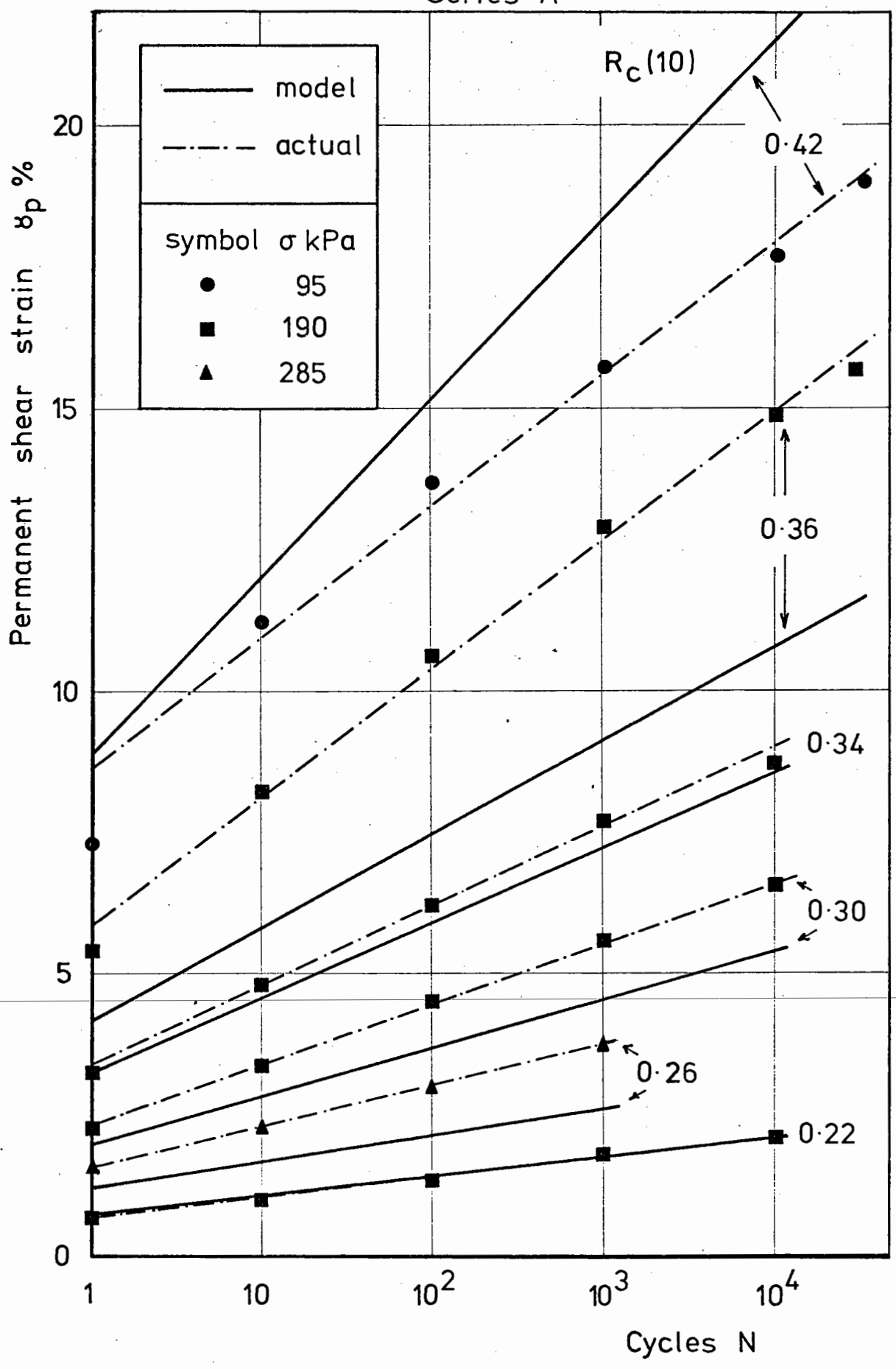

Fig. 38 Comparison of permanent shear strain results with model based on $R_c(10)$

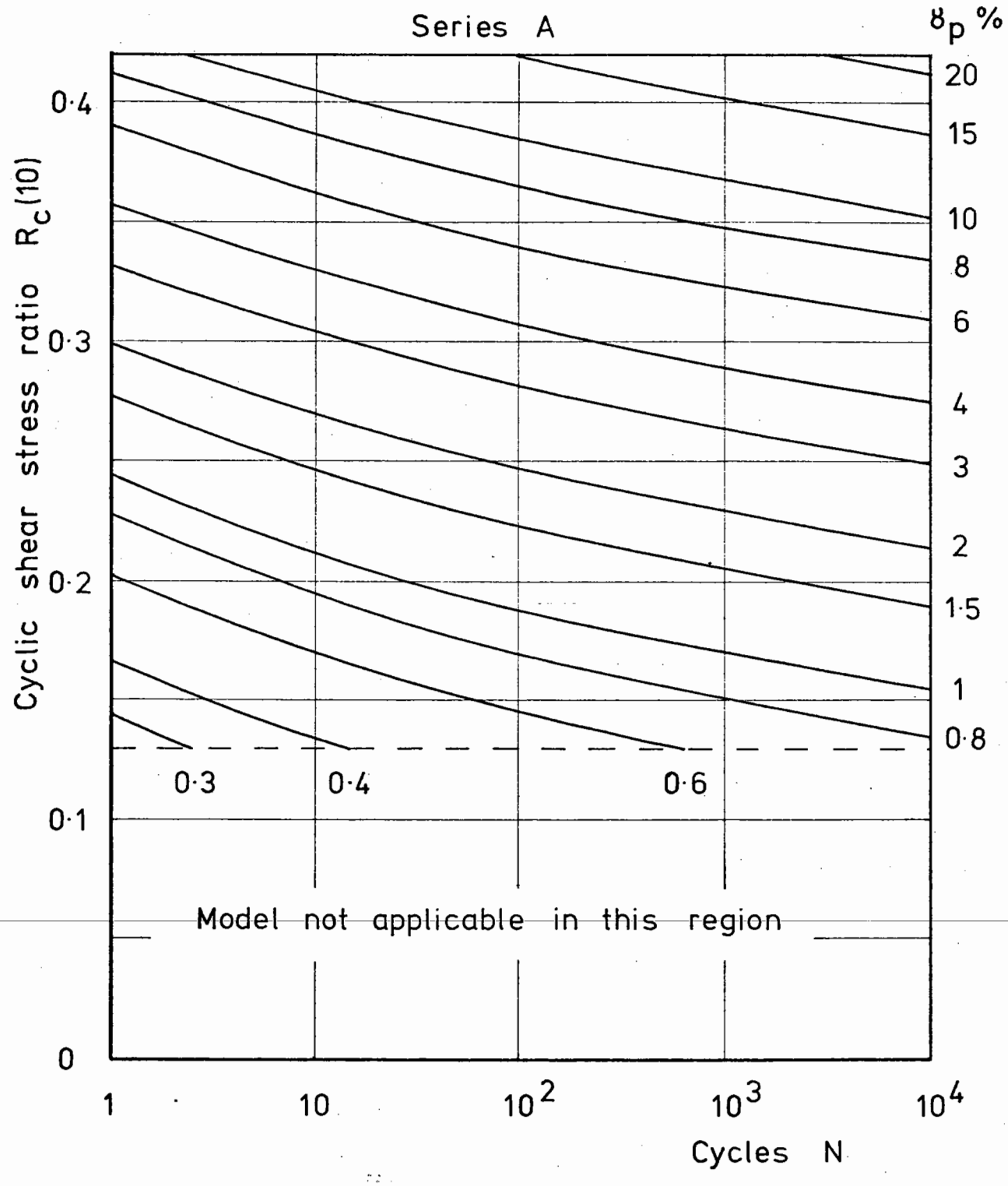

Fig. 39 Permanent shear strain contour chart based on $R_c(10)$

5.5 Recoverable Shear Strain

The recoverable shear strain data for the Series A tests is shown in Fig. 40. At low cyclic shear stress ratios, the recoverable shear strain quickly settled down to a value which subsequently decreased only very slowly. At higher cyclic shear stress ratios, the initial recoverable shear strain was 2 or 3 times its value after 10^4 cycles and the settling down period was much longer; up to 10^4 cycles or more. It can be seen from the model which is developed in Appendix F that the recoverable shear strain does not actually reach a constant value at any stage although the rate of decrease does eventually become extremely small. The model has been developed by correlating the recoverable shear strain results with the cyclic shear stress ratio and it is shown in Fig. 41. The range of applicability is $0.06 < R_c(10) < 0.42$ which is the range of the test data. The model can be represented mathematically in the form:

$$\log \gamma_r(N) = (A + B\log N + C\log^2 N + D\log^3 N + E\log^4 N)R_c(10) - 0.804$$

where $A = 2.848$ $B = -0.554$ $C = 0.140$

$D = -0.022$ $E = 0.0016$

The calculated value of $\gamma_r\%$ should be corrected to 2 significant figures.

Fig. 41 can be used to predict the recoverable shear strain curve for unidirectional repeated loading by plotting the decade points and joining them with a smooth curve. This technique has been used to prepare Fig. 42 which shows a comparison of the model with some of the test data. For reasons similar to those outlined in Section 5.4, this model is also more accurate for low to medium cyclic shear stress ratios at the intermediate level of normal stress.

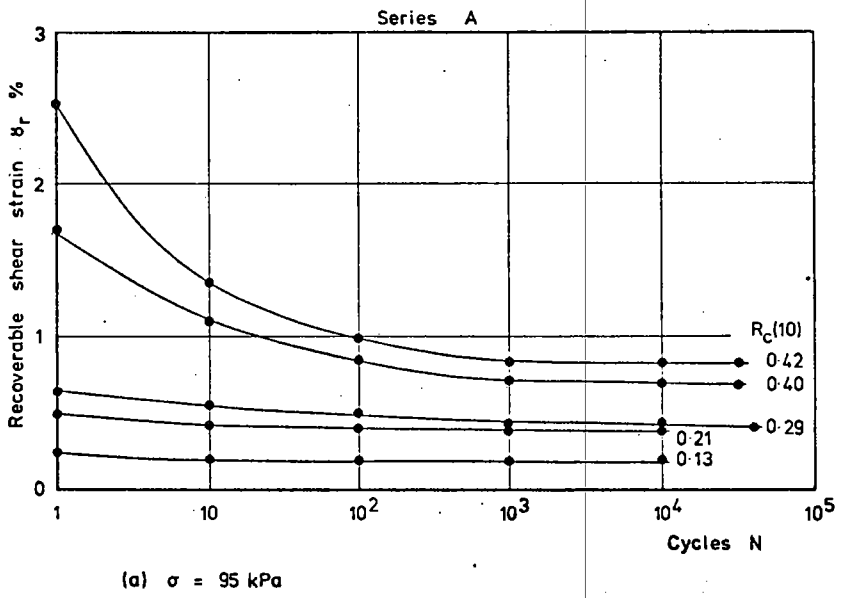

(a) σ = 95 kPa

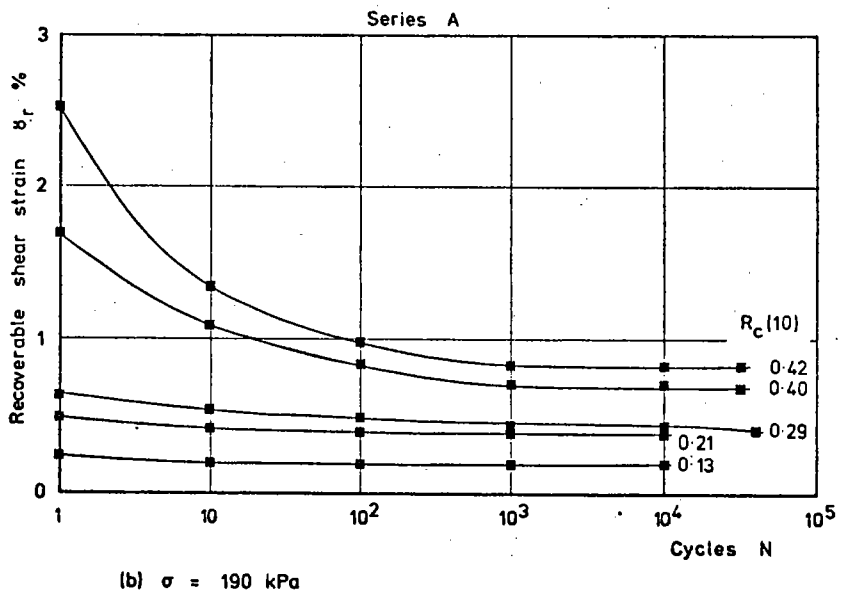

(b) σ = 190 kPa

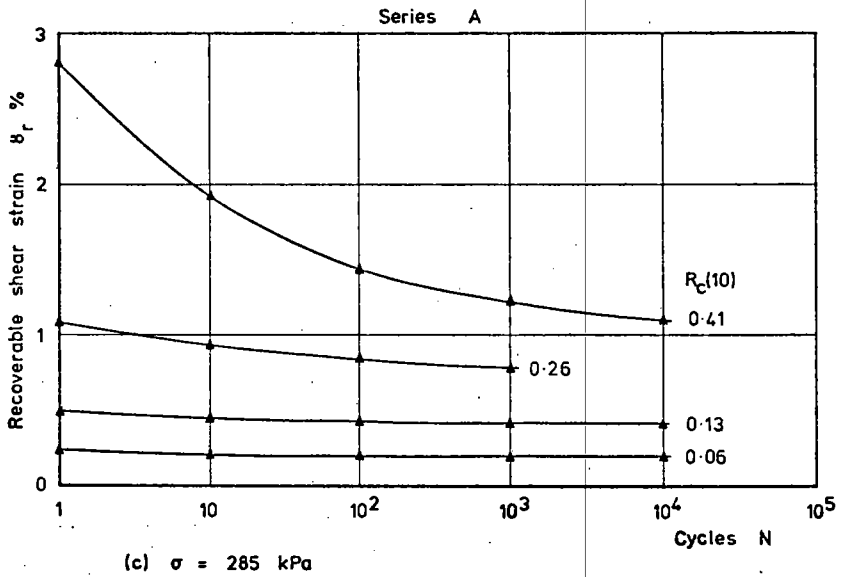

(c) σ = 285 kPa

Fig. 40 Recoverable shear strain results - Series A

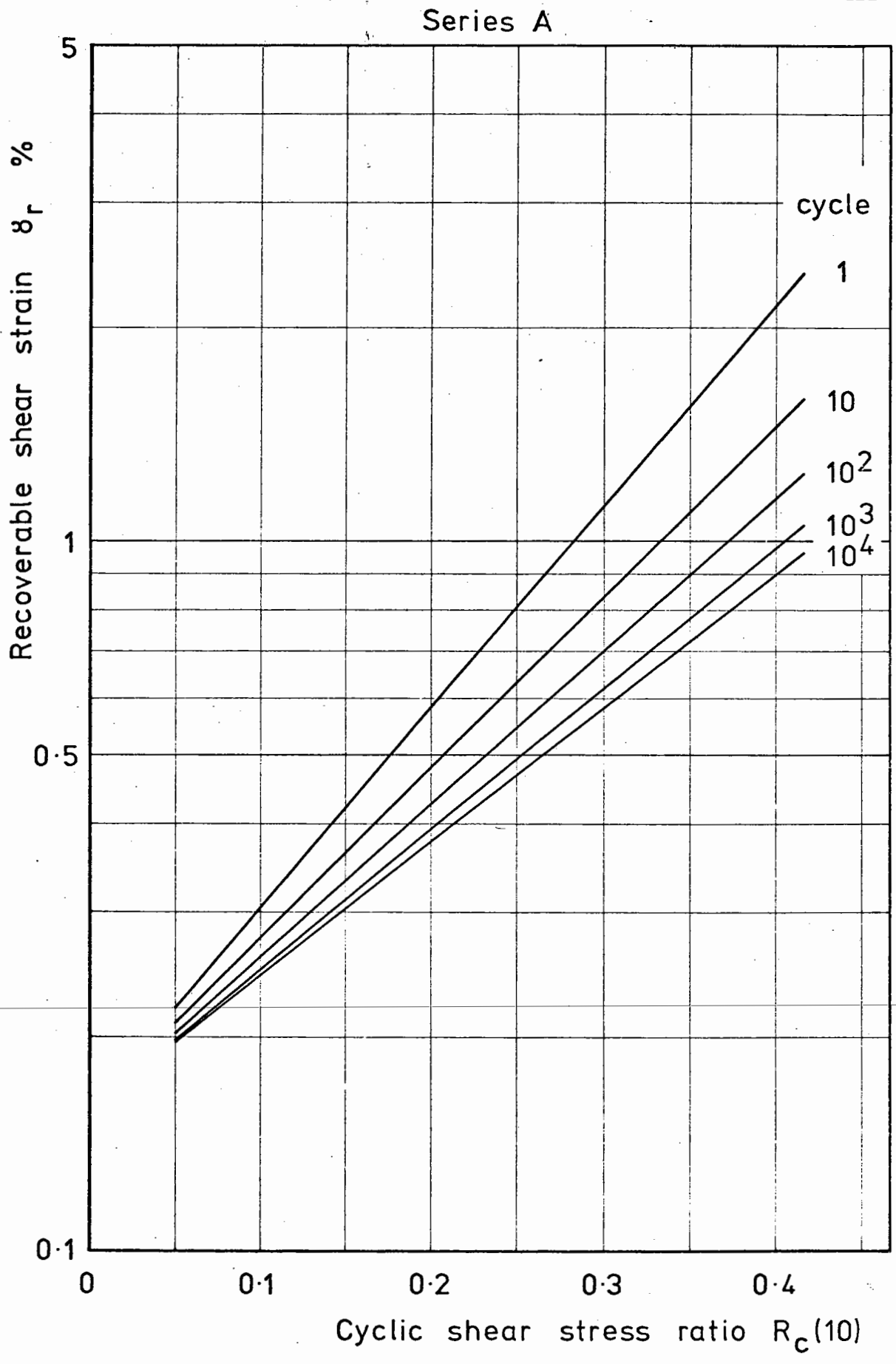

Fig. 41 Adjusted model for recoverable shear strain

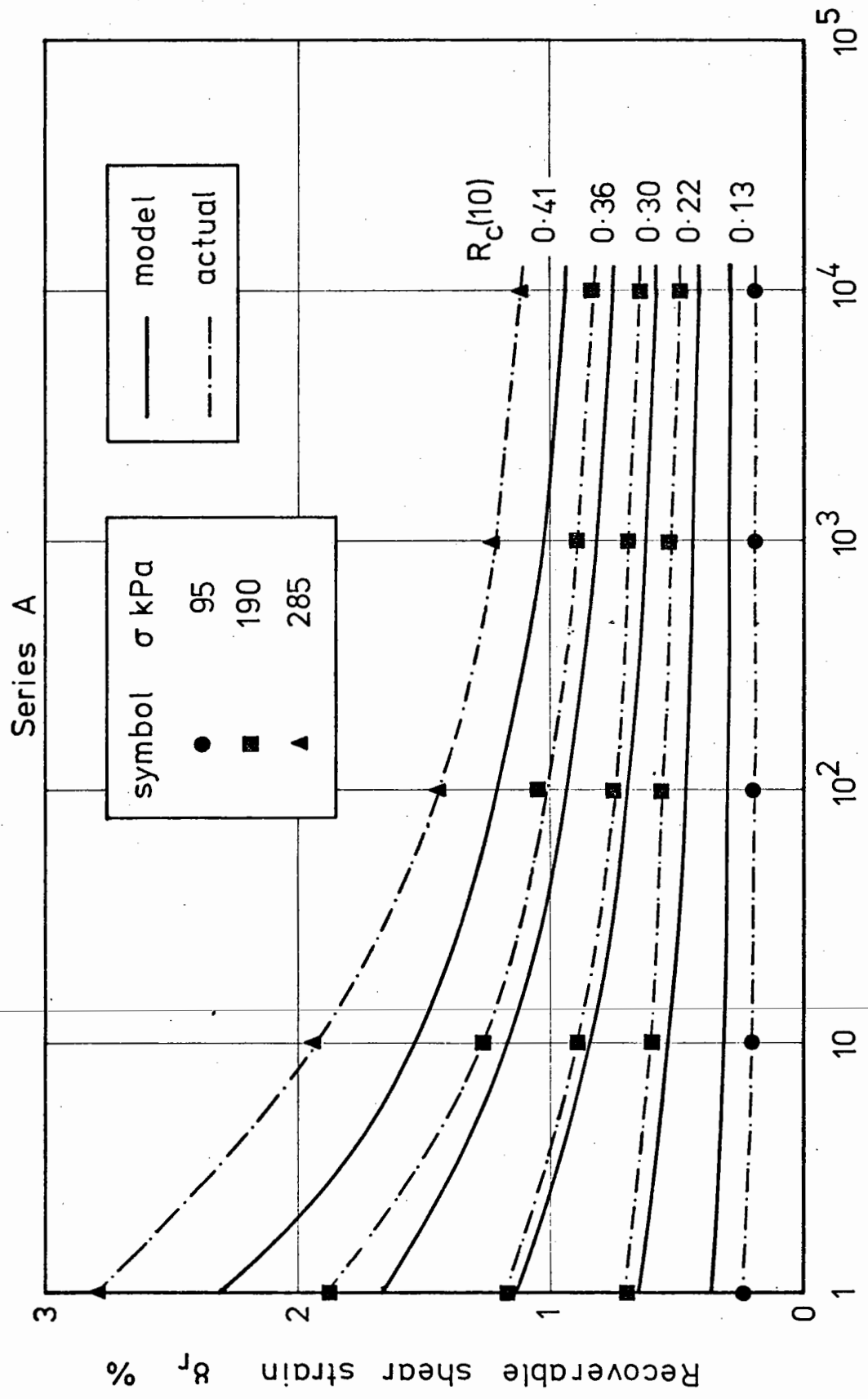

Fig.42 Comparison of recoverable shear strain results with model based on Series A

5.6 Complete Shear Strain Model for Unidirectional Repeated Load

In Appendix G, another permanent shear strain model is developed by correlating the permanent shear strain parameters, I and $\Delta\gamma_p$/decade, with the initial recoverable shear strain. The model is of the form:

$$\gamma_p(N) = I + \Delta\gamma_p/\text{decade} \ (\log N)$$

where $$I = 1.65577 \ (\gamma_r(1))^{1.756}$$

and $$\Delta\gamma_p/\text{decade} = 0.63241 \ (\gamma_r(1))^{1.952}$$

The model is applicable in the range $0.2\% < \gamma_r(1) < 3\%$ and the calculated value of $\gamma_p\%$ should be corrected to 2 significant figures. A graphical representation of this model is given in Fig. 43 and this enables the permanent shear strain after any number of cycles, up to 10^4, to be obtained from the appropriate initial recoverable shear strain.

A comparison of the model with some of the test data is shown in Fig. 44 and this shows that there is some improvement using this model at low to medium initial recoverable shear strains compared with the model described in Section 5.4. This model is also rather inaccurate at higher recoverable shear strains. However, these would be beyond the practical range since permanent shear strains of the order of 10% in the first 10 cycles would almost certainly be unacceptable. A strain contour chart, developed from Fig. 43, is shown in Fig. 45 and further reference is made to this type of chart in Chapter Seven.

From Figs 41 and 43, it can be seen that a mutual correlation exists between the cyclic shear stress ratio, the recoverable shear strain and the parameters I and $\Delta\gamma_p$/decade which define the permanent shear strain behaviour. It is possible, therefore, to combine Figs

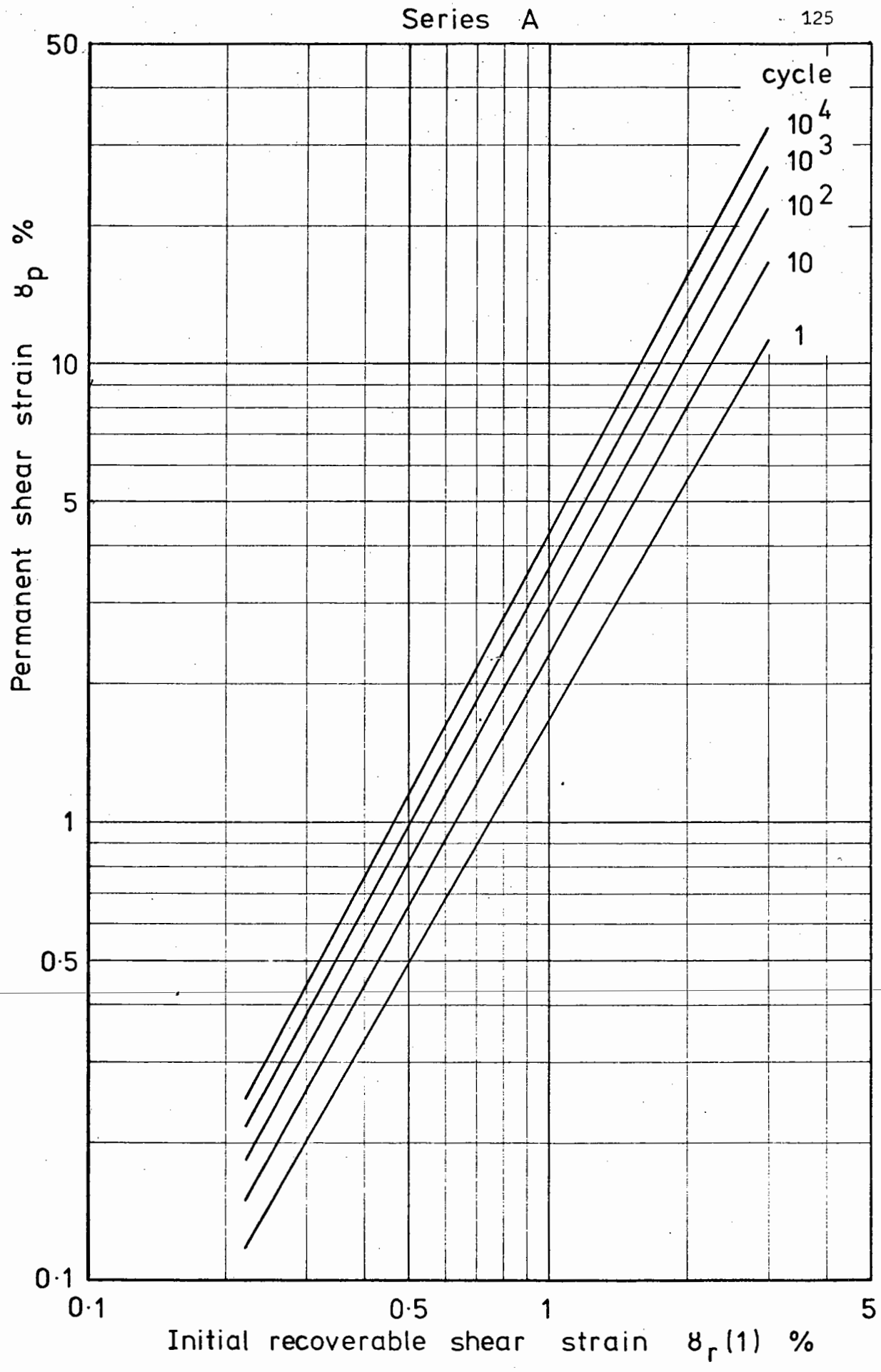

Fig. 43 Model for permanent shear strain based on $\gamma_r(1)$

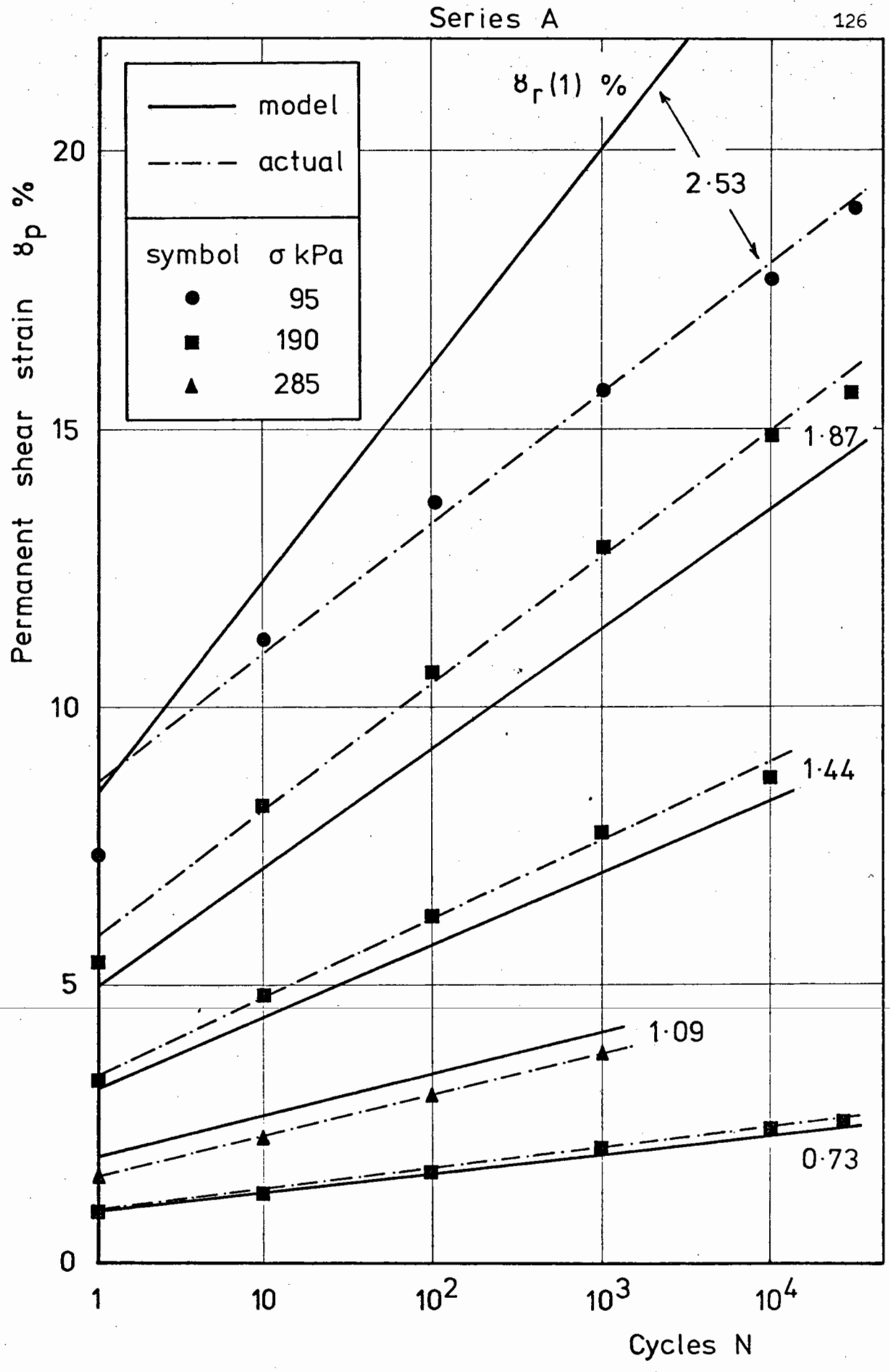

Fig.44 Comparison of permanent shear strain results with model based on $\gamma_r(1)$

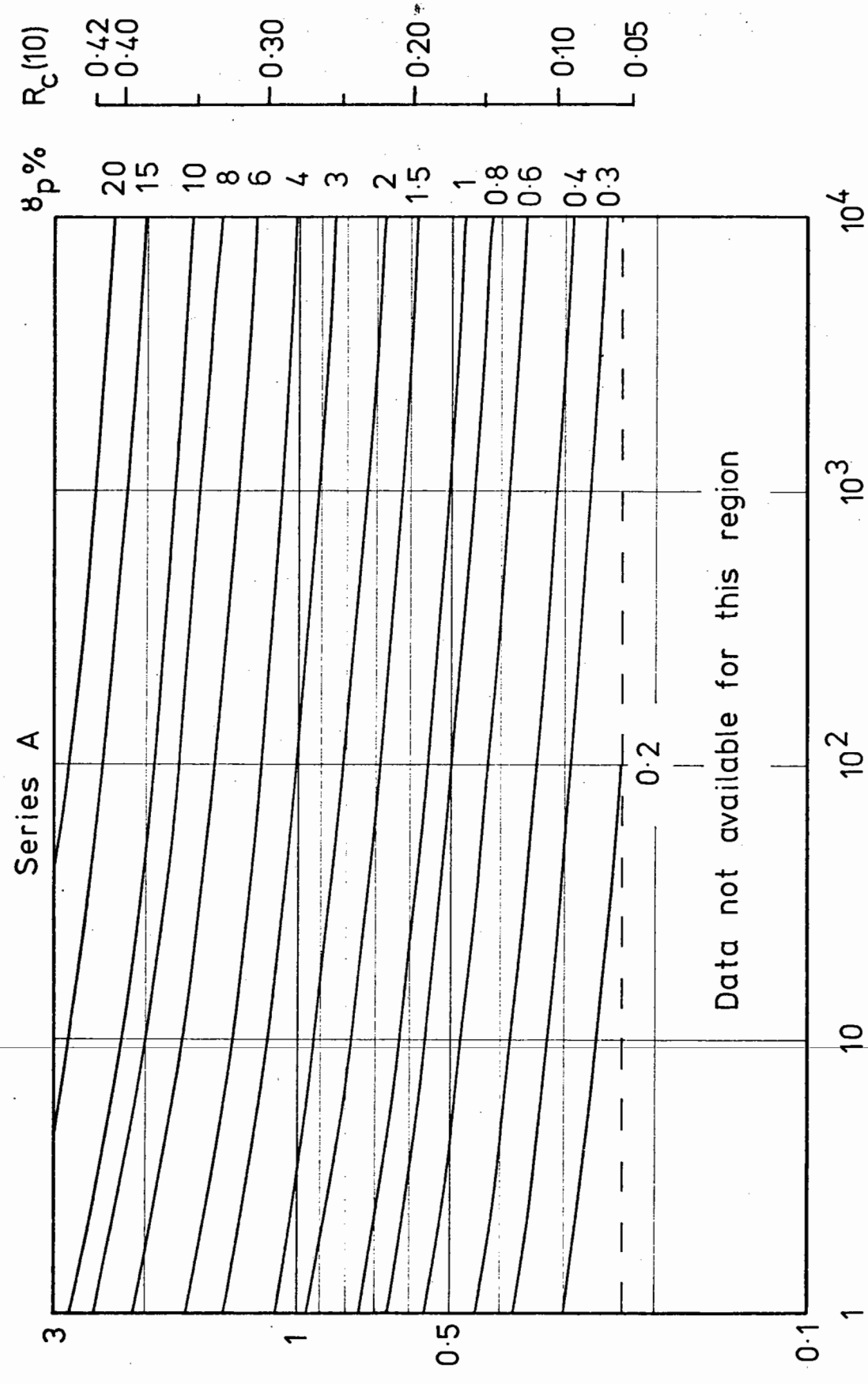

Fig. 45 Permanent shear strain contour chart based on $\gamma_r(1)$

41 and 43 to form a complete shear strain model, Fig. 46. An example of the use of this complete model is superimposed on the diagram. The transfer line between the two sections of the chart is the $\gamma_r(1)$ line since this was used to develop the model in Appendix G. However, a value for the recoverable shear strain after any number of load cycles may be used by moving across the lower section of the chart along the appropriate $R_c(10)$ line to meet the transfer line as shown in Fig. 46. If, for example, a value for the recoverable shear strain was available from an elastic analysis, this could be used as an equilibrium value and the chart entered to meet the γ_r (10^4) line. By moving horizontally to the $\gamma_r(1)$ line and then vertically upwards into the upper half of the chart, the permanent shear strain behaviour could be predicted. This combined model can also be used to predict the permanent shear strain and recoverable shear strain behaviour from the cyclic shear stress ratio. It would be similarly possible to use Figs 41 and 45 in conjunction to allow the permanent shear strain contour chart to be used with any recoverable shear strain value or the applied cyclic shear stress ratio. An equivalent linear scale for cyclic shear stress ratio has been added to Fig. 45 to illustrate this possibility.

It is important to note, however, that the combined model shown in Fig. 46 has been developed from the same data as the model described in Section 5.4 and the overall accuracy of the combined model is controlled by the same data. This means that, although the permanent shear strain model based on the initial recoverable shear strain, Fig. 43, is more accurate over a greater range than the model based on the cyclic shear stress ratio, Fig. 37, the overall accuracy of the combined model can be no better than that of the model developed in Section 5.4 when the cyclic shear stress ratio is used as the starting

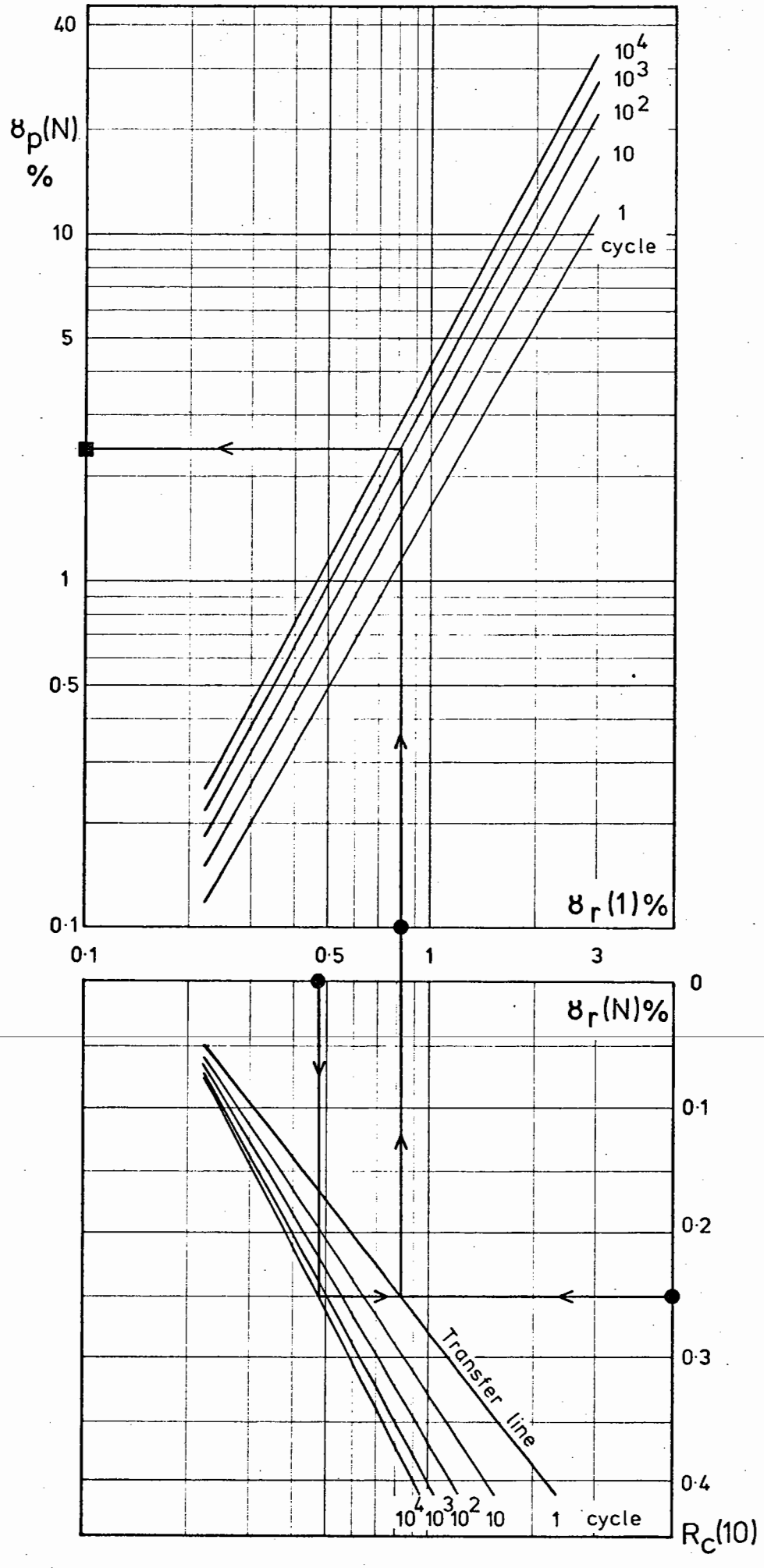

Fig. 46 Complete shear strain model for unidirectional repeated load

point. Similar comments apply to the use of Fig. 41 in conjunction with Fig. 45 referred to in the previous paragraph.

The reason for the improved accuracy of the model based on the initial recoverable shear strain is probably that all the parameters involved are obtained as average values over the whole sample whereas the cyclic shear stress ratio used to develop the previous model is a local value obtained from the central third of the sample. Suggestions for further work to investigate this are discussed in Chapter Nine.

5.7 Permanent Volumetric Strain

The permanent volumetric strain behaviour for the Series A tests is shown in Fig. 47. The overall effect was for the material to compact steadily even though the initial density was thought to be quite high. The shear straining appears to produce further compaction even under a constant vertical load. In general, a considerable proportion of the overall permanent volumetric strain occurred in the first cycle. However, at cyclic shear stress ratios in excess of about 0.35, dilation occurred in the first cycle though the subsequent behaviour was similar to that observed in tests at lower stress ratios. This dilation can be attributed to the large shear strains occurring in the first load cycle of these tests. This indicates the existence of an optimum cyclic shear stress ratio for compaction of the material by this type of loading. If dilation occurs in the first load cycle, then the process of compaction is severely disrupted. It can also be seen that compaction is assisted by increased vertical loading at a given cyclic shear stress ratio. At low cyclic shear stress ratios there was some evidence of the material reaching a limiting density. This indicates that, at high cyclic shear stress ratios, some

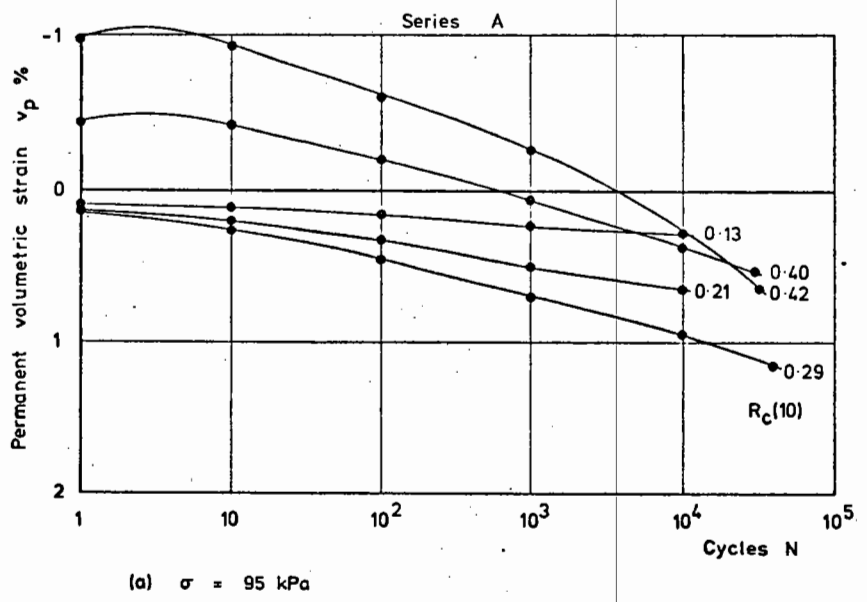

(a) σ = 95 kPa

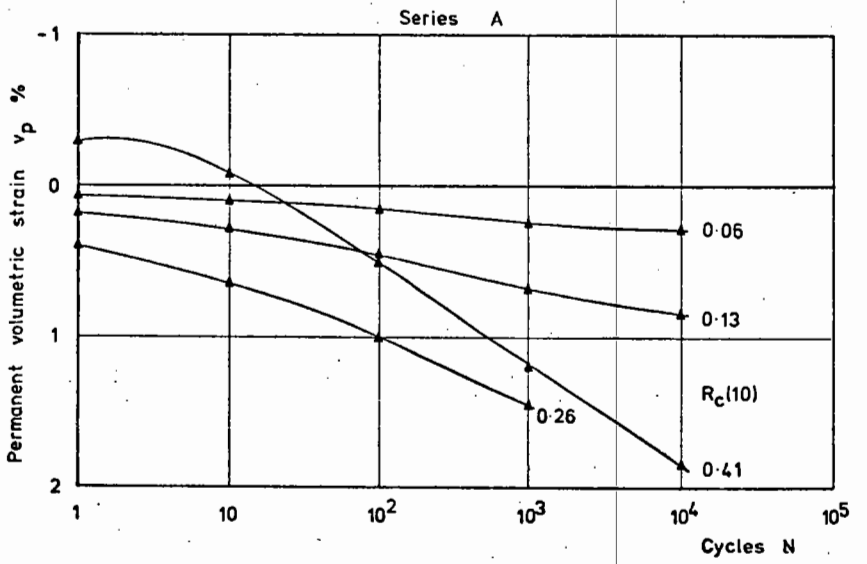

(c) σ = 285 kPa

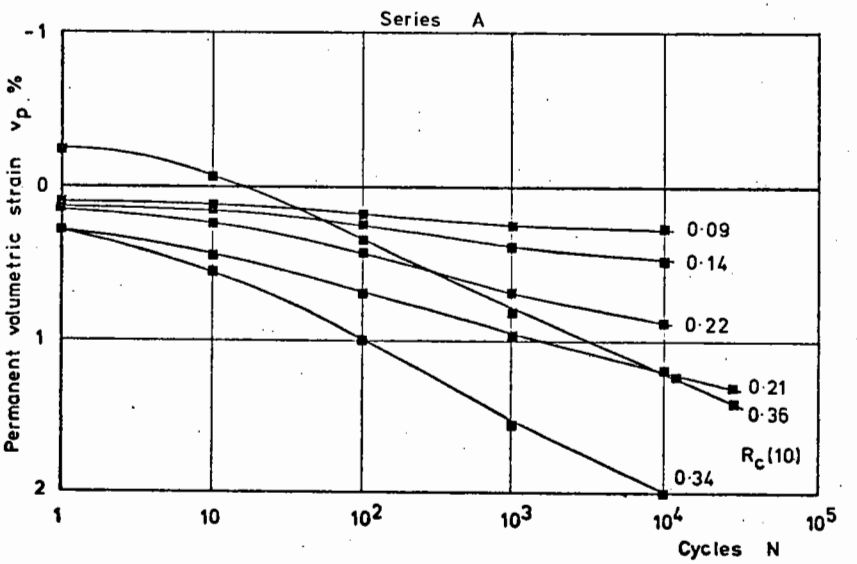

(b) σ = 190 kPa

Fig.47 Permanent volumetric strain results - Series A

degradation of the particles must occur to allow continuing compaction. There was some evidence of degradation on the corners of the particles after testing at high cyclic shear stress ratios but this was not studied quantitatively because of experimental difficulties. The maximum value of permanent volumetric strain in the Series A tests was about 2%. This represents a reduction in porosity from 0.40 to 0.39 or 2.5%.

Due to the different type of response above and below the optimum cyclic shear stress ratio, it has not been possible to develop a model for the permanent volumetric strain behaviour. However, the results have shown the importance of knowing whether dilation is likely to affect the behaviour of the material when subjected to unidirectional repeated load.

5.8 Recoverable Volumetric Strain

Fig. 48 shows the recoverable volumetric strain behaviour observed in the Series A tests and it can be seen that it was dilatant throughout. The curves are of a similar type to those for the recoverable shear strain behaviour; showing a relatively high initial value settling down to an approximately constant value which depended on the cyclic shear stress ratio. Higher stress ratios produced correspondingly higher recoverable volumetric strains.

A model for the recoverable volumetric strain is developed in Appendix H by correlating the results with the cyclic shear stress ratio and this is shown in Fig. 49. The model can be represented mathematically in the form:

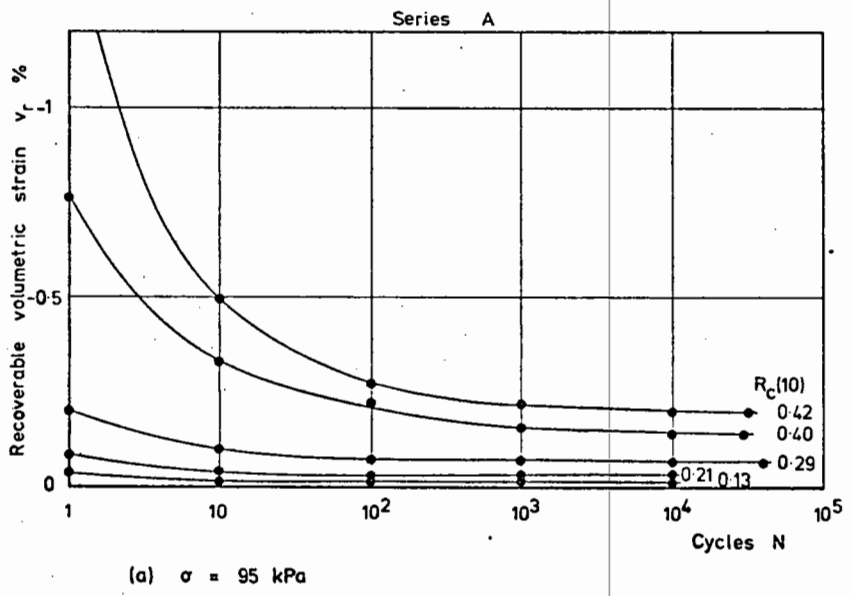

(a) σ = 95 kPa

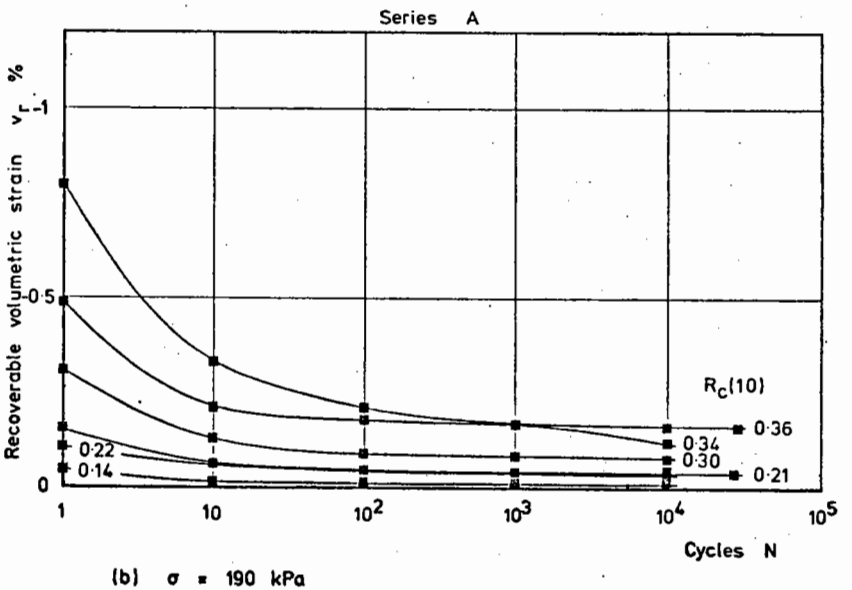

(b) σ = 190 kPa

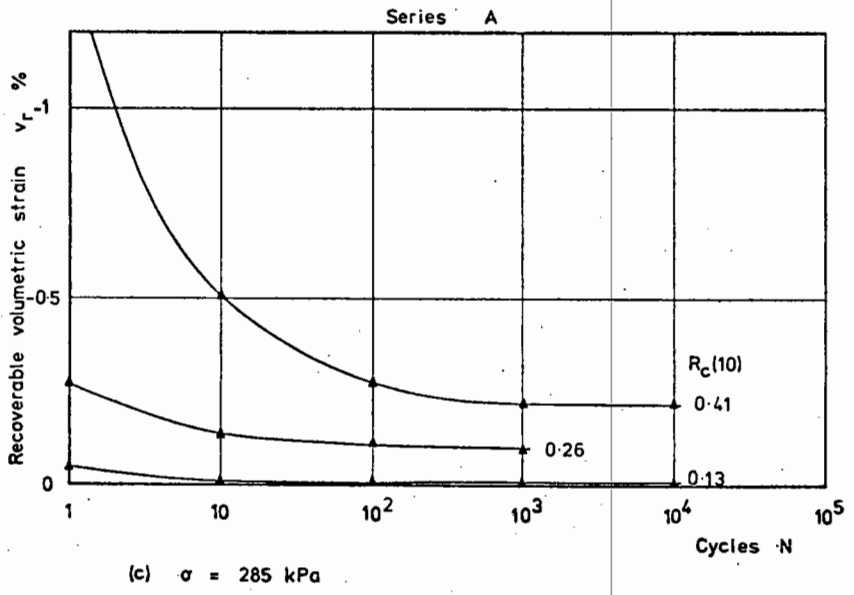

(c) σ = 285 kPa

Fig. 48 Recoverable volumetric strain results - Series A

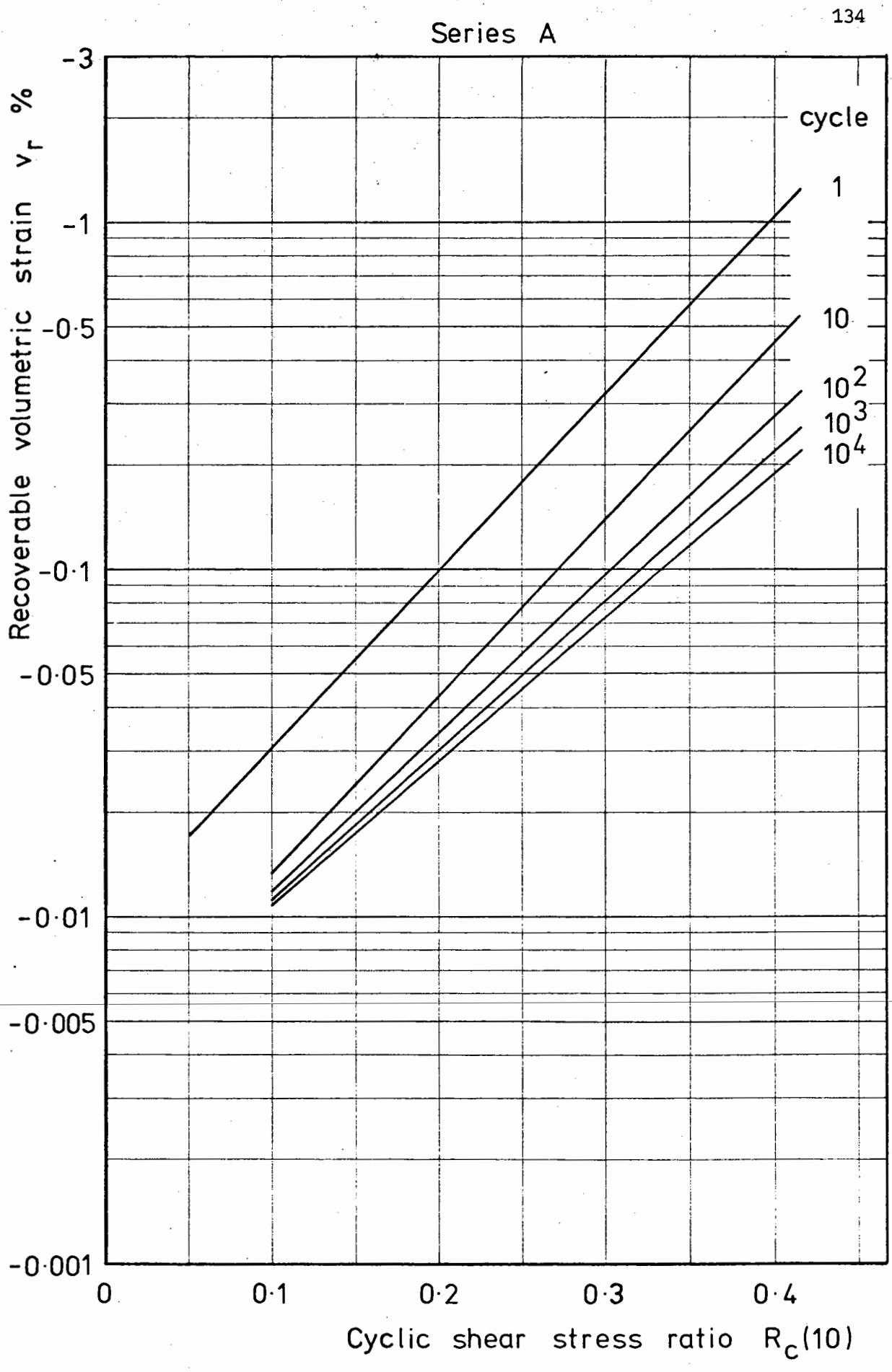

Fig. 49 Adjusted model for recoverable volumetric strain

For the first cycle:

$$\log v_r(1) = 5.097\, R_c(10) - 2.022$$

where $0.06 < R_c(10) < 0.42$

and for cycle 10 onwards:

$$\log v_r(N) = (A + B\log N + C\log^2 N + D\log^3 N)R_c(10) - 2.385$$

where $A = 6.150$ $B = -1.382$ $C = 0.368$ $D = -0.037$

and $0.10 < R_c(10) < 0.42$

The reasons for the discontinuous nature of the model are given in the appendix. The calculated value of v_r% should be corrected to 2 significant figures and the sign convention considered since the calculated value of v_r will always be positive.

A comparison of some of the test data with the model is shown in Fig. 50. Although it is not readily apparent from the examples shown, this model suffers inaccuracies from the same sources as the other models presented in this chapter.

5.9 Shear Modulus

In Section 5.3, the shear modulus, G, was defined as τ_r/γ_r and this has been used to calculate the values of shear modulus presented herein. The consequences of using a local value of shear stress, from the central third, and an overall or average value for the shear strain is discussed later in this section.

The variation of the shear modulus of the material during the Series A tests is shown in Fig. 51. Only the decade and final point values have been evaluated and these have then been connected by

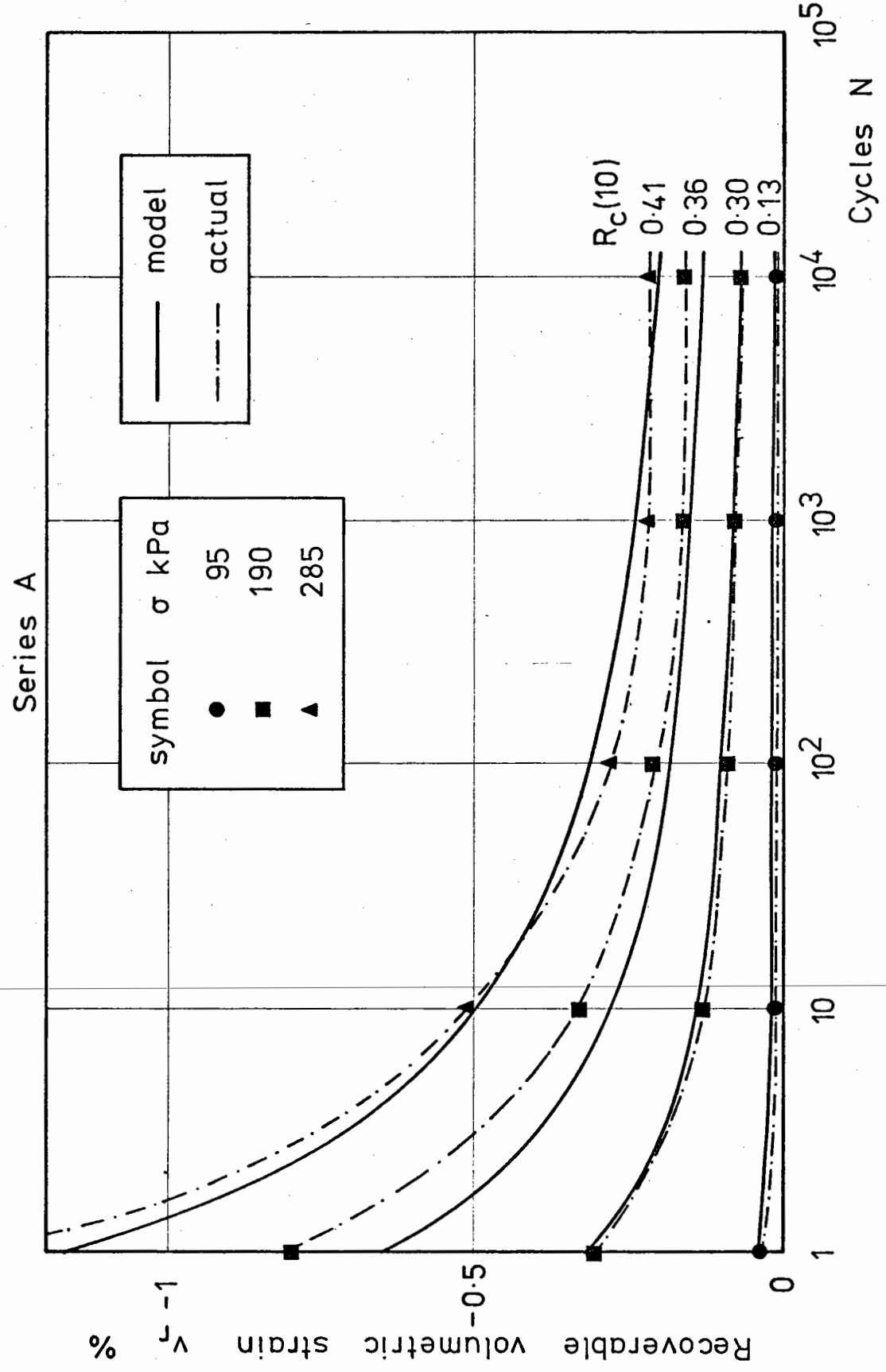

Fig.50 Comparison of recoverable volumetric strain results with model

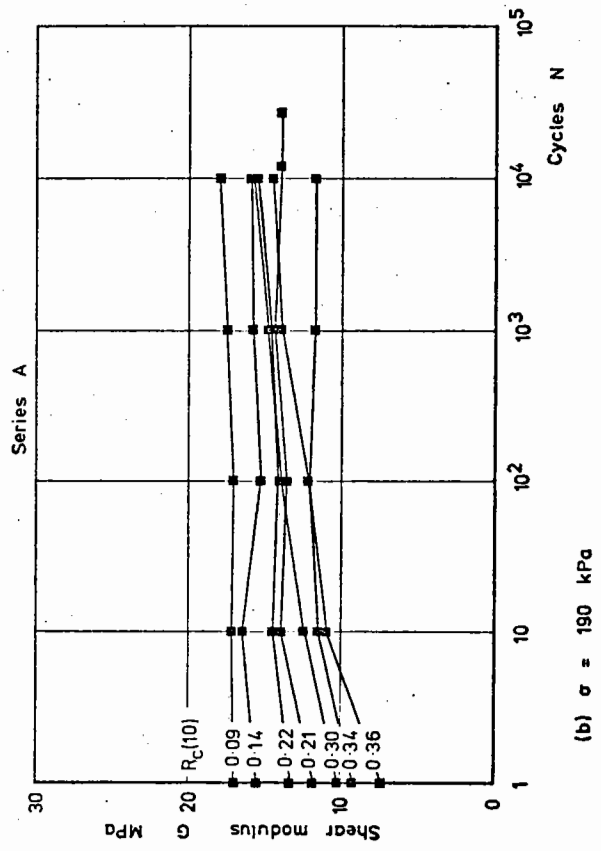

(b) σ = 190 kPa

Fig. 51 Shear modulus - Series A

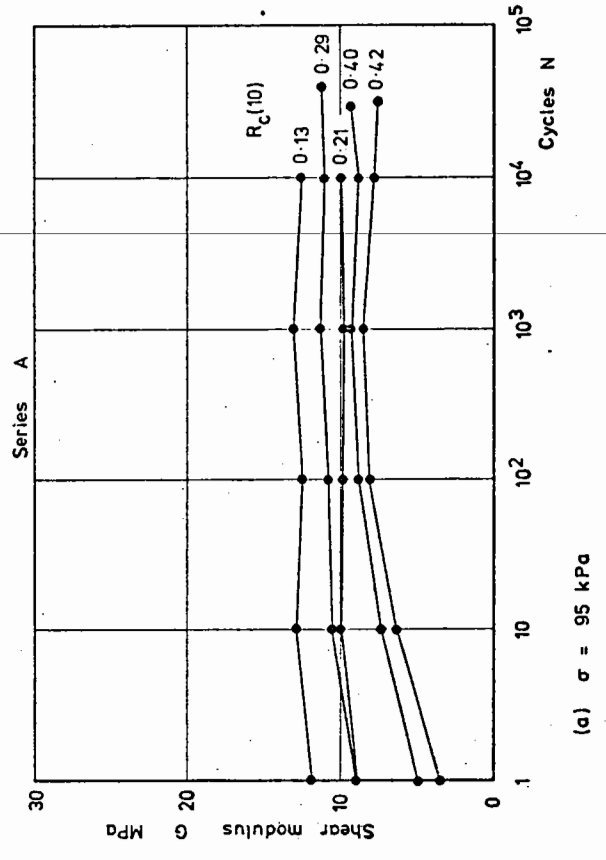

(a) σ = 95 kPa

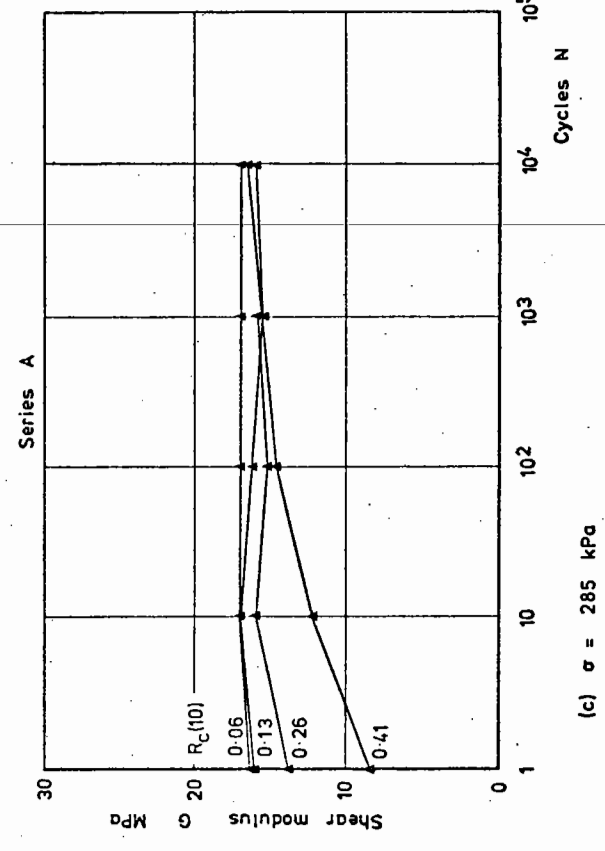

(c) σ = 285 kPa

straight lines. Fig. 51(c) shows the general trend most clearly. At low cyclic shear stress ratios the shear modulus remains approximately constant throughout the test. With increasing values of cyclic shear stress ratio, a lower initial shear modulus was observed followed by an increase to reach an equilibrium value after several hundred cycles. These lower initial shear moduli correspond with an increasing amount of dilation in the first load cycle which tends to soften the material. The subsequent compaction is indicated by the stiffening of the material. This stiffening during the first few cycles can be seen in Fig. 52 which shows a trace from the xy recorder. The accumulation of permanent shear strain can also be clearly seen. It is interesting to note that the hysteresis loop, after settling down, is practically symmetrical in contrast to the banana-shaped hysteresis loop obtained by Boyce (9) from repeated load triaxial tests on well graded samples of the same material. However, the stress conditions in the two types of test were completely different and direct comparison is perhaps not really appropriate.

There is a considerable degree of scatter in the equilibrium values of shear modulus shown in Fig. 51 but there is evidence to show dependency on the cyclic shear stress ratio and the applied normal stress. This evidence is presented and further discussed in Section 6.12 along with the results from the Series B and C repeated load tests.

Since a constant repeated shear load was being applied to the shear box, it would appear that the shear modulus behaviour should be directly related to the recoverable shear strain because the shear modulus has been defined as τ_r/γ_r. Thus, the shear modulus was calculated using an instantaneous local cyclic shear stress and an instantaneous average shear strain. Although the trend of the recoverable shear

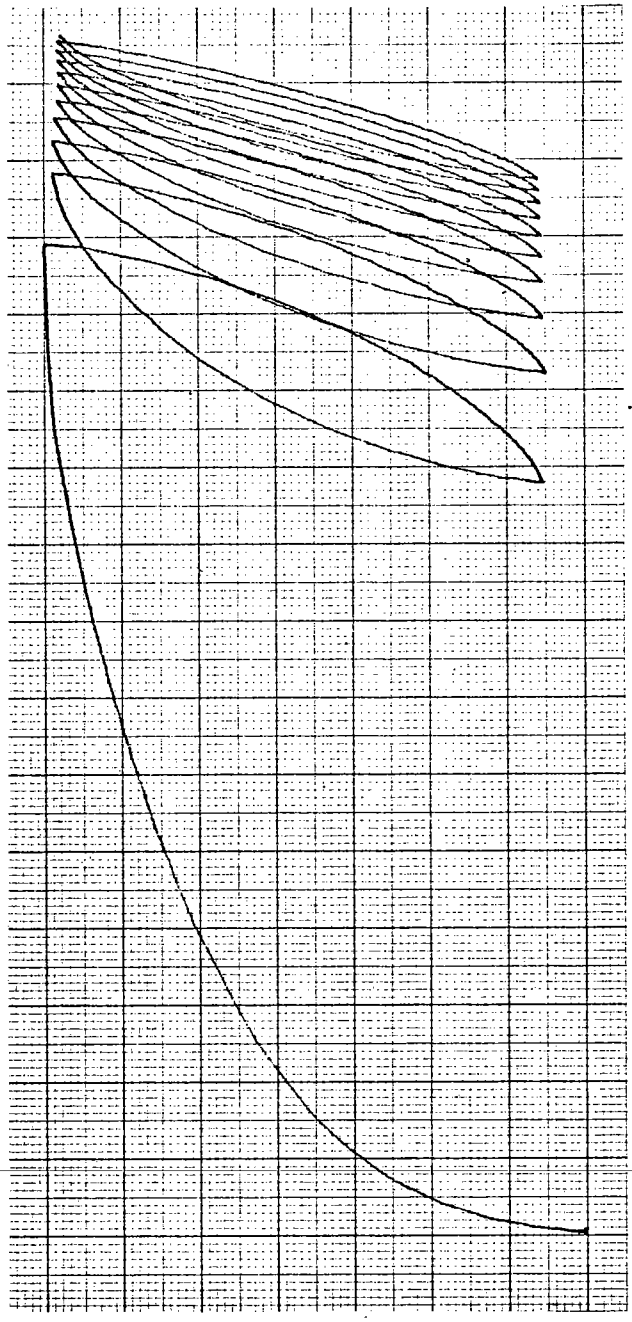

Fig.52 XY recorder trace

strain results is followed, the correlation is not exact because the cyclic shear stress measured over the central third was not constant during a test. This point was also discussed in Section 5.4. Also, any non-uniformity in the shear strain distribution could not be monitored and these limitations of the apparatus lead to the differences noted above. X-ray techniques, such as those used to study the shear strain distribution in the Cambridge Simple Shear Apparatus (6), would not be practicable in the present apparatus because of the steel side plates which are required to support the crossheads for the top platen.

5.10 Concluding Remarks

In this chapter, the results of the unidirectional repeated load tests have been presented and various models developed. These predict the response of the material to a type of loading which exists in the ballast below rail track curves. In situ, this stress regime will be modified by the effect of the rolling wheel load. The general nature of the permanent shear strain behaviour was similar to that observed for permanent axial strain in repeated load triaxial tests by Shenton (73). It should also be noted that no sudden failures occurred in the Series A tests. Having survived the first load cycle, the sample continued to deform in a controlled manner and a failure condition would only be reached if it was predefined as a limiting accumulated permanent shear strain.

The effectiveness of simple shear straining as a means of compacting granular material, noted by Youd (87, 88) for bidirectional repeated constant shear strain tests, has also been observed in these unidirectional repeated constant shear load tests. The response of

the material to this type of loading was, to some extent, dependent on the applied normal stress. However, insufficient data was available to characterise this aspect of the material's response.

Several lines for further investigation are suggested by the results and experience gained from the tests and these are discussed in Chapter Nine.

CHAPTER SIX

BIDIRECTIONAL REPEATED LOAD TESTS (SERIES B AND C)

6.1 Introduction

The second phase of the repeated load testing involved monitoring the response of the material to two types of bidirectional shear stress pulses which were a known fraction of the static failure strength. For the Series B tests, the loading was symmetrical about the zero load level; $R_m = 0$. This stress regime corresponds to the shear stress reversal which occurs in a pavement subjected to a rolling wheel load. A diurnal lateral shear stress reversal can also be caused by thermal stresses in curved rail tracks. An outward shear stress is produced during the day due to expansion of the rails and an inward shear stress is produced at night due to contraction.

Series C involved a few tests to investigate any effect of the mean shear stress ratio in the range $R_c \geq R_m \geq 0$ which are the limits imposed by the Series A and B tests respectively. This asymmetric bidirectional loading produces a stress regime which might occur at points away from the centre line between rail track sleepers. Fig. 53 compares a typical stress path for each of the Series A, B and C tests. With the apparatus in its present form, it is not possible to carry out tests in which $R_m > R_c$ because of limitations imposed by the control equipment. This type of test was not catered for in the original design since it does not utilise the shear stress reversal facility which was a major design feature of the apparatus.

The structure of this chapter is similar to that of Chapter Five and reference will be made to it for those details which are similar to the Series A test programme. The results of the Series C tests are

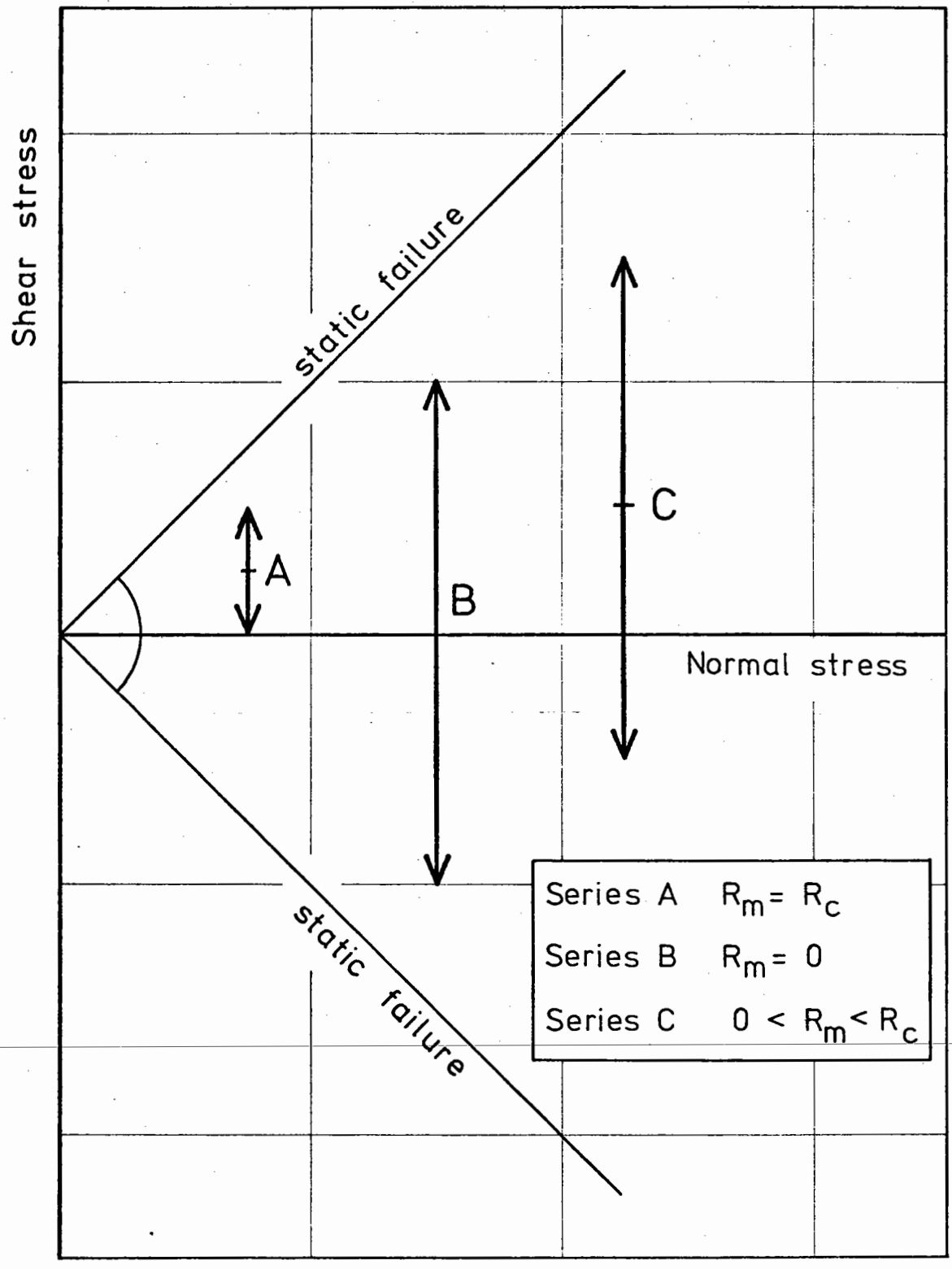

Fig.53 Typical stress paths for repeated load tests

considered separately, following the presentation of the Series B results.

6.2 Test Details

The same three levels of normal stress used in the Series A tests; 95, 190 and 285 kPa nominal, were used for the bidirectional repeated load tests. Series B consisted of fourteen tests: four at the highest and five at the remaining two normal stress levels. Series C consisted of just three tests at the intermediate vertical stress level, 190 kPa.

The sample preparation and setting up procedure for all these tests was the same as that described in Section 5.2 for the Series A tests. Both shear rams were now used to load the sample. In the case of the Series B tests, the two solenoid valves were supplied by the same regulated air supply to ensure that identical air pressures were admitted to each ram in turn. For the Series C tests, each solenoid valve had its own regulated air supply so that asymmetrical shear loads could be applied to the sample. A typical loading waveform for the Series B tests is shown in Fig. 27(b). The frequency of loading for the Series B and C tests was the same as that used for the Series A tests; 0.36 Hz, and the test duration was generally 10^4 cycles. To obtain permanent strain data for the Series C tests it was necessary to stop the test at intervals because of the asymmetric nature of the loading. For the Series B tests, it was assumed that the cyclic shear strains were symmetrical about the instantaneous level of permanent shear strain. However, this led to difficulties with the volumetric strain data for the Series B tests and these are discussed further in Section 6.6.

6.3 Permanent Shear Strain - Series B

Since the shear load pulse for the Series B tests was symmetrical about zero, it was anticipated that very little permanent shear strain would accumulate in these tests and this proved to be the case. A small amount of permanent shear strain built up over the first 100 cycles and then settled down to a steady value which was always less than 1% and generally less than 0.5%. This small permanent shear strain was probably due to slight differences between the two shear load rams. No further study of the permanent shear strain response to symmetric bidirectional repeated load was made.

6.4 Recoverable Shear Strain - Series B

In Section 5.3, γ_r was defined as the peak to peak shear strain and for unidirectional loading this is obviously a recoverable shear strain. However, in the case of bidirectional loading, it is not immediately apparent that this same definition is appropriate since the material is being loaded in two directions. However, in Appendix I, where all the recoverable shear strain results are considered together, it is shown that these definitions are compatible.

The recoverable shear strain data for the Series B tests is shown in Fig. 54 and it can be seen that the general pattern of behaviour was similar to that observed in the Series A tests described in Section 5.5. However, the range of recoverable shear strains is much greater than for the Series A tests because of the bidirectional loading which allows cyclic shear stress ratios up to twice those possible in the unidirectional Series A tests to be applied. This point can be appreciated by reference to Fig. 53.

Fig. 55 shows that the initial recoverable shear strain in the

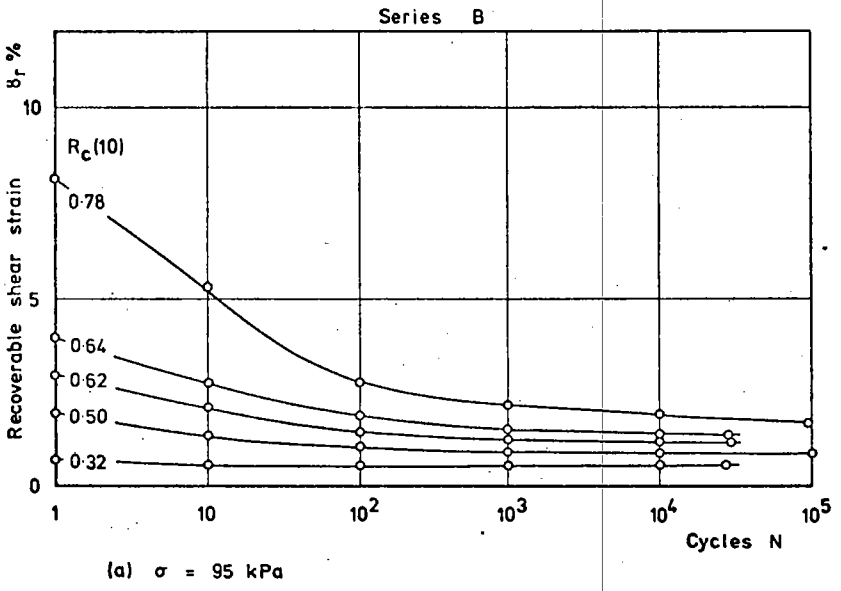

(a) σ = 95 kPa

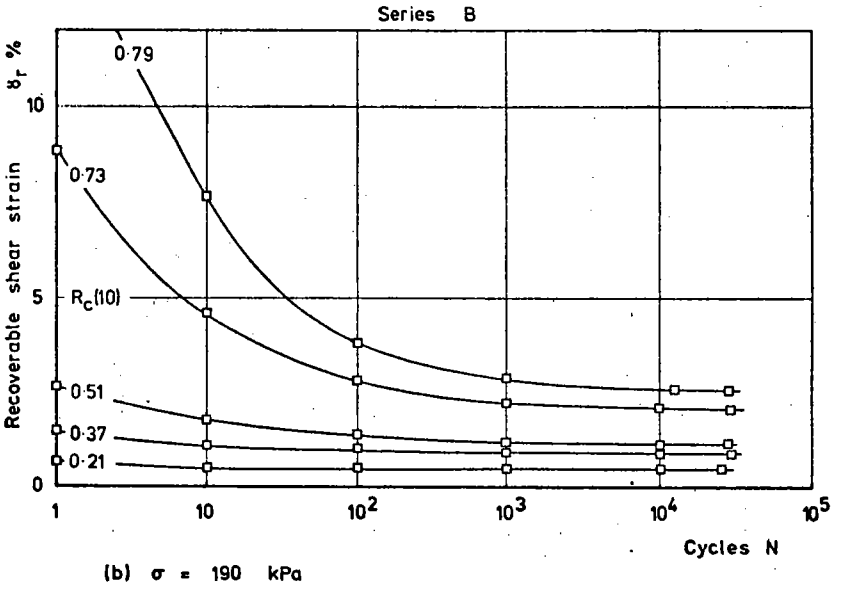

(b) σ = 190 kPa

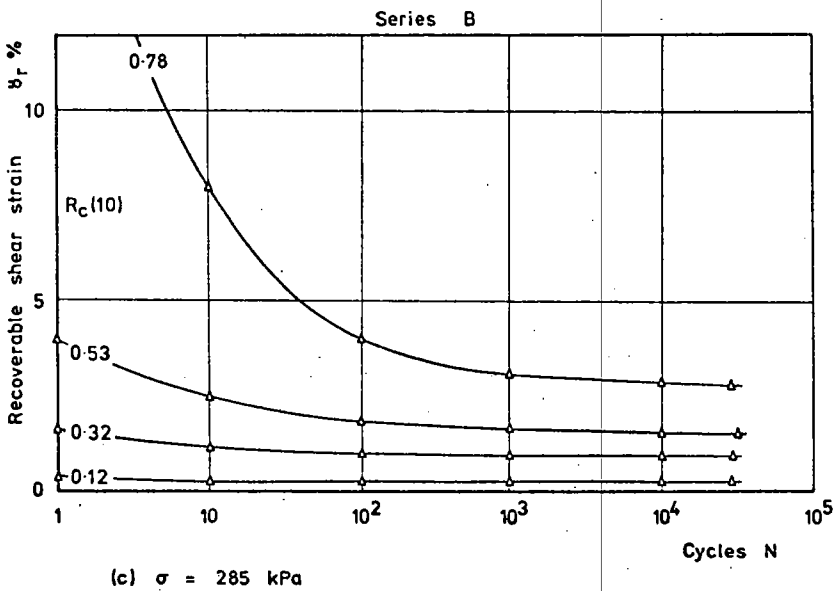

(c) σ = 285 kPa

Fig. 54 Recoverable shear strain results - Series B

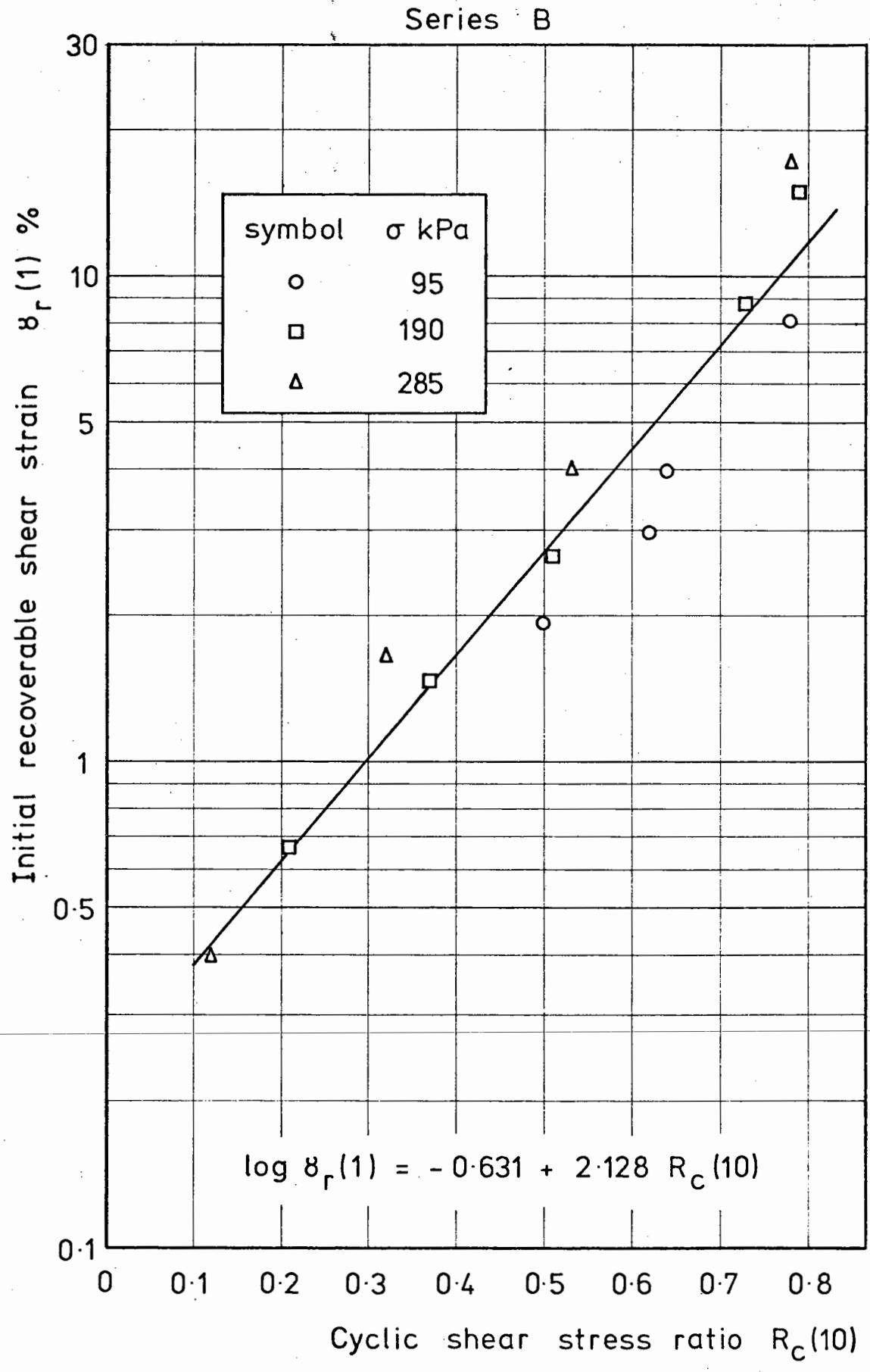

Fig.55 Initial recoverable shear strain versus cyclic shear stress ratio

Series B tests was linearly related to the cyclic shear stress ratio on a log-linear basis as was the case for the Series A tests, Appendix F. Again, a similar type of relationship holds for the other decade points. However, a model for this behaviour will not be developed here since a complete, recoverable shear strain model is presented in Section 6.11.

6.5 Permanent Volumetric Strain - Series B

The results for the permanent volumetric strain behaviour are shown in Fig. 56. The general pattern was again similar to that for the Series A tests, described in Section 5.7. However, it can be seen that dilation does not appear to play such an important role in the first few cycles of tests at relatively high cyclic stress ratios. This was because the material responded to the shear stress reversal as two separate pulses, each half of the cycle being comparable to a single unidirectional load pulse. Thus the shear stress reversal reduced the dilation which occurred in the first half of the first load cycle when, uniquely, there was no difference between the stress paths of the Series A and Series B tests. As with the Series A tests, it can be seen that compaction was assisted by increased vertical loading at a given cyclic shear stress ratio. The change in porosity for the Series B tests was quite considerable at the higher cyclic shear stress ratios. A permanent volumetric strain of 10% represents a reduction in porosity from 0.40 to 0.33 or 17.5%. This decrease in porosity must, to a large extent, have been accommodated by rounding of the corners of the particles and some qualitative evidence of this effect was observed. However, despite the increased density, no evidence of any increase in the angle of shearing resistance could be found when a single load, Series S type test was performed on some

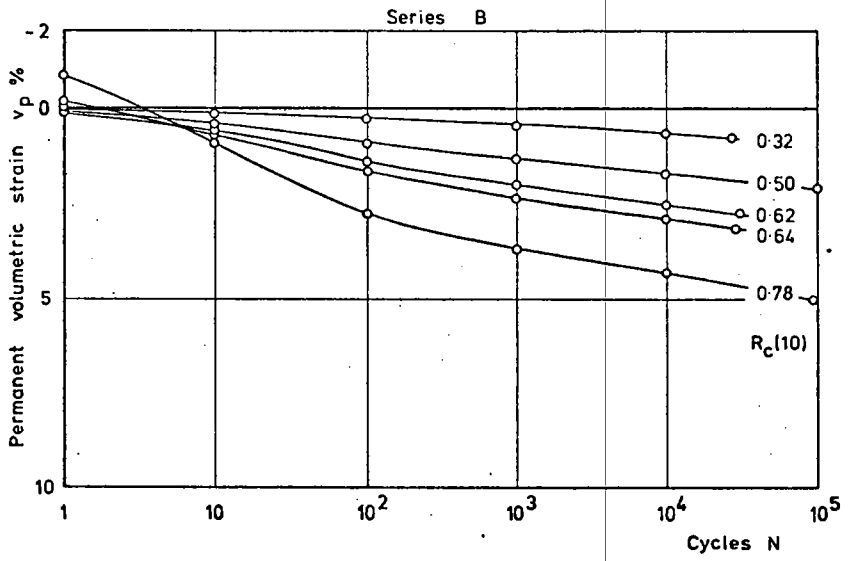

(a) σ = 95 kPa

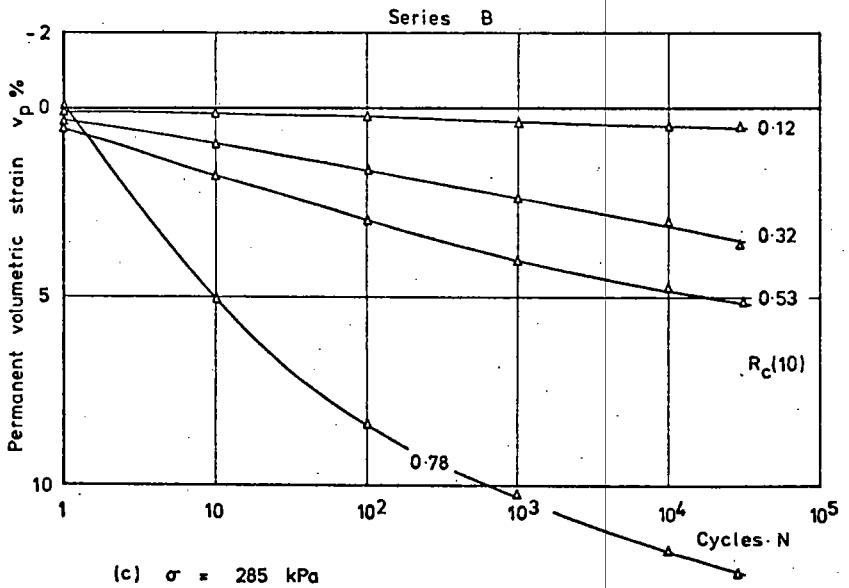

(c) σ = 285 kPa

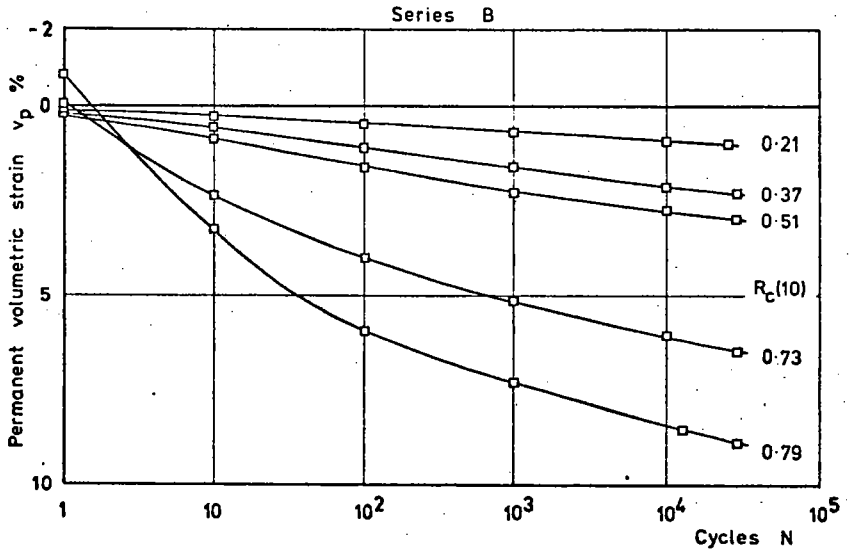

(b) σ = 190 kPa

Fig. 56 Permanent volumetric strain results - Series B

of the samples after completing a Series B test. Support for these results is provided by Pike (59) who observed that the change in the potential for aggregate interlock caused by a change in particle angularity was more significant than that caused by the change in porosity which could be achieved using the same compaction procedure. In effect, the rounding of the corners of the particles was more significant than the change in porosity.

6.6 Recoverable Volumetric Strain - Series B

For the Series B tests, it was found that the recoverable volumetric strain, as indicated by the chart recorder, was very small in comparison with the results presented in Section 5.8 for the Series A tests. This was due to the effect of the shear stress reversal producing two separate volumetric strain pulses as discussed in the previous section. The two halves of the shear stress pulse followed each other so closely that there was insufficient time for elastic recovery as the shear stress pulse passed through the zero level. This prevented any recoverable volumetric strain data being obtained from the Series B tests. Thus, the permanent volumetric strain results presented in the previous section must be slightly smaller than the actual results but this is unlikely to be significant. This problem could be avoided if the technique subsequently used in the Series C tests was employed. This method involved stopping the test at intervals to allow a permanent strain reading to be obtained.

6.7 Shear Modulus - Series B

In Section 6.4, the recoverable shear strain for the Series B tests was defined as the peak to peak shear strain and this value was

used to evaluate the shear modulus of the material. It is shown in Appendix I that this definition is appropriate. The variation of the shear modulus during the Series B tests is shown in Fig. 57. It can be seen that the general pattern was similar to that described in Section 5.9 for the Series A tests though the range of the results was greater because of the higher values of cyclic shear stress ratio which were possible in the bidirectional repeated load tests. These results are discussed further in Section 6.12 when all the shear modulus results are considered together.

6.8 Permanent Shear Strain - Series C

Since the bidirectional loading in the Series C tests was asymmetric, permanent shear strain accumulated in the direction in which the larger shear load was acting. The test results are shown in Fig. 58. No permanent strain data is available for the first cycle because it was felt that stopping the test at this stage might influence the subsequent behaviour. A comparison of these results with the complete shear strain model, Fig. 46, indicates that the larger shear load was the controlling factor in the accumulation of permanent shear strain; the material tended to respond as if it were subjected to a unidirectional repeated load of a magnitude equal to the larger shear load as shown by the dotted lines in Fig. 58. However, the result for the test at the highest cyclic shear stress ratio, $R_c(10) = 0.50$ asymmetrically divided 0.38:0.12 between the two directions, does not fit into this pattern. This could be due to a threshold type situation where the smaller shear load has to reach a certain magnitude before it has any effect. However, there is insufficient evidence to be definite about this point.

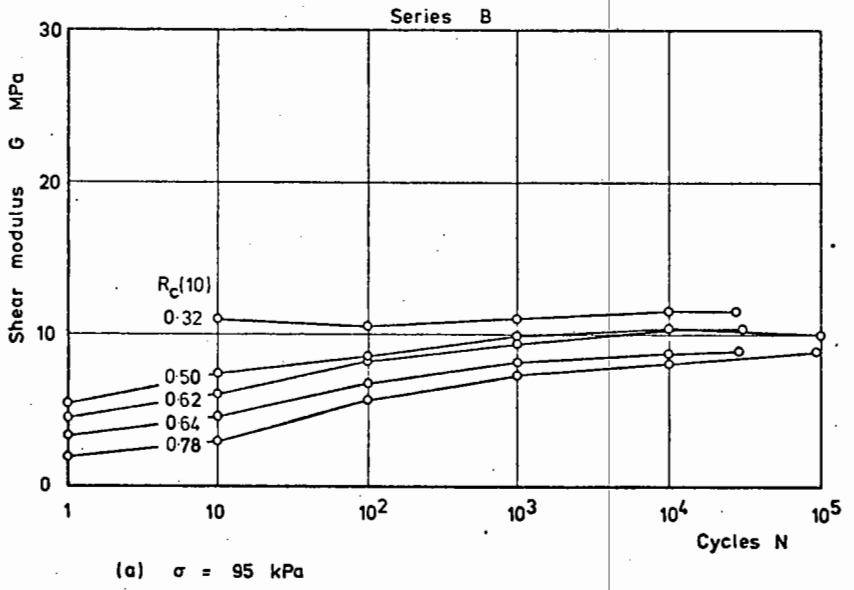

(a) σ = 95 kPa

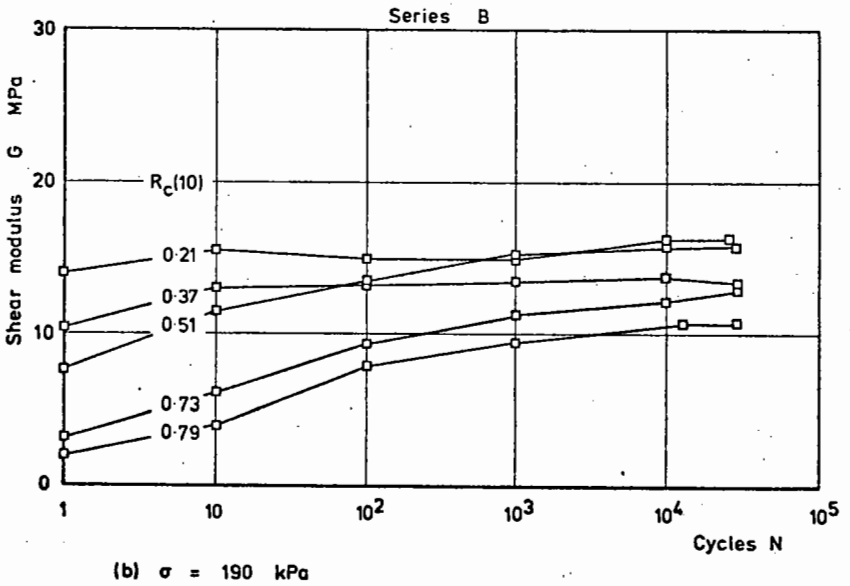

(b) σ = 190 kPa

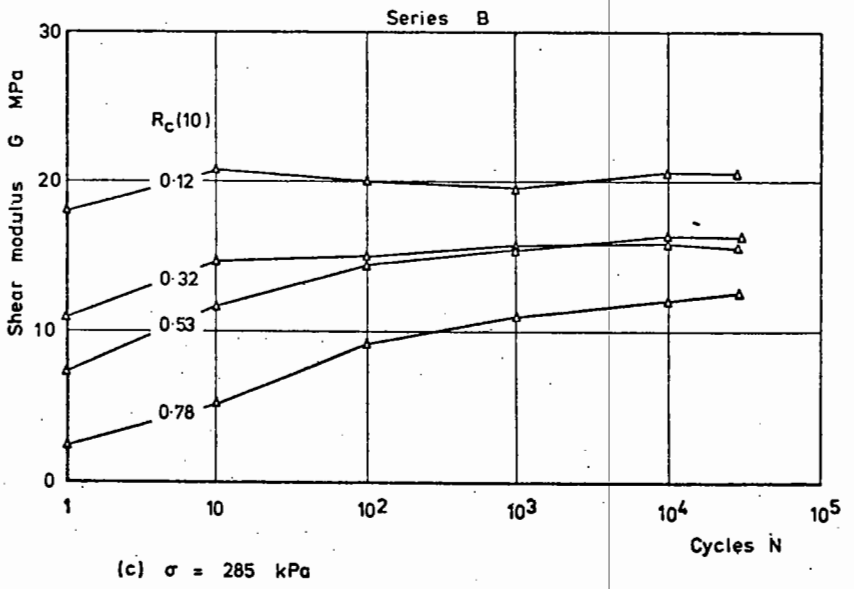

(c) σ = 285 kPa

Fig. 57 Shear modulus - Series B

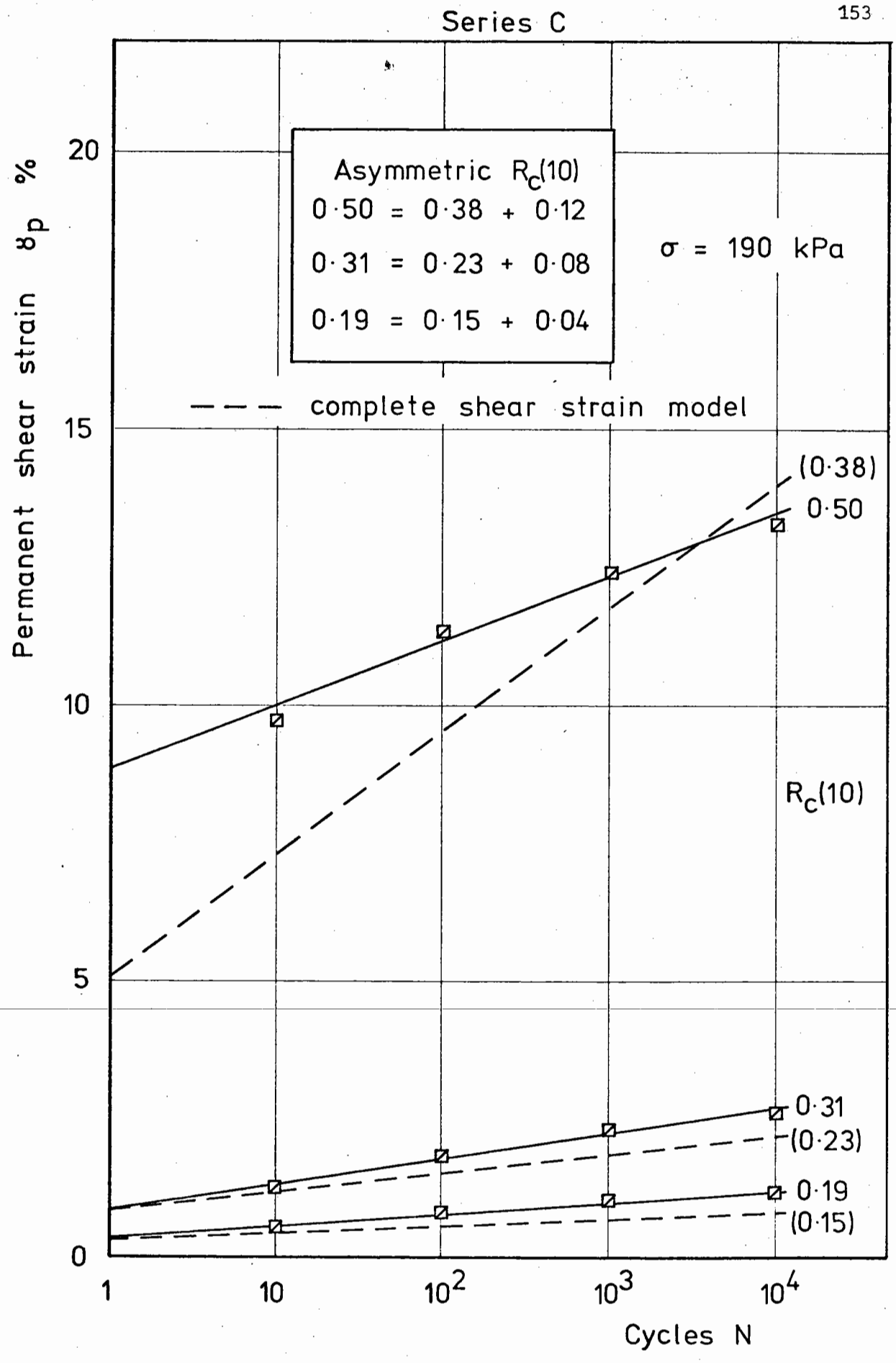

Fig. 58 Permanent shear strain results - Series C

6.9 Recoverable Shear Strain and Shear Modulus - Series C

Fig. 59(a) shows the recoverable shear strain behaviour of the material in the Series C tests. It can be seen that the response was similar to that observed for the Series A and Series B tests described in Sections 5.5 and 6.4 respectively. It can also be seen, in Fig. 59(b), that the variation of the shear modulus during the Series C tests followed a similar pattern to that in the Series A and Series B tests described in Sections 5.9 and 6.7 respectively. These results are discussed further in Sections 6.11 and 6.12.

6.10 Volumetric Strain - Series C

The permanent volumetric strain results are shown in Fig. 60(a) though, as explained earlier, no data is available for the first load cycle. Comparison of these results with those shown in Fig. 56(b) for the Series B tests at the same level of normal stress indicates that the asymmetric nature of the cyclic shear stress had little effect on the permanent volumetric strain behaviour of the material.

Fig. 60(b) shows the recoverable volumetric strain results for the Series C tests. Again, no data is available for the first load cycle. However, the general pattern was similar to that described in Section 5.8 for the Series A tests.

6.11 Overall Recoverable Shear Strain Behaviour

In this section, the recoverable shear strain results from the whole of the repeated load test programme are brought together to show that, within the range considered; $R_c \geq R_m \geq 0$, the mean shear stress ratio, R_m, has very little, or no effect. The results also show, Appendix I, that the definition of recoverable shear strain, given in

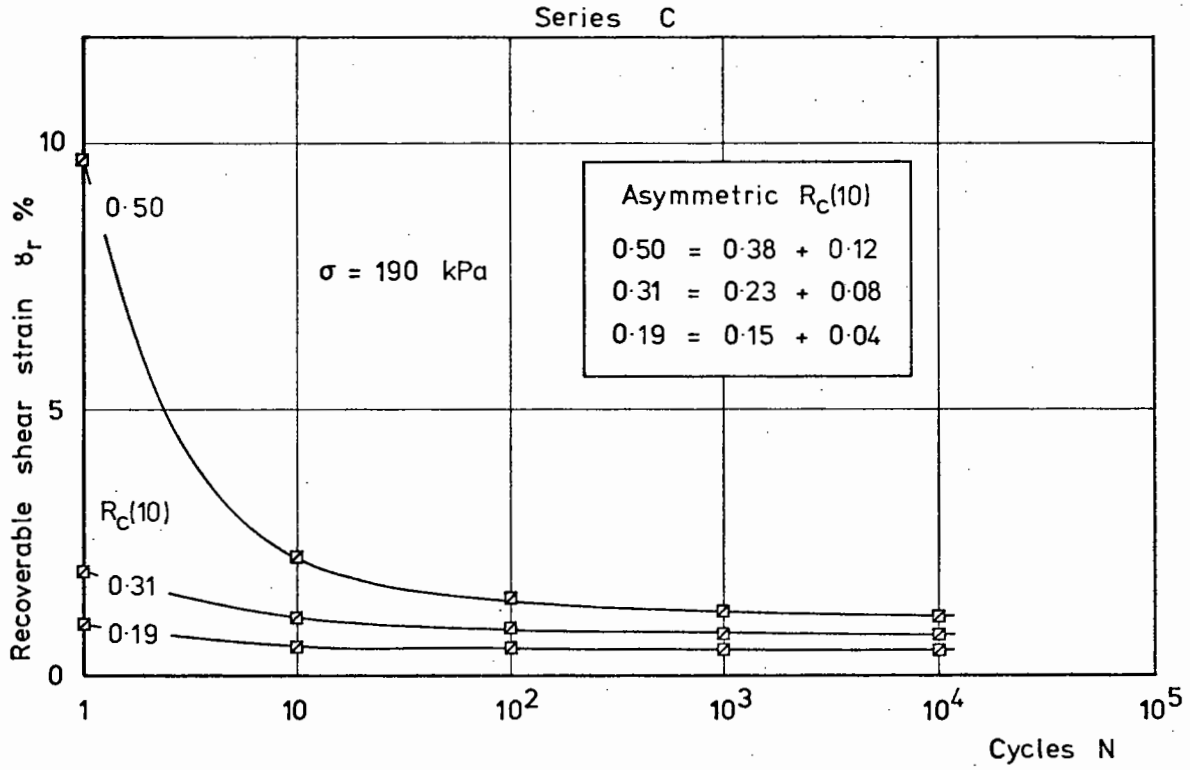

(a) Recoverable shear strain results - Series C

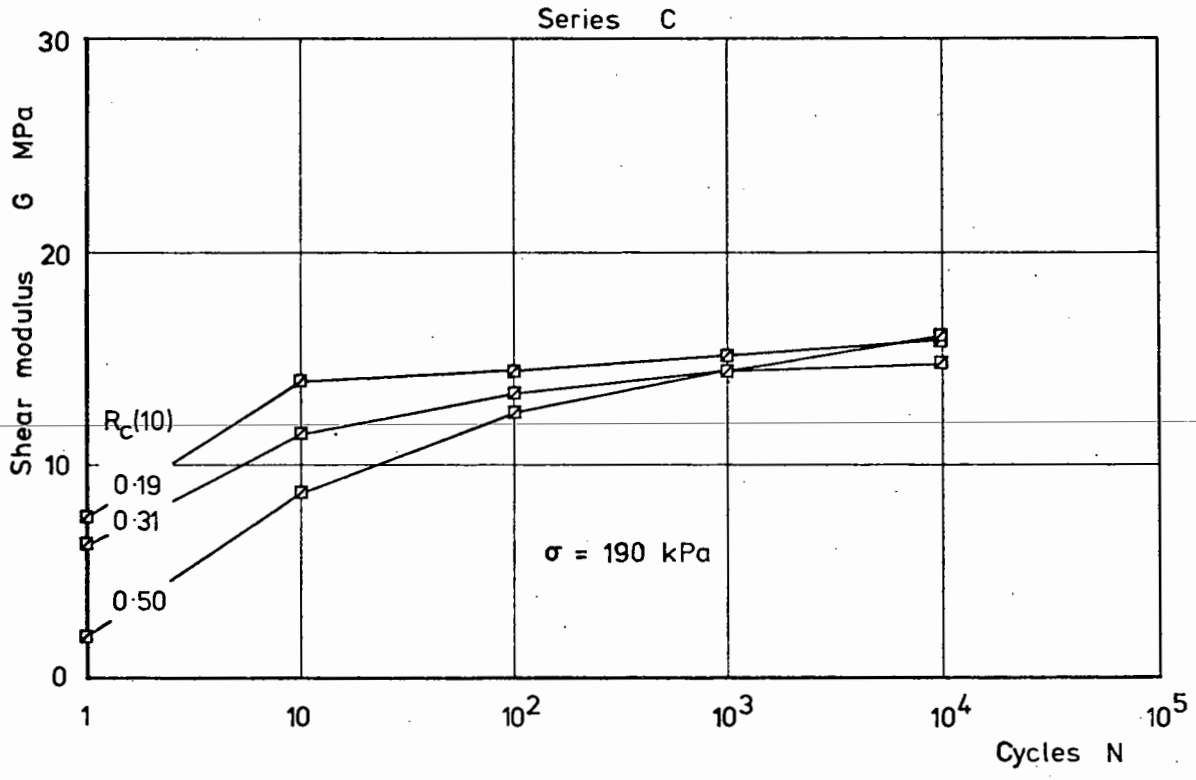

(b) Shear modulus - Series C

Fig. 59

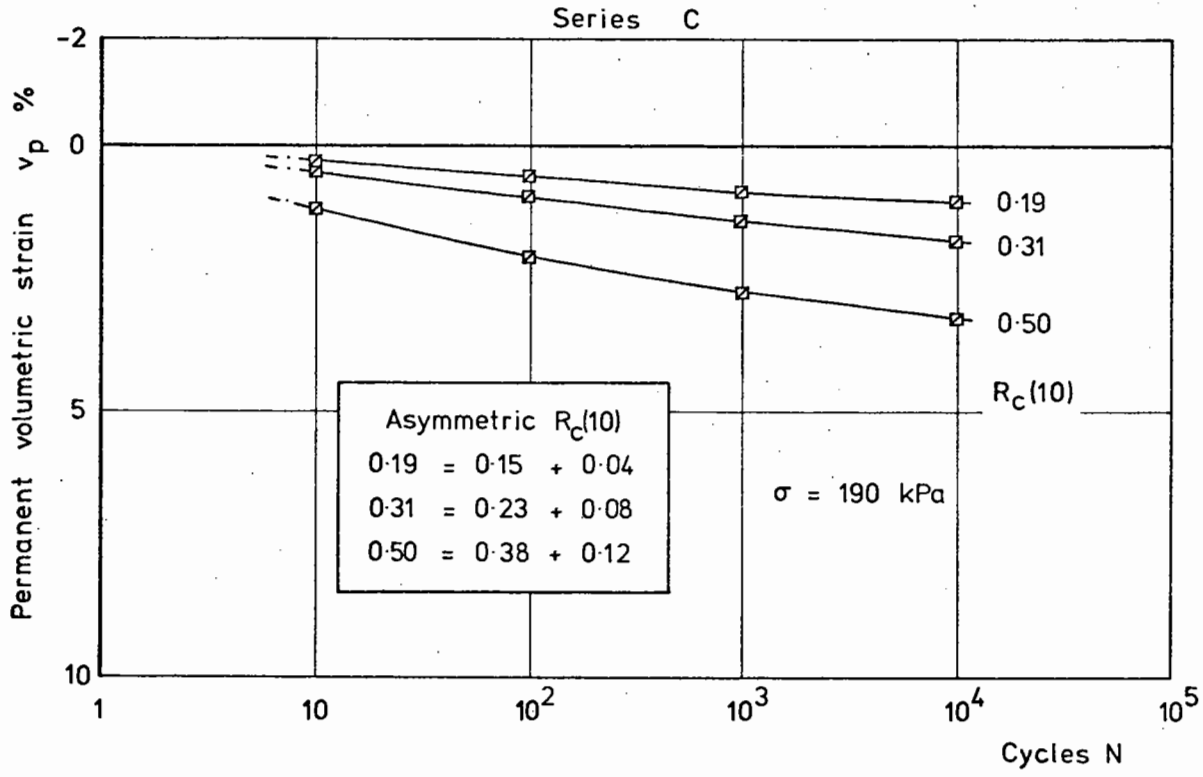

(a) Permanent volumetric strain results - Series C

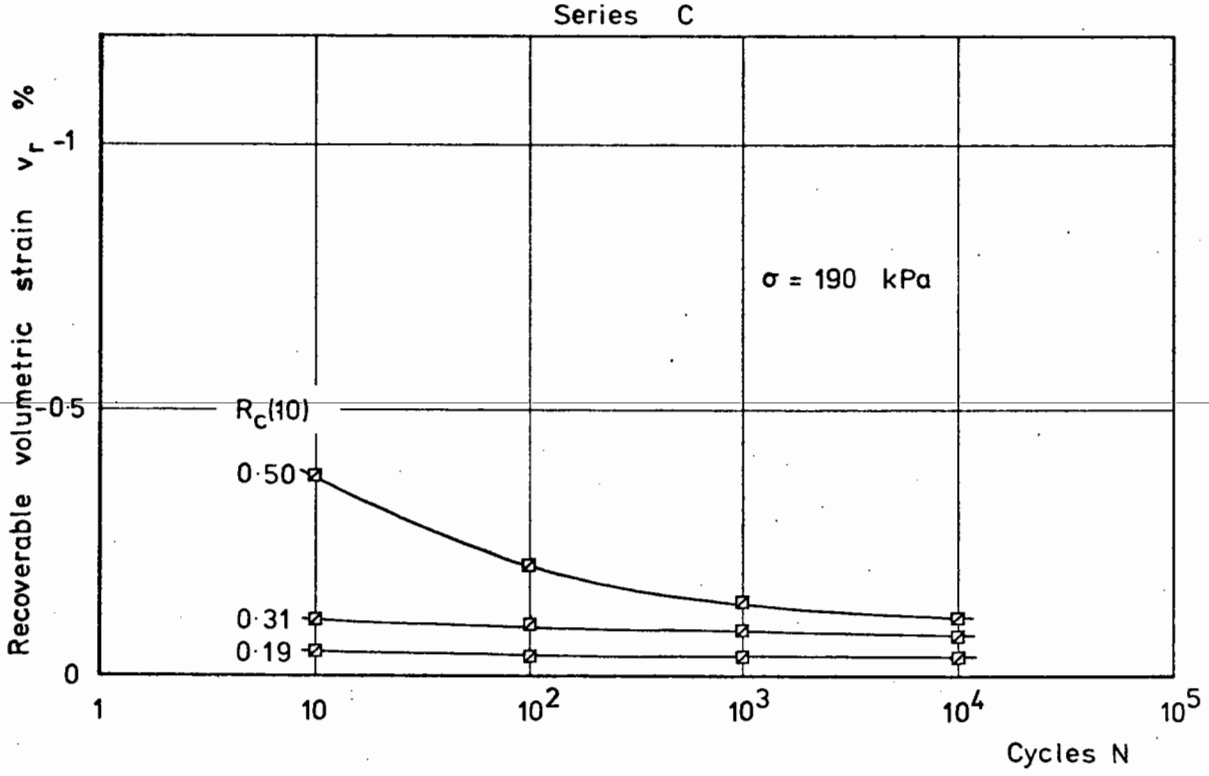

(b) Recoverable volumetric strain results - Series C

Fig. 60

Section 5.3, as the peak to peak shear strain is appropriate for the three types of repeated loading considered herein.

A model for the overall recoverable shear strain behaviour is developed in Appendix I by correlating the Series A, B and C results with the cyclic shear stress ratio in a similar manner to that described in Appendix F for the Series A model. The model is shown in Fig. 61 and it can be applied over the range: $0.05 < R_c(10) < 0.8$ for both unidirectional and bidirectional repeated loading with the possible exception of the initial recoverable shear strain in the asymmetric, bidirectional loading situation as discussed in Appendix I. For unidirectional loading, the upper limit of the range of applicability is, of course, only 0.42. The model can be expressed in the form:

$$\log \gamma_r(N) = (A + B\log N + C\log^2 N + D\log^3 N + E\log^4 N)R_c(10) - 0.664$$

where $A = 2.274$ $B = -0.305$ $C = -0.140$

$D = 0.074$ $E = -0.0095$

The calculated value of $\gamma_r\%$ should be corrected to 2 significant figures.

A comparison of the overall recoverable shear strain model with some of the test data is shown in Fig. 62 and, considering the range of loading conditions covered by this model, the predictions appear to be quite acceptable. Slight inaccuracies, from the same sources as for the other models described herein, are again present. A recoverable shear strain contour chart, developed from the model, Fig. 61, is shown in Fig. 63 and further reference to this type of chart is made in Chapter Seven.

It should be noted that the recoverable shear strain model incorporated in the complete shear strain model for unidirectional

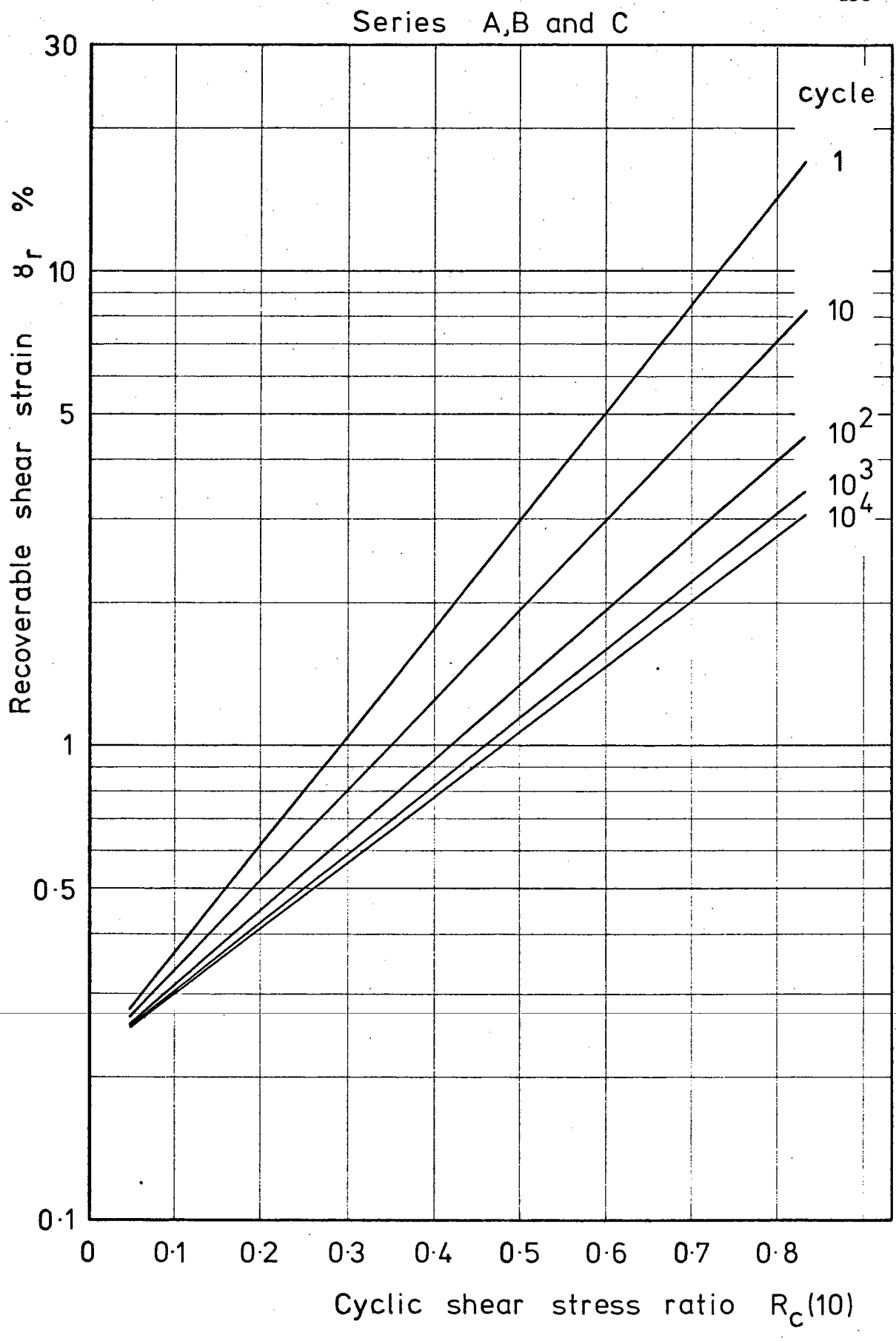

Fig.61 Adjusted model for recoverable shear strain

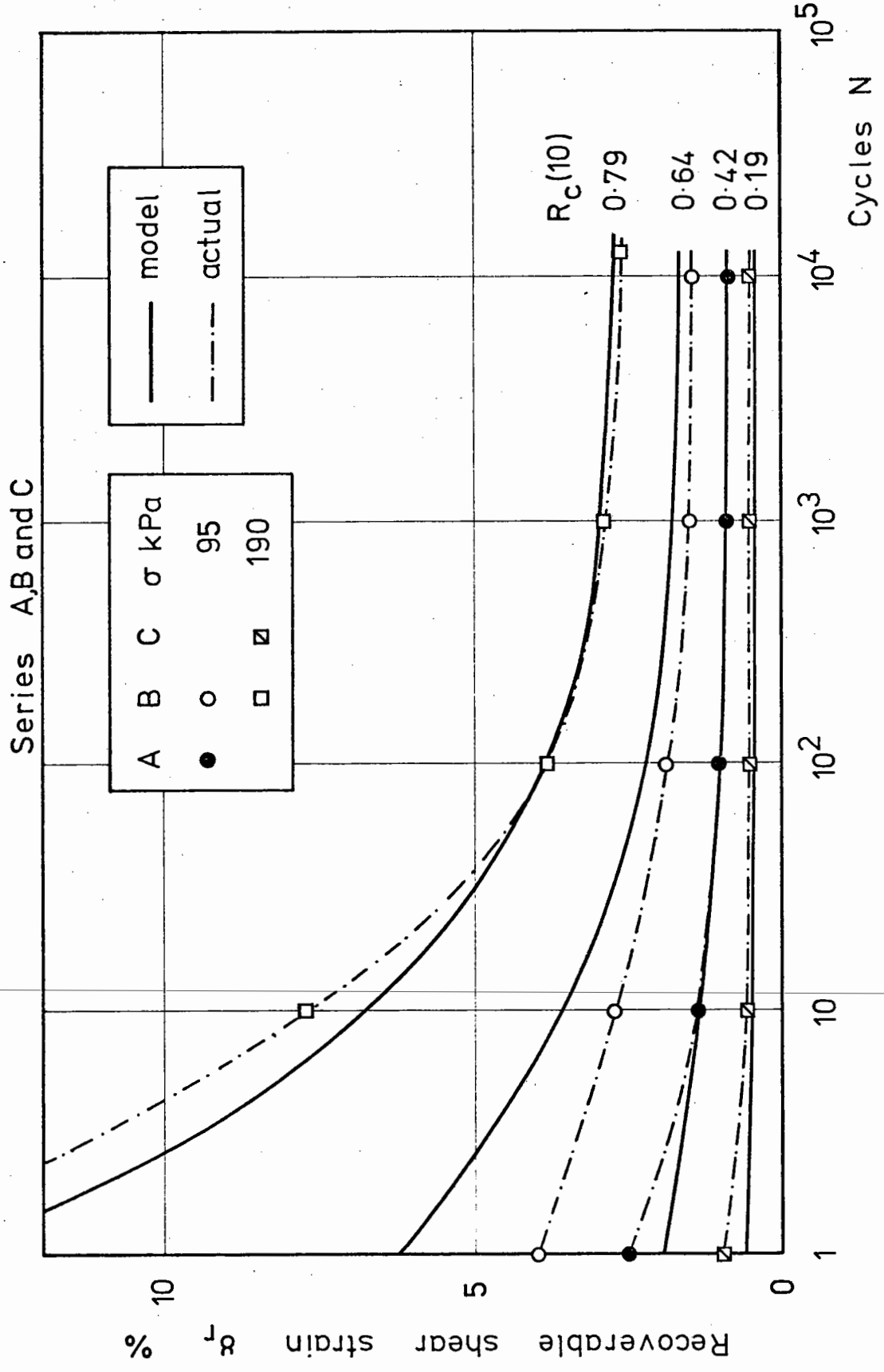

Fig.62 Comparison of recoverable shear strain results with model based on Series A,B and C

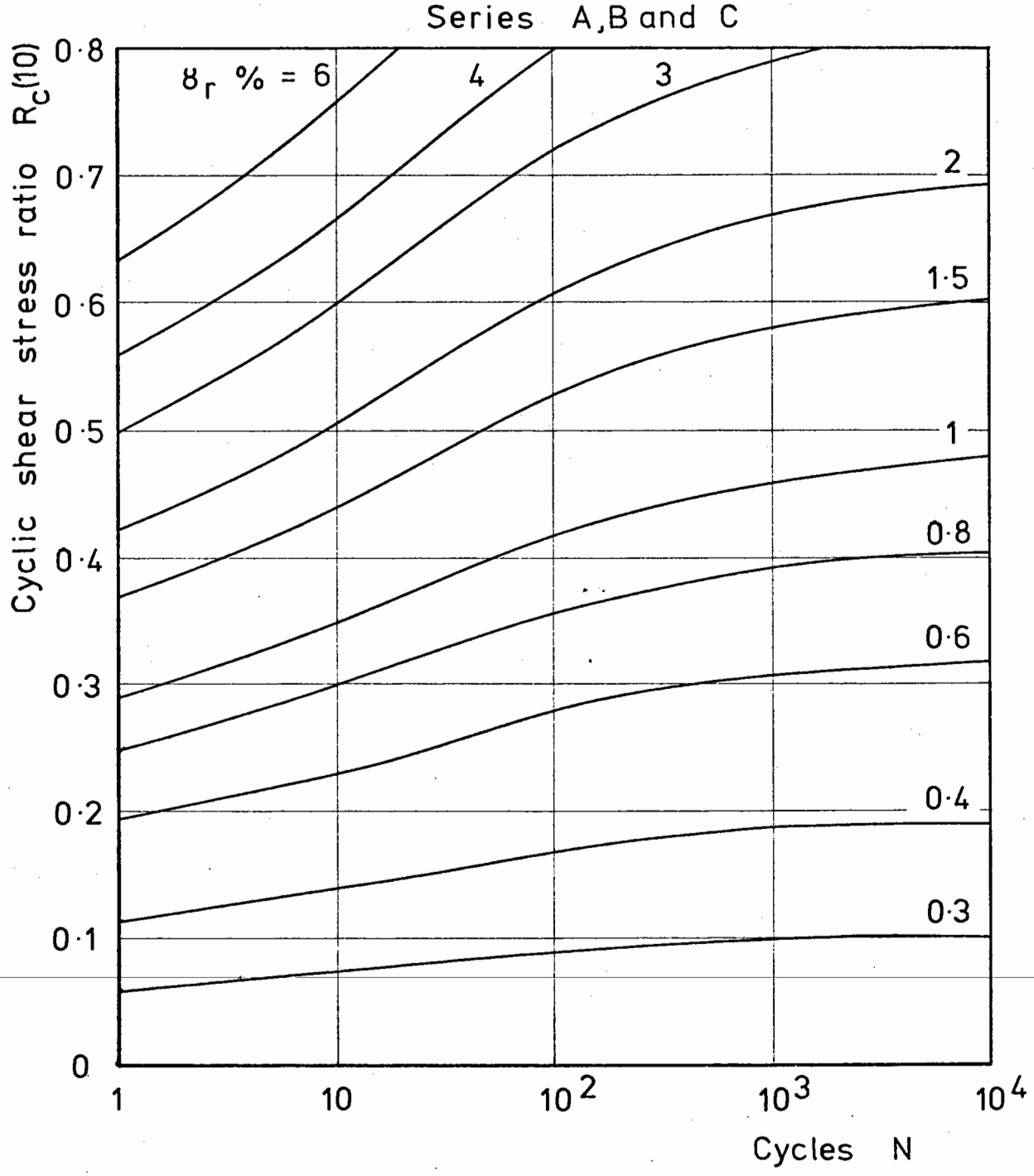

Fig.63 Recoverable shear strain contour chart

load, Section 5.6, was that developed from the Series A results alone in Appendix F. The slight differences in recoverable shear strain predicted by the two models can have a significant effect on the permanent shear strain predicted using the complete shear strain model because of the sensitivity of the logarithmic scales. However, if only the recoverable shear strain is required, then the differences between the two models are unlikely to be significant.

6.12 Combined Shear Modulus Results

In this section, the equilibrium shear modulus values for all the repeated load tests are considered together, the values after 10^4 cycles having been taken in each case.

Fig. 64 shows a plot of the shear modulus against the cyclic shear stress ratio and it can be seen that there was a tendency for the shear modulus to decrease with increasing stress ratio; the shear modulus decreasing by something less than a factor of 2 over the range of stress ratios considered. A decrease in shear modulus of this size would probably be significant in an elastic analysis of a pavement structure, depending upon the importance of the granular layer relative to the rest of the structure. No mathematical analysis of this relationship is presented because of the scatter of the results. However, Fig. 64 does establish a trend which is not entirely surprising considering the disruptive effect of high cyclic shear stress ratios indicated by the dilatant volumetric strains referred to in this and the previous chapter. Part of the scatter referred to above is clearly due to the influence of the vertical stress and Fig. 65 shows a plot of the shear modulus against the nominal vertical stress. The considerable range of the results is now due, at least

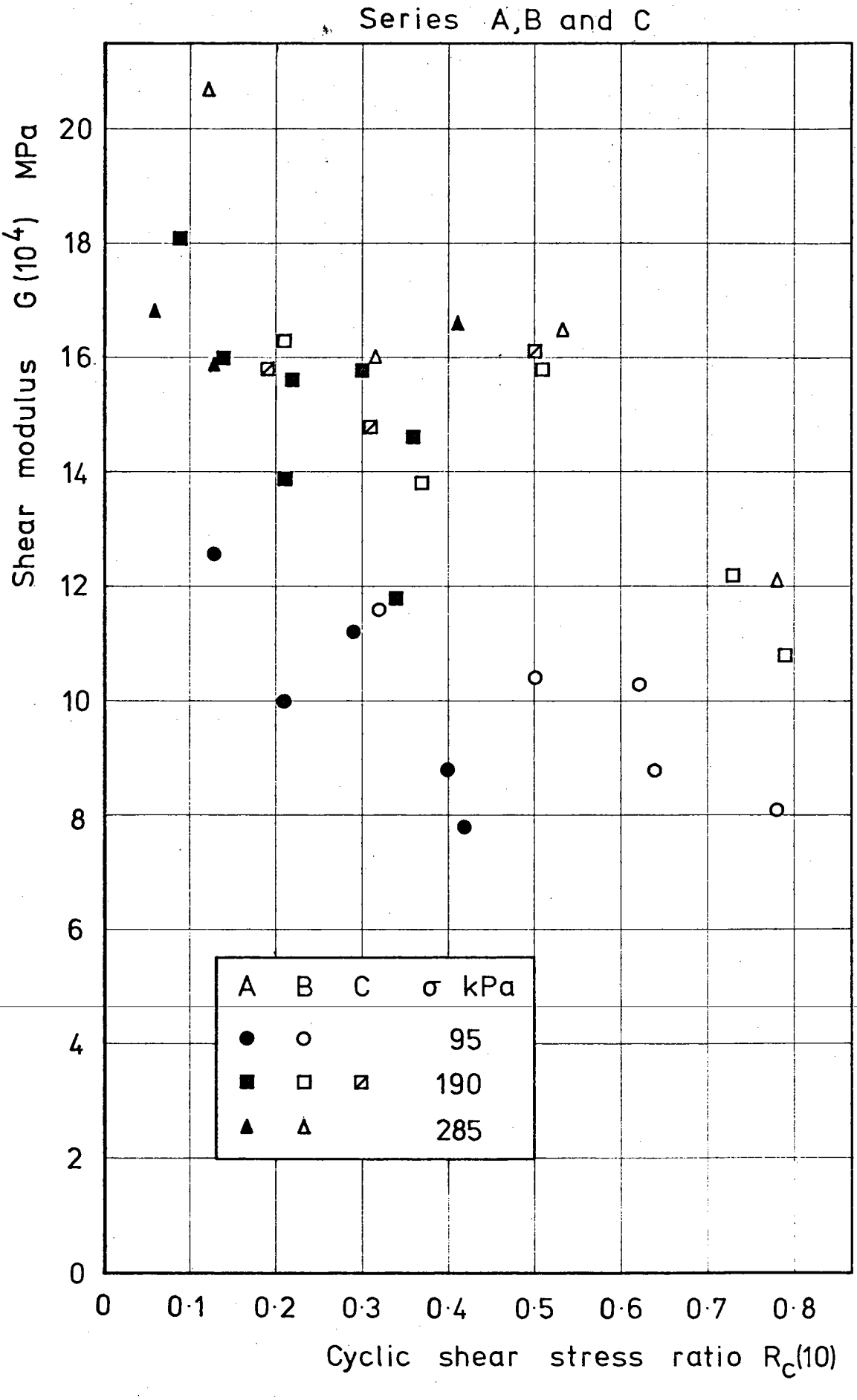

Fig.64 Shear modulus versus cyclic shear stress ratio

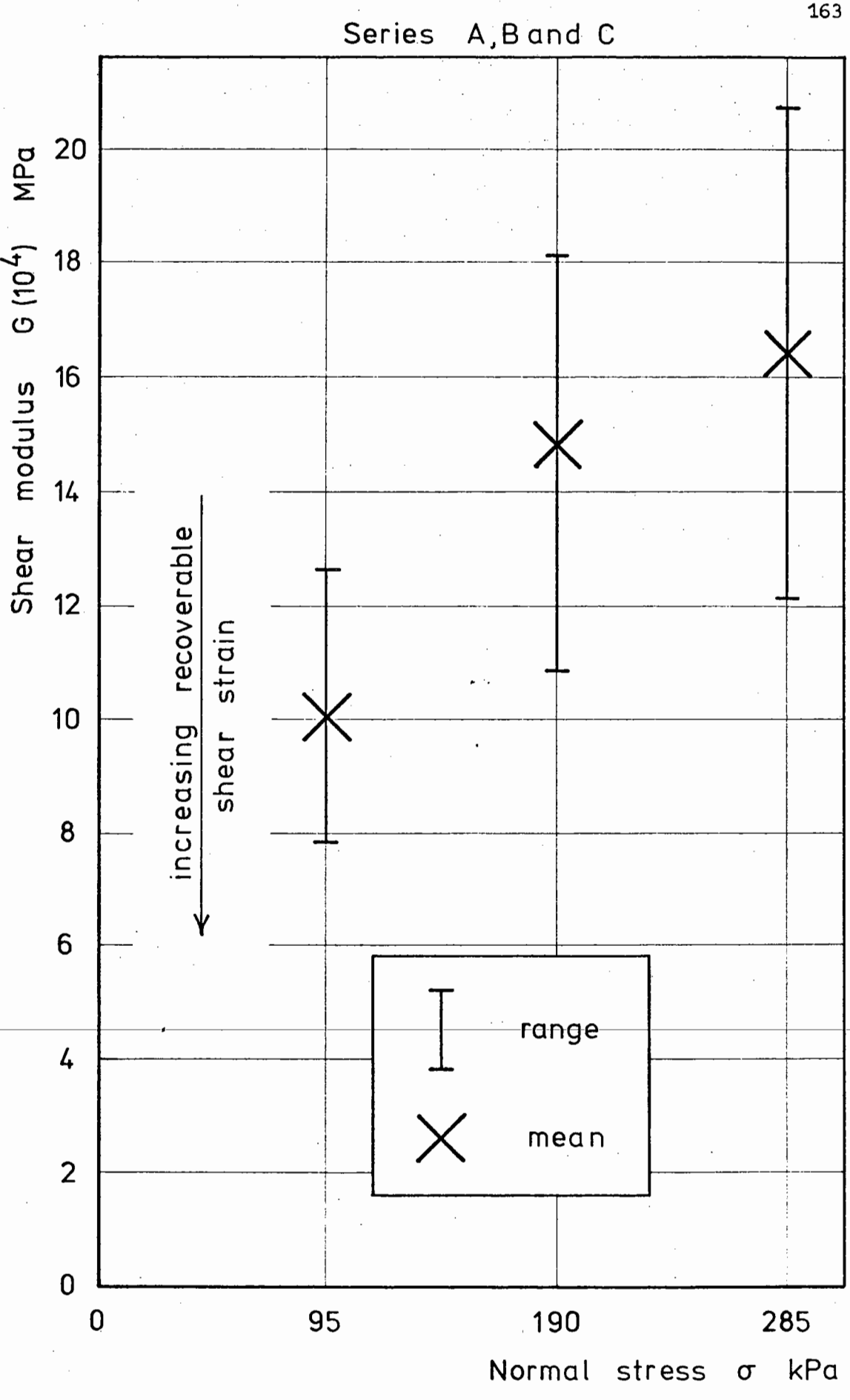

Fig.65 Shear modulus versus normal stress

in part, to the effect of the cyclic shear stress ratio and again no mathematical analysis of the relationship is presented. However, the results do show a trend for the shear modulus to increase with increasing vertical stress. This trend is also not unexpected considering the increased compaction which has been observed with increasing vertical stress. This effect is not incompatible with that referred to in Section 6.5 where no evidence of increased static shear strength could be found following the considerable compaction caused by the cyclic loading since the static shear strength is a parameter which is defined by failure conditions at high shear strains whereas the shear modulus is defined at low shear strain conditions where the potential for aggregate interlock is not likely to be so significant. In fact, it was observed in the single load tests, referred to in Section 6.5, that the shear modulus indicated by the initial section of the stress-strain curve for the single load test was approximately equal to the final value of shear modulus observed in the repeated load test.

The trend of the results shown in Fig. 65 is in agreement with those presented by Park and Silver (56), shown in Fig. 66, except where the initial permanent volumetric strains were dilatant. The disruptive influence of dilation on the behaviour of the material has been discussed earlier. The results shown in Fig. 66 are from simple shear tests on a dry, uniform angular quartz sand. However, direct comparison of the results is not possible because the tests reported by Park and Silver were of a repeated constant shear strain type in the range: γ_c = 0.01 - 0.5%. These shear strains are very small in comparison with the range of recoverable shear strains recorded in the repeated load tests described herein.

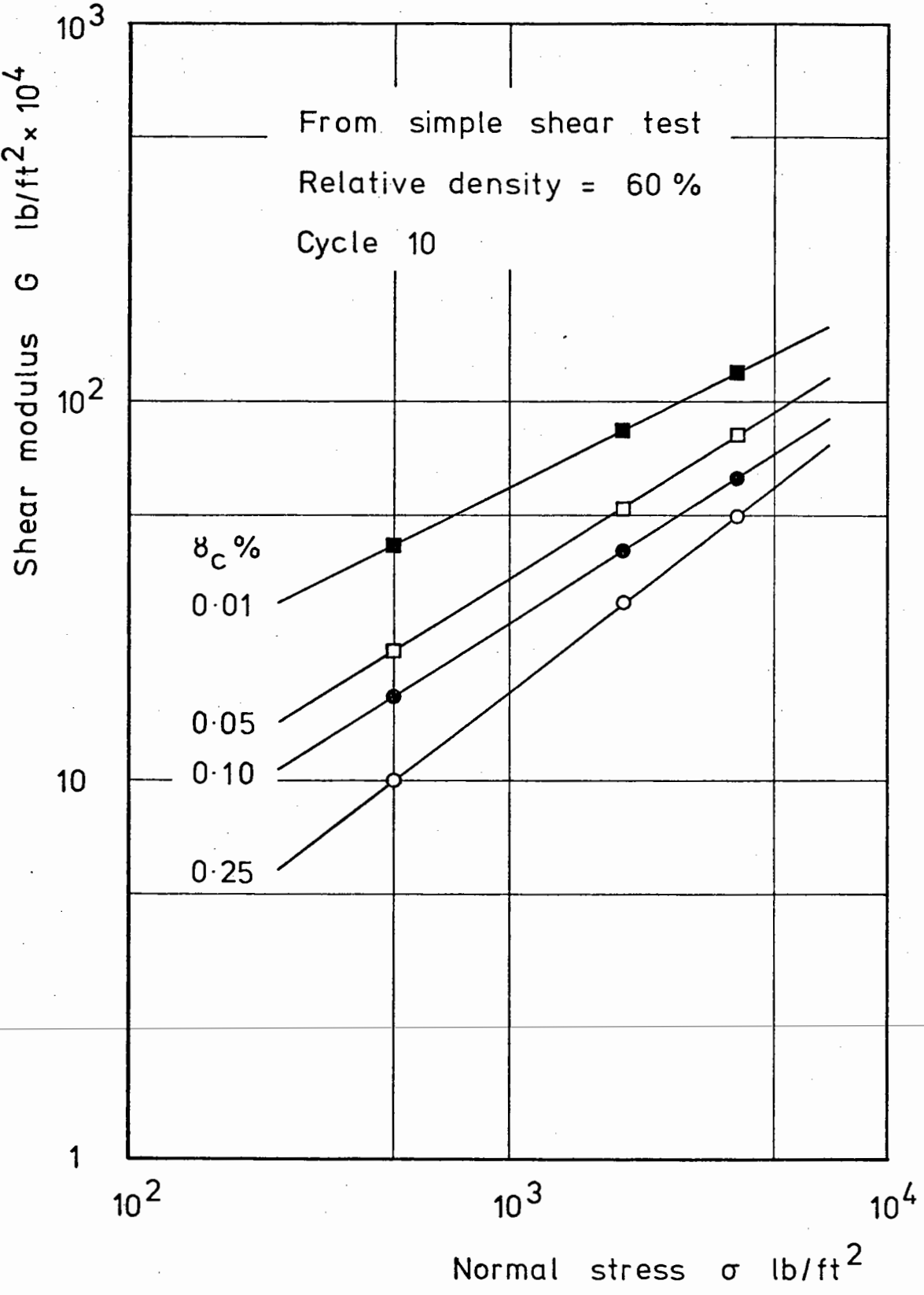

Fig.66 Shear modulus versus normal stress (after Park and Silver (56))

6.13 Concluding Remarks

In this chapter, the results of the bidirectional repeated load tests have been described and a model has been presented which includes the recoverable shear strain data from all the repeated load tests. It has been shown, Appendix I, that within the range $R_c \geq R_m \geq 0$ the influence of the mean shear stress ratio, R_m, is negligible except possibly for the initial recoverable shear strain in the asymmetric bidirectional loading situation. It has also been shown, Appendix I, that the peak to peak shear strain in a bidirectional repeated load test can be considered as a recoverable strain comparable with that measured in a unidirectional repeated load test.

A point of considerable interest in these results is the lack of any increase in static shear strength following quite large decreases in porosity even though the shear modulus had increased significantly during the test. This would seem to be due to the differing relative importance of the effects of particle angularity and porosity on the static shear strength of the material.

The general pattern of behaviour observed in the Series B tests is in agreement with results obtained by other researchers. However, direct comparison is not possible because the cyclic simple shear tests reported in the literature are mainly of a repeated constant shear strain nature. This has been due to the apparent dependency on the cyclic shear strain of some of the factors, such as modulus, being investigated by these researchers. However, the in situ pavement conditions will generally be stress controlled because of the nature of the loading and so a repeated constant shear stress type of test would appear to have considerable merit for investigating the pavement situation. It is possible for strain controlled conditions to occur

in both road pavements and rail track permanent way. Such conditions occur where a weak layer in the structure is supported by a relatively strong, stiff layer. In the road situation, a surfacing layer could be subject to a strain controlled loading due to the influence of the underlying roadbase. However, this case has no direct relevance to the granular material being considered in this work. In the permanent way situation, a strain controlled loading can occur on a bridge section where the deflection of the bridge deck due to the live load may be the controlling factor.

Suggestions for further work in the light of the results presented in this chapter are considered in Chapter Nine.

CHAPTER SEVEN

BLOCK LOAD TESTS (SERIES Y AND Z)

7.1 Introduction

The tests described in Chapters Five and Six were essentially repeated constant stress tests. This chapter describes two further series of tests in which the stress level was altered at discrete intervals during the course of each test. This procedure is known as block loading; each block consists of a train of load pulses at a constant stress level. This type of loading is intermediate between the repeated constant stress levels applied in the laboratory tests previously described and the random loading spectrum which occurs in a pavement under traffic. The purpose of these tests was to investigate any possible stress history effects and to look at the possibility of correlating the results of the block load tests with those from the repeated constant stress tests.

7.2 Test Details

The sample preparation and data recording techniques used for the block load tests were similar to those previously described for the other repeated load tests. Details of the Series Y and Z test programmes are set out in Fig. 67 and Table 2; each series consisted of 3 tests at the intermediate normal stress level, 190 kPa nominal. In all cases, Blocks 1 and 2 were of equal length, N cycles and a package consisting of Block 1 and Block 2 was repeated several times as indicated by the repeat factor.

In the Series Y tests, the cyclic shear load in each direction remained constant and the block length, N cycles, was varied to

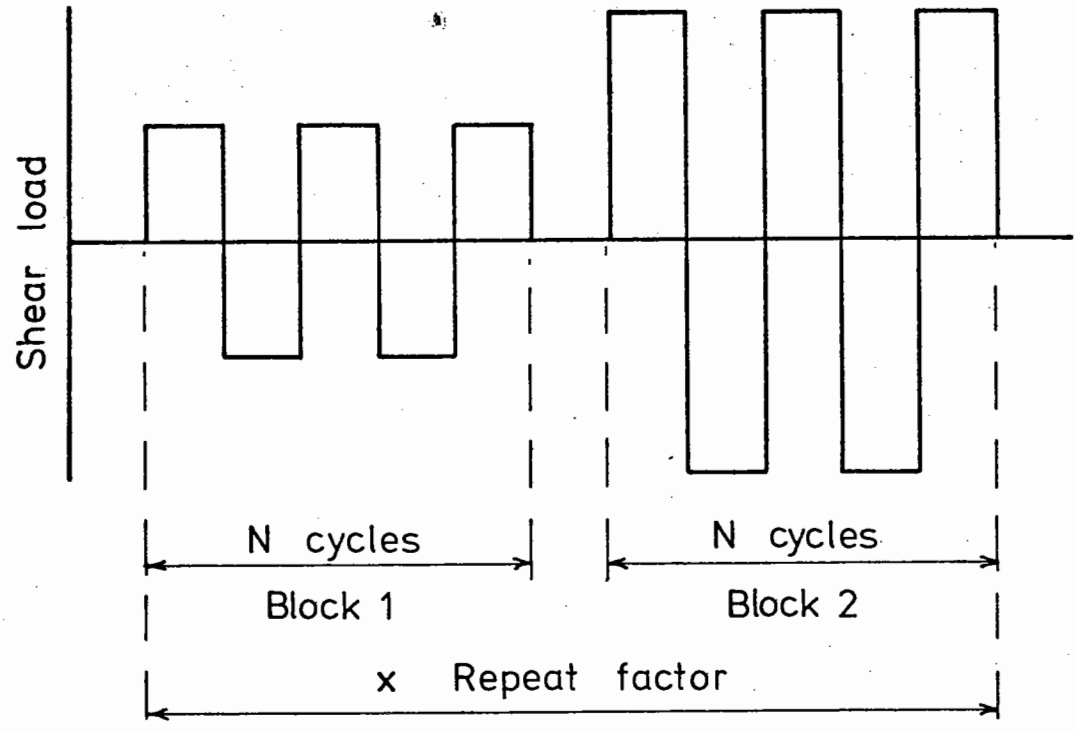

(a) Series Y

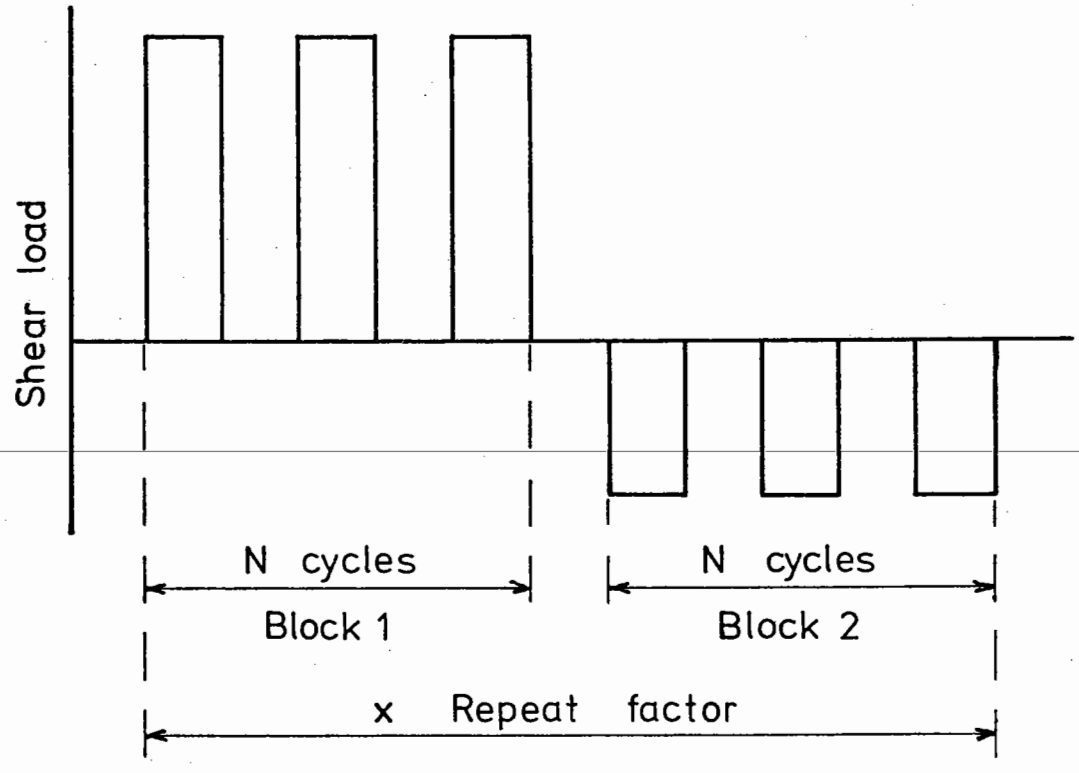

(b) Series Z

Fig.67 Block load patterns

Test	Block	$R_c(10)$	N cycles	Repeat Factor	N cycles	Repeat Factor
Series Y: Symmetric Bidirectional Loading						
Y01	1	0.34	100	5	-	-
	2	0.72	100		-	
Y02	1	0.35	10	10	50	2
	2	0.75	10		50	
Y03	1	0.74	100	2	50	2
	2	0.34	100		50	
Series Z: Unidirectional Loading (Two Way)						
Z01	1	0.11	100	5	-	-
	2	0.10	100		-	
Z02	1	0.26	100	5	-	-
	2	0.10	100		-	
Z03	1	0.36	100	5	-	-
	2	0.08	100		-	

Table 2 Details of Series Y and Z test programmes

investigate any effect this might have. One of the blocks had a cyclic shear stress ratio approximately twice as large as the other. For the Series Z tests, the block lengths remained constant throughout and the relative size of the two unidirectional load pulses was varied for each test. The purpose of this was to investigate the possibility of any healing effects which might be produced by inducing a permanent shear strain in the opposite direction to that in which it was accumulating most rapidly. This type of investigation has parallels with the work by Phillips (58), referred to in Section 2.6, which was concerned, in part, with the effectiveness of tamping of railway ballast as part of the track maintenance procedure. The problem involved is one of trying to break away from the permanent strain versus number of load cycles relationship established by the loading previous to the tamping procedure which leaves the track ballast in an almost virgin state and hence large permanent shear strains are likely to occur during the first few subsequent load cycles.

7.3 Test Results - Series Y

The data for recoverable shear strain and permanent volumetric strain for Test Y01 are shown in Figs 68 and 69 respectively. It should be noted that these figures are plotted on a linear cycles basis in contrast to those presented in Chapters Five and Six which were on a log cycles basis. Also, the straight lines joining the data points do not necessarily represent the actual path taken between the points. These comments apply to all the figures presented in this chapter.

Fig. 68 shows that, after the first package of Blocks 1 and 2, the recoverable shear strains settled down to values which depended primarily upon the applied cyclic shear stress ratios. The block

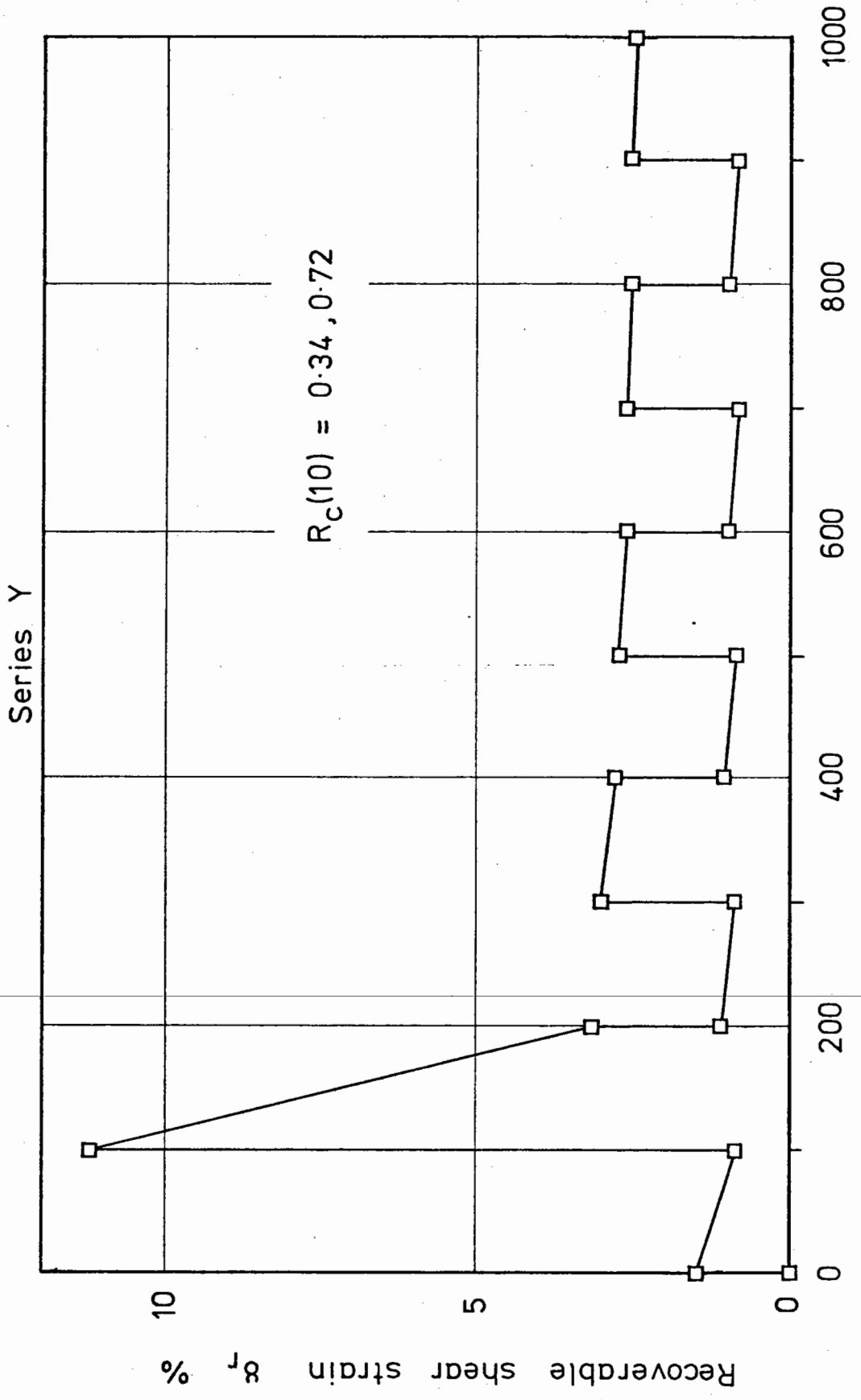

Fig.68 Recoverable shear strain results - Test Y01

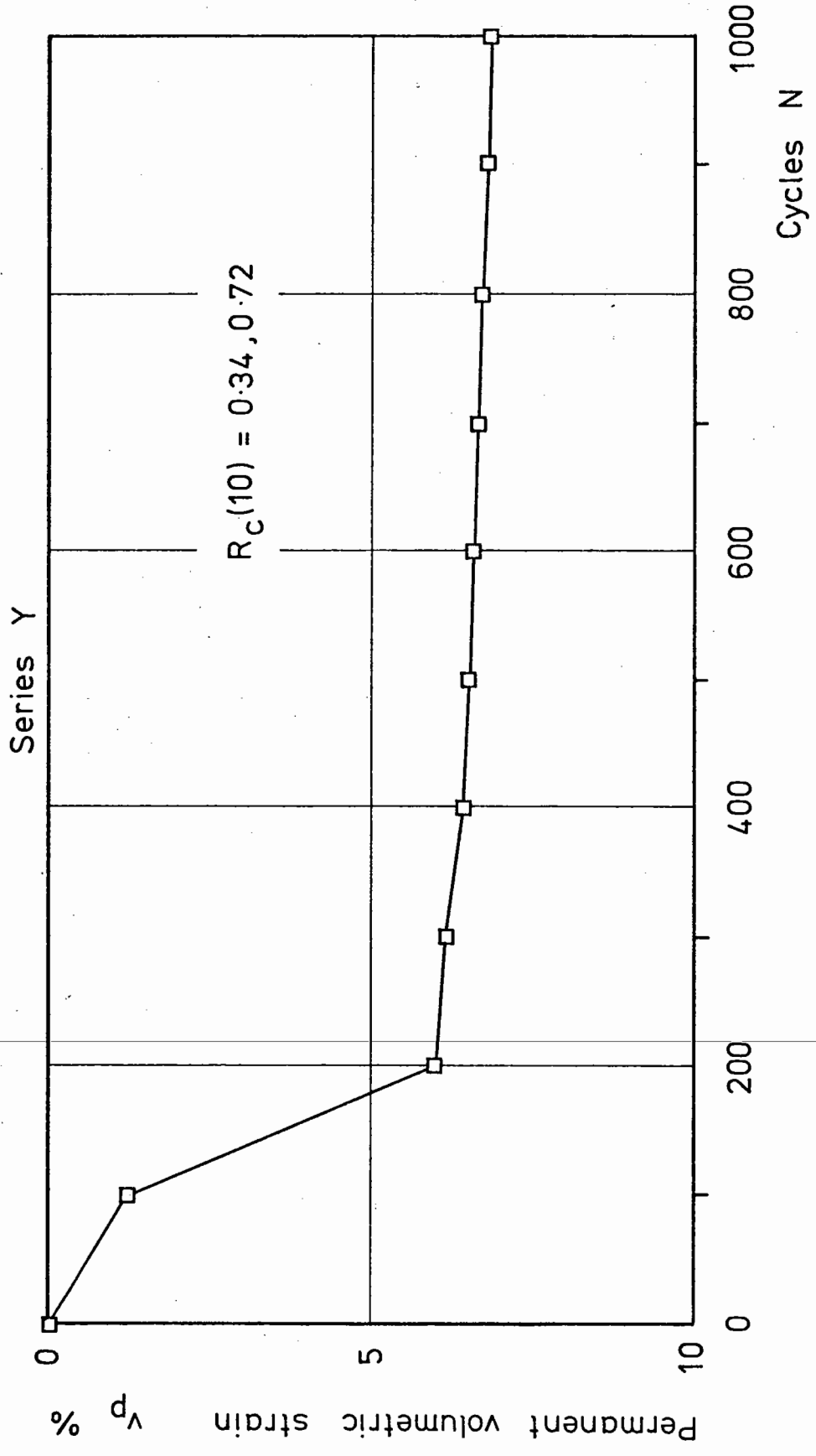

Fig.69 Permanent volumetric strain results - Test Y01

length in this test was 100 cycles and the equilibrium recoverable shear strains correspond with approximately that number of cycles in the model presented in Section 6.11, Fig. 61.

Andersen has described (3) the use of a strain contour chart, developed from the results of repeated constant stress tests, to predict the response of undrained clay samples to block loading and his method is described in Appendix J. It had been hoped that a similar technique could be used to correlate the results of the Series Y and Z tests with the results of the Series A and B using the strain contour charts shown in Figs 39, 45 and 63. However, by reference to Fig. 63, it can be seen that this is not possible for the cyclic shear stress ratios used in the Series Y tests, nominally 0.35 and 0.75, since transfer between the two cyclic shear stress ratios cannot be made along the appropriate strain contour. This is a result of the rather shallow slopes of the strain contours.

Fig. 69 shows the permanent volumetric strain behaviour in Test Y01 and comparison with Fig. 56(b) indicates that the permanent volumetric strain in Test Y01 was controlled by the influence of the larger shear load pulses.

Figs 70 and 71 show the results from the other two Series Y tests compared with the results from Test Y01. In terms of the number of cycles at a given stress level, Test Y02 is directly comparable with Test Y01 after 200 cycles and again after 400 cycles. Test Y03 is directly comparable with Test Y01 after 200, 400 and 600 cycles. From these results, it can be seen that the order in which the load cycles were applied had no significant effect on either the recoverable shear strain or the permanent volumetric strain.

No data for permanent shear strain or recoverable volumetric strain

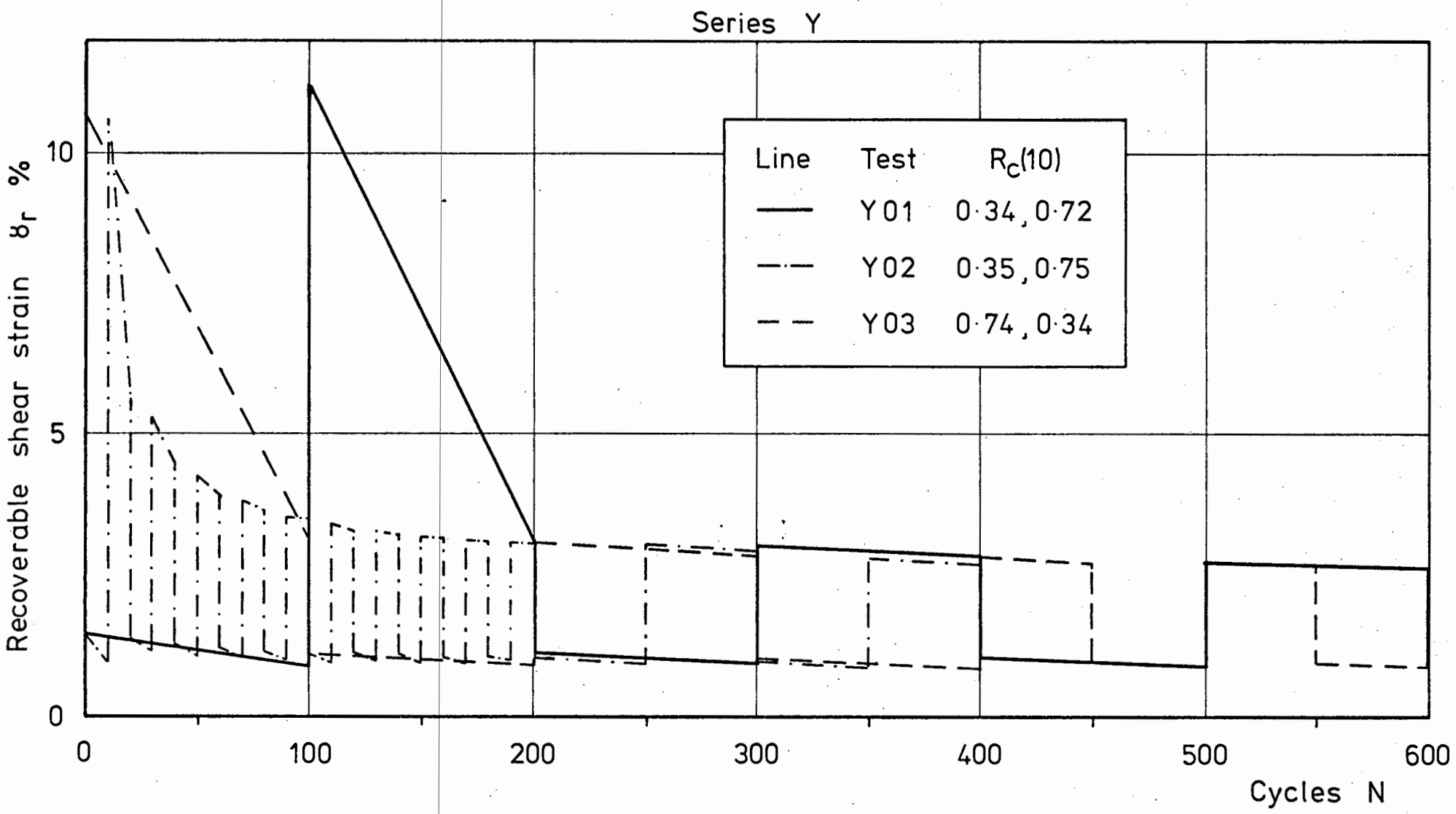

Fig.70 Recoverable shear strain results - Series Y

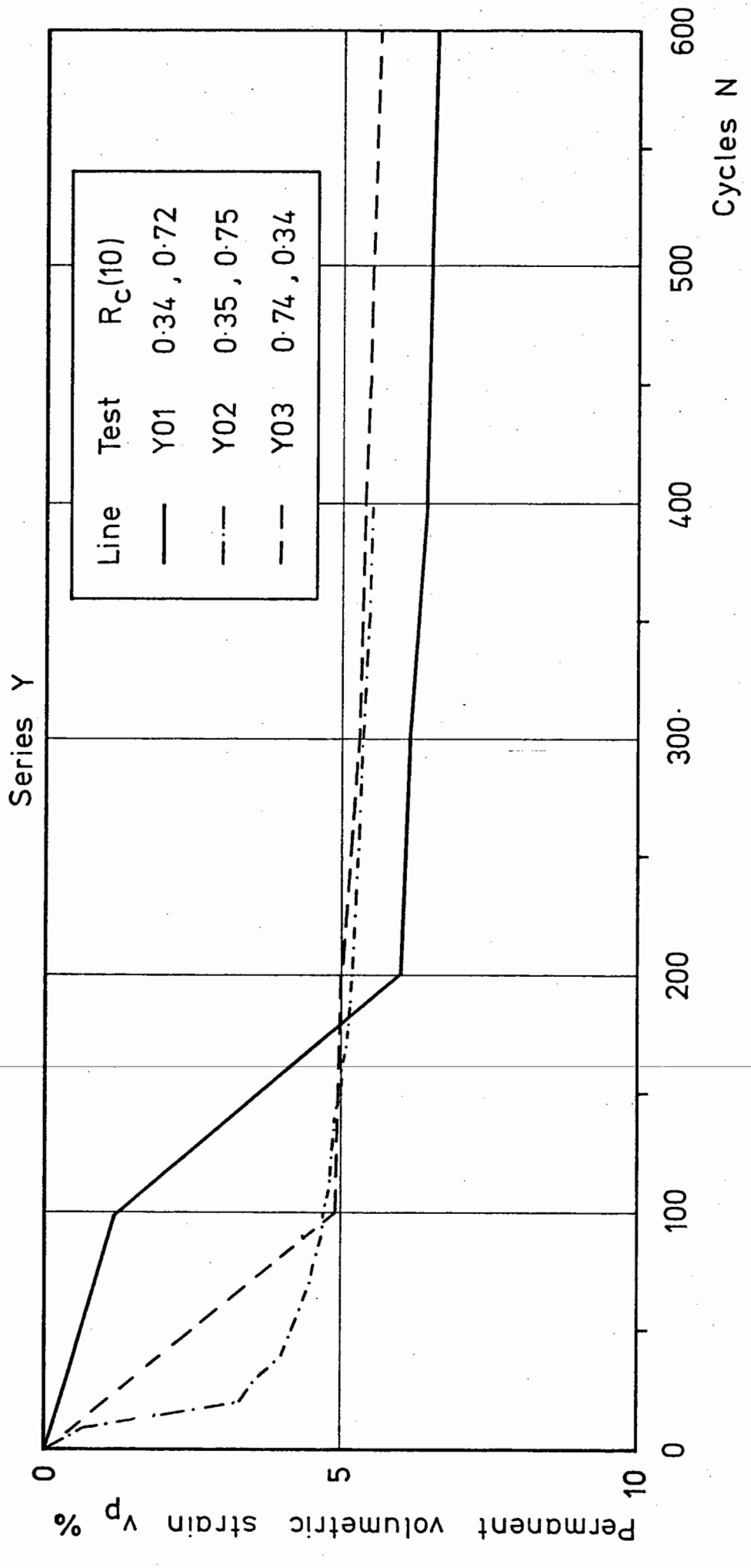

Fig. 71 Permanent volumetric strain results - Series Y

is presented for the Series Y tests for reasons similar to those discussed in Sections 6.3 and 6.6 for the Series B tests.

7.4 Permanent Shear Strain - Series Z

Fig. 72 shows the permanent shear strains developed in the Series Z tests. It should be noted that the ordinate scales used in the three graphs are quite different. Very little permanent shear strain built up in Test Z01 where the cyclic shear stress ratios for Blocks 1 and 2 were virtually equal but opposite in direction. A very small permanent shear strain did accumulate in the direction of the Block 2 loads even though this block had a slightly lower cyclic shear stress ratio. A similar situation was observed in several of the bidirectional Series B tests where the small permanent shear strains which developed tended to be in the direction of the second half of the first load cycle. This could possibly be due to slight differences in the two shear load rams. However, this is unlikely to be important because of the small permanent shear strains being considered. In Tests Z02 and Z03 the permanent shear strain accumulated in the direction of the higher shear loads. The effect of the smaller shear loads was very small because of the logarithmic nature of the response of the material to repeated load, i.e. for a linear increase in the applied load there was a logarithmic increase in the observed strains.

It can be seen, by reference to the strain contour chart in Fig. 39, that the permanent shear strain accumulated in Test Z02 during the first 100 cycles at a cyclic shear stress ratio of 0.26 is much too great to allow transfer along the permanent shear strain contour to the appropriate lower cyclic shear stress ratio, 0.10. This also explains why the smaller shear loads had only a slight effect on the

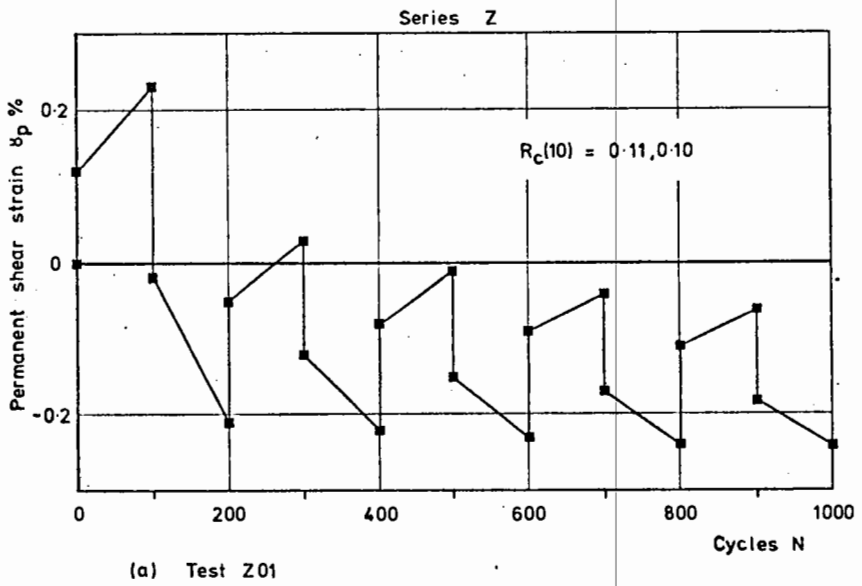

(a) Test Z01

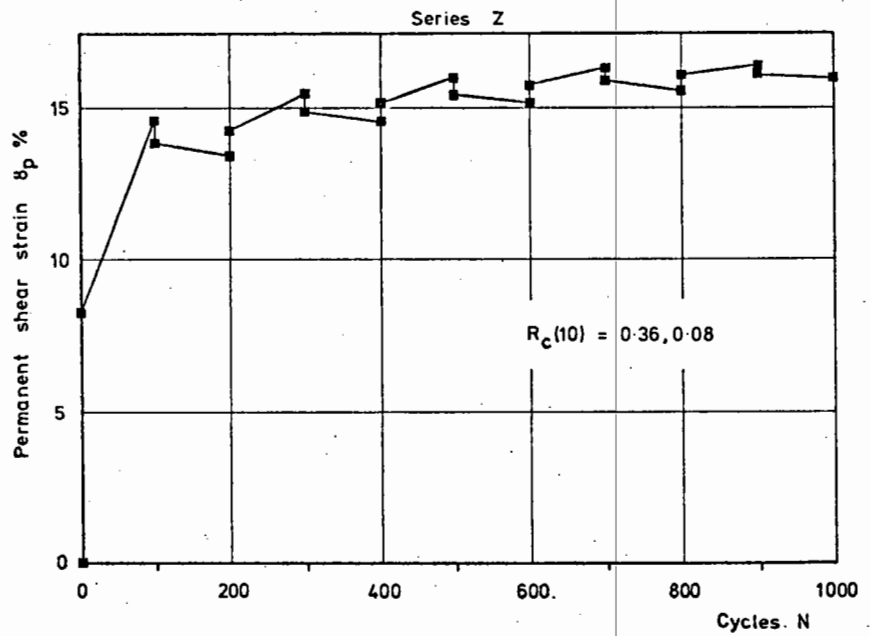

(c) Test Z03

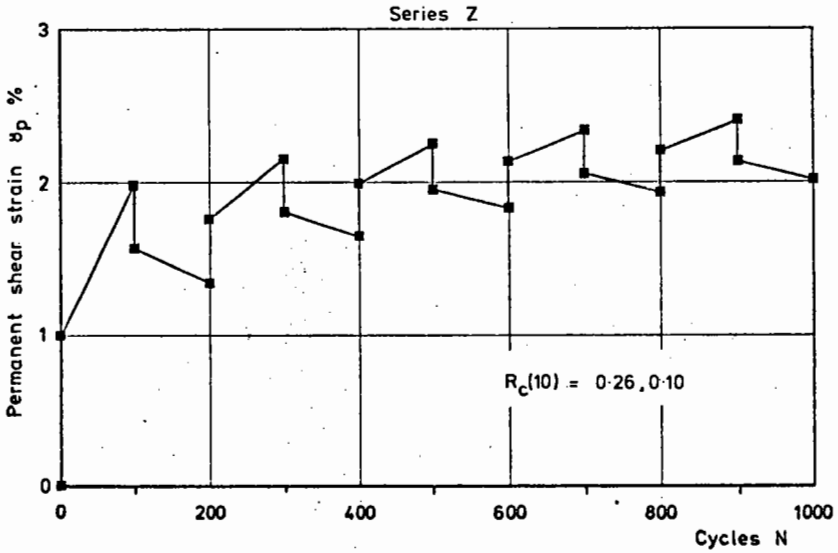

(b) Test Z02

Fig. 72 Permanent shear strain results - Series Z

permanent shear strain response observed in the Series Z tests. It is quite probable that a technique similar to that used by Andersen (Appendix J) would not, in fact, be appropriate for predicting the permanent shear strain behaviour in the Series Z tests because of the two way nature of this block loading. However, it might be possible to predict the response to unidirectional block loads which were all applied in the same direction using this method. Further work would obviously be necessary to clarify the situation where the unidirectional block loads are applied in opposite directions as in the Series Z tests.

For similar reasons, the effect of the smaller shear loads in Test Z03 was even less significant than in Test Z02 since the ratio between the two shear loads was even greater.

7.5 Recoverable Shear Strain - Series Z

The recoverable shear strain behaviour for the Series Z tests is shown in Fig. 73 where it can be seen that the behaviour was similar to that described in Section 7.3 for the Series Y tests. By reference to Fig. 41, which is based on the Series A results, it can be seen that the recoverable shear strains in the Series Z tests settled down to values which depended primarily on the applied cyclic shear stress ratio and were not significantly affected by the stress history. In view of the permanent shear strain behaviour described in the previous section and considering the recoverable shear strain contour model described in Section 6.11, this is not surprising. The influence of the larger shear loads was dominant over the smaller loads because of the logarithmic nature of the response.

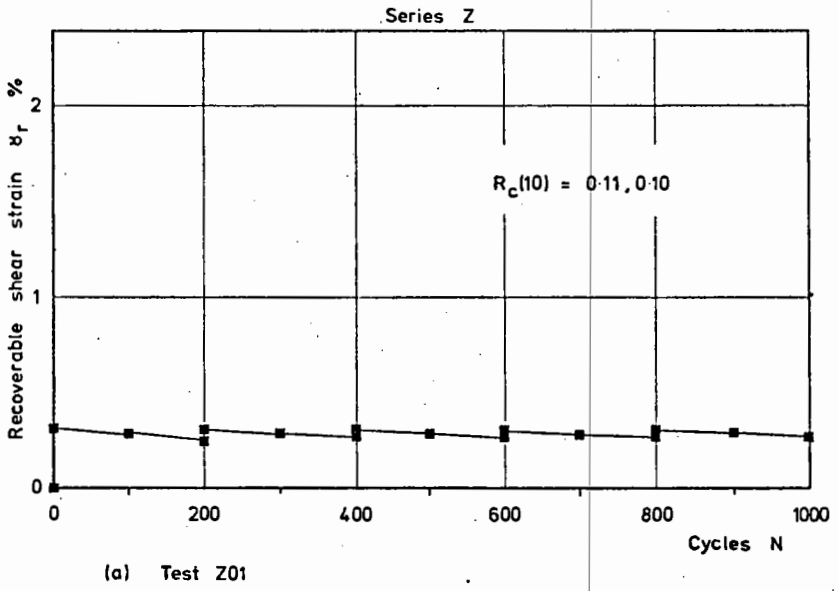

(a) Test Z01

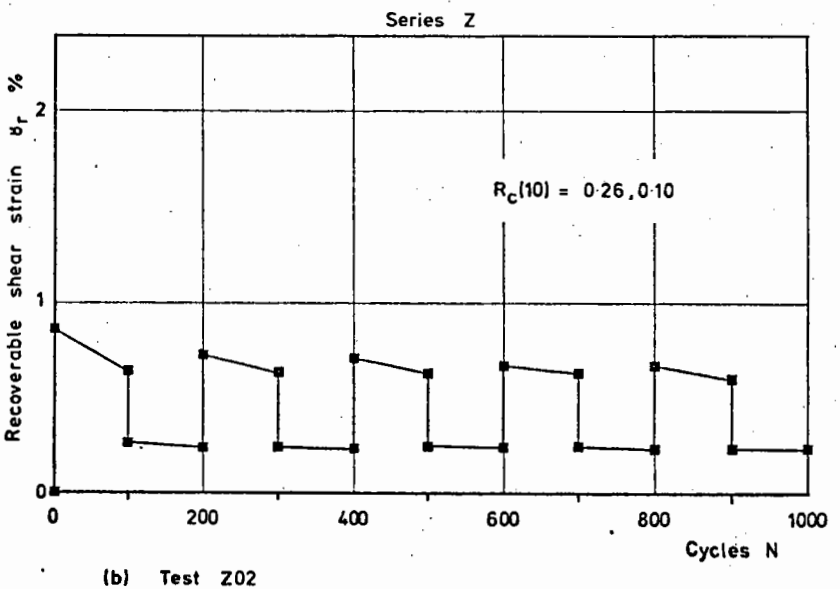

(b) Test Z02

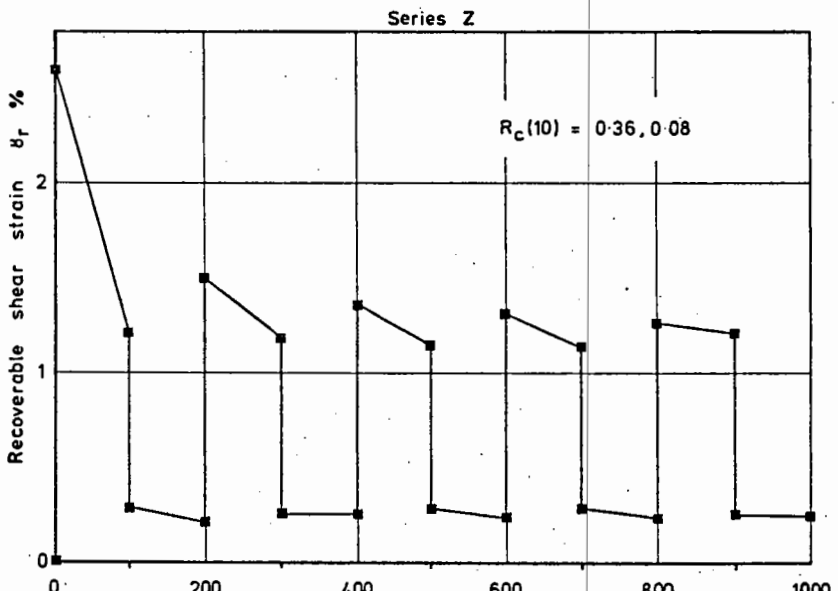

(c) Test Z03

Fig. 73 Recoverable shear strain results - Series Z

7.6 Permanent Volumetric Strain - Series Z

The permanent volumetric strain behaviour for the Series Z tests is shown in Fig. 74 and it can be seen, by comparison with the Series A results, Fig. 47(b), that the strain was again dominated by the response of the material to the larger cyclic shear stresses. However, careful inspection of the results does indicate some evidence to suggest that the two way nature of this block loading does slightly increase the permanent volumetric strain for a given number of cycles. Direct comparison here with the bidirectional Series B results is not really appropriate because of the different dilational responses observed in the unidirectional and bidirectional repeated load tests.

In Test Z03, dilation continued to have an effect throughout the test. Each time the larger block load was started the material dilated initially and then compacted. When the subsequent smaller block load was started, there was an immediate compaction followed by further compaction during the course of that block.

7.7 Recoverable Volumetric Strain - Series Z

The recoverable volumetric strain behaviour for the Series Z tests is shown in Fig. 75. The data for Tests Z01 and Z03 is incomplete because of problems with the chart recorders. By reference to Fig. 49, it can be seen that the recoverable volumetric strains in the Series Z tests were governed by the applied cyclic shear stress ratios and that the stress history had very little effect.

7.8 Concluding Remarks

This chapter has described two short series of block load tests which were carried out partly to investigate any stress history effects

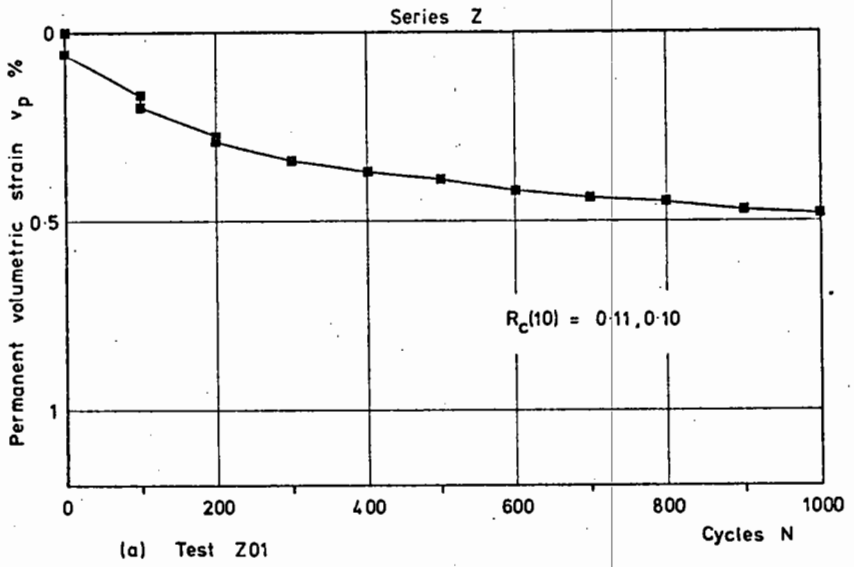

(a) Test Z01

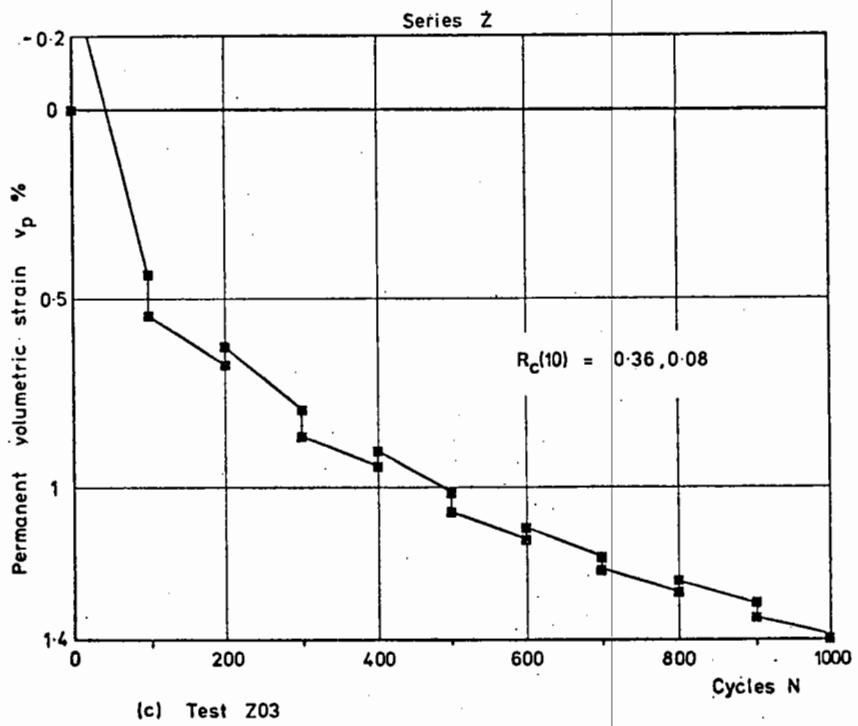

(c) Test Z03

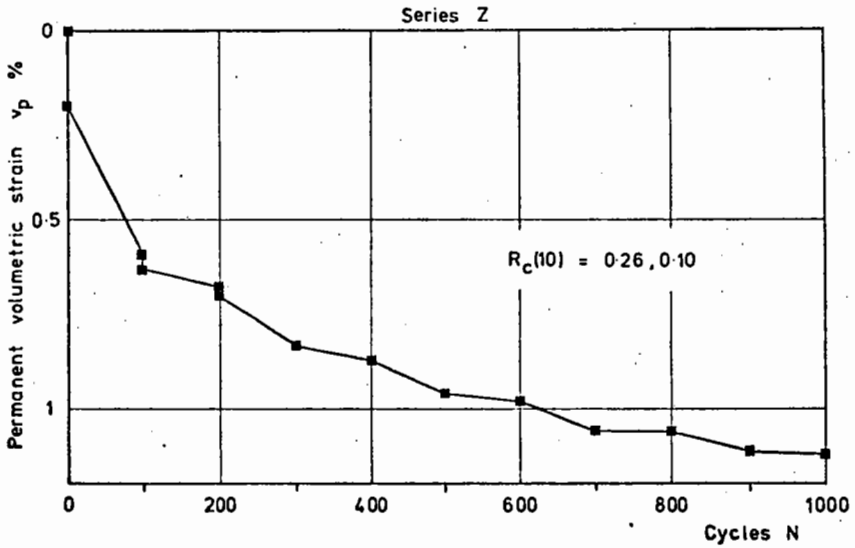

(b) Test Z02

Fig. 74 Permanent volumetric strain results - Series Z

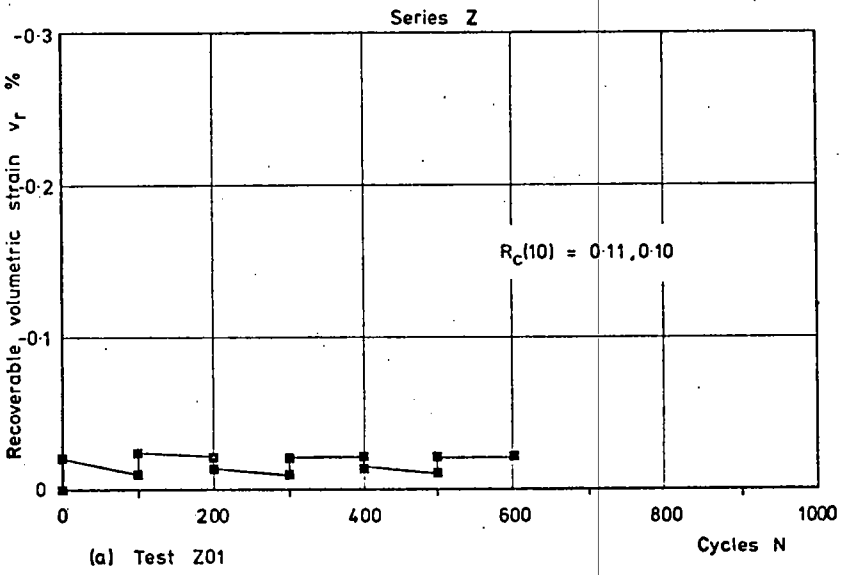

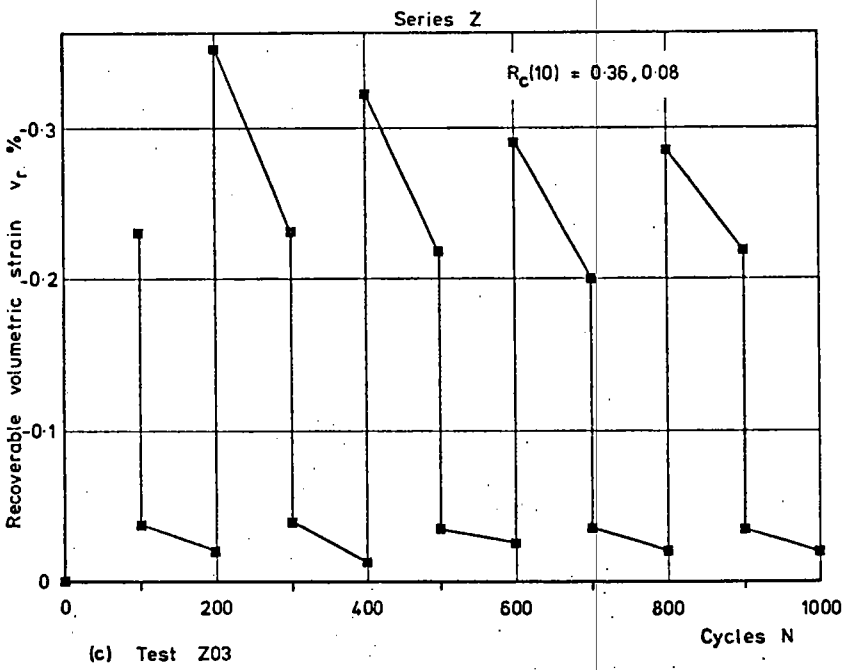

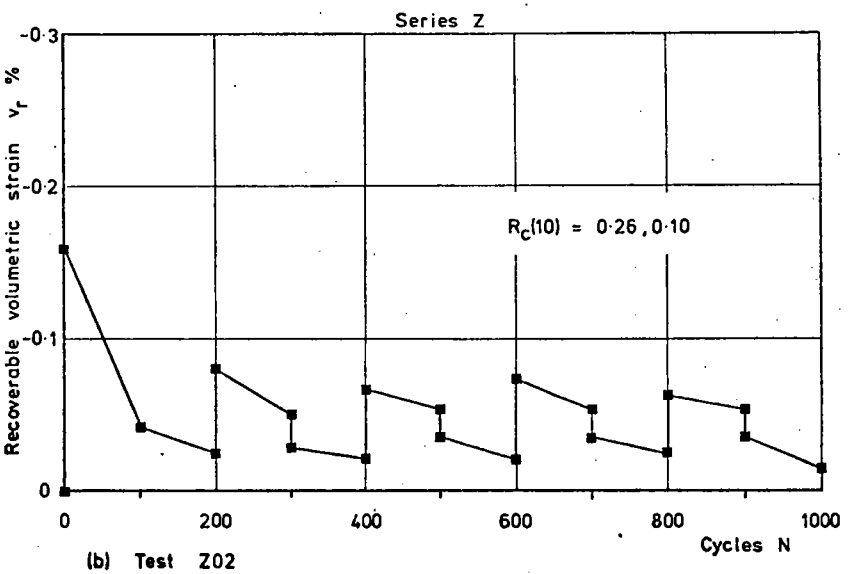

Fig. 75 Recoverable volumetric strain results - Series Z

and partly to determine whether the response of the material to a load spectrum could be predicted from the results of repeated load tests at constant stress levels. In general, it was found that stress history had practically no effect on the subsequent behaviour of the material. Unfortunately, because of the values of cyclic shear stress ratio chosen for the block load tests, it was not possible to compare the strain contour models with the block load tests. The results obtained from these tests indicated that the overall response of the material was dominated by the larger cyclic shear stress pulses, particularly when these were a large proportion of the static failure strength. This dominance of the larger cyclic stress ratio could possibly be hiding any stress history effects which might exist if the smaller cyclic shear stress ratio was somewhat higher.

In practice, the dominant influence of the larger cyclic shear stress ratios is probably of particular interest in the rail track situation where cyclic shear stress ratios are likely to be higher than in a road pavement. In particular, high stress ratios are likely to occur in the ballast which is in the vicinity of the sleepers where the confining stresses are low.

Suggestions for further block load tests are discussed in Chapter Nine; quite severe restrictions would have to be imposed on the cyclic shear stress ratios and the number of load cycles applied in order to investigate the use of strain contour charts to predict block load test behaviour.

CHAPTER EIGHT

CONCLUSIONS

Simple shear tests have been carried out on two nominally single size granular materials. Nominally 1 mm particles were used in the Mk1 apparatus with rigid sample boundaries and nominally 3 mm particles were used in the larger Mk2 apparatus which incorporated a split top platen. The main conclusions of the work described in this thesis are listed below:

1.(a) In a simple shear apparatus with rigid sample boundaries, the stress conditions are such that differential dilation induces a severely non-uniform stress distribution over the length of the sample and this distribution varies during the course of shearing.

(b) These non-uniformities cause a wide discrepancy between the values of the angle of shearing resistance evaluated on an "average stress" basis and on a "local stress" basis using transducer measurements from the central third of the sample.

(c) The use of a simple shear apparatus with the top platen split into three independent, stress controlled sections considerably reduces this discrepancy.

2.(a) The permanent shear strain behaviour under unidirectional repeated load is characterised by a relatively large initial strain representing approximately one half of the strain after 10^4 load cycles.

(b) The accumulation of permanent shear strain is linear with respect to the logarithm of the number of load cycles.

(c) The permanent shear strain which develops under symmetric bidirectional repeated load is negligible.

3.(a) For all types of repeated loading considered herein, the recoverable shear strain can be defined as the peak to peak shear strain.

(b) The logarithm of the recoverable shear strain after a given number of cycles is linearly related to the applied cyclic shear stress ratio.

(c) The material stiffens considerably during the first few hundred load cycles but after several thousand cycles, it settles down to an equilibrium recoverable shear strain except at higher cyclic shear stress ratios where 10^4 cycles, or more, may be required to reach this state.

(d) The shear modulus is dependent on both the cyclic shear stress ratio and the normal stress though there was a considerable degree of scatter in these results.

4.(a) A threshold situation exists for permanent volumetric strain. At cyclic shear stress ratios below the threshold value, which depends on the type of loading, the material initially compacts and continues to do so. A slight tendency to reach a limiting density is only apparent at low cyclic shear stress ratios.

(b) At cyclic shear stress ratios above the threshold value, the permanent volumetric strain is initially dilatant followed by compaction to a density greater than the initial density.

(c) Some qualitative evidence to indicate that this continued compaction is accommodated by particle degradation has been observed, particularly at high cyclic shear stress ratios.

(d) The recoverable volumetric strains are always dilatant and follow a pattern similar to that of the recoverable shear strains; settling down eventually to an equilibrium value

which depends on the cyclic shear stress ratio.

5. In the range considered, $R_c \geq R_m \geq 0$, the mean shear stress ratio, R_m, has no significant effect on the elastic response of the material to repeated load.

6. Despite a considerable reduction in porosity during repeated loading, no subsequent increase in the static shear strength of the material has been observed.

7. From the results obtained, it appears that stress history effects are negligible for this material.

8. Various empirical models for the response of the material to repeated load have been developed. The slight effect of normal stress, which was independent of its direct influence on the cyclic shear stress ratio, has been ignored in the development of these models. This means that they are generally most accurate for the intermediate level of normal stress considered; 190 kPa nominal. The models have been presented in both graphical and mathematical form. In the latter case, they are suitable for incorporation into a computer program.

CHAPTER NINE

RECOMMENDATIONS FOR FURTHER WORK

9.1 Introduction

This chapter includes an appraisal of the Mk2 Simple Shear Apparatus and recommendations for its further development and future work are discussed in the light of experience gained during the test programme described in the preceding chapters. These recommendations depend, to some extent, on the desired nature of the future test programme and a decision on this point would seem to be necessary before any major modifications are made to the apparatus.

9.2 Recommendations for Further Work and the Development of the Simple Shear Apparatus

In order to more closely simulate the stress conditions under a rolling wheel load, it would be necessary to incorporate a cyclic normal load into the control system and the difficulties likely to be encountered with this were referred to in Section 4.4. The phasing of the normal and shear stress pulses would have to be such that the shear stress did not build up too quickly in relation to the normal stress otherwise very large shear deformations might occur. Considering the logarithmic nature of the response of the material to different cyclic shear stress ratios, the problems encountered might well be considerable and extensive continuous data logging facilities would almost certainly be required to do this. A two-gun cathode ray oscilloscope would probably be necessary to compare the two stress pulses directly.

The introduction of such a cyclic normal load facility would probably increase the cycle time to something of the order of 5 to 10

seconds to allow the stress pulses to be phased correctly. This would increase the length of a test; 10^4 cycles at a cycle time of 5 seconds would take almost 14 hours. For tests using a constant normal load, it may be worthwhile investigating the possibility of using different cycle times at different stages of a test. For example, 5 seconds for each of the first 10 cycles, 3 seconds each up to 10^3 cycles and 2 seconds for each cycle thereafter. Test of 10^4 cycles would only take about 6 hours using this arrangement. Different frequencies were used during the repeated load triaxial tests described by Shenton (73) with apparently no significant adverse effects.

The problems involved with phasing the two stress pulses might be reduced if a servo-hydraulic loading arrangement such as that referred to in Section 5.2 were used since this would reduce the response time of the control system due to the hydraulic oil being practically incompressible. If the present pneumatic system were, in fact, to be retained the response time of the system could probably be reduced by filling the loading rams with hydraulic oil and having air/oil interfaces at a suitable points in the pipelines.

From the results presented in the preceding chapters, it can be seen that the apparatus has generally behaved in a consistent manner using the sample preparation technique and test control arrangements described. The split top platen would seem to have removed the problem of differential dilation which caused considerable changes in the stress distribution over the length of the sample during single load tests in the Mk1 apparatus. The total shear load cells were the only unsatisfactory components of the Mk2 apparatus. A considerable time was devoted to developing a suitable total shear load cell but the final design proved unsatisfactory because of seating difficulties. It is suggested that

a load cell on the lines of the normal load cells used in the top platen might prove suitable since no real problems were encountered in their development and seating was not such a problem with this load cell because of its layout. The use of steel for these load cells should allow suitable transducers of a reasonable size to be produced. In connection with the total shear load, it may well be desirable to change the position of the shear rams so that their mutual line of action is on a level with the mid-height of the sample. This would minimise any moment effects caused by the lever arm of the shear load. However, this does not appear to have been a great problem with the present arrangement. Realignment of the shear load rams would require a loading bracket to be fixed to each end of the shear box to clear the clamping frame which controls the end plates. As a further refinement, it may be worthwhile to line the side boundaries of the sample with hardened steel plates so as to reduce any frictional effects at these two interfaces.

Following these modifications to the apparatus, some of the tests could be repeated to investigate the correlation between the total shear load and the strains produced. In addition, the influence of normal stress, which has been ignored in the analysis herein, could be further investigated to provide more information on the stress dependency of the material properties. If more extensive data logging facilities were available, it would also be useful to check the correlation between the shear strains and the sum of the outputs from the three shear stress transducers. The results from these tests should help to clarify the problems associated with correlating average strain parameters with local stress parameters previously referred to in Sections 5.6 and 5.9. It seems possible that the sum of the three

shear stress transducer outputs might be a useful parameter on which to base these correlations. These results would also provide information on the stress distribution over the length of the sample and how this changes during the course of a test. A more complete data logging system would be required for this because it seems probable that the stress distribution changes quite rapidly during the early stages of the test. It is rather difficult to make recommendations as to what form the data logging system should take since this will depend on the intended future programme and the amount of money available for its development. Any addition to the number of two-pen chart recorders in use would be unmanageable. Multi-channel ultra violet chart recorders have restrictions in their chart width and their resolution may be unsatisfactory, partly because of the lack of clarity of the trace and partly because of the confusion which can arise from having several traces of one colour on the same chart. The possibility of using a 14 channel FM tape recorder for data logging in alalogue form was briefly discussed in Section 4.3. Development of this system to meet the requirements of the simple shear apparatus would probably take some time but this would almost certainly cost less than a fully computerised Solartron data logging system which would be necessary to overcome the problem of scanning speed which precludes the data logging system used for the single load Series S tests described in Section 4.7.

Further block load tests are necessary to provide more comprehensive information on the effects of stress history on the subsequent response of the material. These tests should use cyclic shear stress ratios which are closer together than those used in the block load tests described in Chapter Seven. Also, the number of

cycles of the larger load should be restricted so that its effect does not entirely dominate that of the smaller load pulses. The results of these tests should allow the possible use of strain contour charts for predicting the response to block loading to be investigated.

An entirely different line of approach for further work is suggested by the permanent volumetric strain results obtained from the repeated load tests. Shear straining would appear to be a very useful method of inducing vertical compaction even under a constant vertical load as was used in the tests described herein. In practice, it might be possible to compact granular material by attaching a rotating eccentric mass to a heavy steel plate resting on the surface of the material. Attention would have to be paid to providing an efficient mechanism to transfer the shear loads to the material to be compacted. A system similar to that used in this work would probably be effective. However, a simpler system using ribs on the base of the plate might well be equally effective and more practical. The speed of rotation of the eccentric could be varied to achieve an optimum rate of compaction. Too great a speed might cause problems with dilation effects. A prototype Dynamic Track Stabiliser which compacts railway ballast by dynamic lateral loading of the track itself is currently being developed by Plasser and Thuerer Limited. Wheeled clamps are suspended beneath a slowly moving wagon and they apply a constant vertical load to the rails by means of jacks. The lateral loads are provided by means of rotating eccentrics and the loads are transmitted into the ballast via the sleepers (74).

In order to directly compare the results from this simple shear apparatus with those obtained by other researchers, it would be necessary to carry out some repeated constant shear strain tests and

these could well be useful even though the repeated constant shear stress situation is generally more relevant to the pavement situation. A cam and lever arm system similar to that used by Silver and Seed (75) would probably be suitable for this type of test since it allows direct control over the frequency and amplitude of the loading. Also, a series of strain controlled single load tests would probably provide a fuller understanding of the behaviour of granular material in simple shear than that obtained from the stress controlled, Series S tests.

All the tests reported in this thesis have involved a nominally single size material which has been used to model a railway ballast. The use of a dry, well graded material, such as that used by Boyce (9), would be an obvious next step though the maximum particle size would have to be much less than that used by him. It would also probably be instructive to carry out some repeated load triaxial tests on the nominally single size material used in the Mk2 apparatus for comparison with the results presented herein.

With the Mk2 Simple Shear Apparatus in its present form, the lateral normal stresses on the sample are unknown and the principal stresses cannot be evaluated. Thus, analysis of the data on the basis of stress invariants, such as those used at Cambridge for triaxial tests (69), cannot be carried out. It might be possible to measure some of the required lateral stresses by incorporating load cells into the sides of the shear box. Their design could be based on that used for the existing normal stress transducers. However, rigidly mounting these load cells on the apparatus may be difficult because of the limited space available between the shear box and the main frame. Even with this additional information, the stress conditions are not completely defined. The normal stress on the faces parallel to the

end plates are still unknown though it might be possible, in the first instance, to assume these as being equal to the normal stresses on the other side faces of the sample. These limitations of the apparatus do not, however, detract from the usefulness of the apparatus for investigating the overall deformation characteristics of granular material and developing some form of model for its response to repeated load.

REFERENCES

1. ALLEN, J.J. and THOMSON, M.R., "Resilient Response of Granular Materials Subjected to Time-Dependent Lateral Stresses", Transportation Research Record, No. 510, 1974, pp. 1-13.
2. ALLEN, J.J. and THOMSON, M.R., "Significance of Variably Confined Triaxial Testing", Transportation Engineering Journal, Proceedings A.S.C.E., Vol. 100, No. TE4, Proc. Paper 10911, November 1974, pp. 827-843.
3. ANDERSEN, K.H., "Behaviour of Clay Subjected to Undrained Cyclic Loading", Proceedings of the International Conference on the Behaviour of Off-Shore Structures, BOSS '76, Trondheim, 1976, Vol. 1, pp. 392-403.
4. ARTHUR, J.R.F. and ROSCOE, K.H., "An Earth Pressure Cell for the Measurement of Normal and Shear Stresses", Civil Engineering and Public Works Review, Vol. 56, June 1961, pp. 765-770.
5. BARKSDALE, R.D., "Laboratory Evaluation of Rutting in Base Course Materials", Proceedings of the Third International Conference on the Structural Design of Asphalt Pavements, London, 1972, Vol. 1, pp. 161-174.
6. BASSETT, R.H., The Simple Shear Apparatus, Lecture Notes for Course on "Research Techniques and Equipment in Soil Mechanics", CUED/C-SOILS/LN2(1973), Department of Engineering, University of Cambridge.
7. BJERRUM, L., "Geotechnical Problems Involved in Foundations of Structures in the North Sea", Geotechnique, Vol. 23, No. 3, 1973, pp. 319-358.
8. BJERRUM, L. and LANDVA, A., "Direct Simple-Shear Tests on a

Norwegian Quick Clay", Geotechnique, Vol. 16, No. 1, 1966, pp. 1-20.

9. BOYCE, J.R., The Behaviour of a Granular Material Under Repeated Loading, Ph.D. Thesis, Department of Civil Engineering, University of Nottingham, 1976.

10. BRANSBY, P.L., Cambridge Contact Stress Transducers, Lecture Notes for Course on "Research Techniques and Equipment in Soil Mechanics", CUED/C-SOILS/LN2(1973), Department of Engineering, University of Cambridge.

11. BRANSBY, P.L., Private oral communication, September 1975.

12. BRITISH STANDARDS INSTITUTION, British Standard 1377:1967, Methods of Testing Soils for Civil Engineering Purposes, British Standards Institution, London, 1967.

13. BRITISH STANDARDS INSTITUTION, PD 5686:1972, The Use of SI Units, British Standards Institution, London, 1972.

14. BROWN, S.F., "Repeated Load Testing of a Granular Material", Journal of the Geotechnical Engineering Division, Proceedings A.S.C.E., Vol. 100, No. GT7, Proc. Paper 10864, July 1974, pp. 825-841.

15. BROWN, S.F. and HYDE, A.F.L., "The Significance of Cyclic Confining Stresses in Repeated Load Triaxial Testing of Granular Material", Transportation Research Record, No. 537, 1975, pp. 825-841.

16. BURMISTER, D.M., "The Place of the Direct Shear Test in Soil Mechanics", Symposium on Direct Shear Testing of Soils, A.S.T.M. Special Technical Publication No. 131, 1952, pp. 3-18.

17. CHAN, C.K. and MULILIS, J.P., "Pneumatic Sinusoidal Loading System", Journal of the Geotechnical Engineering Division,

Proceedings A.S.C.E., Vol. 102, No. GT3, Technical Note, Proc. Paper 11953, March 1976, pp. 277-282.

18. CULLINGFORD, G., LASHINE, A.K.F. and PARR, G.B., "Servo-Controlled Equipment for Dynamic Triaxial Testing of Soils", Geotechnique, Vol. 22, No. 2, Technical Note, 1972, pp. 526-529.

19. D'APPOLONIA, E., "Dynamic Loadings", Journal of the Soil Mechanics and Foundations Division, Proceedings A.S.C.E., Vol. 96, No. SM1, Proc. Paper 7010, January 1970, pp. 42-72.

20. DEHLEN, G.L. and MONISMITH, C.L., "Effect of Nonlinear Material Response on the Behaviour of Pavements under Traffic", Highway Research Record, No. 310, 1970, pp. 1-16.

21. DEPARTMENT OF THE ENVIRONMENT, Specification for Road and Bridge Works, Her Majesty's Stationery Office, London, 1969.

22. DEPARTMENT OF THE ENVIRONMENT, A Guide to the Structural Design of Pavements for New Roads, Road Note 29, Third Edition, Her Majesty's Stationery Office, London, 1970.

23. DUNCAN, J.M. and DUNLOP, P., "Behaviour of Soils in Simple Shear Tests", Proceedings of the Seventh International Conference on Soil Mechanics and Foundation Engineering, Mexico City, 1969, Vol. 1, pp. 101-109.

24. DUNCAN, J.M., MONISMITH, C.L. and WILSON, E.L., "Finite Element Analyses of Pavements", Highway Research Record, No. 228, 1968, pp. 18-33.

25. ELLIS, G.P., The Behaviour of North Sea Sand Under Cyclic Loading Conditions, M.Sc. Thesis, University of Manchester, 1975.

26. EMBANKMENT-DAM ENGINEERING, Casagrande Volume, John Wiley and Sons Inc., New York, 1973.

27. FINN, W.D.L., BRANSBY, P.L. and PICKERING, D.J., "Effect of

Strain History on Liquefaction of Sand", Journal of the Soil Mechanics and Foundations Division, Proceedings A.S.C.E., Vol. 96, No. SM6, Proc. Paper 7670, November 1970, pp. 1917-1934.

28. FINN, W.D.L., PICKERING, D.J. and BRANSBY, P.L., "Sand Liquefaction in Triaxial and Simple Shear Tests", Journal of the Soil Mechanics and Foundations Division, Proceedings A.S.C.E., Vol. 97, No. SM4, Proc. Paper 8039, April 1971, pp. 639-659.

29. GREEN, G.E. and READES, D.W., "Boundary Conditions, Anisotropy and Sample Shape Effects on the Stress-Strain Behaviour of Sand in Triaxial Compression and Plane Strain", Geotechnique, Vol. 25, No. 2, 1975, pp. 333-356.

30. HEATH, D.L., SHENTON, M.J., SPARROW, R.W. and WATERS, J.M., "Design of Conventional Rail Track Foundations", Proceedings of the Institution of Civil Engineers, Vol. 51, February 1972, pp. 251-267.

31. HENNES, R.G., "The Strength of Gravel in Direct Shear", Symposium on Direct Shear Testing of Soils, A.S.T.M. Special Technical Publication No. 131, 1952, pp. 51-62.

32. HORN, H.M. and DEERE, D.U., "Frictional Characteristics of Minerals", Geotechnique, Vol. 12, No. 4, 1962, pp. 319-335.

33. HOUSEL, W.S., "The Shearing Resistance of Soil - Its Measurement and Practical Significance", Proceedings A.S.T.M., Vol. 39, 1939, pp. 1084-1099.

34. HVORSLEV, M.J., "A Ring Shear Apparatus for the Determination of the Shearing Resistance and Plastic Flow of Soils", Proceedings of the International Conference on Soil Mechanics and Foundation Engineering, Cambridge, Massachusetts, 1936, Vol. 2, pp. 125-129.

35. HYDE, A.F.L., Repeated Load Triaxial Testing of Soils, Ph.D.

Thesis, Department of Civil Engineering, University of Nottingham, 1974.

36. ISHIBASHI, I. and SHERIF, M.A., "Soil Liquefaction by Torsional Simple Shear Device", Journal of the Geotechnical Engineering Division, Proceedings A.S.C.E., Vol. 100, No. GT8, Proc. Paper 10752, August 1974, pp. 871-888.

37. KIRKPATRICK, W.M., "Effects of Grain Size and Grading on the Shearing Behaviour of Granular Materials", Proceedings of the Sixth International Conference on Soil Mechanics and Foundation Engineering, Montreal, 1965, Vol. 1, pp. 273-277.

38. KJELLMAN, W., "Testing the Shear Strength of Clay in Sweden", Geotechnique, Vol. 2, No. 3, 1951, pp. 225-232.

39. KOERNER, R.M., "Effect of Particle Characteristics on Soil Strength", Journal of the Soil Mechanics and Foundations Division, Proceedings A.S.C.E., Vol. 96, No. SM4, Proc. Paper 7393, July 1970, pp. 1221-1234.

40. KOERNER, R.M., "Behaviour of Single Mineral Soils in Triaxial Shear", Journal of the Soil Mechanics and Foundations Division, Proceedings A.S.C.E., Vol. 96, No. SM4, Proc. Paper 7432, July 1970, pp. 1373-1390.

41. KOLBUSZEWSKI, J., "An Experimental Study of the Maximum and Minimum Porosities of Sands", Proceedings of the Second International Conference on Soil Mechanics and Foundation Engineering, Rotterdam, 1948, Vol. 1, pp. 158-165.

42. KOLBUSZEWSKI, J. and ALYANAK, I., "Effects of Vibrations on the Shear Strength and Porosity of Sands", The Surveyor and Municipal Engineer, Vol. 123, No. 3756, 30 May 1964, pp. 23-27, and No. 3757, 6 June 1964, pp. 31-34.

43. LADD, R.S., "Specimen Preparation and Liquefaction of Sands", Journal of the Geotechnical Engineering Division, Proceedings A.S.C.E., Vol. 100, No. GT10, Technical Note, Proc. Paper 10857, October 1974, pp. 1180-1184.

44. LAMBE, T.W. and WHITMAN, R.V., Soil Mechanics, John Wiley and Sons Inc., London, 1969.

45. LAREW, H.G. and LEONARDS, G.A., "A Strength Criterion for Repeated Loads", Proceedings of the Highway Research Board, Vol. 41, 1962, pp. 529-556.

46. LEE, K.L., The Influence of End Restraint in the Cyclic Triaxial Test, Report to U.S. Army, Contract Report No. S-76-1, March 1976.

47. LEE, K.L. and FITTON, J.A., "Factors Affecting the Cyclic Loading Strength of Soil", Vibration Effects of Earthquakes on Soils and Foundations, A.S.T.M. Special Technical Publication No. 450, 1969, pp. 71-95.

48. LEE, K.L. and SEED, H.B., "Cyclic Stress Conditions Causing Liquefaction of Sand", Journal of the Soil Mechanics and Foundations Division, Proceedings A.S.C.E., Vol. 93, No. SM1, Proc. Paper 5058, January 1967, pp. 47-70.

49. LEE, K.L. and SEED, H.B., "Drained Strength Characteristics of Sands", Journal of the Soil Mechanics and Foundations Division, Proceedings A.S.C.E., Vol. 93, SM6, Proc. Paper 5561, November 1967, pp. 117-141.

50. LEPS, T.M., "Review of Shearing Strength of Rockfill", Journal of the Soil Mechanics and Foundations Division, Proceedings A.S.C.E., Vol. 96, No. SM4, Proc. Paper 7394, July 1970, pp. 1159-1170.

51. LUCKS, A.S., CHRISTIAN, J.T., GREGG, E.B. and HOEG, K., "Stress

Conditions in NGI Simple Shear Test", Journal of the Soil Mechanics and Foundations Division, Proceedings A.S.C.E., Vol. 98, No. SM1, Technical Note, Proc. Paper 8618, January 1972, pp. 155-160.

52. MARACHI, N.D., CHAN, C.K. and SEED, H.B., "Evaluation of Properties of Rockfill Materials", Journal of the Soil Mechanics and Foundations Division, Proceedings A.S.C.E., Vol. 98, No. SM1, Proc. Paper 8672, January 1972, pp. 95-115.

53. MARSH, A.D., Determination of Residual Shear Strength of Clay by a Modified Shear Box Method, T.R.R.L. Report LR 515, Department of the Environment, 1972.

54. MARTIN, G.R., FINN, W.D.L. and SEED, H.B., "Fundamentals of Liquefaction Under Cyclic Loading", Journal of the Geotechnical Engineering Division, Proceedings A.S.C.E., Vol. 101, No. GT5, Proc. Paper 11284, May 1975, pp. 423-438.

55. MORGAN, J.R., "The Response of Granular Materials to Repeated Loading", Proceedings of the Australian Road Research Board, Third Conference, 1966, Vol. 3, Part 2, Paper No. 255, pp. 1178-1191.

56. PARK, T.K. and SILVER, M.L., "Dynamic Triaxial and Simple Shear Behavior of Sand", Journal of the Geotechnical Engineering Division, Proceedings A.S.C.E., Vol. 101, No. GT6, Proc. Paper 11347, June 1975, pp. 513-529.

57. PEACOCK, W.H. and SEED, H.B., "Sand Liquefaction under Cyclic Loading Simple Shear Conditions", Journal of the Soil Mechanics and Foundations Division, Proceedings A.S.C.E., Vol. 94, No. SM3, Proc. Paper 5957, May 1968, pp. 689-708.

58. PHILLIPS, S.J., Repeated Loading of Railway Ballast, B.Sc. Thesis,

Department of Civil Engineering, University of Nottingham, 1975.

59. PIKE, D.C., Shear Box Tests on Graded Aggregates, T.R.R.L. Report LR 584, Department of the Environment, 1973.

60. POELLOT, J.H. and YOSHIMI, Y., "A Direct Shear Apparatus for Rheological Soil Testing", Soil and Foundation, Vol. 4, No. 1, 1963, pp. 44-49.

61. PREVOST, J.H. and HOEG, K., "Reanalysis of Simple Shear Soil Testing", Canadian Geotechnical Journal, Vol. 13, No. 4, November 1976, pp. 418-429.

62. RAYMOND, G.P., "Triaxial Research on a Dolomite Railroad Ballast", Proceedings of the Second Seminar on the Behaviour of Granular Materials Under Repeated Loading, Department of Civil Engineering, University of Nottingham, July 1976.

63. RAYMOND, G.P., Private oral communication, July 1976.

64. ROSCOE, K.H., "An Apparatus for the Application of Simple Shear to Soil Samples", Proceedings of the Third International Conference on Soil Mechanics and Foundation Engineering, Zurich, 1953, Vol. 1, pp. 186-191.

65. ROSCOE, K.H., BASSETT, R.H. and COLE, E.R.L., "Principal Axes Observed during Simple Shear of a Sand", Proceedings of the Geotechnical Conference, Oslo, 1967, Vol. 1, pp. 231-237.

66. ROUND, D.J., The Solution of Load/Deformation Behaviour of a Discrete Particle Material by Digital Computer, Ph.D. Thesis, Department of Civil Engineering, University of Nottingham, 1976.

67. ROUND, D.J., Private communication, October 1976.

68. ROWE, P.W., "The Stress-Dilatancy Relation for Static Equilibrium of An Assembly of Particles in Contact", Proceedings of the Royal Society, Series A, Vol. 269, 1962, pp. 500-527.

69. SCHOFIELD, A.N. and WROTH, C.P., Critical State Soil Mechanics, McGraw-Hill Publishing Company Limited, London, 1968.

70. SEED, H.B. and LEE , K.L., "Liquefaction of Saturated Sands during Cyclic Loading", Journal of the Soil Mechanics and Foundations Division, Proceedings A.S.C.E., Vol. 92, No. SM6, Proc. Paper 4972, November 1966, pp. 105-134.

71. SEED, H.B. and PEACOCK, W.H., "Test Procedures for Measuring Soil Liquefaction Characteristics", Journal of the Soil Mechanics and Foundations Division, Proceedings A.S.C.E., Vol. 97, No. SM8, Proc. Paper 8330, August 1971, pp. 1099-1119.

72. SEED, H.B. and SILVER, M.L., "Settlement of Dry Sands During Earthquakes", Journal of the Soil Mechanics and Foundations Division, Proceedings A.S.C.E., Vol. 98, No. SM4, Proc. Paper 8844, April 1972, pp. 381-397.

73. SHENTON, M.J., Deformation of Railway Ballast Under Repeated Loading (Triaxial Tests), Report RP5, Soil Mechanics Section, British Railways Research Department, Derby, 1974.

74. SHENTON, M.J., Private oral communication, January 1977.

75. SILVER, M.L. and SEED, H.B., "Deformation Characteristics of Sands Under Cyclic Loading", Journal of the Soil Mechanics and Foundations Division, Proceedings A.S.C.E., Vol. 97, No. SM8, Proc. Paper 8334, August 1971, pp. 1081-1098.

76. SILVER, M.L. and SEED, H.B., "Volume Changes in Sands During Cyclic Loading", Journal of the Soil Mechanics and Foundations Division, Proceedings A.S.C.E., Vol. 97, No. SM9, Proc. Paper 8354, September 1971, pp. 1171-1182.

77. SOWERS, G.F., "Strength Testing of Soils", Laboratory Shear Testing of Soils, A.S.T.M. Special Technical Publication No. 361, 1963, pp. 3-21.

78. SPARROW, R.W., "A Direct Shear Apparatus for Repeated Loading Tests on Cohesive Soils", Civil Engineering and Public Works Review, Vol. 60, April 1965, pp. 531-533.

79. SPARROW, R.W., "A Repeated Load Biaxial Shear Box for Tests on Railway Ballast", Proceedings of the Second Seminar on the Behaviour of Granular Materials Under Repeated Loading, Department of Civil Engineering, University of Nottingham, July 1976.

80. STROUD, M.A., The Behaviour of Sand at Low Stress Levels in the Simple-Shear Apparatus, Ph.D. Thesis, Department of Engineering, University of Cambridge, 1971.

81. TAYLOR, D.W., Fundamentals of Soil Mechanics, John Wiley and Sons Inc., New York, 1948.

82. THIERS, G.R. and SEED, H.B., "Cyclic Stress-Strain Characteristics of Clay", Journal of the Soil Mechanics and Foundations Division, Proceedings A.S.C.E., Vol. 94, No. SM2, Proc. Paper 5871, March 1968, pp. 555-569.

83. THIERS, G.R. and SEED, H.B., "Strength and Stress-Strain Characteristics of Clays Subjected to Seismic Loading Conditions", Vibration Effects of Earthquakes on Soils and Foundations, A.S.T.M. Special Technical Publication No. 450, 1969, pp. 3-56.

84. THROWER, E.N., LISTER, N.W. and POTTER, J.F., "Experimental and Theoretical Studies of Pavement Behaviour Under Vehicular Loading in Relation to Elastic Theory", Proceedings of the Third International Conference on the Structural Design of Asphalt Pavements, London, 1972, Vol. 1, pp. 521-535.

85. TIMMERMAN, D.H. and WU, T.H., "Behaviour of Dry Sands Under Cyclic Loading", Journal of the Soil Mechanics and Foundations Division, Proceedings A.S.C.E., Vol. 95, No. SM4, Proc. Paper

6698, July 1969, pp. 1097-1112.

86. YOUD, T.L., "Densification and Shear of Sand During Vibration", Journal of the Soil Mechanics and Foundations Division, Proceedings A.S.C.E., Vol. 96, No. SM3, Proc. Paper 7272, May 1970, pp. 863-880.

87. YOUD, T.L., "Maximum Density of Sand by Repeated Straining in Simple Shear", Highway Research Record, No. 374, 1971, pp. 1-6.

88. YOUD, T.L., "Compaction of Sands by Repeated Shear Straining", Journal of the Soil Mechanics and Foundations Division, Proceedings A.S.C.E., Vol. 98, No. SM7, Proc. Paper 9063, July 1972, pp. 709-725.

89. YOUD, T.L. and CRAVEN, T.N., "Lateral Stress in Sands During Cyclic Loading", Journal of the Geotechnical Engineering Division, Proceedings A.S.C.E., Vol. 101, No. GT2, Technical Note, Proc. Paper 11093, February 1975, pp. 217-221.

APPENDIX A

Stress Conditions in the Simple Shear Test

It has been seen in Chapter Two that the applied shear stress, τ, is not the maximum shear stress in a sample subject to simple shear, Fig. 14. The maximum shear stress, τ_{max}, is given by (71):

$$\tau_{max}^2 = \tau^2 + \left[\frac{\sigma_o'(1 - K_o)}{2}\right]^2$$

Substituting $K_o = 1 - \sin \varphi'$ and rearranging gives

$$\left[\frac{\tau_{max}}{\sigma_o'}\right]^2 = \left[\frac{\tau}{\sigma_o'}\right]^2 + \left[\frac{\sin \varphi'}{2}\right]^2$$

If we now define τ_{max}/σ_o' as $\tan(\varphi' + \Delta\varphi')$ where $\varphi' = \tan^{-1}(\tau/\sigma_o')$, a graph showing the relationship between $\Delta\varphi'$ and φ' can be produced, Fig. A1. It can be seen that $\Delta\varphi'$ reaches a maximum value of only 2.18° when $\varphi' = 30^\circ$.

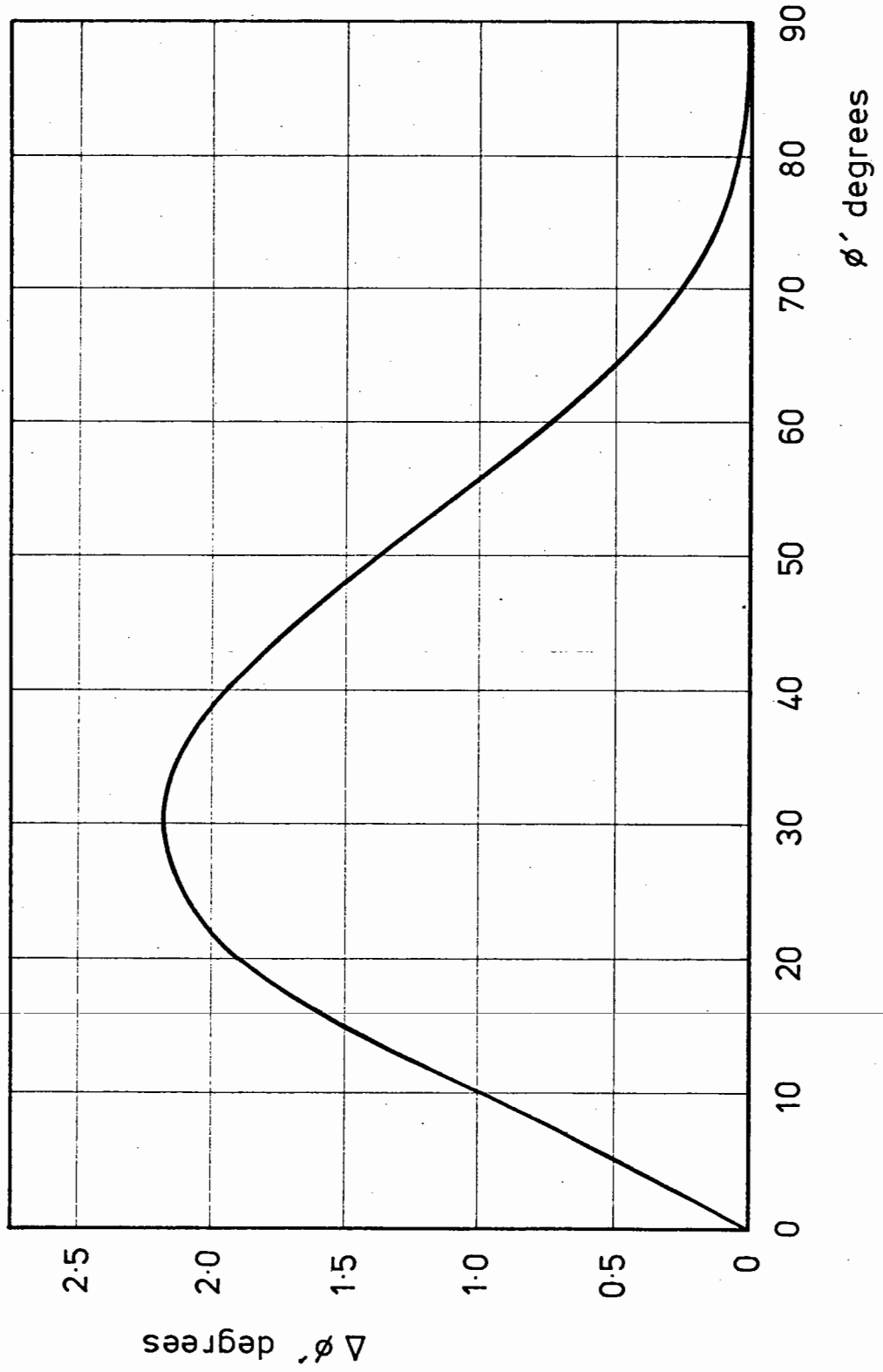

Fig.A1 Correction for stress conditions in simple shear test

APPENDIX B

Contact Stress Transducers (Load Cells)

B.1 Design Considerations

The Cambridge load cell described by Arthur and Roscoe (4) and the subsequently modified cells described by Bransby (10) are able to measure both normal and shear stresses and also determine the eccentricity of the line of action of the applied normal load. These transducers operate by monitoring the direct strains induced in the thin web elements of the load cell. Somewhat simpler load cells were designed for use in this apparatus and the basic layout of the Mk1 versions are shown in Figs B1 and B2. Separate cells were used to measure the applied normal and shear stresses which were monitored by measuring the bending strains produced in the webs of the load cells. This arrangement allowed thicker web sections than those in the Cambridge load cells to be used. Thus, the cells were somewhat easier to manufacture while still providing adequate sensitivity. Bransby (10) has indicated the need for this type of transducer to be made from a material which is linearly elastic, easy to machine and of a reasonably low Young's modulus. These conditions are fulfilled by the aluminium alloy HE15W. The 0.1% proof stress is quoted as 220 MPa and the Young's modulus as 70 GPa. A maximum bending stress of 100 MPa was used for design purposes. This represents 0.45 of the proof stress. The various Cambridge load cells were designed (10) for a maximum working stress of between 0.33 and 0.67 of the proof stress.

The measuring elements shown in the cells shown in Figs B1 and B2 are four strain gauged webs 5 mm x 2 mm x 10 mm long. In the design, it was assumed that the webs acted as fixed end beams and that the

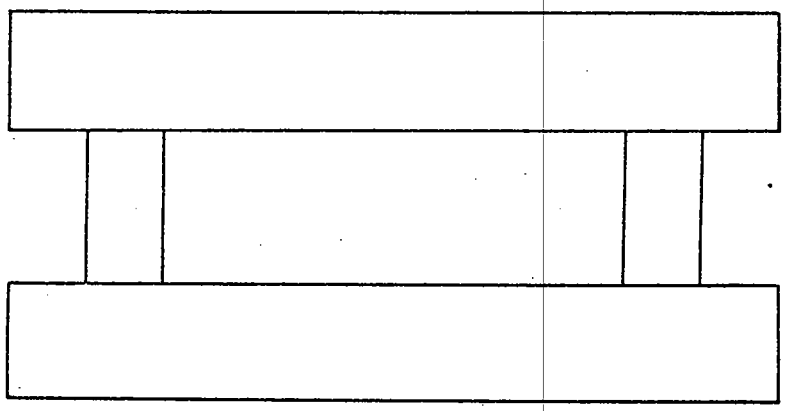

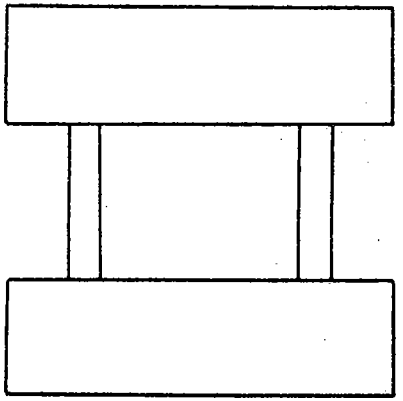

20 mm

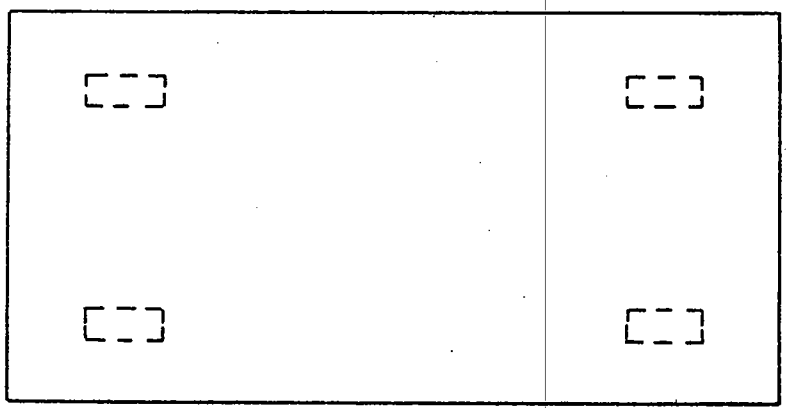

NOTES

1. Material - Aluminium HE15 W
2. Maximum radii on all web root faces 1/16 inch
3. All fixing holes omitted

Fig.B1 General design of shear load cell

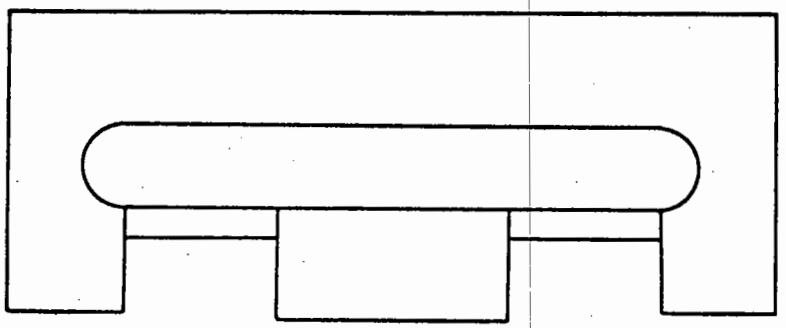

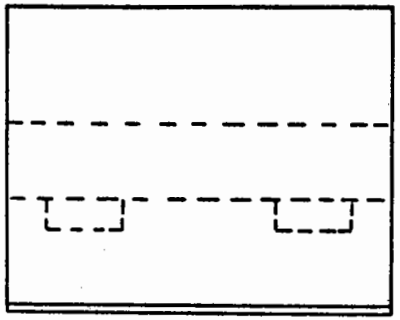

20 mm

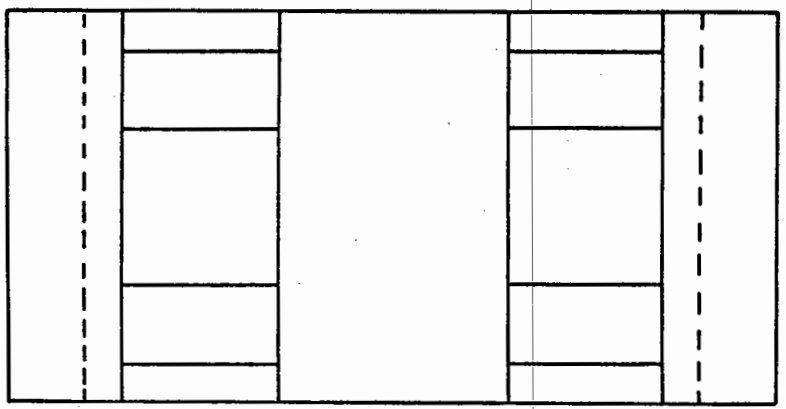

NOTES

1. Material - Aluminium HE15W
2. Maximum radii on all web root faces 1/16 inch
3. All fixing holes omitted

Fig.B2 General design of normal load cell

gauges were positioned at the roots of the webs. The webs were also assumed to be prismatic, however, for reasons of easy of manufacture and fatigue problems, fillet radii were specified at the roots. TML Foil Gauge - Series 'F' Type FLE-1 strain gauges were used for the Mk1 load cells. They had a nominal resistance of 120 Ω, a gauge factor of approximately 2.1 and a gauge length of 1 mm. The adhesive used was Micro-Measurements M-Bond 43-B. This adhesive proved satisfactory but had the slight disadvantage of requiring a rather high curing temperature of about 175°C. The gauges were connected in a 4-arm active bridge circuit, Fig. B3, to give maximum sensitivity and inherent temperature compensation. The calculated maximum deflection of the load cells in the direction of the load being measured was 0.025 mm.

B.2 Calibration of the Mk1 Load Cells

For calibration, the load cell was fixed to a thick steel plate supported by a frame, Plate BI. The cell was held by screws passing through the plate into its base and a steel calibration plate was similarly fixed to the active face. The calibration plate had provision for applying normal loads from a weight hanger at various eccentricities relative to the central position. The plate also retained a steel wire which passed over a pulley mounted on a circular ball race to allow shear loads to be applied by a weight hanger attached to the wire. Packing plates were placed under the load cell so that the wire was parallel to the active face.

Prior to calibration, the load cell was fully loaded and unloaded three or four times. This procedure strain cycles both the gauges and the cell itself and so helps to reduce hysteresis effects. Fairly extensive calibration checks were carried out to investigate any

T - Tension C - Compression

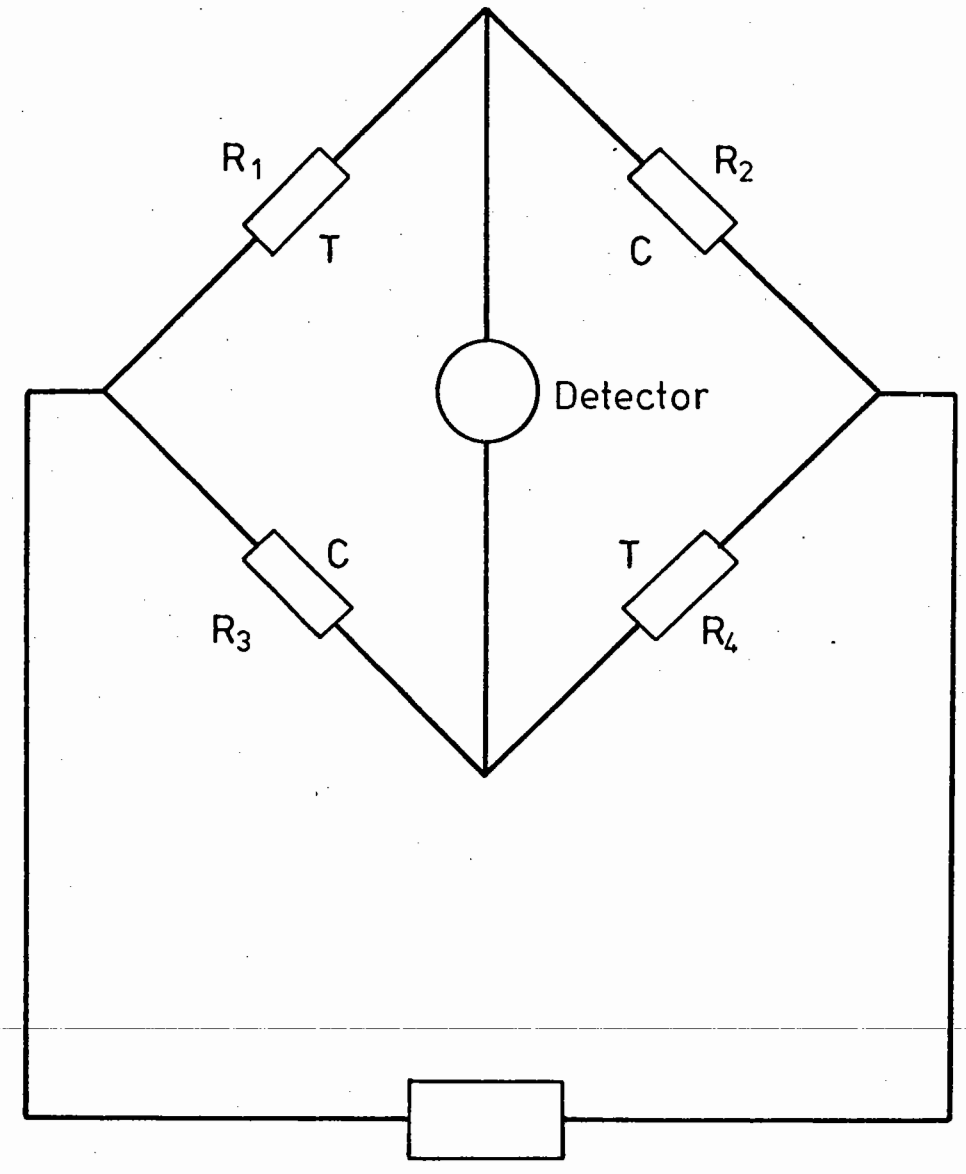

Fig.B3 4-arm active bridge circuit used in contact stress transducers

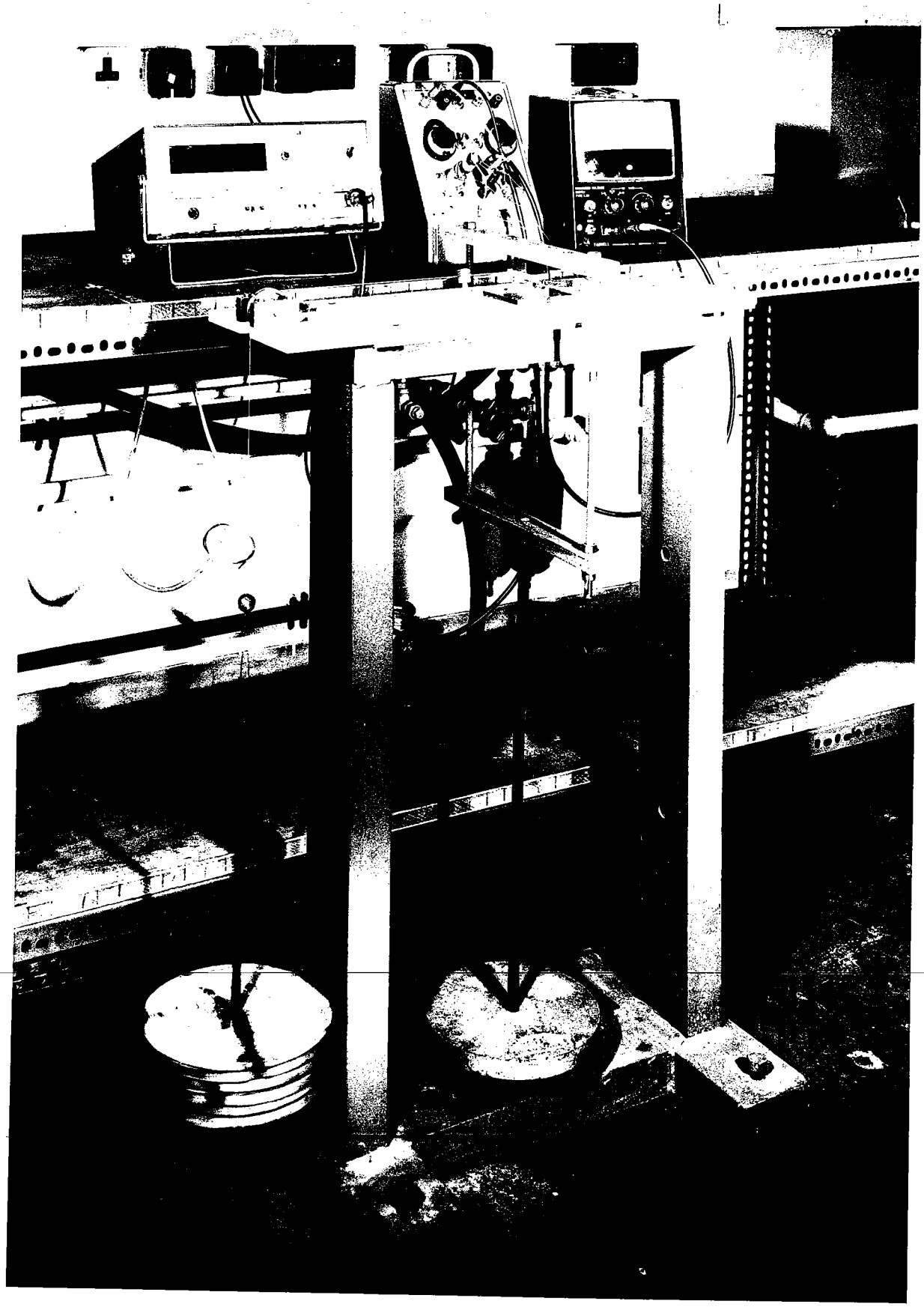

Plate BI Mk1 Calibration Bench

possible cross sensitivity effects and the influence of eccentricity of the line of action of the applied load. A calibration chart for the normal load cell is shown in Fig. B4 and it can be seen that the linearity and lack of hysteresis effects is excellent. Some problems with creep in the bond between the gauges and the webs was experienced initially but this was overcome by using the M-Bond 43-B adhesive. Following a rearrangement of some of the gauge positions, cross sensitivity and eccentricity effects were reduced to negligible proportions. The active face stress sensitivities of the normal and shear load cells were 40.7 and 34.4 kPa/mV respectively for a 4.0 V bridge input.

B.3 The Mk2 Load Cells

The initial designs for the load cells used in the Mk2 apparatus were basically the same as those for the Mk1 apparatus except for size. The active face of each load cell was 140 mm x 70 mm. The webs of the shear load cells were 20 mm x 8 mm x 28 mm long. In the normal load cells they were 20 mm x 7 mm x 28 mm long. These dimensions were chosen to give stress sensitivities of a similar order of magnitude to those for the Mk1 load cells. One refinement in the design of the shear load cells was that the webs were positioned so that, for a uniformly distributed load on the active face, there would be no tendency for rotation to occur at the support points which could lead to spurious outputs. With reference to Fig. B5, it can be shown, using Mohr's theorems, that there will be zero rotation at the support points for a value of $\alpha = 0.55$. The assumption was made that the active face of the load cell was simply supported by the webs at their centre lines.

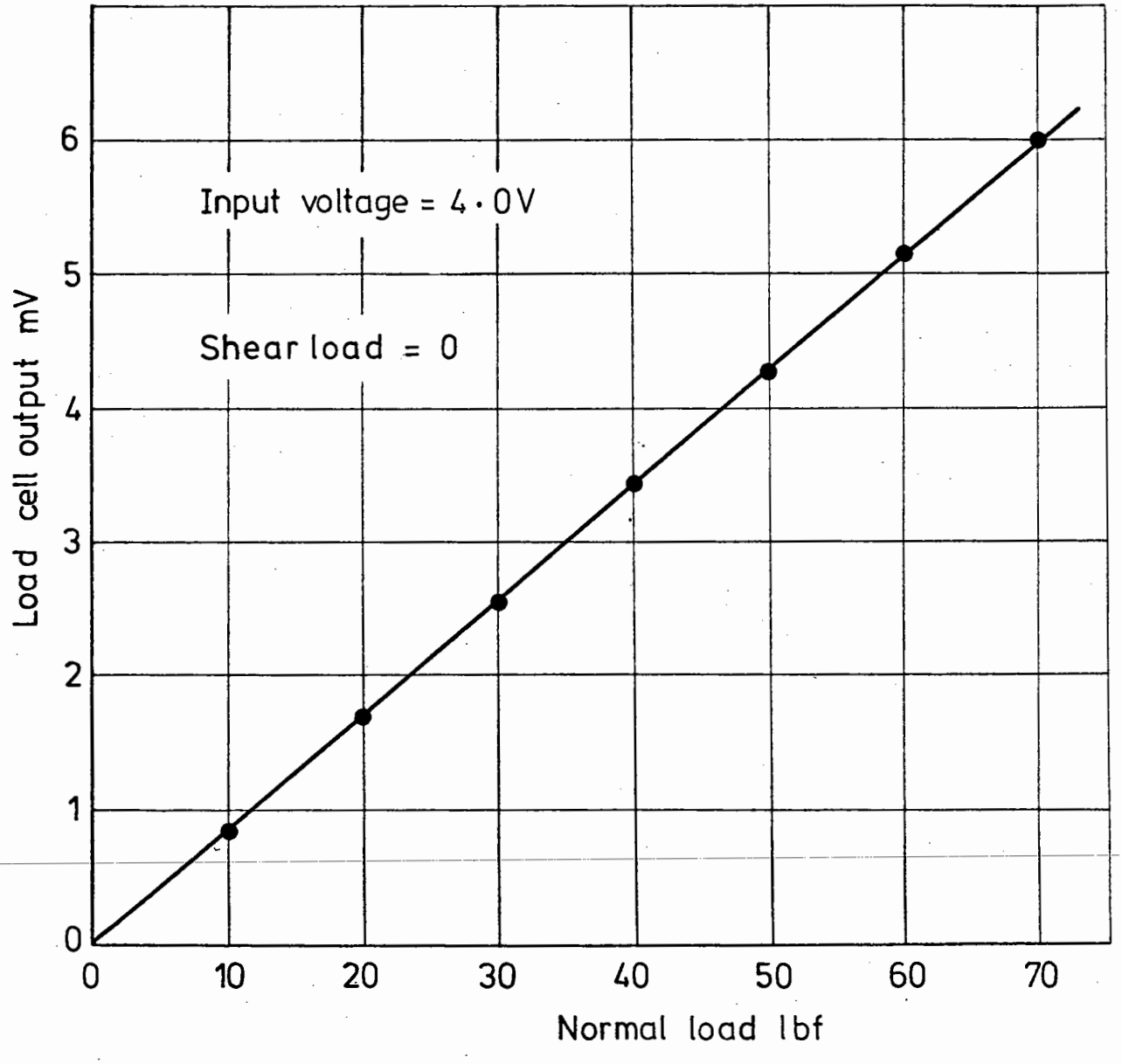

Fig.B4 Calibration of normal load cell

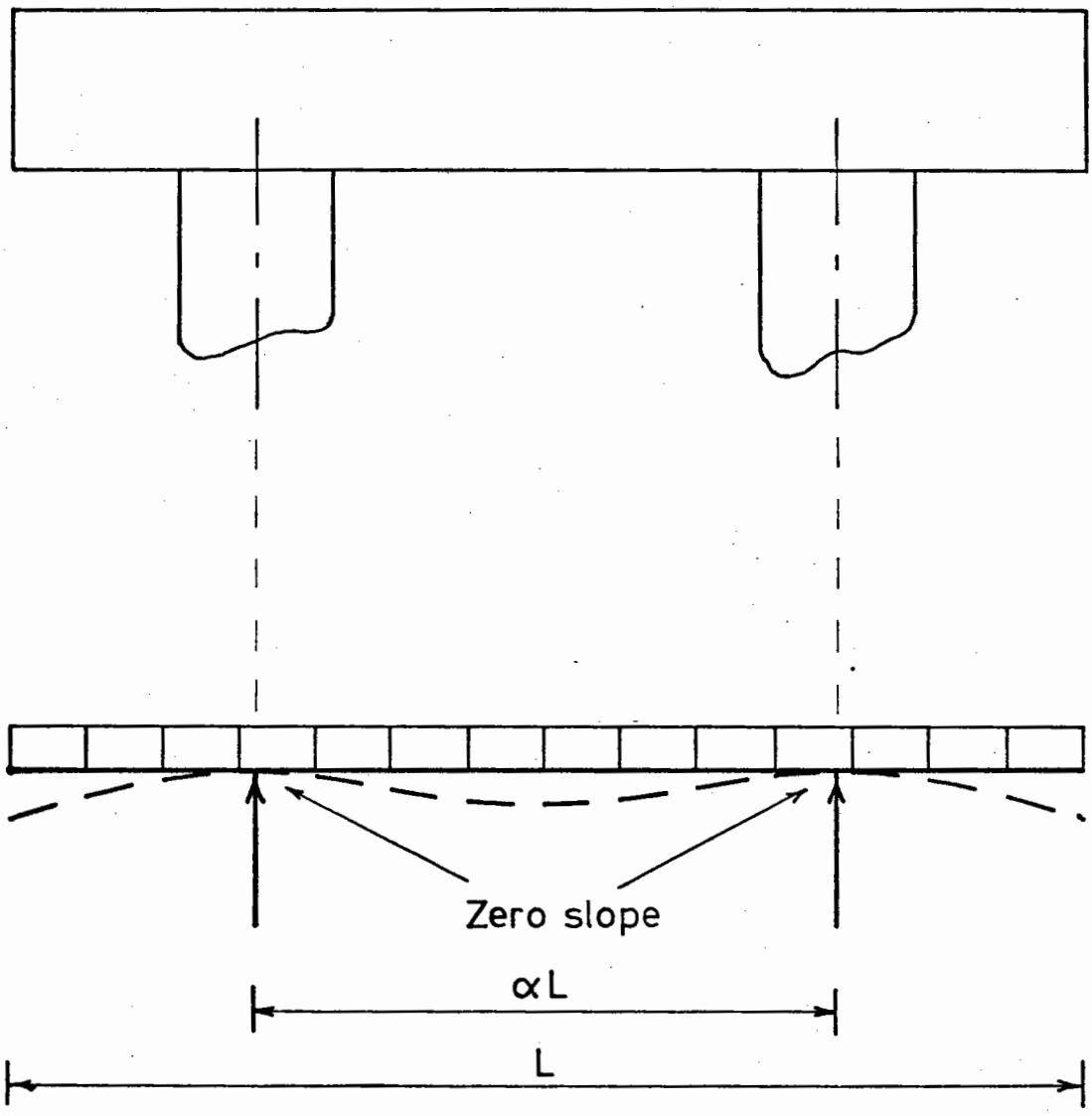

Fig. B5 Web spacing for load cells

The load cells were machined from the same aluminium alloy, HE15W, as was used for the Mk1 load cells. The strain gauges were TML Foil Gauge Series 'F' Type FLA-3-23 having a nominal resistance of 120 Ω, a gauge factor of 2.15 and a gauge length of 3 mm. The adhesive used in this case was Araldite AY 103 mixed with HY 951 in the proportions 10:1 by weight respectively. This adhesive has a lowering curing temperature than the M-Bond 43-B used for the Mk1 load cells and no creep problems were encountered. The gauges were again connected in a 4-arm active bridge circuit as shown in Fig. B3 and, with experience gained from the Mk1 load cells, the gauges were arranged so as to minimise eccentricity effects. The calculated maximum deflection of the load cells in the direction of the load being measured was 0.045 mm.

The calibration loads required for these load cells were approximately 1000 lbf and it was not practicable to use weight hangers and steel wire as was done before. A proving ring frame was therefore built to provide the loads through a calibration plate fitted to the active face of the transducer, Plate BII. Again, prior to calibration, each load cell was cycled to full load three or four times so as to reduce hysteresis effects.

B.4 Modifications to the Mk2 Load Cells

On calibration, it was found that relative movement was occurring between the baseplate of the calibration bench, the load cell and the calibration plate. This would have led to severe problems when the apparatus was assembled because of the small working clearances involved in the design. To overcome this, extra fixing holes were provided for the base of the shear load cells. Locating slots were also cut along the edges of the active face and these engaged with

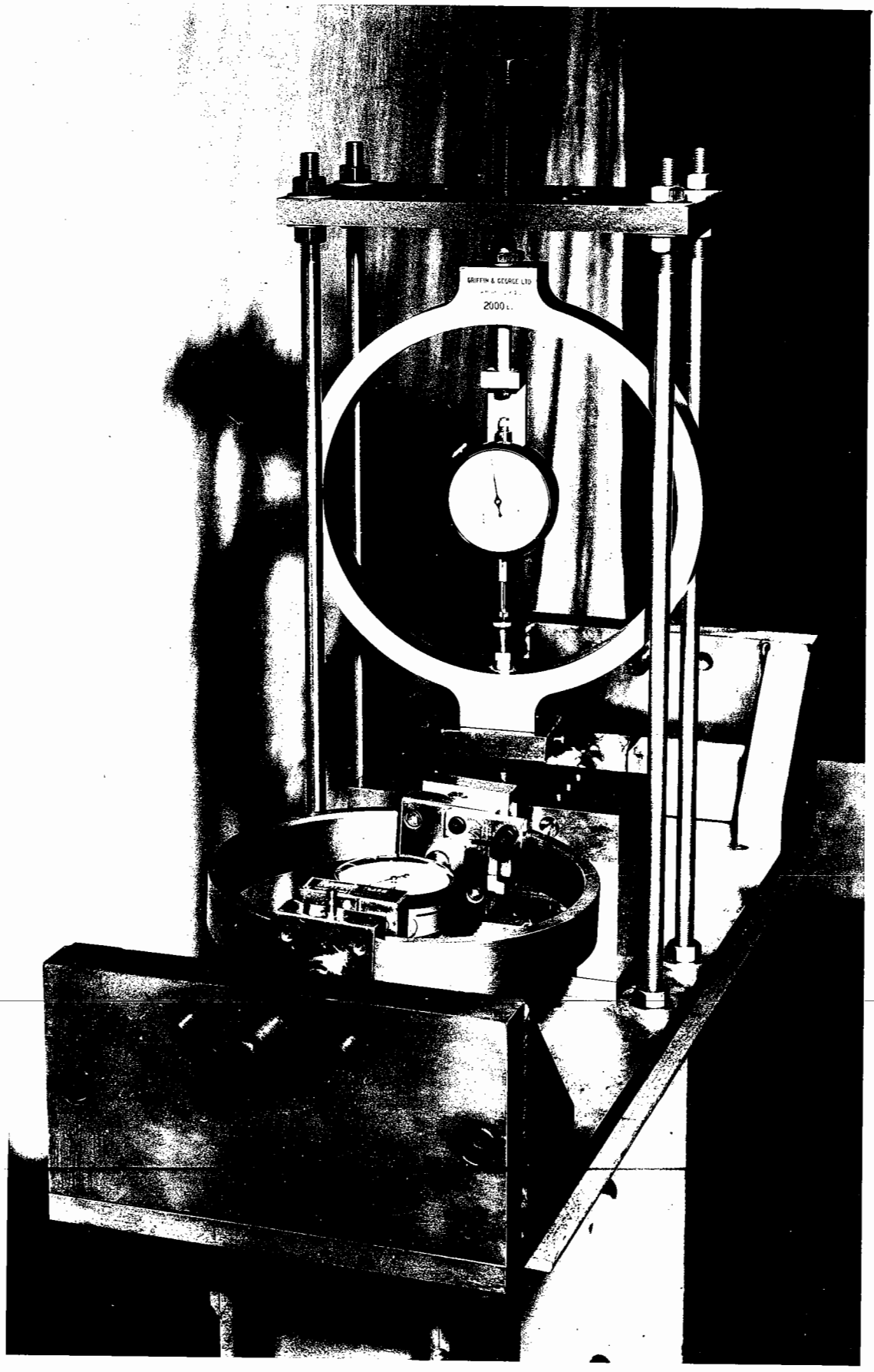

Plate BII Mk2 Calibration Bench

ribs on the lower face of the calibration plate. The ends of the ribs on the loading plates can be seen in Plate VI.

Cross sensitivity and eccentricity effects were negligible in the case of the shear load cells. However, in the case of the normal load cells, cross sensitivity effects were found to be very large. This was attributed to a moment effect due partly to the large lever arm which a shear load had about the strain gauged webs and partly to the small separation of these webs, Fig. B6. Twisting of the webs by the shear load was causing the cross sensitivity. The normal load cells were redesigned by inverting the original design to put the webs closer to the active face, Fig. B7. This reduced the lever arm of the shear load about the webs by a factor of 2.04. In addition, the separation of the webs of the central load cell was increased by a factor of 1.14. In the case of the outer normal load cells, the separation of the webs had to be reduced by a factor of 0.8 because of the vee-slots in the sides of these cells. Following these modifications, the normal load cells performed very well with only minor cross sensitivity and eccentricity effects. With its wider web separation, the cross sensitivity of the central load cell was less than that of the outer cells. The active face stress sensitivities of the central normal and shear load cells were 67.0 and 92.8 kPa/mV respectively for a 4.0 V bridge input.

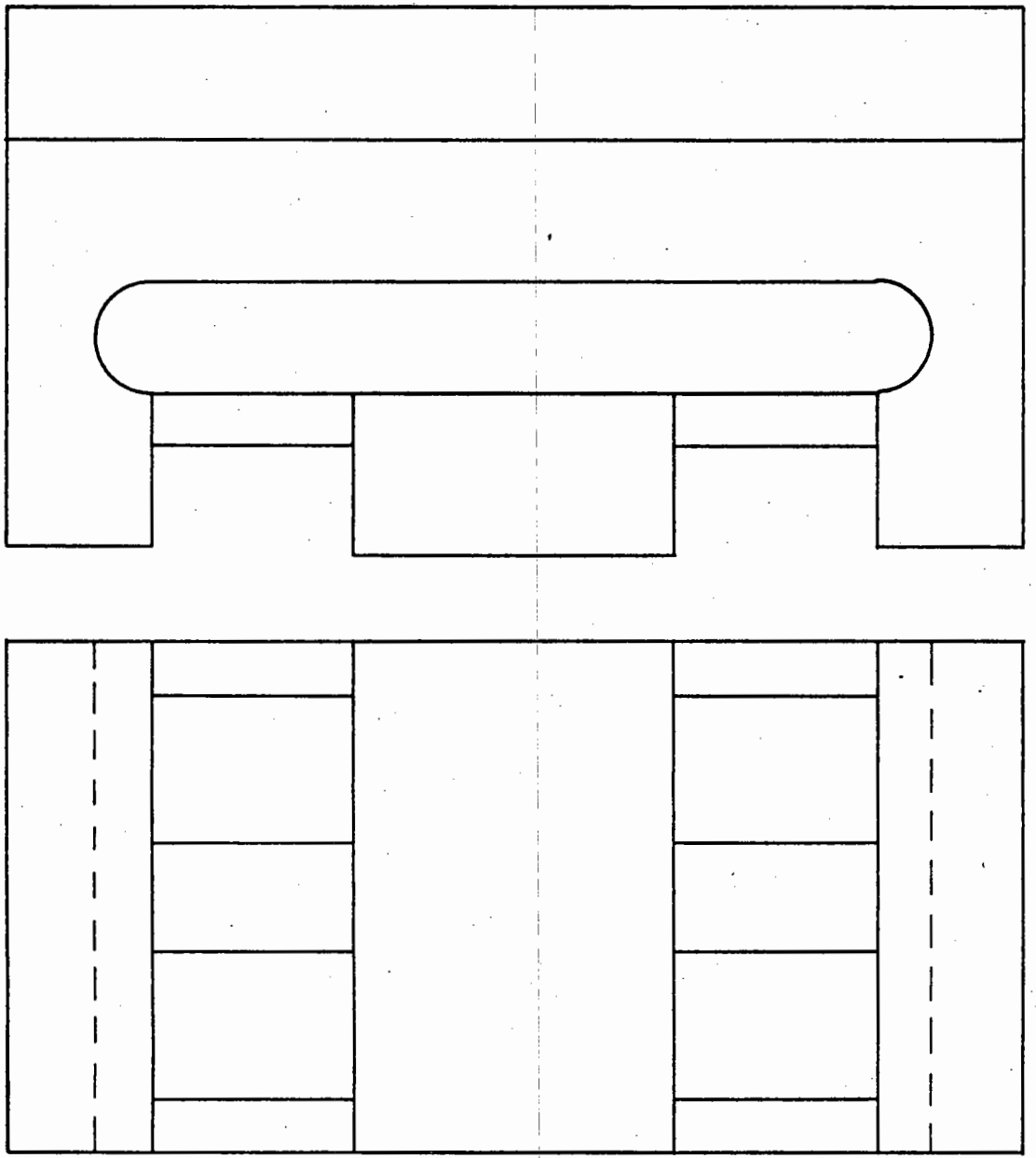

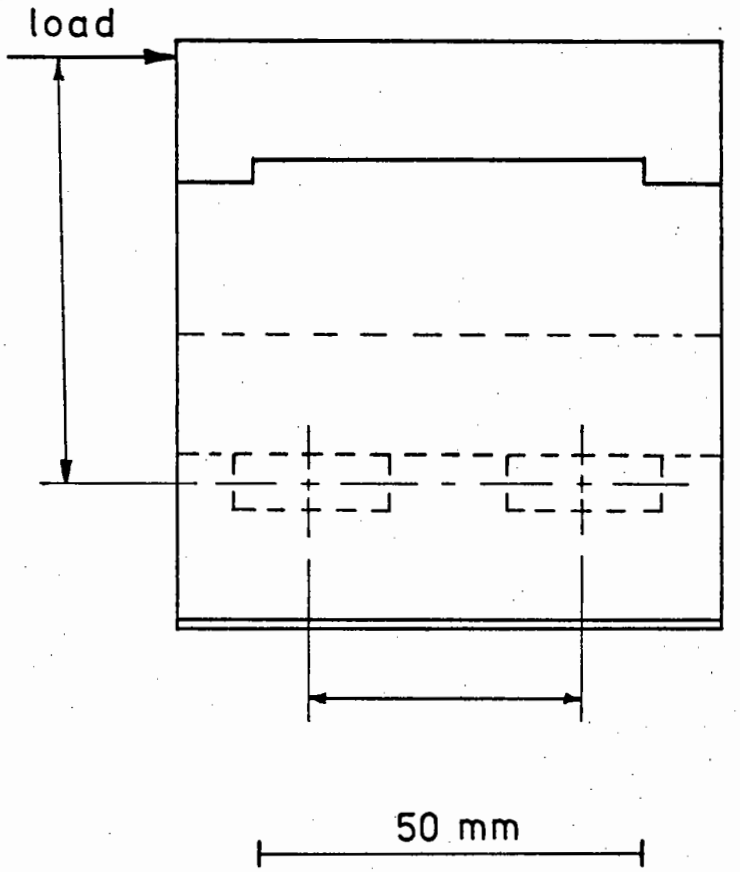

Fig.B6 Mk 2 normal load cell – original design

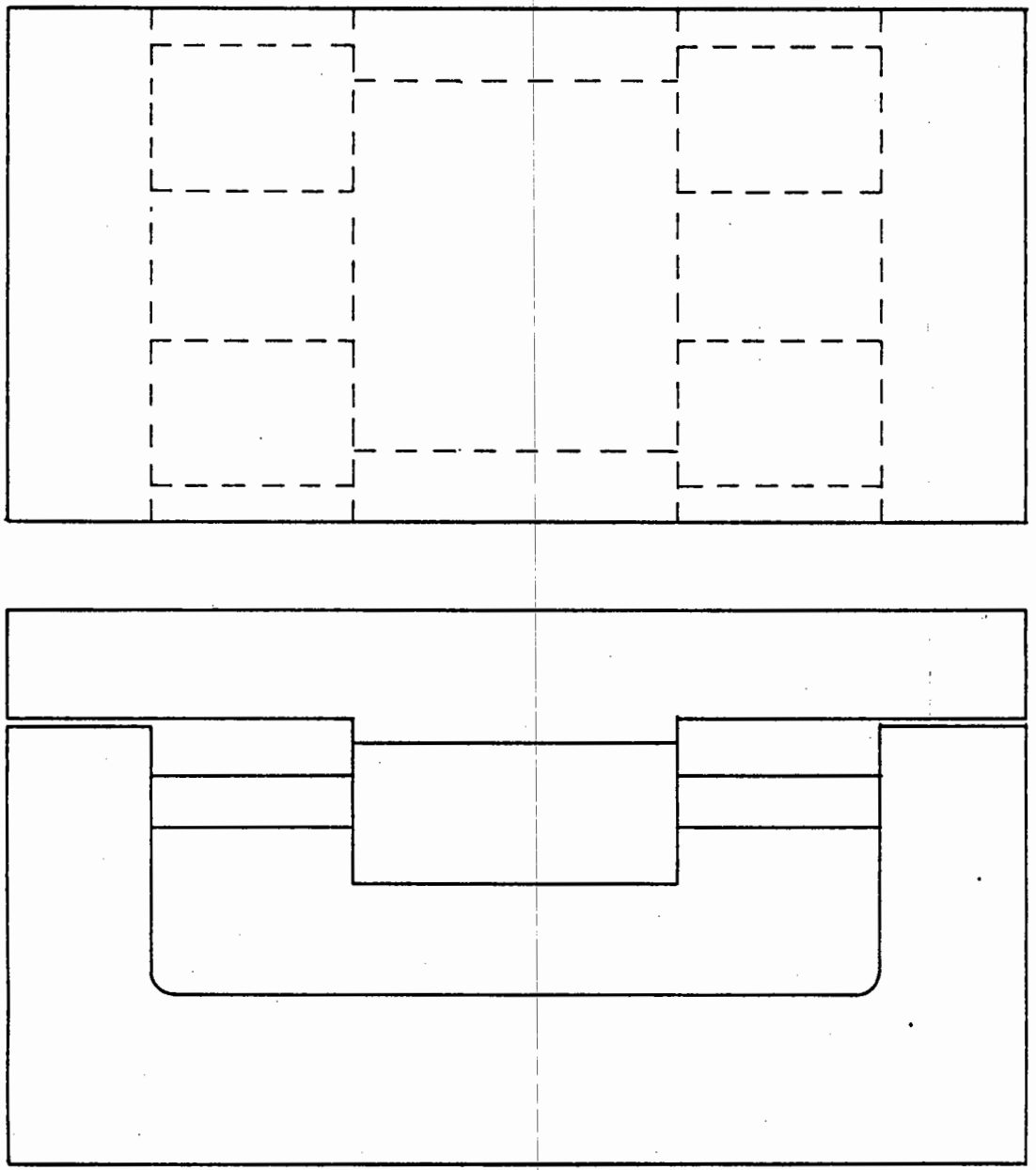

Fig.B7 Mk2 normal load cell - modified design

APPENDIX C

Standard Strength Tests

C.1 Standard Direct Shear Tests

For the standard direct shear tests, the 1 mm material was compacted by clamping the shear box to the vibrating table. The density obtained was 1.48 Mg/m^3 which is slightly lower than that obtained in the preliminary compaction trials, Section 3.5.2. This was probably due to the effect of the ribbed loading plates which might have caused a reduced density in the region immediately adjacent to them. The results of these tests are tabulated in Table C1 and they are plotted in Figs C1 to C3. The rather high φ value of 55° is supported by the good fit of the line to the data, Fig. C1, and also Hennes (31) has reported φ values in excess of 45° for similar granular material. Fig. C3 indicates that the material was behaving as a dense material at the level of compaction achieved.

C.2 Triaxial Compression Tests

Two series of static triaxial tests were carried out to establish angles of shearing resistance for the materials used in the Mk1 and Mk2 Simple Shear Apparatus. The material used in the Mk1 apparatus passed BS Sieve No. 14 and was retained on BS Sieve No. 25. The material used in the Mk2 apparatus passed a $\frac{3}{16}$ in. BS Sieve and was retained on BS Sieve No. 7. These materials are referred to as nominally 1 mm and 3 mm particles respectively. In the case of the smaller material, the triaxial test was used to provide a check on the value of 55° obtained for the angle of shearing resistance obtained from the standard direct shear test. For the larger material, the triaxial

Normal Load lb	20		40		60		80	
Horiz. def. mm	Shear stress kPa	Vert. def. mm	Shear stress kPa	Vert. def. mm	Shear stress kPa	Vert. def. mm	Shear stress kPa	Vert. def. mm
0	0	0	0	0	0	0	0	0
0.2	2.6	0	3.4	0	13.2	0	7.9	0
0.4	10.5	0	12.0	0	26.3	0	19.9	0
0.6	18.8	0	21.8	0	43.2	0	34.2	0
0.8	26.3	0	32.0	0	59.4	0	54.1	0
1.0	32.7	0	43.2	0	72.6	0	69.5	0
1.2	40.6	0	55.6	0	83.8	0	79.7	0
1.4	51.5	0	66.5	0	93.6	0	89.8	0
1.6	58.3	0.004	77.1	0	102.6	0	101.9	0
1.8	62.8	0.014	84.6	0.006	108.3	0.002	113.5	0
2.0	65.4	0.030	90.6	0.014	115.4	0.012	124.4	0
2.2	66.5	0.044	95.1	0.020	122.6	0.020	131.2	0.004
2.4	67.3	0.058	98.5	0.034	126.7	0.032	149.2	0.010
2.6	67.7	0.074	100.7	0.050	128.9	0.042	157.5	0.018
2.8	66.9	0.092	101.1	0.060	130.8	0.054	164.3	0.028
3.0			104.1	0.074	131.6	0.070	168.4	0.042
3.2			104.5	0.094	131.9	0.082	170.3	0.054
3.4			104.5	0.104	131.9	0.116	170.7	0.066
3.6							170.7	0.082

Shear deformation rate = 1.304 mm/min

Mass of hanger and top plates = 15.6 lb

$\therefore$ Applied normal stresses are: 44.0, 68.7, 93.4 and 118.1 kPa

(based on an area of 36 cm^2)

Table C1 Results of Standard Direct Shear Tests

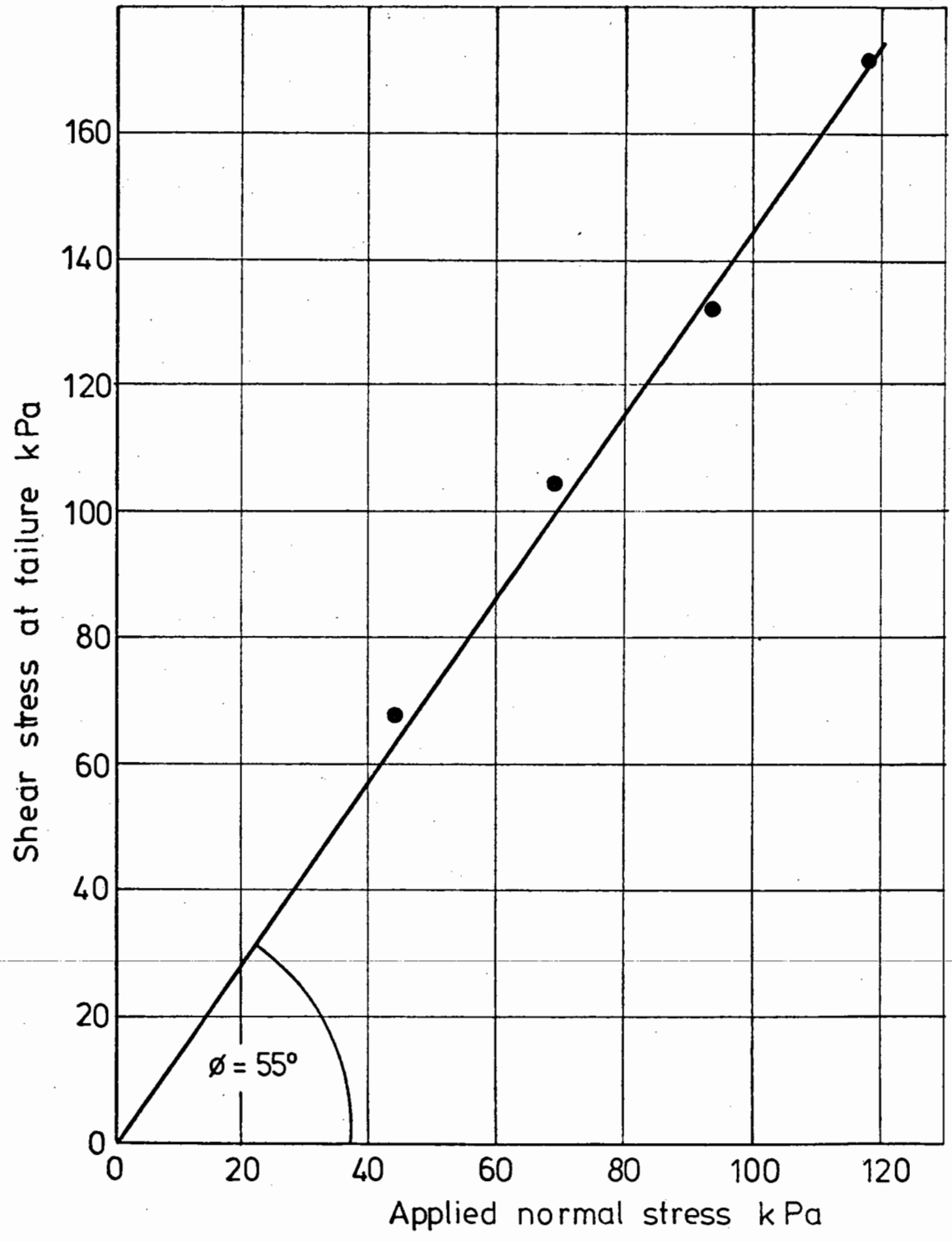

Fig. C1 Determination of angle of shearing resistance

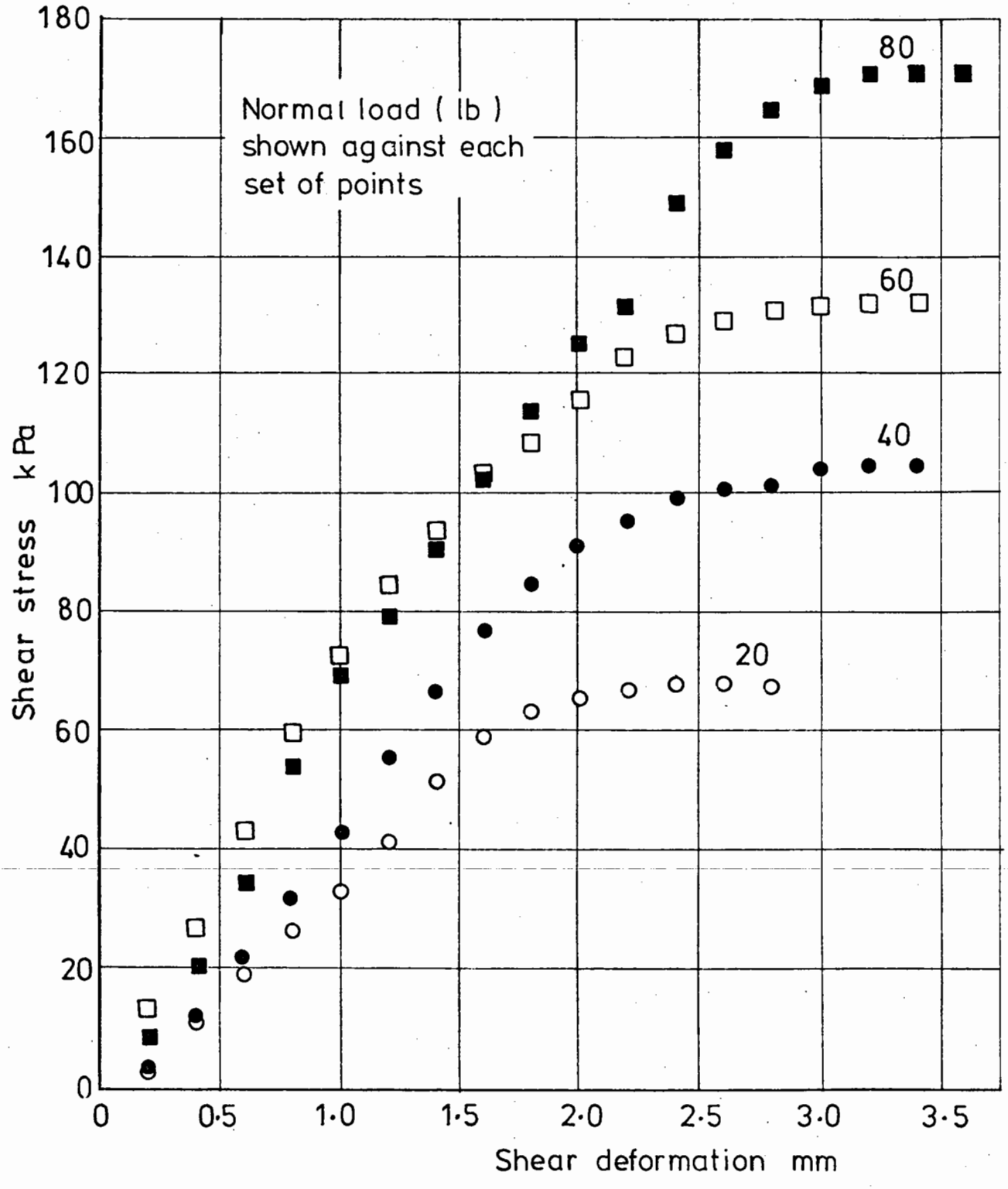

Fig. C2 Shear stress - shear deformation

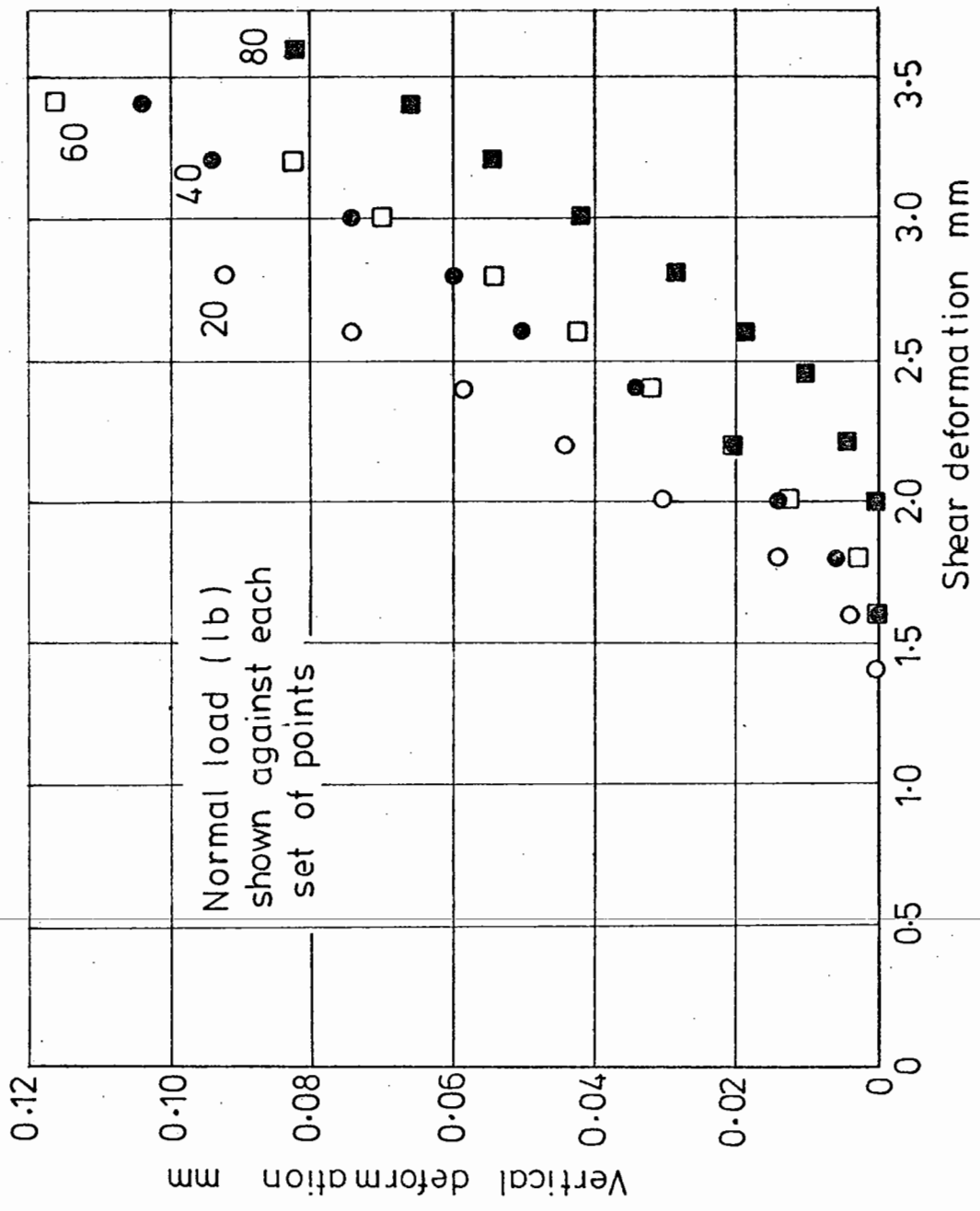

Fig. C3 Vertical deformation - shear deformation

test was used to provide a ϕ value because a large, standard direct shear box was not available.

A standard triaxial testing machine was used for both series of tests with a crosshead speed of approximately 1 mm/min. The samples were tested air dry and an internal vacuum was used to provide confining pressures of up to 70 kPa. This simplified the setting up and testing procedure. For the 1 mm material, the samples were approximately 65 mm high and 37 mm in diameter. In the case of the 3 mm material, the samples were approximately 185 mm high and 101 mm in diameter. All the samples were formed using a membrane lined split-mould with a vacuum applied to hold the membrane against the mould. The assembled mould was placed over a triaxial cell base which was clamped to a vibrating table. A known weight of material was put inside the mould and the top platen placed on this. The compaction of the sample was monitored using an LVDT to check the level of top platen in a manner similar to that described in Section 3.6. Average densities of 1.54 and 1.49 Mg/m^3 corresponding to porosities of 0.44 and 0.45 were obtained for the smaller and larger materials respectively.

To reduce frictional restraint at the ends of the samples, a sandwich of two layers of latex rubber membrane smeared with silicone grease was used on both loading platens. The lower sandwich had a small hole at its centre to allow the internal vacuum to be applied. This technique prevented barrelling quite effectively and it was assumed, in calculating the failure stresses, that the sample deformed as a right cylinder of constant volume. For such a strongly dilatant material, this latter assumption is obviously invalid. However, obtaining volume change data for this type of sample would have complicated the experimental procedure to an unjustifiable extent

considering the purpose of these preliminary tests.

The results of the triaxial tests were analysed in terms of the Lambe and Whitman parameters, p and q, which are defined (44) as:

$$p = \frac{(\sigma_1 + \sigma_3)}{2} \quad \text{and} \quad q = \frac{(\sigma_1 - \sigma_3)}{2}$$

It can be seen that p defines the centre and q the radius of the conventional Mohr's circle. These parameters are plotted at failure for the two series of tests in Figs C4 and C5. With this method of presentation, the Mohr failure circle for each test is represented by a single point and a regression analysis can be used to evaluate the slope of the line, $\tan \alpha$. It can then be shown that $\sin \varphi = \tan \alpha$. The least squares line constrained to pass through the origin indicates φ values of 52° and 50° for the smaller and larger materials respectively.

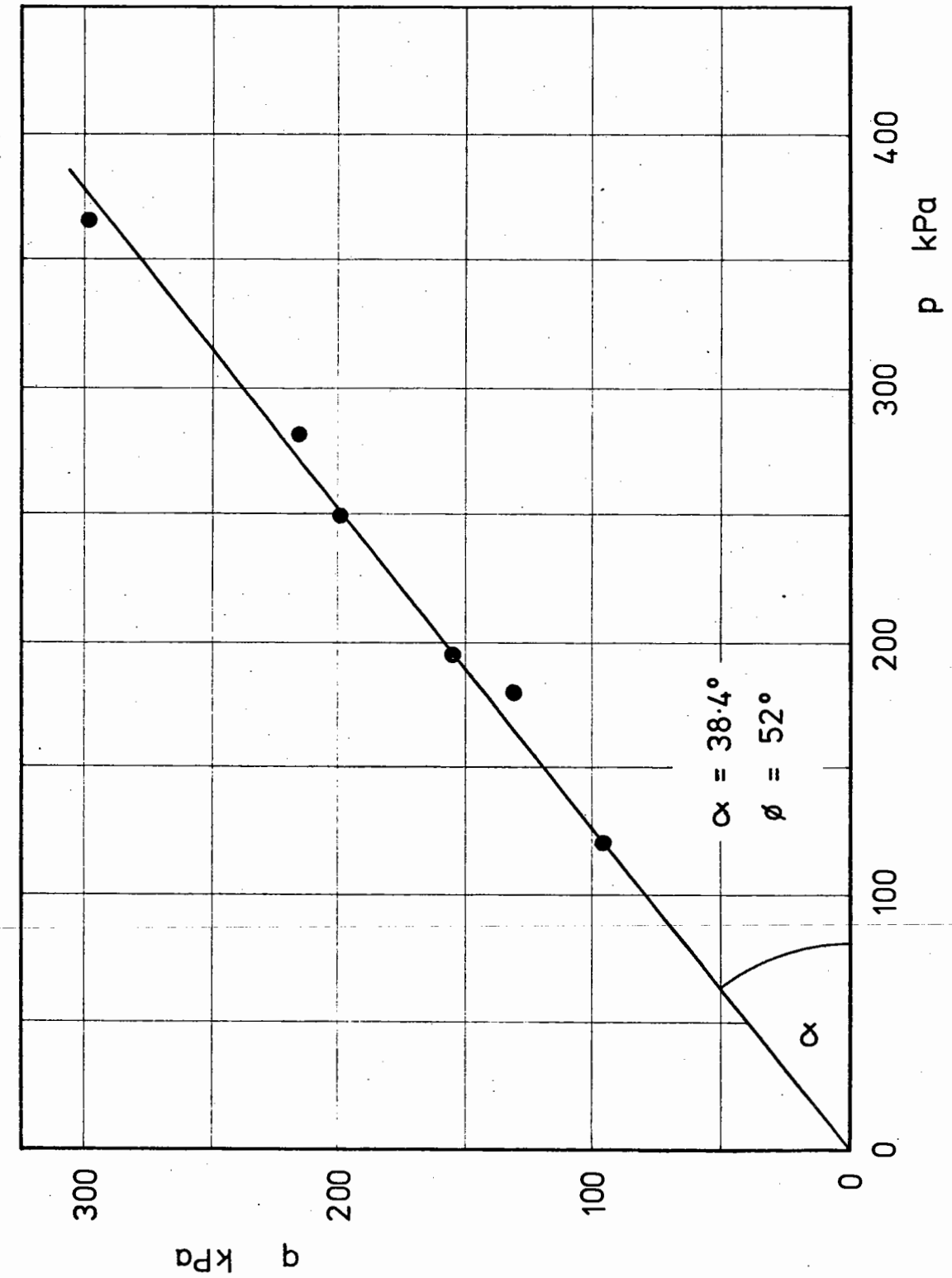

Fig.C4 Triaxial test results - 1mm material

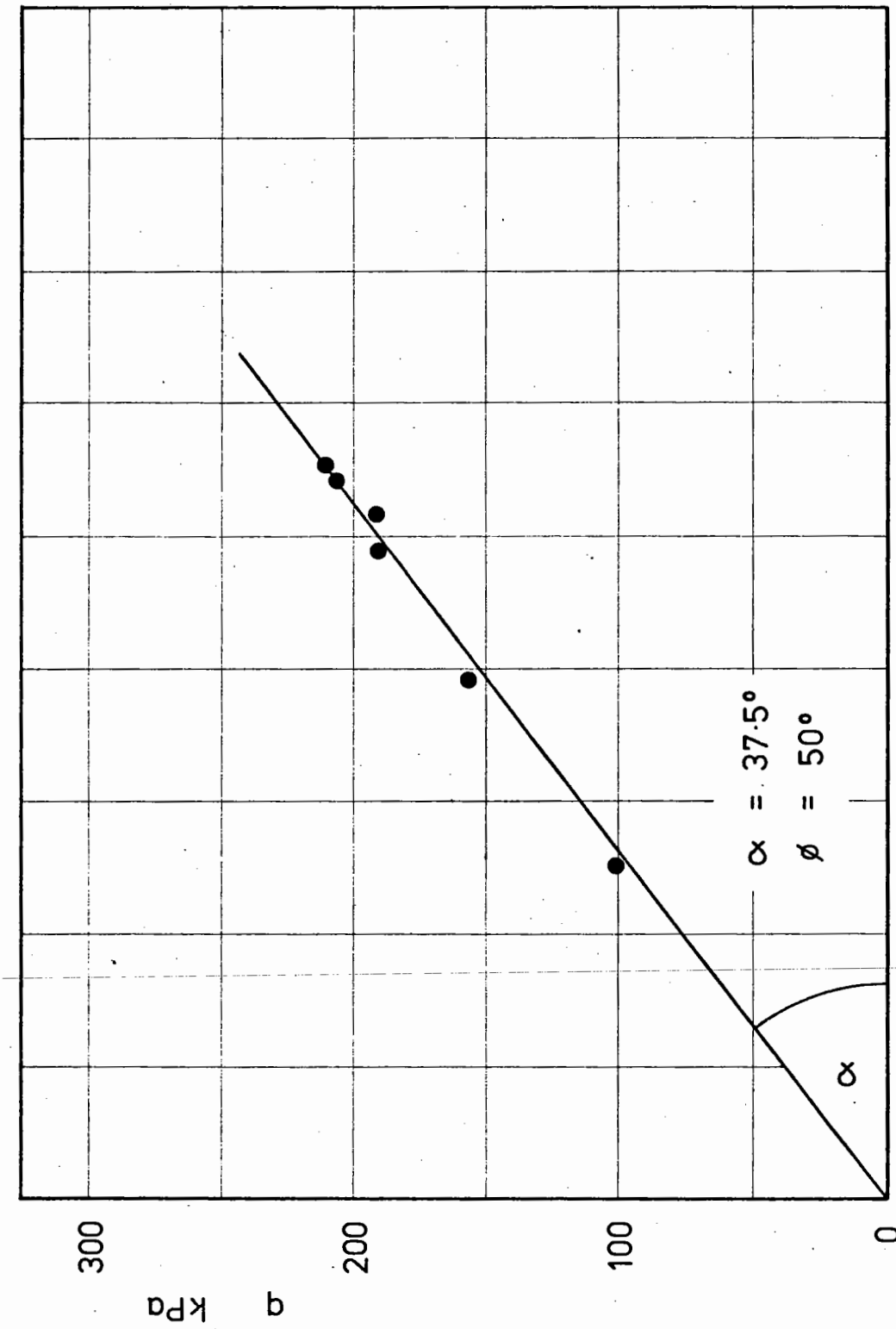

Fig.C5 Triaxial test results - 3 mm material

APPENDIX D

Test Results from Series A, B and C

D.1 Series A - Unidirectional Repeated Load

D.1.1 Series A - Basic test data

Test	σ kPa	Final N cycles	R_m (10)	R_c (10)
A01	95	38750	0.35	0.29
A02	95	30000	0.44	0.40
A03	95	32030	0.48	0.42
A04	95	10100	0.21	0.13
A05	95	10000	0.27	0.21
A06	190	27505	0.27	0.21
A07	190	10000	0.15	0.09
A08	190	10000	0.41	0.34
A09	190	10000	0.20	0.14
A10	190	12200	0.29	0.22
A11	190	28900	0.44	0.36
A12	190	12500	0.35	0.30
A13	285	1400	0.32	0.26
A14	285	10000	0.20	0.13
A15	285	10000	0.10	0.06
A16	285	10000	0.47	0.41

D.1.2 Series A - Permanent shear strain

Test	Permanent shear strain γ_p%					
	Cycle 1	10	10^2	10^3	10^4	Final
A01	1.27	1.85	2.42	3.05	3.55	3.78
A02	3.72	5.84	7.62	9.64	11.52	12.56
A03	7.30	11.20	13.70	15.71	17.72	19.02
A04	0.20	0.24	0.27	0.31	0.35	-
A05	0.48	0.64	0.85	1.13	1.38	-
A06	0.98	1.27	1.66	2.11	2.44	2.57
A07	0.17	0.20	0.23	0.26	0.28	-
A08	3.28	4.82	6.20	7.72	8.70	-
A09	0.25	0.32	0.41	0.53	0.60	-
A10	0.69	0.98	1.36	1.82	2.13	2.15
A11	5.42	8.22	10.57	12.86	14.91	15.67
A12	2.34	3.42	4.48	5.58	6.55	6.62
A13	1.62	2.28	2.97	3.79	-	3.89
A14	0.36	0.48	0.62	0.80	0.92	-
A15	0.11	0.15	0.17	0.20	0.21	-
A16	9.70	14.94	18.66	21.71	24.18	-

D.1.3 Series A - Recoverable shear strain

Test	Recoverable shear strain γ_r%					
	Cycle 1	10	10^2	10^3	10^4	Final
A01	0.64	0.55	0.50	0.43	0.43	0.41
A02	1.71	1.09	0.84	0.72	0.71	0.68
A03	2.53	1.35	0.98	0.83	0.83	0.84
A04	0.25	0.20	0.20	0.19	0.20	-
A05	0.49	0.42	0.40	0.38	0.38	-
A06	0.73	0.59	0.55	0.50	0.50	0.50
A07	0.23	0.20	0.19	0.18	0.18	-
A08	1.44	1.13	0.97	0.88	0.77	-
A09	0.39	0.34	0.34	0.33	0.33	-
A10	0.70	0.60	0.56	0.53	0.50	0.50
A11	1.87	1.27	1.05	0.89	0.84	0.85
A12	1.17	0.89	0.75	0.70	0.65	0.67
A13	1.09	0.94	0.86	0.78	-	0.78
A14	0.49	0.45	0.43	0.42	0.42	-
A15	0.24	0.22	0.22	0.21	0.21	-
A16	2.82	1.93	1.44	1.24	1.12	-

D.1.4 Series A - Permanent volumetric strain

Test	Permanent volumetric strain v_p%					
	Cycle 1	10	10^2	10^3	10^4	Final
A01	0.14	0.27	0.47	0.71	0.96	1.16
A02	-0.43	-0.42	-0.18	0.07	0.38	0.55
A03	-0.98	-0.93	-0.60	-0.26	0.29	0.65
A04	0.09	0.12	0.17	0.24	0.28	-
A05	0.13	0.22	0.34	0.51	0.66	-
A06	0.28	0.44	0.69	0.97	1.24	1.32
A07	0.09	0.12	0.18	0.25	0.27	-
A08	0.28	0.55	1.00	1.55	1.99	-
A09	0.10	0.15	0.25	0.38	0.48	-
A10	0.14	0.24	0.43	0.69	0.88	0.91
A11	-0.24	-0.07	0.35	0.82	1.20	1.41
A12	0.26	0.50	0.81	1.16	1.45	1.48
A13	0.39	0.64	1.00	1.45	-	1.51
A14	0.18	0.28	0.46	0.68	0.84	-
A15	0.06	0.10	0.16	0.25	0.28	-
A16	-0.29	-0.08	0.51	1.19	1.83	-

D.1.5 Series A - Recoverable volumetric strain

Test	Recoverable volumetric strain v_r%					
	Cycle 1	10	10^2	10^3	10^4	Final
A01	-0.20	-0.10	-0.076	-0.073	-0.066	-0.066
A02	-0.77	-0.33	-0.22	-0.16	-0.14	-0.14
A03	-1.43	-0.50	-0.27	-0.22	-0.20	-0.19
A04	-0.038	-0.014	-0.014	-0.014	-0.014	-
A05	-0.086	-0.042	-0.028	-0.035	-0.035	-
A06	-0.16	-0.063	-0.049	-0.042	-0.049	-0.039
A07	-0.024	-	-	-	-	-
A08	-0.49	-0.21	-0.18	-0.17	-0.12	-
A09	-0.049	-0.014	-0.014	-0.014	-0.014	-
A10	-0.11	-0.063	-0.042	-0.038	-0.028	-
A11	-0.80	-0.33	-0.21	-0.16	-0.16	-0.16
A12	-0.31	-0.13	-0.091	-0.081	-0.074	-
A13	-0.28	-0.14	-0.12	-0.10	-	-
A14	-0.052	-0.014	-0.014	-0.014	-0.014	-
A15	-0.021	-	-	-	-	-
A16	-1.36	-0.51	-0.28	-0.22	-0.22	-

D.1.6 Series A - Shear modulus

Test	Shear modulus G MPa					
	Cycle 1	10	10^2	10^3	10^4	Final
A01	9.0	10.6	10.8	11.4	11.2	11.3
A02	4.9	7.3	8.8	9.3	8.8	9.4
A03	3.5	6.3	8.2	8.6	7.8	7.6
A04	11.9	13.0	12.6	13.2	12.6	-
A05	8.9	10.0	9.8	9.8	10.0	-
A06	11.8	14.0	13.7	14.5	13.9	13.9
A07	17.0	17.2	17.1	17.6	18.1	-
A08	9.3	11.6	12.2	11.8	11.8	-
A09	15.5	16.4	15.3	15.8	16.0	-
A10	13.3	14.5	14.2	14.7	15.6	15.4
A11	7.4	11.0	12.3	14.0	14.6	14.7
A12	10.2	12.5	13.9	14.8	15.8	15.2
A13	13.8	15.9	15.2	15.8	-	-
A14	16.1	16.9	16.2	15.5	15.9	-
A15	16.2	16.9	16.9	16.8	16.8	-
A16	8.4	12.3	14.6	15.5	16.6	-

D.2 Series B - Symmetric Bidirectional Repeated Load

D.2.1 Series B - Basic test data

Test	σ kPa	Final N cycles	R_m (10)	R_c (10)
B01	95	27100	0.00	0.32
B02	95	100000	0.01	0.50
B03	95	30000	0.00	0.62
B04	95	28100	0.00	0.64
B05	95	90800	-0.01	0.78
B06	190	26000	0.00	0.21
B07	190	28000	-0.03	0.51
B08	190	28000	-0.01	0.79
B09	190	29500	-0.01	0.37
B10	190	29000	0.00	0.73
B11	285	30600	0.00	0.53
B12	285	29100	-0.02	0.78
B13	285	29200	0.01	0.32
B14	285	28300	-0.01	0.12

D.2.2 Series B - Recoverable shear strain

Test	Recoverable shear strain γ_r%					
	Cycle 1	10	10^2	10^3	10^4	Final
B01	0.73	0.58	0.58	0.55	0.55	0.55
B02	1.95	1.36	1.07	0.90	0.86	0.87
B03	2.97	2.10	1.46	1.26	1.17	1.16
B04	3.98	2.74	1.87	1.52	1.38	1.36
B05	8.14	5.30	2.81	2.15	1.88	1.69
B06	0.67	0.53	0.52	0.51	0.49	0.49
B07	2.67	1.75	1.39	1.21	1.16	1.16
B08	14.93	7.73	3.80	2.90	2.60	2.58
B09	1.47	1.12	1.03	0.96	0.90	0.88
B10	8.94	4.59	2.82	2.30	2.14	2.05
B11	4.01	2.50	1.90	1.64	1.54	1.53
B12	17.27	7.96	4.01	3.13	2.89	2.79
B13	1.66	1.20	1.07	0.96	0.93	0.94
B14	0.40	0.32	0.31	0.31	0.30	0.31

D.2.3 Series B - Permanent volumetric strain

Test	Permanent volumetric strain v_p%					
	Cycle 1	10	10^2	10^3	10^4	Final
B01	0.06	0.12	0.26	0.47	0.66	0.74
B02	0.05	0.41	0.88	1.30	1.70	2.03
B03	-0.05	0.58	1.35	1.97	2.47	2.72
B04	-0.18	0.63	1.61	2.33	2.88	3.19
B05	-0.90	0.92	2.73	3.70	4.33	5.05
B06	0.09	0.24	0.43	0.70	0.91	0.95
B07	0.18	0.86	1.58	2.24	2.72	2.93
B08	-0.86	3.21	5.90	7.26	8.48	8.85
B09	0.18	0.55	1.06	1.58	2.09	2.26
B10	-0.06	2.28	3.97	5.10	6.02	6.44
B11	0.49	1.77	2.97	4.05	4.77	5.11
B12	-0.11	5.05	8.39	10.20	11.73	12.33
B13	0.37	0.95	1.66	2.40	3.02	3.66
B14	0.03	0.11	0.24	0.40	0.52	0.56

D.2.4 Series B - Shear modulus

Test	Shear modulus G MPa					
	Cycle 1	10	10^2	10^3	10^4	Final
B01	-	11.0	10.6	11.1	11.6	11.6
B02	5.4	7.4	8.6	9.9	10.4	10.0
B03	4.4	6.1	8.3	9.4	10.3	10.3
B04	3.3	4.7	6.8	8.2	8.8	8.9
B05	1.9	3.0	5.7	7.3	8.1	9.0
B06	14.0	15.6	15.0	14.9	16.3	16.3
B07	7.7	11.5	13.6	15.3	15.8	15.9
B08	2.0	4.0	7.9	9.6	10.8	10.8
B09	10.4	13.1	13.3	13.5	13.8	13.4
B10	3.2	6.2	9.4	11.3	12.2	12.9
B11	7.4	11.7	14.4	15.6	16.5	16.3
B12	2.5	5.2	9.2	11.1	12.1	12.6
B13	10.9	14.7	14.9	15.7	16.0	15.6
B14	18.1	20.8	20.0	19.7	20.7	20.6

D.3 Series C - Asymmetric Bidirectional Repeated Load

D.3.1 Series C - Basic test data

Test	σ kPa	Final N cycles	R_m (10)	R_c (10)
C01	190	10000	-0.27	0.50
C02	190	10000	-0.11	0.19
C03	190	10000	-0.16	0.31

D.3.2 Series C - Permanent shear strain

Test	Permanent shear strain γ_p%				
	Cycle 1	10	10^2	10^3	10^4
C01	-	9.74	11.32	12.43	13.32
C02	-	0.57	0.78	1.02	1.15
C03	-	1.29	1.82	2.30	2.62

D.3.3 Series C - Recoverable shear strain

Test	Recoverable shear strain γ_r%				
	Cycle 1	10	10^2	10^3	10^4
C01	9.72	2.22	1.45	1.20	1.13
C02	0.99	0.54	0.51	0.48	0.47
C03	1.98	1.07	0.88	0.79	0.77

D.3.4 Series C - Permanent volumetric strain

Test	Permanent volumetric strain v_p%				
	Cycle 1	10	10^2	10^3	10^4
C01	-	1.18	2.08	2.78	3.26
C02	-	0.31	0.58	0.88	1.06
C03	-	0.52	0.97	1.43	1.80

D.3.5 Series C - Recoverable volumetric strain

Test	Recoverable volumetric strain v_r%				
	Cycle 1	10	10^2	10^3	10^4
C01	-	-0.38	-0.21	-0.14	-0.11
C02	-	-0.052	-0.038	-0.039	-0.035
C03	-	-0.11	-0.098	-0.081	-0.074

D.3.6 Series C - Shear modulus

Test	Shear modulus G MPa				
	Cycle 1	10	10^2	10^3	10^4
C01	2.0	8.8	12.5	14.5	16.1
C02	7.7	13.9	14.4	15.1	15.8
C03	6.3	11.5	13.3	14.4	14.8

APPENDIX E

Model for Permanent Shear Strain based on R_c (10) - Series A

This model is developed from the permanent shear strain results obtained from the Series A tests which are presented in Section 5.4 where the permanent shear strain was shown to be linearly related to the logarithm of the number of load cycles. Each line can be defined in terms of an intercept, I, with the cycle 1 ordinate and a slope, $\Delta\gamma_p$/decade. Figs E1 and E2 show that these parameters correlate with the cyclic shear stress ratio, R_c (10) on a log-linear basis. There is some effect of normal stress but this has been ignored throughout since the data is insufficient to characterise the behaviour independently for each normal stress level.

In Fig. E2 it can be seen that the data points for the lowest stress ratios fall well below the regression line, shown dotted, which includes these points. This is probably due to the fact that the data must become asymptotic to the R_c (10) = 0 ordinate. If these points are rejected, the fit of the regression line, shown full in Fig. E2, is improved. While this improves the accuracy of the model obtained, it also restricts it to the range $0.13 < R_c\ (10) < 0.42$. The upper limit is defined by the range of the data.

Using the regression lines in Figs E1 and E2, an empirical model for the permanent shear strain behaviour can be developed in the form:

$$\gamma_p(N) = I + \Delta\gamma_p/\text{decade}\ (\log N)$$

where $$\log I = -1.291 + 5.311\ R_c\ (10)$$

giving $$I = 0.05117\ (204644)^{R_c\ (10)}$$

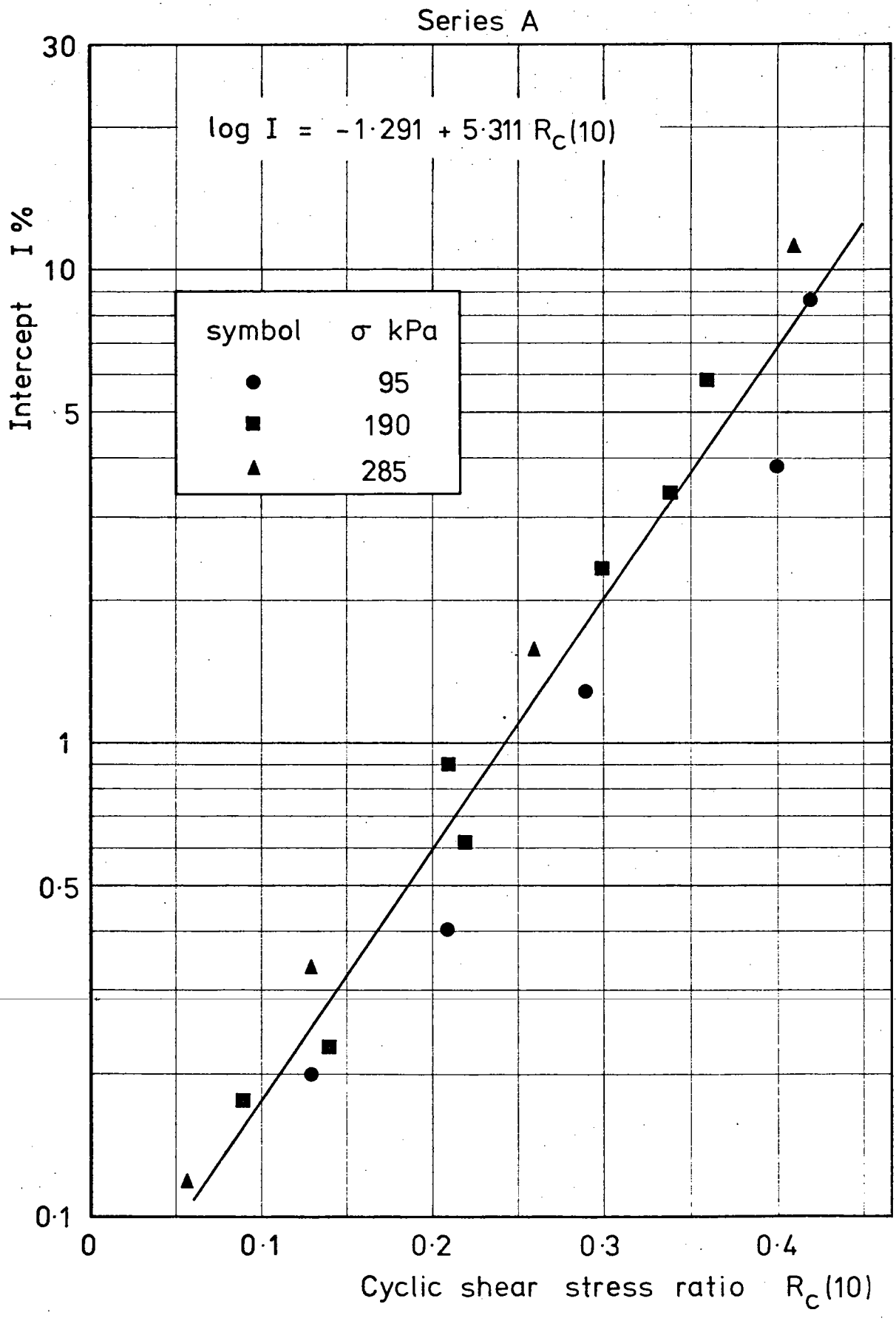

Fig. E1 Intercept versus cyclic shear stress ratio

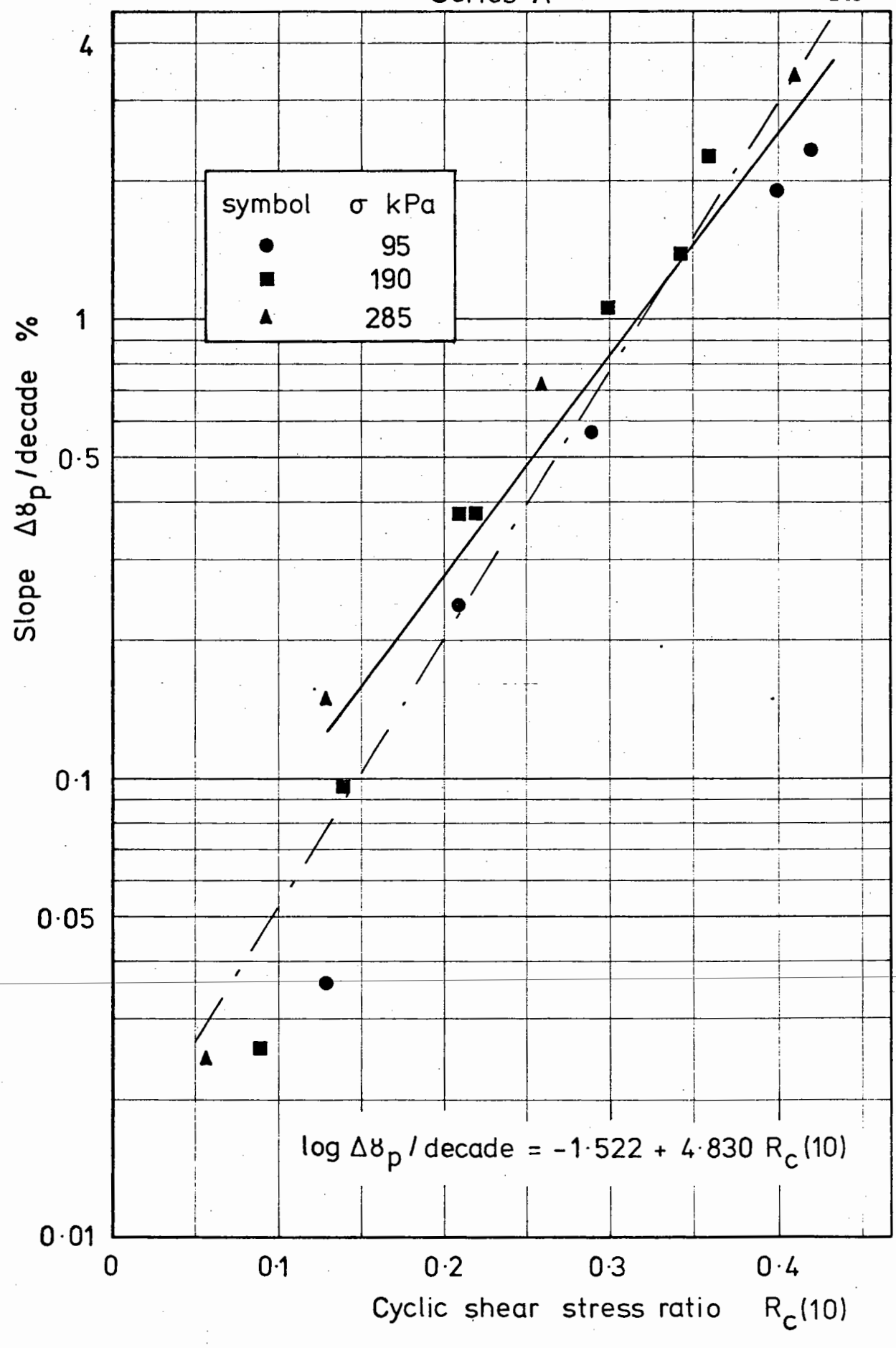

Fig. E2 Slope versus cyclic shear stress ratio

and $$\log \Delta\gamma_p/\text{decade} = -1.522 + 4.830\ R_c \quad (10)$$

giving $$\Delta\gamma_p/\text{decade} = 0.03006\ (67608)^{R_c} \quad (10)$$

The implied accuracy of the coefficients must be disregarded when considering the calculated value of $\gamma_p(N)\%$.

APPENDIX F

Model for Recoverable Shear Strain - Series A

This model is developed from the recoverable shear strain results obtained from the Series A tests which are presented in Section 5.5. It can be seen in Fig. F1 that the initial recoverable shear strain, $\gamma_r(1)$, correlates with the cyclic shear stress ratio, R_c (10), over the range of the test data on a log-linear basis. A similar relationship exists at each of the decade points and the regression lines for these are shown in Fig. F2. The effect of normal stress was again difficult to quantify and has been ignored in the development of this model.

As it stands, Fig. F2 is obviously unacceptable as a model since the regression lines intersect each other at various points. To overcome this, the intercepts for the five lines have been averaged and this value used as a focus. Each line has been rotated about its original value at R_c (10) = 0.4 in the adjustment. The adjusted model is shown in Fig. 41.

A mathematical recoverable shear strain model can be developed from Fig. 41 using a fourth order regression curve to obtain the slope of each line:

$$\log \gamma_r(N) = (A + B\log N + C\log^2 N + D\log^3 N + E\log^4 N)R_c(10) - 0.804$$

where A = 2.848 B = -0.554 C = 0.140 D = -0.022 E = 0.0016

The model is applicable in the range $0.06 < R_c$ (10) < 0.42 and, in this form, it could be incorporated into a computer program. The implied accuracy of the coefficients must be disregarded when considering the calculated result.

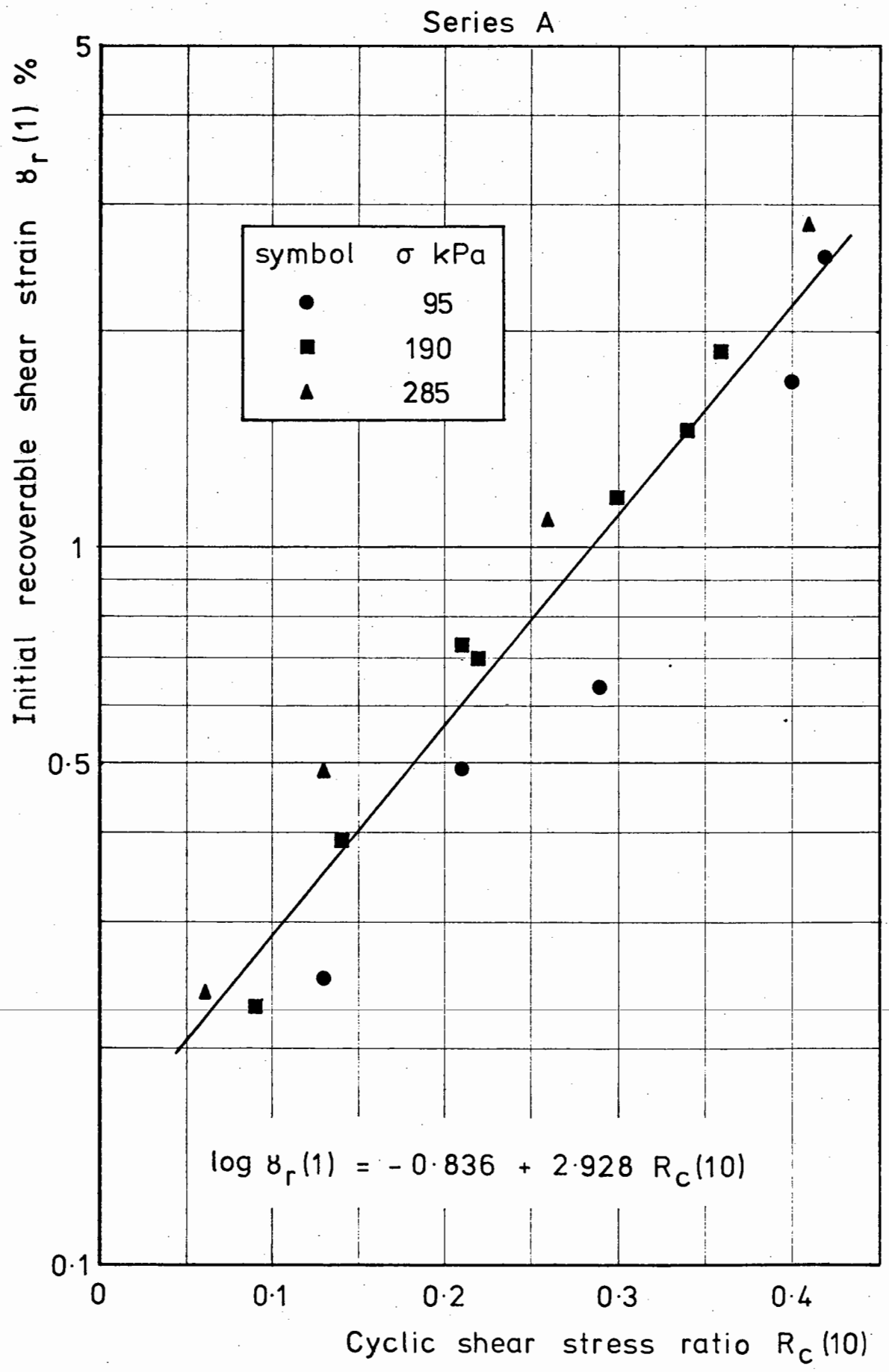

Fig. F1 Initial recoverable shear strain versus cyclic shear stress ratio

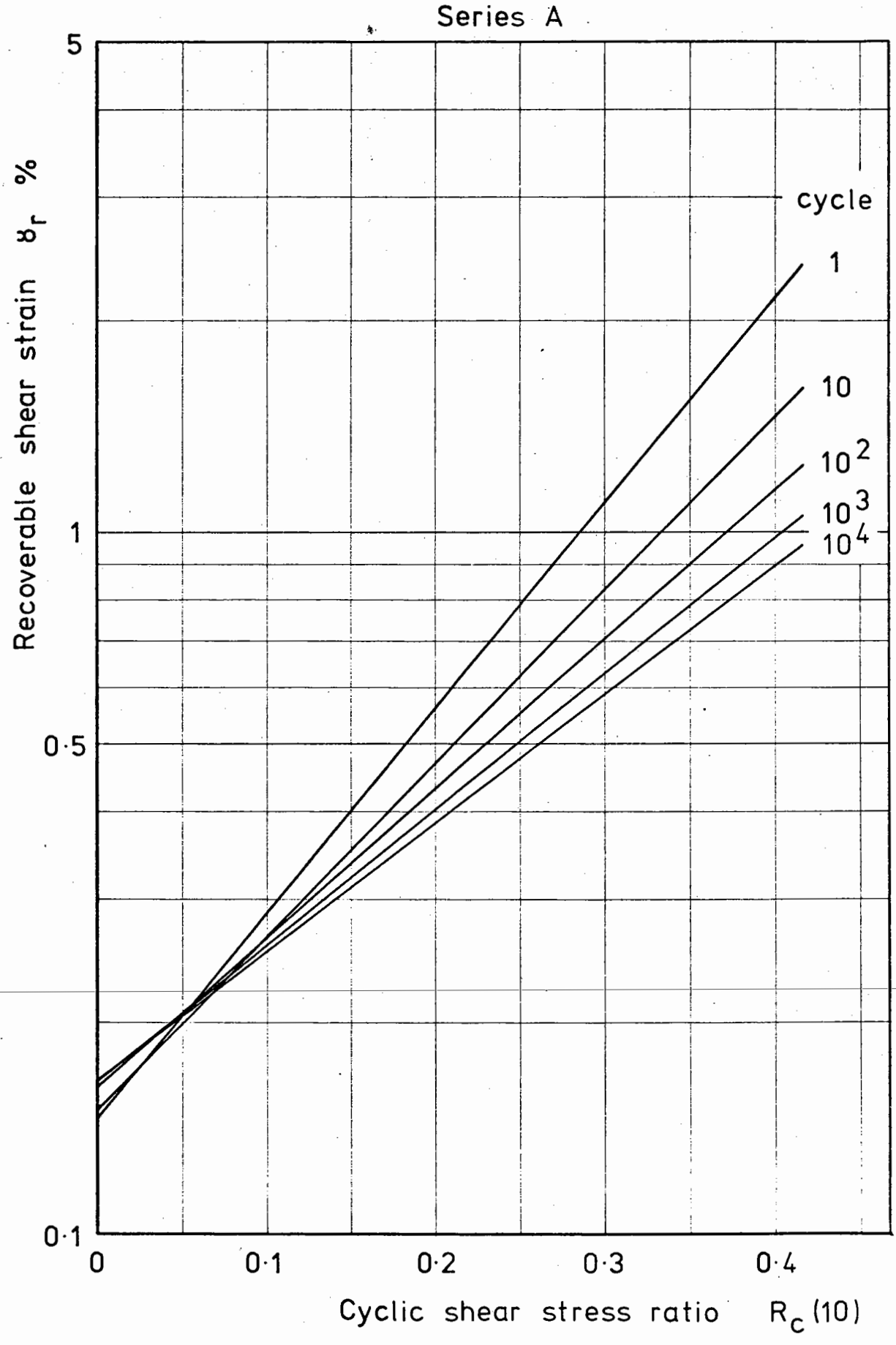

Fig.F2 Unadjusted model for recoverable shear strain

APPENDIX G

Model for Permanent Shear Strain based on $\gamma_r(1)$ - Series A

This model is developed from the permanent and recoverable shear strain results obtained from the Series A tests which are presented in Sections 5.4 and 5.5 respectively. In Appendix E it was shown that, for permanent shear strain, a linear relationship exists between the cyclic shear stress ratio, R_c (10), and the logarithms of both the intercept, I, and the slope, $\Delta\gamma_p$/decade, which define the permanent shear strain behaviour. In Appendix F, it was shown that a linear relationship also exists between the cyclic shear stress ratio and the logarithm of the recoverable shear strain, γ_r. Consequently, a relationship must exist between the recoverable shear strain and both the intercept, I, and the slope, $\Delta\gamma_p$/decade, for permanent shear strain. Figs G1 and G2 show these relationships for $\gamma_r(1)$. $\gamma_r(1)$ has been used since this gives a greater range of recoverable shear strains which is useful in the development of the model. From Fig. G2, it can be seen that this model can accommodate the three points which were omitted in the permanent shear model developed in Appendix E and the reason for this is considered in Section 5.6.

Using the regression lines in Figs G1 and G2, an empirical model for the permanent shear strain behaviour can be developed in the form:

$$\gamma_p(N) = I + \Delta\gamma_p/\text{decade} \ (\log N)$$

where $$\log I = 0.219 + 1.756 \log \gamma_r(1)$$

giving $$I = 1.65577 \ (\gamma_r(1))^{1.756}$$

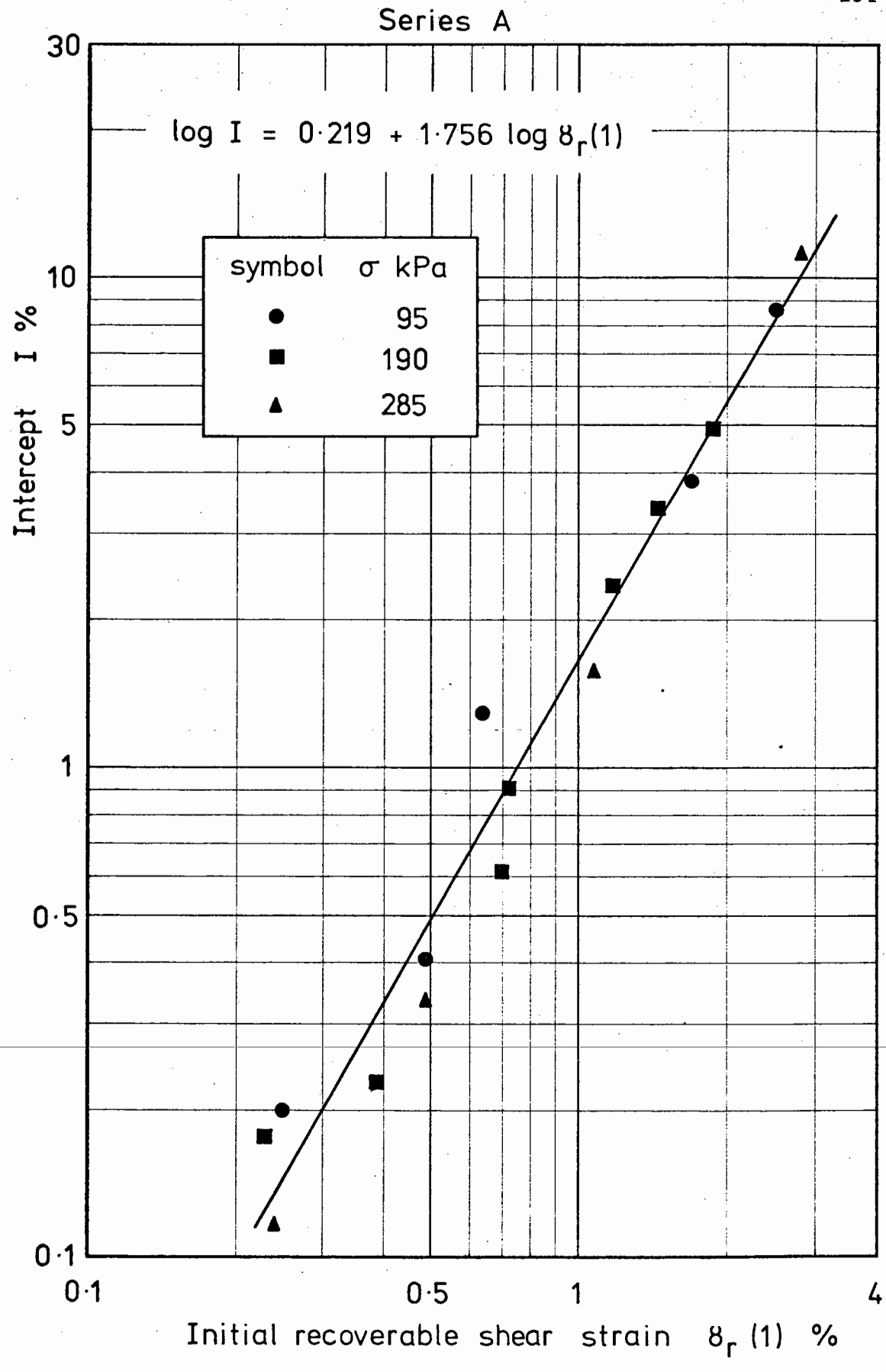

Fig. G1 Intercept versus initial recoverable shear strain

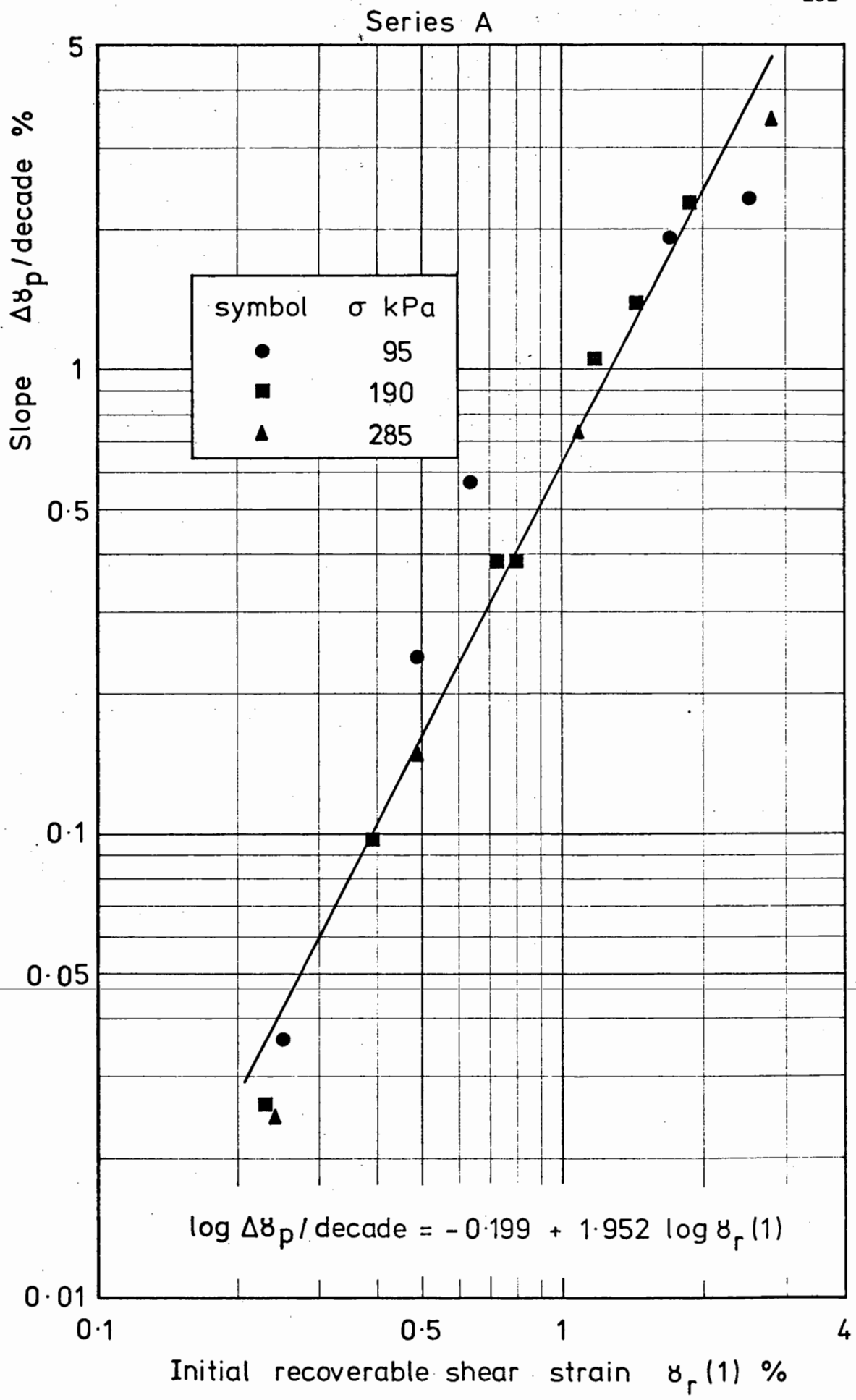

Fig. G2 Slope versus initial recoverable shear strain

and $$\log \Delta\gamma_p/\text{decade} = -0.199 + 1.952 \log \gamma_r(1)$$

giving $$\Delta\gamma_p/\text{decade} = 0.63241 \, (\gamma_r(1))^{1.952}$$

The model is applicable in the range $0.2\% < \gamma_r(1) < 3\%$. The implied accuracy of the coefficients must be disregarded when considering the calculated result.

APPENDIX H

Model for Recoverable Volumetric Strain - Series A

This model is developed from the recoverable volumetric strain results obtained from the Series A tests which are presented in Section 5.8. The relationship between the initial recoverable volumetric strain, $v_r(1)$ and the cyclic shear stress ratio, R_c (10), is shown in Fig. H1. Similar relationships exist at the other decade points and these are shown in Fig. H2. To produce a feasible model from these lines it was necessary to adjust them in a similar manner to that described in Appendix F for the recoverable shear strain model. However, the line for $v_r(1)$ appears to be independent of the other four lines and so the intercept of this line has not been adjusted. This independence of the $v_r(1)$ line is probably due to the high shear strains associated with the first cycle and so its treatment as a separate case appears reasonable. The adjusted model produced by this method is shown in Fig. 49 for its range of applicability. Again, the adjusted lines have been rotated about their original value at R_c (10) = 0.4 so as to pass through the average of their original intercepts. The range of the model is curtailed after the first cycle because the strains become so small that the data from the tests is unreliable.

The mathematical model for the recoverable volumetric strain is in two parts; one for the first cycle and another for cycle 10 onwards using a third order regression curve to obtain the slope of the lines in Fig. 49.

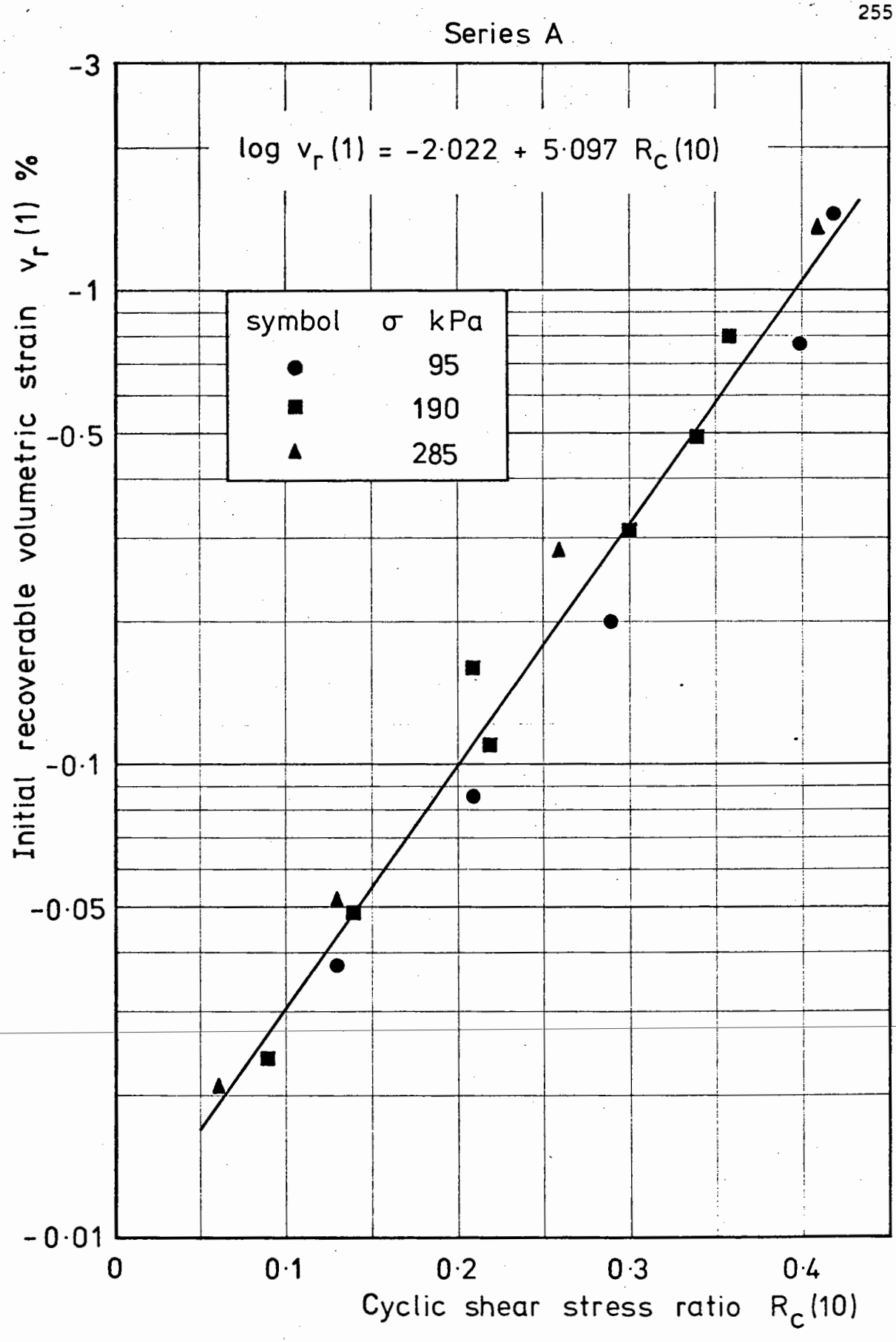

Fig. H1 Initial recoverable volumetric strain versus cyclic shear stress ratio

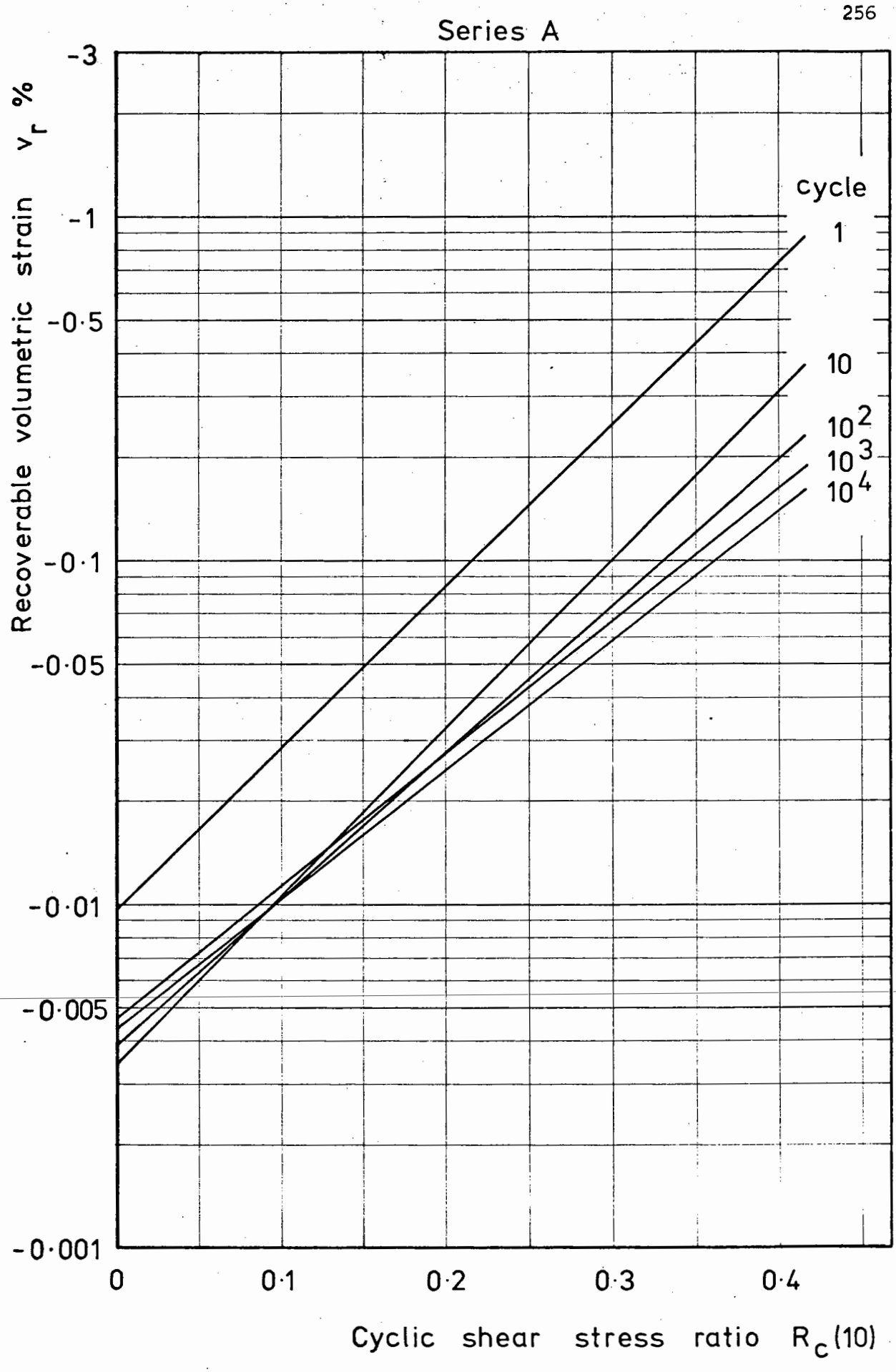

Fig. H2 Unadjusted model for recoverable volumetric strain

For the first cycle:

$$\log v_r(1) = 5.097\, R_c(10) - 2.022$$

$$0.06 < R_c(10) < 0.42$$

and for cycle 10 onwards:

$$\log v_r(N) = (A + B\log N + C\log^2 N + D\log^3 N)R_c(10) - 2.387$$

where $A = 6.150$ $B = -1.382$ $C = 0.368$ $D = -0.037$

$$0.10 < R_c(10) < 0.42$$

The implied accuracy of the coefficients must be disregarded when considering the calculated result. In addition, the sign convention, which would represent dilatant volumetric strains as negative, has been ignored in the mathematical model for ease of presentation. All recoverable volumetric strains were dilatant so no real difficulty arises in considering the appropriate sign.

APPENDIX I

Model for Recoverable Shear Strain - Series A, B and C

This model is developed from the recoverable shear strain results obtained from the Series A, B and C tests which are presented in Sections 5.5, 6.4 and 6.9 respectively and is thus applicable to repeated loading at any mean shear stress ratio in the range considered; $R_c \geq R_m \geq 0$.

Fig. I1 shows the relationship between the recoverable shear strain and the cyclic shear stress ratio at cycle 10 for the Series A, B and C results. Similar relationships exist for the other decade points, Fig. I2, with the possible exception of cycle 1 where it was found that the initial recoverable shear strains in the three Series C tests were somewhat higher than those in the Series A and B tests. However, at subsequent decade points, the Series C results conformed with the rest of the data points. This effect at cycle 1 has not been modelled because of the small amount of data available from the Series C tests. The slight effect of normal stress has again been ignored in this model since it was difficult to quantify with the data available.

Fig. I1 also provides justification for the definition, given in Section 5.3, of the recoverable shear strain as the peak to peak shear strain because, using this definition, all the recoverable shear strain results obey a similar relationship with the cyclic shear stress ratio. This point was also discussed in Sections 6.4 and 6.7.

Having brought all the recoverable shear strain data together, a model for the overall recoverable shear strain behaviour can be developed by adjusting the regression lines shown in Fig. I2 using the technique described in Appendix F for the Series A model. The

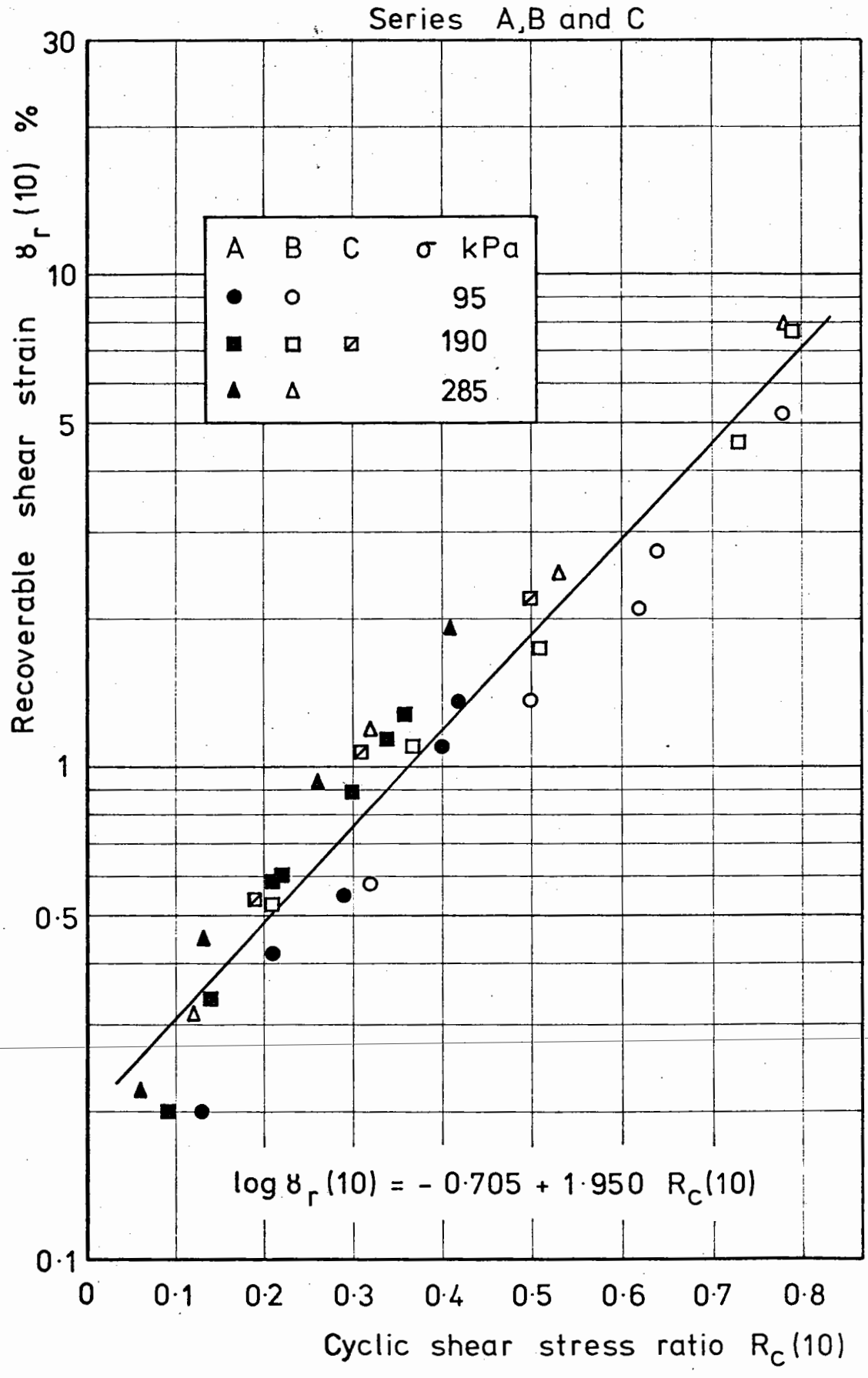

Fig. I1 Recoverable shear strain versus cyclic shear stress ratio

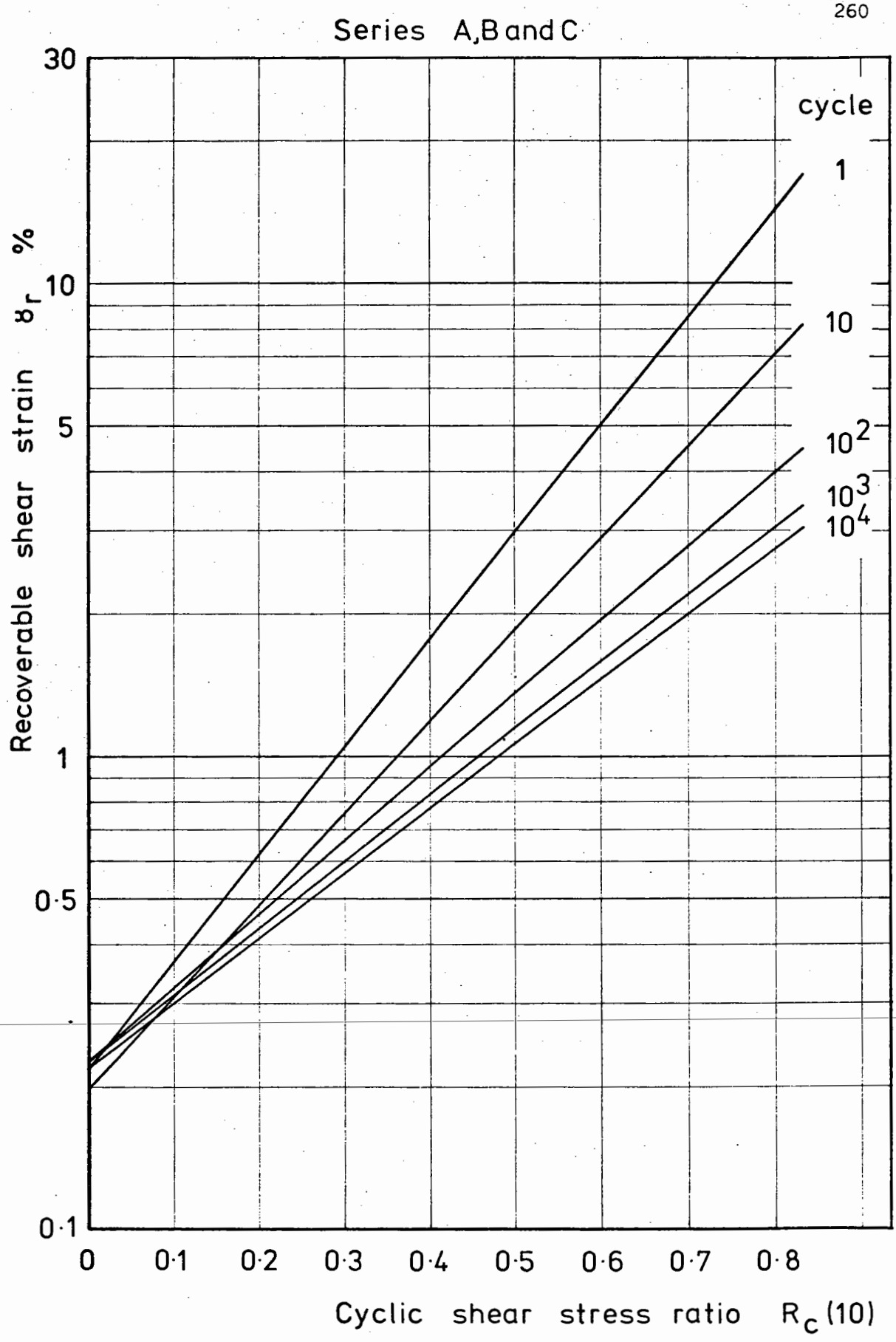

Fig. I2 Unadjusted model for recoverable shear strain

regression lines in Fig. I2 were adjusted by rotating them about their original value at $R_c(10) = 0.8$ so as to give them a common intercept. The adjusted model is shown in Fig. 61.

A mathematical recoverable shear strain model can be developed from Fig. 61 using a fourth order regression curve to obtain the slope of each line:

$$\log \gamma_r(N) = (A + B\log N + C\log^2 N + D\log^3 N + E\log^4 N)R_c(10) - 0.664$$

where $A = 2.274$ $B = -0.305$ $C = -0.140$ $D = 0.078$ $E = -0.0095$

The model is applicable in the range $0.05 < R_c(10) < 0.8$ and, in this form, it could be incorporated into a computer program. The implied accuracy of the coefficients must be disregarded when considering the calculated result.

APPENDIX J

Andersen's Method for Predicting the Response to Block Loading

The technique described in this appendix was successfully used by Andersen (3) to predict the cyclic shear strains for saturated clay samples subjected to varying cyclic shear stresses from the results of repeated constant stress tests. His work was concerned with the behaviour of saturated clay subjected to undrained cyclic loading such as might occur below offshore gravity structures in the North Sea during a storm.

Andersen's proposals are as follows: the cyclic shear strain after $N + \Delta N$ cycles, $\gamma_{c,N+\Delta N}$ may be expressed by the equation:

$$\gamma_{c,N+\Delta N} = \gamma_{c,N} + \Delta\gamma_{c,i} + \Delta\gamma_{c,\Delta N}$$

where

$\gamma_{c,N}$ = the cyclic strain in cycle N with a cyclic shear stress, $\tau_{c,N}$

$\Delta\gamma_{c,i}$ = the "immediate change in cyclic shear strain" which is due to a change in cyclic shear stress from $\tau_{c,N}$ to $\tau_{c,N+1}$

$\Delta\gamma_{c,\Delta N}$ = the increase in cyclic shear strain due to ΔN cycles with a cyclic shear stress, $\tau_{c,N+1}$

A graphical method of using this equation is shown in Fig. J1 using a strain contour chart developed from the stress controlled tests and a graph relating the cyclic shear strain to the cyclic shear stress level for the first load cycle. In the example shown in Fig. J1, the clay sample is subjected to a cyclic shear stress level of ± 0.45 and starts at point A for the first cycle. The sample is subjected to 100 cycles at this stress level and moves horizontally to point B in the diagram

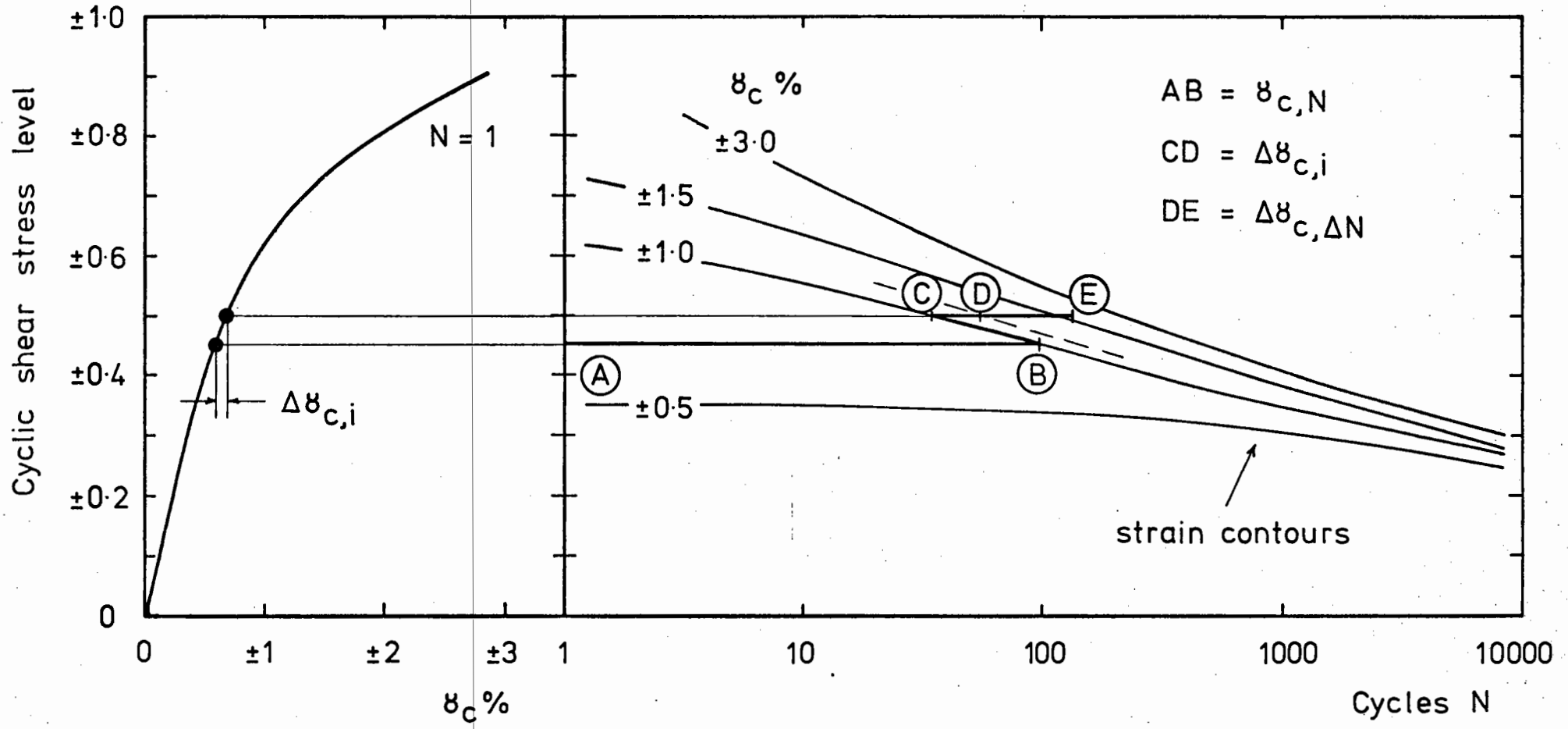

Fig. J1 Andersen's method for predicting the response to block loading

and the cyclic shear strain is:

$$\gamma_{c,N} = \gamma_{c,1} + \Delta\gamma_{c,\Delta N} = \pm 1\%$$

The cyclic shear stress level is then increased to ±0.50 taking the clay along the strain contour from point B to point C. The shear stress increase causes an "immediate cyclic shear strain", $\Delta\gamma_{c,i}$ which is found from the left hand diagram in Fig. J1 by assuming that the immediate change in shear strain due to the change in cyclic shear stress level is the same as it would have been for the first load cycle. This assumption is considered (3) good enough for any practical solution. The immediate strain, which is found to be ±0.1%, takes the clay from point C to point D and the subsequent cycles are counted from this point. After 100 cycles at a cyclic shear stress level of ±0.50, point E is reached at which the accumulated cyclic shear strain will be $\gamma_{c,N + \Delta N} = \pm 1.6\%$. Further cyclic loading, with increasing or decreasing cyclic shear stress levels, may be considered in a similar manner and the method may be used to evaluate the cyclic shear strains throughout a storm which cause arbitrary variations in cyclic load on the foundation of a gravity-type oil production platform.